UNIVERSITÉ DU QUÉBEC À RIMOUSKI

RECONSTITUTIONS DE LA VARIABILITÉ CLIMATIQUE DANS L'AXE PRINCIPAL DU PASSAGE DU NORD-OUEST AU COURS DE L'HOLOCÈNE

THÈSE
PRÉSENTÉE À
L'UNIVERSITÉ DU QUÉBEC À RIMOUSKI
comme exigence partielle
du programme de doctorat en océanographie

PAR
DAVID LEDU

Octobre 2009

AVANT-PROPOS

Les études doctorales sont comme une évolution pathologique en trois étapes. La première étape s'inscrit dans un délire paranoïde de type mégalomaniaque s'exprimant par le fait de vouloir tout comprendre. Puis, vient la deuxième étape où l'on croit tout comprendre ou presque laissant place à une décompensation importante et à l'installation de la pathologie de manière profonde. Enfin, la troisième étape est l'installation du trouble bipolaire, qui se traduit par la manie toujours persistante d'apprendre et de comprendre, accompagnée par un doute croissant de ce que l'on sait au point de douter plus qu'au départ. La Science est basée sur cet état d'insatisfaction permanente et de satisfaction passagère, qui en fait toute sa beauté et sa splendeur. Elle nous force à l'humilité par son caractère infini, immense et insaisissable. Elle nous murmure doucement les mots des Anciens: « Tout ce que je sais, c'est que je ne sais rien » (Socrate), nous donnant la chance immense, et peut-être inégalée, de côtoyer l'infini à travers le désir inébranlé, inébranlable pour certains, d'apprendre et de comprendre. Je voudrais remercier mes parents, Jeanne et Daniel, de m'avoir transmis ce désir permanent de connaissance et de curiosité, et de m'avoir toujours soutenu dans mes démarches: je leur dédie ce doctorat.

Je souhaite également remercier mon directeur de recherche, le Dr André Rochon (ISMER/UQAR-GEOTOP), de m'avoir permis de réaliser un de mes vœux les plus chers, et de m'avoir fait confiance dans des moments très difficiles. N'oublie pas, je ne lâche jamais ! J'ai énormément appris avec toi, et je te suis éternellement reconnaissant.

Ma reconnaissance va également vers ma co-directrice, le Dr Anne de Vernal (UQAM/GEOTOP/ISMER), qui a accepté de me superviser, et qui m'a également fait confiance. C'est une personne qui a une passion inébranlable pour la recherche, je trouve cela exceptionnel. Même si tu ne le sais peut-être pas, une phrase dite dans ton bureau à Montréal a tout changé dans ma tête, et m'as remis sur les rails... J'espère sincèrement t'avoir convaincu intellectuellement.

Je remercie aussi le Dr Guillaume St-Onge (ISMER/UQAR/GEOTOP) d'avoir été toujours disponible même dans les périodes difficiles où le temps manquait. Je le remercie aussi de m'avoir permis d'utiliser le magnétomètre cryogénique, et de m'avoir formé sur son fonctionnement.

Mes remerciements vont aussi vers le Dr Michel Gosselin (ISMER/UQAR/QUÉBEC-OCÉAN) qui a accepté d'être le président de mon jury de thèse, et vers le Dr Sarah A. Finkelstein (Université de Toronto) qui a accepté d'en être l'examinateur externe.

Je souhaite adresser ma sincère reconnaissance à Sylvain Leblanc (ISMER/UQAR, analyse granulométrique), Pierre Simard et Guillaume Auclair (UQAR, préparation palynologique), Bassam Ghaleb et Jean-François Hélie (UQAM/GEOTOP, analyses géochimiques et isotopes stables). Je remercie également l'équipage du brise-glace de recherche canadien *Amundsen* ainsi que Trecia Schell (Université Dalhousie) et Robbie Bennett (Institut Océanographique de Bedford) pour l'échantillonnage des sédiments.

Un grand merci à Jacques Labrie (ISMER/UQAR) pour avoir réglé les problèmes informatiques, et pour le temps passé avec moi sur les «wavelets». Sans oublier le fameux Mac qui nous a posé tant de soucis.

Taoufik Radi, Maryse Henry (UQAM-GEOTOP) et Thomas Richerol (Université Laval/ISMER) ont aussi contribué à cette recherche par les discussions que nous avons pu avoir, sur les « épineux », mais aussi sur les fonctions de transfert.

Francesco Barletta, merci d'être ce que tu es. Tu serais capable de faire aimer la physique au plus grand des réfractaires.

Ma pensée va vers le Dr Jean-Claude Brêthes et le Dr Jean-François Dumais qui m'inspirent un respect immense pour leur vision des choses et leur sens de l'humain.

Je remercie également tout le personnel administratif de l'ISMER et, en particulier, Sylvie Fillon pour sa gentillesse et sa douceur ainsi que Nycole Bérubé.

Enfin, mon affection va vers le regretté Dr François Saucier qui a su me conseiller à un moment décisif. Merci.

Cette recherche n'aurait pu être possible sans le soutien financier du Réseau des centres d'excellence ArcticNet et du Conseil de recherches en sciences naturelles et en génie (CRSNG) du Canada Cette recherche est une contribution au projet 1.6 du réseau ArcticNet : « L'ouverture du passage du Nord-Ouest, Ressources, Navigation, Souveraineté et Sécurité ». Elle est également une contribution au réseau pour la stabilité du climat polaire (Polar Climate Stability Network, PCSN) financé par la Fondation canadienne des sciences du climat et de l'atmosphère (FCSCA).

En plus d'une introduction et d'une conclusion générale, cette thèse est organisée en trois grands chapitres. Le premier chapitre est publié dans la revue *Canadian Journal of Earth Sciences* sous la référence suivante:

> Ledu, D.; Rochon, A.; de Vernal, A.; St-Onge, G. 2008. «Palynological Evidence of Holocene Climate Change in the Eastern Arctic: a Possible shift in the Arctic Oscillation at the Millennial Time Scale». **Canadian Journal of Earth Science**, vol. 45, n°11, pp. 1363-1375.

Le second chapitre est accepté dans la revue *Quaternary Science Reviews*, sous la référence suivante:

> Ledu, D.; Rochon, A.; de Vernal, A.; St-Onge, G. (accepté). Holocene paleoceanography of the Northwest Passage, Canadian Arctic Archipelago: the possible onset of an Arctic Oscillation climate mode». **Quaternary Science Reviews.**

Enfin le troisième chapitre est soumis dans la revue *Paleoceanography* sous la référence suivante:

> Ledu, D.; Rochon, A.; de Vernal, A.; Barletta, F.; St-Onge, G. (soumis à **Paleoceanography**). Holocene sea-ice history and climate variability along the main axis of the Northwest Passage, Canadian Arctic.

Les résultats de cette recherche ont également été présentés dans plusieurs congrès nationaux et internationaux : Association Géologique et Minéralogique du Canada (AGC-AMC, Montréal, 2006), les congrès ArcticNet (Collingwood, ON, 2007 ; Québec, 2008), American Geophysical Union (AGU, San Francisco, 2007), Huitième conférence internationale sur les dinoflagellés modernes et fossiles (Dino8, Montréal, 2008).

RÉSUMÉ

Des analyses palynologiques et géochimiques ont été réalisées sur trois carottes sédimentaires prélevées, dans les détroits de Lancaster, Barrow et Dease, le long de l'axe principal du passage du Nord-Ouest (APPNO). La chronologie des carottes sédimentaires est basée sur l'utilisation combinée d'âges radiocarbones et de corrélations magnétostratigraphiques. Les modèles d'âge indiquent que les carottes sédimentaires des détroits de Lancaster, Barrow et Dease couvrent respectivement les derniers 11,1, 10,8 et 7,7 ka calibrées BP. Les taux de sédimentation calculés sont compris entre 43 et 140 cm/ka pour le détroit de Lancaster et entre 15 et 118 cm/ka pour le détroit de Barrow. Un taux de sédimentation constant de 61 cm/ka caractérise le site du détroit de Dease. L'application de la technique des analogues modernes aux assemblages de kystes de dinoflagellés (dinokystes) a permis des estimations quantitatives des paramètres de surface (température, salinité et durée du couvert de glace) pour les trois séquences sédimentaires couvrant la quasi-totalité des 10 000 dernières années. L'Holocène ancien (entre ~11 et ~8,5 ka calibrées BP) est marqué par des conditions instables avec d'importants apports terrigènes. Au détroit de Lancaster, cet intervalle se caractérise par une absence de dinokystes accompagnée d'importants apports terrigènes entre 11,1 et 10,8 ka calibrées BP suivie de conditions relativement froides comparées aux conditions modernes avec dominance des taxons hétérotrophes. Au détroit de Barrow, l'intervalle entre ~11 et ~8,5 ka calibrées BP est caractérisé dans son ensemble par d'importants apports terrigènes avec des températures (août) relativement froides comparées aux conditions modernes, et un couvert de glace fluctuant autour des valeurs modernes. De telles conditions, enregistrées aux détroits de Lancaster et de Barrow sont associées aux derniers stades de la déglaciation inuitienne dans la région. En particulier, la présence de courants de glace actifs jusqu'à environ 8,5 ka calibrées BP au niveau du bassin de Kane et du détroit de Smith pourrait avoir contribuée aux conditions froides enregistrées au détroit de Lancaster. La présence d'un courant de glace dans le chenal de Wellington accompagnée par un maximum d'épaisseur de glace dans le centre de l'archipel arctique canadien expliquent probablement l'importance des apports terrigènes pendant plus de 2000 ans au niveau du détroit de Barrow.

La comparaison des reconstitutions quantitatives des paramètres de surface entre les trois sites à partir de ~8 ka calibrées BP jusqu'à l'Holocène récent a permis de mieux comprendre la nature et la variabilité du gradient climatique est-ouest caractéristique du réchauffement climatique actuel dans l'Arctique. Ce gradient, dont la présence a été documentée dès le début de l'Holocène entre la baie de Baffin, la mer de Beaufort et de Chukchi, n'avait encore jamais été étudié le long de l'APPNO sur une base quantitative. Les résultats de cette recherche indiquent une variabilité climatique relativement importante à l'échelle millénaire le long de l'APPNO. L'Holocène moyen apparaît comme une période de transition importante. Durant cet intervalle, les enregistrements du détroit de Dease suggèrent la mise en place du courant du Mackenzie dans sa configuration moderne. Des changements marqués des conditions de surface sont également enregistrés de manière synchronique au niveau des trois sites. Cette période de transition est associée à un

changement de phase de l'oscillation arctique (OA^+ vers OA^-). La comparaison du $\delta^{18}O$ d'une carotte de glace prélevée sur l'île de Devon avec la température reconstituée (août) du détroit de Lancaster suggère, en effet, un fort couplage atmosphère-océan durant la quasi-totalité de l'Holocène similaire aux effets de l'oscillation arctique. Cette dernière pourrait avoir opéré à l'échelle millénaire depuis le début de l'Holocène. Cependant, les estimations quantitatives des conditions de surface pour les détroits de Lancaster et de Dease indiquent que la durée saisonnière du couvert de glace a été plus importante que les conditions modernes durant la quasi-totalité de l'Holocène. Ces résultats indiquent que le gradient climatique est-ouest est plus complexe qu'une simple opposition dipolaire entre le secteur oriental et occidental de l'archipel arctique canadien (AAC). Des facteurs locaux incluant que la proximité de glaciers, la présence de courants de côte ou la structure de l'halocline peuvent avoir amplifié, atténué ou renversé le signal climatique de mécanismes supra-régionaux tels que l'oscillation arctique.

TABLE DES MATIÈRES

LISTE DES TABLEAUX

LISTE DES FIGURES

INTRODUCTION GÉNÉRALE

CHAPITRE 1. PALYNOLOGICAL EVIDENCE OF HOLOCENE CLIMATE CHANGE IN THE EASTERN ARCTIC: A POSSIBLE SHIFT IN THE ARCTIC OSCILLATION AT THE MILLENNIAL TIME SCALE

LISTE DES ABRÉVIATIONS

ABBREVIATIONS	SIGNIFICATIONS
AAC	Archipel Arctique Canadien
AF	Alternative Field
AMS	Accelerator Mass Spectrometry
AO	Arctic Oscillation
APPNO	Axe Principal du Passage du Nord-Ouest
BC	Baffin Current
BG	Beaufort Gyre
BP	Before Present
BSB	Barents Sea Branch
CAA	Canadian Arctic Archipelago
ChRM	Characteristic Remanent Magnetization
EGC	East Greenland Current
FSB	Fram Strait Branch
G/P ratio	Gonyaulacales/Peridiniales Ratio
GAD	Geocentric Axial Dipole
GIN seas	Greenland-Iceland-Norwegian seas
GIS	Greenland Ice Sheet
IC	Irminger Current
IIS	Innuitian Ice Sheet
IRD	Ice Rafted Debris
K_{LF}	Low Field volumetric magnetic susceptibility
LIS	Laurentide Ice Sheet
MAD	Maximum Angular Deviations
MANWP	Main Axis of the Northwest Passage
MAT	Modern Analogue Technique
MDF	Median Destructive Field
MSCL	Multi Sensor Core Logger
NAC	North Atlantic Current
NAM	North Annular Mode
NAO	North Atlantic Oscillation
NRM	Natural Remanent Magnetization
NwAC	Norwegian Atlantic Current
OL	Organic Linings
PML	Polar Mixed Layer
PSV	Paleomagnetic Secular Variations
RSL	Relative Sea-Level
SB	Svalbard Branch
SSS	Sea-Surface Salinity
SSSs	Summer Sea-Surface Salinity
SST	Sea-Surface Temperature
SSTs	Summer Sea-Surface Temperature
TPD	Transpolar Drift
WGC	West Greenland Current
YB	Yermack Branch

INTRODUCTION GÉNÉRALE

L'océan Arctique dans le contexte du réchauffement climatique

Au cours des 40 dernières années, les données instrumentales indiquent que l'océan Arctique a enregistré des modifications climatiques importantes. Le réchauffement climatique, commencé à la fin des années 1970, s'est cependant fortement amplifié au cours de la dernière décennie [*Comiso,* 2006; *Serreze et al.,* 2007; *Comiso et al.,* 2008; *Deser and Teng,* 2008; *Drobot et al.,* 2008; *Overland et al.,* 2008; *Parkinson and Cavalieri,* 2008; *Stroeve et al.,* 2008; *Wang and Overland,* 2009]. Ce réchauffement s'est traduit par une diminution marquée de la surface occupée par les glaces de mer avec notamment une disparition des glaces pérennes dans certains secteurs centraux de l'archipel arctique canadien (AAC) [*Parkinson and Cavalieri,* 2002; *Atkinson et al.,* 2006]. En septembre 2007, par exemple, l'étendue du couvert de glace de mer de l'océan Arctique était environ 40% inférieure à celui de la période 1979-2006 mesurée à partir des données satellites [*Comiso et al., 2008*; *Schweiger et al.,* 2008]. Les plus fortes diminutions ont été enregistrées au niveau de la mer de Beaufort, du détroit de Béring et des marges continentales sibériennes [*Steele et al.,* 2008] indiquant une opposition marquée entre les secteurs orientaux et occidentaux de l'Arctique face aux effets de la tendance climatique actuelle. Les simulations climatiques indiquent que l'océan Arctique pourrait être libre de glace, au moins sur une base saisonnière, dans la deuxième moitié du 21^{ième} siècle [*Zhang and Walsh,* 2006; *IPCC,* 2007]. Des rétroactions positives du système atmosphère-océan-glace de mer ont été proposées pour expliquer les anomalies climatiques décennales

[*Lindsay and Zhang*, 2005; *Kay et al.,* 2008]. L'émission anthropique de gaz à effet de serre tel que le CO_2 est considérée comme un mécanisme majeur du réchauffement climatique [*Vinnikov et al.,* 1999; *Karl and Trenberth*, 2003; *Johannessen et al.,* 2004].Cependant, la grande majorité des changements climatiques récents a été associée aux forçages atmosphériques à grande échelle tels que l'oscillation arctique (OA) ou l'oscillation nord-atlantique (ONA) [*Hurrell, 1995*; *Thompson and Wallace*, 1998; *Deser et al.,* 2000; *Dickson et al.,* 2000; *Kwok,* 2000; *Rigor et al.,* 2002; *Wallace and Thompson*, 2002; *Hurrell and James*, 2003; *Vavrus and Harrison*, 2003; *Zhang et al.,* 2003; *Rigor and Wallace*, 2004; *Steele et al.,* 2004; *Steele and Ermold*, 2004; *Serreze et al.,* 2007; *Ogi and Wallace*, 2007, 2008]. La diminution du couvert de glace à la fin des années 1970 a, en effet, été synchrone avec une modification de la circulation atmosphérique à l'échelle hémisphérique. Cette modification s'est traduite par le passage de conditions anticycloniques associées à une phase négative de l'OA vers des conditions cycloniques correspondant à une phase positive de l'OA. Il est reconnu que l'impact de l'OA aux échelles annuelle, interannuelle et décennale se traduit par une importante structure dipolaire des conditions climatiques telle qu'observée au cours des dernières décennies entre les secteurs occidentaux et orientaux de l'océan Arctique [*Rigor et al.,* 2002; *Vavrus and Harrison*, 2003; *Zhang et al.,* 2003]. Cependant, les données instrumentales ne couvrent tout au plus que les 40 dernières années rendant difficile l'interprétation et la compréhension des mécanismes responsables du réchauffement climatique observé. En particulier, le recul temporel des données mesurées n'est généralement pas suffisant pour replacer le contexte actuel dans une variabilité naturelle du climat à des échelles séculaires

ou millénaires. Le développement de traceurs paléoclimatiques tels que les traceurs dendroclimatiques et géochimiques enregistrés dans les coraux, les carottes de glace ou les spéléothèmes, les traceurs micropaléontologiques (kystes de dinoflagellés, foraminifères, coccolithes, diatomées, radiolaires, pollen) ou les biomarqueurs ont permis de dépasser les limites temporelles des données instrumentales. Par exemple, les températures de surface lors du dernier maximum glaciaire ont été reconstruites à partir de fonctions de transfert appliquées aux assemblages de kystes de dinoflagellés, de foraminifères et de diatomées (projet MARGO[1]). Cette démarche a permis de tester la capacité des modèles de circulation générale couplés atmosphère-océan à reproduire des conditions climatiques différentes des conditions modernes (projet PMIP[2]). Cependant, le dernier maximum glaciaire représente des conditions climatiques généralement extrêmes en relation avec les paramètres orbitaux de la Terre. L'Holocène (les 10 000 dernières années) est en revanche une période adéquate pour replacer le contexte climatique actuel dans une perspective à plus long terme. En effet, l'Holocène, bien que marqué par des évènements climatiques relativement abrupts (événement à 8.2 ka, hypsithermal, Petit-Âge glaciaire, optimum médieval), correspond à une période géologique de transition relativement stable, pendant laquelle les conditions climatiques peuvent être comparées avec les conditions modernes en isolant les facteurs anthropiques. Depuis le milieu des années 1990, plusieurs études basées sur des traceurs micropaléontologiques à partir de carottes sédimentaires marines ont fourni des reconstitutions quantitatives des conditions de surface dans l'océan Arctique durant l'Holocène [*de Vernal et al.*, 1994, 1997, 2001, 2005b, 2008; *Kunz-Pirrung et al.*, 2001;

[1] Multiproxy Approach for the Reconstruction of the Glacial Ocean Surface
[2] Paleoclimate Modelling Intercomparison Project

Levac et al., 2001; *Koç and Jansen*, 2002; *Bauch and Polyakova*, 2003; *Andersen et al.,* 2004a, 2004b; *Polyakova et al.,* 2004, 2005; *de Vernal and Hillaire-Marcel*, 2006; *Klyuvitkina et al.,* 2006; *Rochon et al.,* 2006; *Justwan et al.,* 2008; *Knudsen et al.,* 2008; *McKay et al.,* 2008; *Olyunina et al.,* 2008; *Ran et al.,* 2008; *Richerol et al.,* 2008b; *Schell et al.,* 2008; *Ren et al.,* 2009; *Scott et al.*, 2009]. La synthèse de ces études indique une nette opposition des conditions de surface entre l'Ouest et l'Est de l'Arctique au cours de l'Holocène. Plus précisément, une tendance aux anomalies négatives du couvert de glace dans l'Est, mais des anomalies positives dans l'Ouest sont indiquées au début de l'Holocène, tandis que la tendance inverse est enregistrée au cours de l'Holocène moyen à récent. Cette structure climatique dipolaire durant l'Holocène est similaire à l'impact de l'OA. En dépit des études précédemment citées, les reconstitutions paléocéanographiques sur une base quantitative n'ont encore jamais été réalisées le long de l'axe principal du passage du Nord-Ouest (APPNO), dans l'AAC. Or, cette région joue un rôle essentiel dans l'exportation des flux d'eau douce et de glace vers l'Atlantique Nord [*Dickson et al.,* 2007]. La marge continentale de l'ACC représente plus de 20% de la surface totale des marges continentales de l'Arctique [*Jakobsson,* 2002; 2004] connectant la mer de Beaufort à la baie de Baffin. La production primaire annuelle est estimée à 55 Mt C a^{-1}soit 1/3 de la production primaire totale des marges continentales de l'océan Arctique [*Vinogradov et al.,* 2000; *Michel et al.,* 2006]. Ces caractéristiques font de l'AAC une région unique pour étudier et mieux comprendre le gradient climatique est-ouest.

L'archipel arctique canadien et l'axe principal du passage du Nord-Ouest

L'AAC est composé de nombreuses îles séparées par des chenaux creusés par l'érosion fluviatile et glaciaire durant le Quaternaire. Par conséquent, plus de la moitié des chenaux dans l'AAC a des profondeurs inférieures à 200 m [*Prinsenberg and Bennett*, 1987; *Jakobsson,* 2002, 2004; *McLaughlin et al.,* 2004]. Seule la région du détroit de Lancaster, sous contrôle structural lors de la formation de la baie de Baffin, enregistre des profondeurs supérieures à 500 m [*Prinsenberg and Bennett*, 1987; *Okulitch and Trettin*, 1991]. D'est en ouest, l'APPNO traverse les détroits de Lancaster, Barrow, Victoria et Dease en passant entre les îles du Prince de Galles et de Somerset (Fig. 1). Les conditions de glace sont relativement sévères le long de l'APPNO, et, de novembre à mai, toute la région est généralement couverte par la glace [*Parkinson et al.,* 1999]. Le couvert minimum de glace est observé au début du mois de septembre avec plusieurs chenaux ouverts, à l'exception de la partie centrale de l'APPNO où des bouchons de glace épais se forment [*Parkinson and Cavalieri*, 2002; *Howell et al.,* 2008]. Les glaces nouvelles (de 1^{ière} année) couvrent l'essentiel de l'AAC, et sont particulièrement développées dans la partie ouest, tandis que les glaces anciennes (plusieurs années) et épaisses occupent les chenaux centraux de l'archipel.

L'APPNO représente dans l'AAC un des conduits principaux d'exportation des eaux et de glace de mer de l'ouest de l'Arctique vers l'Atlantique Nord. En raison de la structure bathymétrique de l'archipel et hormis la région du détroit de Lancaster, la colonne d'eau ne contient peu ou pas d'eau Atlantique. La majeure partie de la colonne d'eau de l'AAC est composée d'une couche de mélange saisonnière et d'une halocline Pacifique relativement

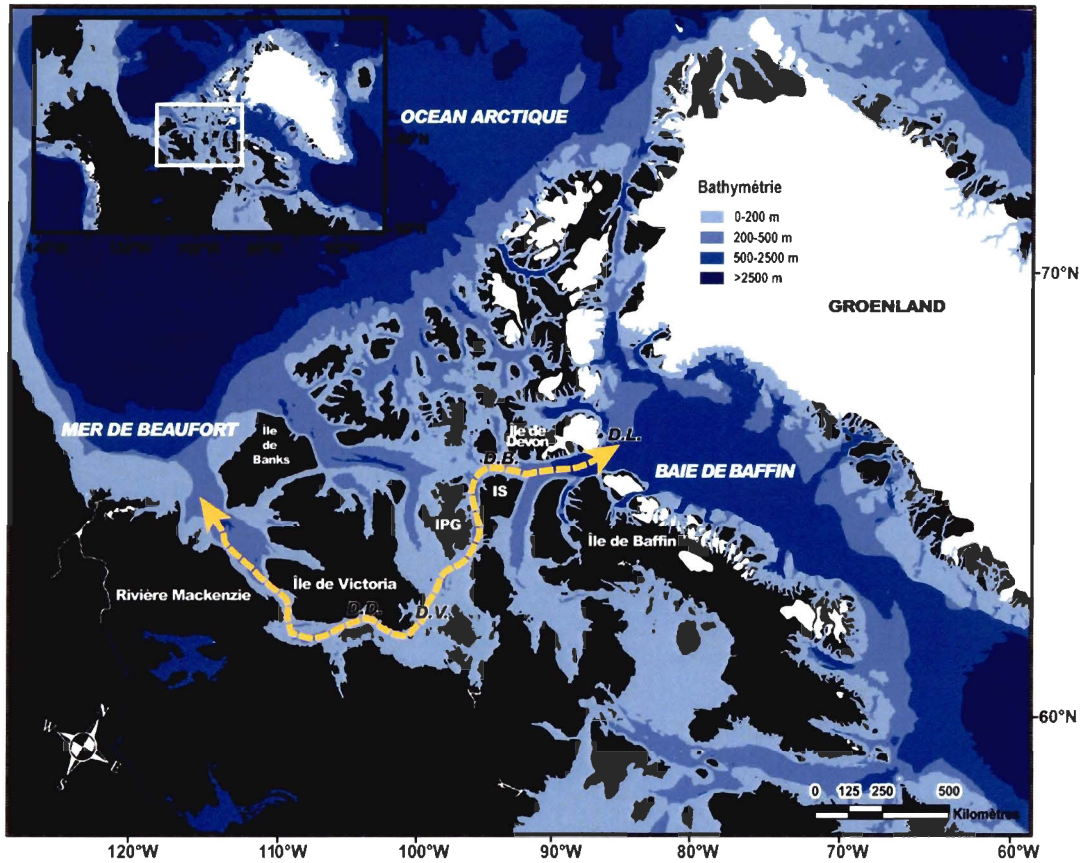

Figure 1. L'archipel arctique canadien. L'axe principal du passage du Nord-Ouest (flèche pointillée jaune) traverse les détroits de Lancaster (D.L.), de Barrow (D.B.), de Victoria (D.V.) et de Dease (D.D.) en passant entre l'île de Somerset (IS) et les îles du Prince-de-Galles (IPG).

complexe et variable [*Jones et al.*, 2003; *Woodgate et al.*, 2005; *Steele et al.*, 2008]. L'halocline supérieure comporte une masse d'eau relativement chaude et peu salée issue du courant de côte Alaskien (influencée par les rivières Yukon et Mackenzie), et repose sur une masse d'eau plus froide et plus salée provenant de la partie plus centrale du détroit de Béring. L'halocline inférieure est composée d'une masse d'eau froide et salée se formant en hiver et particulièrement riche en nutriments. Dans l'AAC, la circulation de surface s'effectue d'ouest en est, et les entrées d'eau provenant du bassin du Canada se font

principalement par le golfe d'Amundsen et le détroit de M'Clure. Or, la structure de l'halocline, c'est-à-dire l'importance relative des différentes masses d'eau qui la composent, dépend non seulement du secteur géographique considéré, mais aussi des phases de l'OA. Cette eau Pacifique, relativement peu salée par rapport à l'eau Atlantique sous-jacente est régulièrement intégrée dans les bilans d'eau douce de l'océan Arctique [*Dickson et al.,* 2007; *Carmack et al.,* 2008]. Récemment, *Dickson et al.,* (2007) ont estimé que l'exportation d'eau douce à travers l'AAC était d'environ 100 mSv soit environ la totalité des précipitations annuelles dans l'océan Arctique. Bien que ces estimations soient variables, en particulier suivant les composantes d'eau douce prise en compte (voir par exemple les estimations de [*Serreze et al.,* 2006]), il n'en demeure pas moins que l'AAC joue un rôle fondamental dans l'exportation d'eau douce de l'ouest de l'Arctique vers l'Atlantique Nord. Dans un contexte de réchauffement climatique, une augmentation des flux d'eau douce à travers l'AAC pourrait altérer les processus convectifs dans la mer du Labrador. Plusieurs études suggèrent une augmentation des flux d'eau douce à travers l'AAC au cours des prochaines décennies [*Haak et al.,* 2005; *Holland et al.,* 2006; *Koenigk et al.,* 2007]. Selon *Haak et al.* (2005), d'ici à la fin du 21^{ième} siècle, l'augmentation des flux d'eau douce à travers l'AAC pourrait être de 75%. Or, *Goosse et al.* (1997) indiquent que si l'AAC devenait libre de glace la circulation thermohaline Atlantique pourrait être réduite de 10%, tandis que *Wadley and Bigg* (2002) estiment cette diminution à 35%.

Dans ce contexte, mieux comprendre la variabilité naturelle du climat de l'Arctique a été un des fondements de cette recherche. Cette dernière s'est attachée à savoir si les conditions climatiques actuelles, notamment la fonte du couvert de glace, sont le signe de

conditions irréversibles ou simplement la manifestation d'une fluctuation climatique s'inscrivant dans une variabilité naturelle du climat à plus grande échelle. L'objectif premier de cette thèse a été de comprendre pourquoi l'Ouest de l'Arctique se réchauffe plus vite que l'Est en essayant de mieux comprendre la nature du gradient climatique est-ouest et sa variabilité au cours de l'Holocène.

Pour ce faire, trois carottes sédimentaires ont été échantillonnées le long de l'APPNO suivant un transect est-ouest au niveau des détroits de Lancaster, de Barrow et de Dease. La technique des analogues modernes [*de Vernal et al.*, 2001, 2005a; *Guiot and de Vernal*, 2007] a été appliquée aux assemblages de kystes de dinoflagellés, permettant ainsi une reconstitution quantitative des paramètres de surface (température, salinité, durée du couvert de glace) au cours de l'Holocène le long de l'APPNO.

Les kystes de dinoflagellés comme traceurs paléocéanographiques des conditions de surface

Les dinoflagellés sont des organismes planctoniques unicellulaires dont la taille varie généralement entre 20 et 100 μm. Ils sont responsables, avec les diatomées et les coccolithophoridés, de la majeure partie de la production primaire. Environ 40 à 60% des dinoflagellés sont photosynthétiques, le reste étant composé d'hétérotrophes, de parasites ou de symbiotes [*Taylor*, 1987]. Les dinoflagellés sont présents dans la plupart des domaines aquatiques (océans, lacs) des hautes et des basses latitudes, mais sont particulièrement abondants au niveau des marges continentales et plus généralement dans les zones néritiques (estuaires, mers épicontinentales).

Pendant leur cycle de reproduction, après la fusion des gamètes, environ 10 à 15% des espèces produisent un kyste très résistant constitué d'un polymère appelé dinosporine protégeant la cellule diploïde pour une période de dormance plus ou moins longue [*Fensome et al.,* 1993]. La distribution des assemblages de kystes de dinoflagellés (ou dinokystes) dans les sédiments modernes des océans a été l'objet de nombreuses investigations. En particulier, des bases de données régionales d'assemblages de dinokystes présents à la surface des sédiments ont été développées pour l'Atlantique Nord, les basses latitudes de l'océan Atlantique, l'océan Arctique et la façade ouest et est de l'océan Pacifique [*de Vernal et al.,* 1997, 2001, 2005a; *Radi et al.,* 2008]. Régulièrement mises à jour, ces bases de données ont été utilisées pour établir des corrélations entre la distribution des assemblages de dinokystes et les paramètres océanographiques de surface (température, salinité et couvert de glace). Elles ont aussi permis l'accès à des reconstitutions quantitatives des conditions paléocéanographiques de surface. Ainsi, de nombreuses études dans l'océan Arctique et les mers sub-polaires ont établi d'une part, des corrélations entre les paramètres de surface et les assemblages de dinokystes, mais aussi fourni des reconstitutions des conditions de surface au cours de l'Holocène (voir [*Marret and Zonneveld*, 2003] et [*de Vernal and Marret,* 2007] pour une synthèse sur le sujet). Les assemblages de dinokystes dans les sédiments du Quaternaire de l'océan Arctique sont relativement variés [*Mudie and Rochon*, 2001; *Rochon,* 2009]. Le fait que les dinoflagellés se retrouvent dans une grande variété d'environnements et de conditions de surface a permis des investigations dans des milieux physiques extrêmes comme l'Arctique. En particulier, leur bonne conservation ainsi que leur diversité dans les milieux polaires

comparées aux microfossiles carbonatés ou siliceux en font un des traceurs paléocéanographiques le mieux adapté pour l'environnement polaire.

Objectifs de recherche

Comprendre pourquoi l'Ouest de l'Arctique se réchauffe plus vite que l'Est et comparer les impacts physiques et sociétaux des changements climatiques dans le Haut Arctique canadien le long du gradient est-ouest ont été au centre des objectifs du réseau de recherche international et pluridisciplinaire ArcticNet (http://www.arcticnet.ulaval.ca/). La recherche présentée ici s'inscrit dans le cadre du projet 1.6 de ce réseau («L'ouverture du passage du Nord-Ouest, Ressources, Navigations, Souveraineté et Sécurité»). Les objectifs principaux de cette dernière ont été de:

- Mieux comprendre la variabilité naturelle du climat de l'Arctique. En particulier, établir la nature et la variabilité du gradient climatique est-ouest le long de l'APPNO en isolant les facteurs anthropiques.
- Développer un cadre chronostratigraphique pour l'APPNO.
- Identifier des tendances climatiques à l'échelle séculaire ou millénaire afin d'intégrer le contexte climatique actuel et sub-actuel dans une évolution paléoclimatique.
- Proposer des mécanismes potentiellement récurrents susceptibles d'expliquer la variabilité climatique enregistrée au cours de l'Holocène dans l'APPNO.

- Fournir, pour la première fois dans l'APPNO, des données quantitatives des conditions de surface couvrant les 10 000 dernières années pouvant servir de limites réalistes pour les simulations climatiques.

Les reconstitutions quantitatives des paramètres de surface au cours de l'Holocène pour le site du détroit de Lancaster sont présentées dans le chapitre 1. L'hypothèse de recherche du chapitre 1 a été l'existence d'une variabilité climatique à l'échelle millénaire s'inscrivant dans une évolution climatique régionale. L'objectif principal a été de replacer le contexte climatique actuel dans une évolution paléoclimatique à l'échelle millénaire isolé des facteurs anthropiques. Les reconstitutions quantitatives des paramètres de surface du détroit de Lancaster ont été comparées avec d'autres études dans les secteurs orientaux et occidentaux de l'océan Arctique. Cela a permis de proposer des mécanismes susceptibles d'expliquer la variabilité climatique enregistrée au détroit de Lancaster durant l'Holocène.

Dans le chapitre 2, les estimations quantitatives des paramètres de surface au cours de l'Holocène sont présentées pour le détroit de Barrow. L'hypothèse de recherche pour ce second chapitre a été l'existence d'un gradient climatique est-ouest, variable à l'échelle millénaire dans l'APPNO au cours de l'Holocène, se manifestant par des tendances climatiques opposées entre les détroits de Lancaster et Barrow. L'établissement d'un cadre chronostratigraphique ainsi que la compréhension de la nature et de la variabilité du gradient est-ouest ont été les objectifs majeurs de ce chapitre.

La comparaison des reconstitutions quantitatives des paramètres de surface des détroits de Dease, Barrow et Lancaster est présentée dans le chapitre 3. L'hypothèse de ce dernier chapitre a été l'existence de tendances climatiques opposées et variables à l'échelle

millénaire au cours de l'Holocène entre l'extrémité orientale (détroit de Lancaster) et occidentale (détroit de Dease). Développer le cadre chronostrastigraphique pour l'APPNO a été un des objectifs de ce chapitre. Afin de dégager une structure thermique dipolaire au cours de l'Holocène, la comparaison des reconstitutions quantitatives des conditions de surface des trois sites dans ce cadre chronostratigraphique a été effectuée. Elle a permis de proposer des mécanismes atmosphériques supra-régionaux récurrents susceptibles d'expliquer la variabilité climatique au cours de l'Holocène dans l'APPNO. Des facteurs locaux agissant comme des boucles de rétroactions positives ou négatives ont pu également être isolés. Enfin, une base quantitative des conditions de surface isolées des facteurs anthropiques a été présentée pour la première fois le long de l'APPNO.

CHAPITRE 1

PALYNOLOGICAL EVIDENCE OF HOLOCENE CLIMATE CHANGE IN THE EASTERN ARCTIC: A POSSIBLE SHIFT IN THE ARCTIC OSCILLATION AT THE MILLENNIAL TIME SCALE

1.1 Abstract/Résumé

Dinocyst assemblages and the physical properties of two sediment cores collected in the easternmost part of the main axis of the Northwest Passage, Canadian Arctic Ocean (cores 2004-804-009 BC and 2004-804-009 PC, 74°11.2'N, 81°11.7'W) were used to reconstruct changes in sea-surface conditions and to characterize changes in the depositional environment. Core 2004-804-009 PC spans the last 12 180 calibrated (cal) years BP, with sedimentation rates ranging from 45 to 122 cm/ka. Quantitative estimates of sea-surface parameters reveal relatively large hydrographic variability at millennial time scale. Before 11 000 cal years BP, our records suggest terrigenous inputs related to the last deglaciation. Between 11 000 and 9600 cal years BP, harsh conditions prevailed with August sea-surface temperatures <2°C and the dominance of heterotrophic taxa. This episode was followed by a gradual increase in the relative abundance of phototrophic taxa and the establishment of milder condition with sea-surface temperature (SST) reaching ~2 °C ~8300 cal years BP, possibly related to increased exchange between the Arctic Ocean and the North Atlantic Ocean. From 6000 cal years BP to the late Holocene, climate variability could be the results of changes in the synoptic-scale atmospheric pattern such as the Arctic oscillation.

Les assemblages de dinokystes et les propriétés physiques de deux carottes sédimentaires (carottes 2004-804-009 BC et 2004-804-009 PC, 74°11.2'N, 81°11.7'O) prélevées dans la partie la plus à l'est de l'axe principal du passage du Nord-Ouest, dans l'Arctique canadien, ont été utilisés pour reconstruire les changements de conditions de surface, et caractériser les changements dans l'environnement de dépôt. La carotte 2004-804-009 PC couvre les dernières 12 180 années calibrées avant le présent (années cal. BP) avec des taux de sédimentation qui varient entre 45 et 122 cm/ka. Les estimations quantitatives des paramètres de surface révèlent une variabilité hydrographique relativement grande sur une échelle millénaire. Avant 11 000 années cal. BP, nos données suggèrent des apports terrigènes liés à la dernière déglaciation. Entre 11 000 et 9600 années cal. BP, des conditions difficiles prévalaient avec des températures de surface d'août inférieures à 2°C aux conditions modernes et une dominance de taxons hétérotrophes. Cet épisode a été suivi d'une augmentation graduelle de l'abondance relative de taxons phototrophes, et l'établissement de conditions plus douces avec des températures de surface

qui atteignaient environ 2°C vers 8300 années cal. BP, possiblement relié à un échange accru entre l'océan Atlantique Nord et l'océan Arctique. De 6000 années cal. BP à l'Holocène tardif, la variabilité du climat pourrait découler de changements dans les patrons atmosphériques à grandes échelles tels que l'oscillation arctique.

1.2 Introduction

The Arctic has undergone dramatic changes over the past three decades. Instrumental data reveal a decline in perennial sea-ice cover by as much as 10% between 1978 and 2000. The minimum ice cover extent was observed in September 2007 and was ~38% less than long-term historical averages [*Comiso,* 2002, 2006; *Comiso et al.,* 2008]. Moreover, there has been a marked thinning of the cold halocline layer insulating the ice from the underlying warm Atlantic water [*Steele and Boyd*, 1998]. However, these decadal changes show regional pattern, with the warming being more pronounced in the western than in the eastern Arctic. Similarly, regionalism in the pattern of sea-ice cover has been inferred for the early Holocene based on marine records, terrestrial data, and model experiments [e.g., *Vavrus and Harrison,* 2003; *Kaufman et al.,* 2004; *Fisher et al.,* 2006; *Rochon et al.,* 2006]. Arctic weather patterns are strongly related to the Arctic oscillation (AO), whose index is defined as the first leading mode of empirical orthogonal function [*Thompson and Wallace,* 1998]. In its positive phase, the AO results in a marked west–east variation in sea-ice-cover thickness across the Arctic [*Rigor et al.,* 2002], operating on a decadal time scale [*Venegas and Mysak,* 2000]. In the context of recent changes, long-term climate variability in the Arctic takes on increasing importance because the recognition of recurrent climatic patterns in the past may explain the actual climate trend. Such variability cannot be assessed from short-term observational data but requires longer time series. However, biological tracers commonly used for reconstruction of hydrographic parameters such as foraminifers and diatoms are generally poorly preserved in Arctic sediments because of dissolution of calcium carbonate and siliceous biological remains. In contrast, organic-walled microfossils

or palynomorphs, in particular the cysts of dinoflagellates (or dinocysts), are highly resistant and well preserved in the sediments, allowing the reconstruction of sea-surface conditions. Moreover, dinocysts, which include both phototrophic and heterotrophic taxa, relate to production in the surface water layer. Their assemblages in sediment from Arctic and subarctic seas are useful for reconstruction of sea-surface conditions, including sea-ice cover extent, sea-surface temperature (SST), and sea-surface salinity (SSS) [*de Vernal et al.*, 2001, 2005a].

To document climate changes in Arctic Canada, to improve our understanding of the mechanisms behind Arctic climate variability, and to provide realistic boundary conditions for climate simulations, sediment cores were collected in Lancaster Sound at the easternmost part of the main axis of the Northwest Passage during leg 9 of the ArcticNet oceanographic campaign in the summer of 2004. Cores 2004-804-009 PC and 2004-804-009 BC contain well-preserved dinocyst assemblages, which allow us to use transfer functions (here the modern analogue technique) to reconstruct summer SST and SSS as well as sea-ice cover during the last 12 180 years.

1.3 Environmental settings

1.3.1 Hydrography of the eastern Arctic

Owing to large freshwater inputs (mainly via river discharge), the Arctic water column is strongly stratified. Typically, a low-density surface layer, the Polar Mixed Layer (PML) occupies the top ~50 to 100 m of the water column above the relatively low-salinity Pacific water, which is generally observed between 100 and 300 m in depth [*Jones et al.*, 2003]. Nearly all of the deep water is supplied by dense saline water from the Atlantic

Ocean, which enters the Arctic Ocean through Fram Strait with the West Spitsbergen Current and through the Barents Sea with the Svalbard and Yermak branches [*Woodgate et al.,* 2007]. This deep water then flows counter-clockwise along the Siberian shelves before recirculating in the Canada, Makarov, and Nansen basins. Finally, the water exits the Arctic Ocean via Fram Strait through the East Greenland Current. The latter then mixes with North Atlantic water to form the West Greenland Current flowing northwards to the Labrador Sea and Baffin Bay. It is then deflected toward the west in northern Baffin Bay where it mixes with Arctic water flowing south through Nares Strait to form the Baffin and Labrador currents (Fig. 1).

The Arctic freshwater export to the North Atlantic is accomplished through three gateways: Fram Strait, Nares Strait, and the Canadian Arctic Archipelago (CAA), mainly via Lancaster and Jones sounds [*Dickson et al.,* 2007]. The AO can strongly affect this pattern of circulation mainly in terms of flux and freshwater pathways [*Rigor et al.,* 2002]. The positive phase of the AO enhances more freshwater export through Fram Strait and an increase of Atlantic water flux to the Arctic Ocean because of more cyclonic conditions [*Proshutinsky et al.,* 2002; *Hakkinen and Proshutinsky,* 2004]. In contrast, the negative phase of the AO (more anticyclonic conditions) leads to more freshwater accumulation in the western Arctic and more inflow of Pacific water into the Arctic Ocean [*McLaughlin et al.,* 2002].

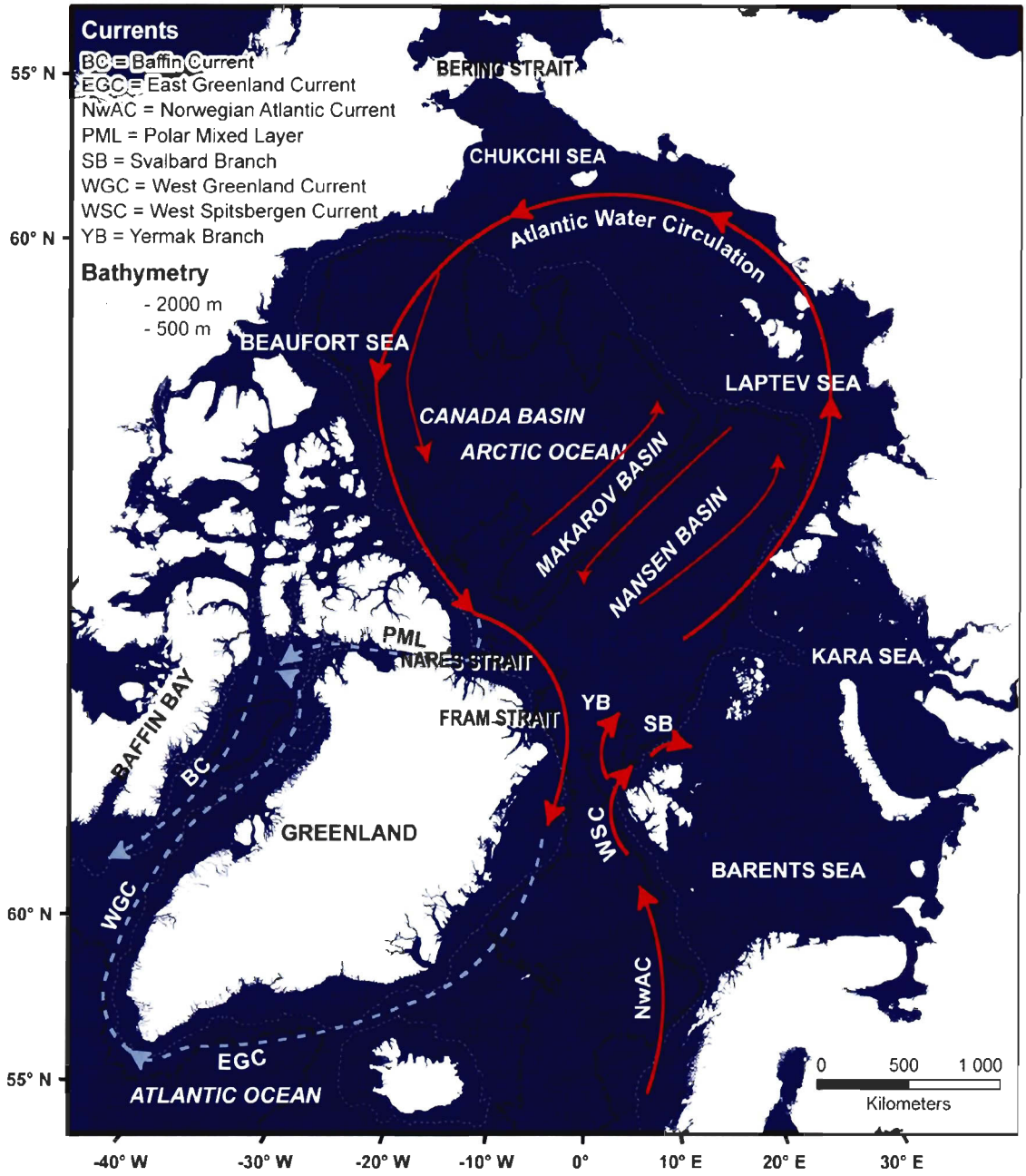

Figure 1. Map showing the major surface currents in the Arctic Ocean. The red arrows correspond to the Atlantic water inflow, which moves counter-clockwise, and the dashed blue arrows show the polar mixed layer (PML) exiting the Arctic Ocean through Fram and Nares straits.

1.3.2 Hydrographic parameters and water mass properties in Lancaster Sound

The CAA has numerous channels between islands. These channels connect the Arctic Ocean to the Atlantic Ocean across a vast continental shelf representing ~20% of the Arctic Ocean shelf area [*Melling,* 2000; *McLaughlin et al.,* 2004; *Michel et al.,* 2006]. The Northwest Passage, one of the main passages in this system, connects the western and eastern part of the Canadian Arctic through Dease, Victoria, and Barrow straits and through Lancaster Sound. All the channels of the CAA are seasonally covered by multiyear and first-year sea-ice, with freeze-up starting in September–October and melt beginning in May–June. Between freeze-up and minimum sea-ice cover, large areas are characterized by landfast ice. The SST is close to the freezing point of ~ –1.8°C during the period marked by sea-ice cover and ranges between –1.6 and +5°C in late August–September. The SSS is 32–33 in winter and ranges from 30–31 in the west to 32–33 in the east during summer [*Mudie and Rochon*, 2001; *Prinsenberg and Hamilton*, 2005].

The general water mass circulation in the CAA has an eastward component (Fig. 2) principally because of steric sea-level difference between the Pacific Ocean and the North Atlantic Ocean and to a strong Coriolis force. Although the CAA is considered to be a key area for freshwater flux from the Arctic Ocean to the North Atlantic, little is known about the water-mass properties and circulation in this area. *Jones et al.* [2003], using nitrate to phosphate ratios, have shown that all the water flowing under the PML (~100 m) in Lancaster Sound is of Pacific origin, with a SSS < 33.2. In contrast, *Prinsenberg and Hamilton* [2005] found that the bottom water is of Atlantic origin with SSS ranging between 33.7 and 34. At the study site 2004-804-009, the present sea-surface summer

temperature (SSTs) is 2°C with a sea-surface summer salinity (SSSs) of 31. Sea-ice cover extends for 8.5 months of the year.

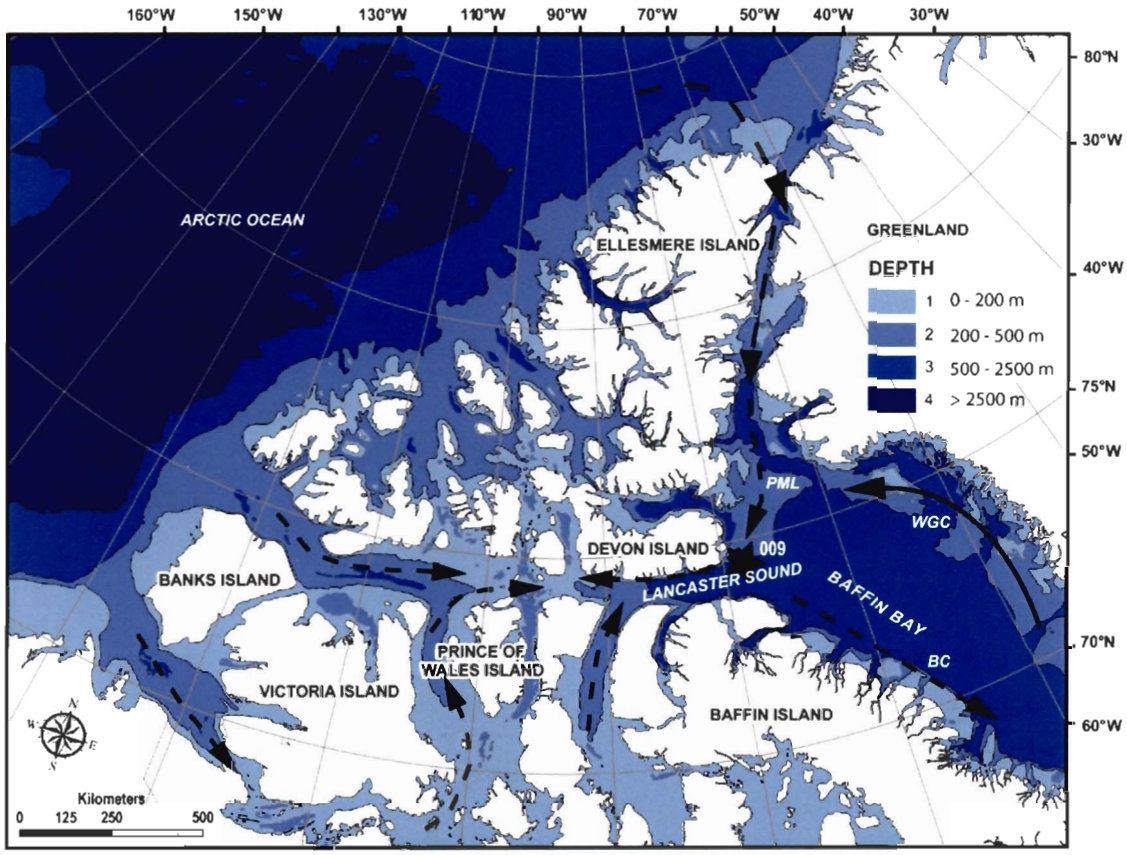

Figure 2. Location of the coring site at the entrance of the Lancaster Sound (black star) and major surface currents in the Canadian Arctic Archipelago (CAA). The circulation in the CAA has an eastward component. Dashed black arrows correspond to the polar mixed layer and solid black arrow corresponds to the Atlantic water. BC, Baffin Current; PML, polar mixed layer; WGC, West Greenland Current. (Modified from[*Rochon et al.* 2006]).

1.4 Material and methods

1.4.1 Sampling site and palynological preparation

Sampling in Lancaster Sound was carried out in the summer of 2004 during leg 9 of ArcticNet oceanographic campaign on board the Canadian Coast Guard Ship (CCGS) *Amundsen* [*Rochon and onboard participants,* 2004]. The sampling sites were selected

using a Simrad EM300 multibeam sonar allowing to avoid disturbed sediment areas (i.e., erosion, mud flows, and (or) mass movements). Core 2004-804-009 PC (74°11.2′N, 81°11.7′W, water depth 781 m, length 6 m) was collected using a piston corer. The sedimentary sequence was then subsampled every 10 cm for palynological analyses. Sequence 2004-804-009 BC (74°11.2′N, 81°11.7′W, water depth 781 m, length 35 cm) was collected using a box corer and subsampled every 5 cm for palynological analyses. Each subsample was then processed according to the standard palynological method described by *Rochon et al.* [1999]. Approximately 5 cm^3 of wet sediment was collected and put in a graduate cylinder filled with distilled water. A tablet of *Lycopodium clavatum* spores (University of Lund 1984, Batch N° 414831) of known concentration (12 100 ± 1892 spores per tablet) was added to each sample at the start of processing to permit the calculation of palynomorph concentration. Sieving was performed using Nitex sieves of 100 and 10 µm mesh to eliminate coarse sand, fine silt, and clay. The fraction between 10 and 100 µm was then preserved in a tube with a few drops of phenol for subsequent chemical treatments.

The chemical processing consists of repeated hot HCl and hot HF treatments to dissolve carbonate and silica particles, respectively. A final sieving at 10 µm was then performed to remove fine silt and clay. A drop of the remaining fraction was mounted in glycerine gel between slide and cover slide. Palynomorphs (dinocysts, pollen grains and spores, acritarchs, organic linings of benthic foraminifers, and chlorococcales) were systematically counted using an optical microscope (Nikon Eclipse 80 – I) with a magnification factor of 400x. A minimum of 300 dinocysts was counted in each sample to

obtain the best statistical representation. Dinocyst concentrations were evaluated using the marker grain method [*Matthews,* 1969] and expressed in terms of individuals per volume unit (cysts/cm^3). The nomenclature of dinocyst taxa used in this paper follows *Head et al.* [2001] and *Rochon et al.* [1999]. All the samples used in this study are stored in the palynological laboratory at the institut des sciences de la mer de Rimouski, Quebec (ISMER; collection number 179-1 to 200-D) and the cores are archived at the Bedford Institute of Oceanography (BIO) in Dartmouth, Nova Scotia.

1.4.2 Methodology for the reconstruction of sea-surface hydrographic parameters

Dinoflagellates are unicellular organisms found in marine and freshwater environments. About half of them are photosynthetic and these make up the largest group of eukaryotic algae aside from diatoms. During their life cycle, after the fusion of the gametes for sexual reproduction, some dinoflagellate taxa produce a highly resistant organic-walled cyst constituted by a polymer called dinosporine that is not affected by dissolution [*Kokinos et al.,* 1998].

Many studies on dinocyst assemblages in modern sediments have shown their close relationship with sea-surface parameters (see [*Marret and Zonneveld,* 2003 and *de Vernal and Marret,* 2007] for synthesis on the subject). In particular, it has been shown that annual thermal amplitude, salinity, and duration of sea-ice cover in high latitudes are determinant factors on the distribution of dinocysts taxa especially in the northern North Atlantic Ocean [*de Vernal et al.,* 1994, 1997, 2000; *Rochon et al.,* 1999], the Labrador Sea [*Rochon and de Vernal,* 1994], the Canadian Arctic Ocean, including the Beaufort Sea, the CAA, northern Baffin Bay and Hudson Bay [*Mudie and Rochon,* 2001; *Hamel et al.,* 2002; *Richerol et al.,*

2008a,b], the Laptev Sea [*Kunz-Pirrung,* 2001], and the Bering and Chukchi seas [*Radi et al.,* 2001]. The close relationship between the dinocyst assemblages in surface sediments and observed sea-surface conditions have been shown from databases that are regularly updated [*Rochon et al.,* 1999; *de Vernal et al.,* 2001, 2005a]. The reference dinocyst database used in this work results from palynological analyses performed on 1189 surface sediment samples. The samples are from the North Atlantic Ocean and adjacent seas, the Arctic Ocean and sub-arctic seas and the North Pacific Ocean and include 64 dinocyst taxa. The list of all taxa and corresponding abbreviations is presented in appendix 1. The modern hydrographical environmental parameters used for statistical analyses include SST and SSS compiled from a radius of 30 nautical miles around each reference site using the 2001 version of the World Ocean Atlas [*NODC*, 2001]. However, at some sites in the Arctic and sub-arctic seas, hydrographic data (especially salinity) are very scarce and the compilation of SST and SSS has been done from a 60 nautical miles radius. Sea-ice cover data were compiled at a 1° by 1° grid scale from the 1953-2000 AD dataset provided by the National Snow and Ice Data Center (*NSIDC*) in Boulder, Colorado. Sea-ice is expressed here as the number of months per year with >50% of sea-ice coverage. Of the 1189 sites, 584 are characterized by the occurrence of sea-ice during the 1953-2000 AD interval, which is used as the modern reference. In order to reconstruct sea-surface conditions, we used the modern analogue technique (MAT) as described by Guiot and *Goeury* [1996] with the software R following the procedure described by *de Vernal et al.* [2005a]. MAT has been applied to Holocene time series in Baffin Bay [*Levac et al.,* 2001; *Rochon et al.,* 2006], Chukchi Sea [*de Vernal et al.,* 2005b], Beaufort Sea [*Rochon et al.,* 2006], Laptev Sea [*Kunz-Pirrung et*

al., 2001], Barents Sea [*Voronina et al.,* 2001], Nares Strait [*Mudie et al.,* 2006], and the eastern part of the Canadian Arctic Ocean [*Mudie et al.,* 2005].

This method yields good results as indicated by coefficients of correlation >0.90 between estimated and instrumental hydrographic parameters. The degree of accuracy of the estimated reconstructions is obtained by the calculation of the standard deviation of the residual (estimated minus observed values); they are ±1.7°C and ±1.7 for SSTs and SSSs respectively, and ±1.1 months/year for the duration of sea-ice cover (see appendix 2).

1.4.3 Stable isotopes, grain-size analysis, and magnetic susceptibility

Organic carbon (C_{org}), nitrogen (N), and inorganic carbon (C_{inorg}) contents were measured using a Carlo–Erba elemental analyser at the Geochemistry and Geodynamics Research Center (GEOTOP), Montréal, Quebec. The procedure consists of taking a sediment sample aliquot that is dried, ground, and analyzed for its total carbon and nitrogen content. A second aliquot is acidified with HCl (1 N) to dissolve carbonates, washed, and analyzed for its N and residual C content, which is considered to represent only the C_{org} content. C_{inorg} is then calculated by the difference between the two measurements. The $CaCO_3$ content of each sample was determined from the molar weight of $CaCO_3$ (100 g) and its content in C_{org} (12 g) allowing calculating the calcium carbonate equivalent.

Grain-size analysis was performed at the Institut des sciences de le mer de Rimouski (ISMER), Quebec, using a Beckman Coulter LS 13320 laser diffraction grain-size analyser. The software Gradistat [*Blott and Pye,* 2001] was used to derive the grain-size distribution and statistical parameters (mean, standard deviation). The whole core volumetric magnetic

susceptibility of the sediments was determined at 1 cm intervals using a GEOTEK multisensor core logger (MSCL) on board the CCGS *Amundsen*.

1.4.4 Chronostratigraphy of the sedimentary sequence

A constant-rate supply ^{210}Pb model [*Appleby and Oldfield,* 1983] was used to estimate ages and to determine sedimentation rates in core 2004-804-009 BC (Fig. 3).

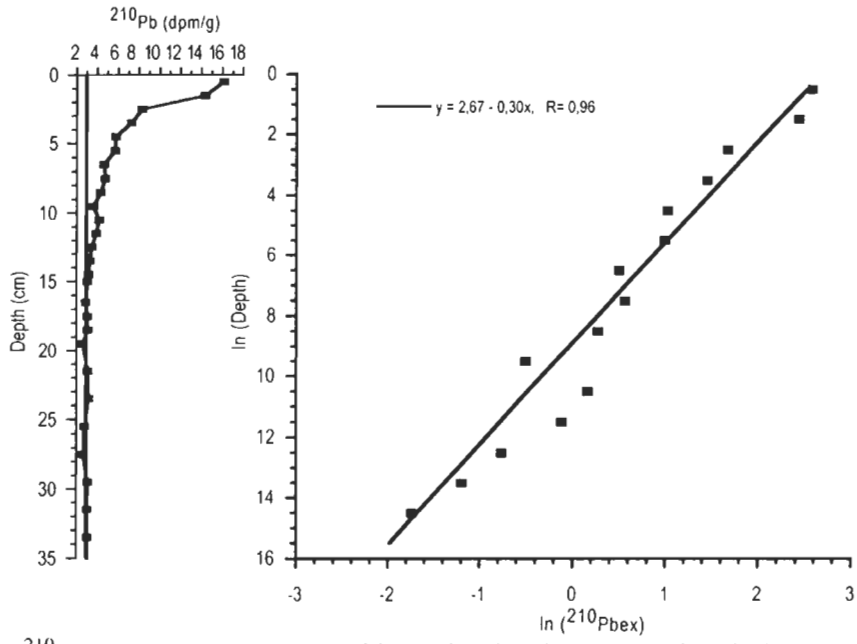

Figure 3. (a) ^{210}Pb activity in core 2004-804-009 BC. The vertical black line (asymptote = 3) corresponds to supported ^{210}Pb. (b) Neperian logarithm of the excess ^{210}Pb, which is used for estimating sedimentation rates.

The data indicate negligible biological mixing at the top of the sequence and the ^{210}Pb excess in the upper 15 cm of the core suggests an average sedimentation rate of ~60 cm/ka. Assuming constant sediment accumulation rate from the top to the base of the core, the sequence would cover approximately the last 580 years, from ~1420 AD at the base to the beginning of the present decade at the top.

The chronostratigraphy of the core 2004-804-009 PC (Table 1) was established using accelerator mass spectrometry (AMS) ^{14}C measurements on pelecypod shell fragments and foraminifera. We obtained four radiocarbon ages, from which calibrated years have been

Table 1. Radiocarbon ages used to develop age-depth model for core 2004-804-009 PC

Depth (cm)	Material dated	Laboratory numbers	Conventional radiocarbon ages (years BP)[a]	Calibrated ages (cal years BP)[b]
217-220	Mixed benthic foraminifers	Ugams# - 02317	6370±30	6376
317	Bivalve fragment shells	Beta-203496	8490±40	8543
525	Bivalve fragment shells	Beta-203498	9770±50	10240
571-572	Mixed benthic foraminifers	Ugams# - 02318	10 480±40	11060

[a]This column lists the AMS ^{14}C ages as reported from the laboratory after normalization for a $\delta^{13}C$ value of –25‰.

[b]Calibrated ages were estimated using the software Calib version 5.0.2 [*Stuiver et al.*, 2005] with ΔR local reservoir effect of 400 years, which means a total correction of 800 years to account for the air–sea reservoir difference. The calibrated ages are computed from the arithmetic average of the calibrated age range based on two standard deviations (i.e., a confidence interval of 95%).

calculated using the Calib version 5.0.2 software [*Stuiver et al.*, 2005] to calculate sedimentation rates and construct an age model. A reservoir (400 years) and the local marine reservoir (regional) ΔR of 400 years (i.e., correction total of 800 years) have been applied for the regional air–sea $^{14}CO_2$ in the Canadian Arctic Ocean [*Mangerud and Gulliksen*, 1975; *Blake*, 1987]. We applied a linear interpolation to construct an age model indicating that core 2004-804-009 PC spans about 11 000 – 2000 cal years BP with sedimentation rate ranging from 122 cm/ka in the middle part of the core to minimum possible values of 34 cm/ka in the upper part of the core (Fig. 4). Based on these

sedimentation rates and the sampling intervals of 10 cm, we calculated that time resolution of the analyses we made ranges between 80 and 220 years.

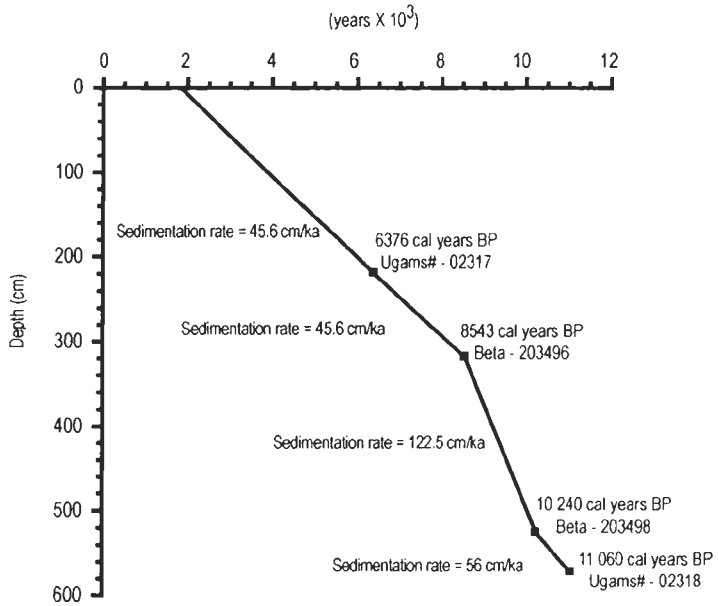

Figure 4. Age versus depth relationship in core 2004-804-009 PC according to accelerator mass spectrometry (AMS) ^{14}C ages on bivalve shells or mixed benthic foraminifers (see Table 1). The age model is based on a linear interpolation between the ages. It suggests variable sedimentation rates ranging from 45 to 122 cm/ka.

1.5 Results

1.5.1 Sediment description, grain size, geochemical and magnetic properties

Core 2004-804-009 PC consists of a uniform olive-coloured silty clay throughout its entire length with few mottles generally between 3 and 10 cm in size and especially abundant between 250 and 280 cm. Grain-size analysis (Fig. 5) shows predominant silt and clay in most of the core. Only the base of the sedimentary sequence, between 600 and 560 cm, records a high percentage of sand (~50%) and coarse silt. Geochemical analyses indicate that the C_{org} content ranges from 0.34% to 2.12%, averaging 1.24%, with values increasing gradually from the base to the top of the core. $\delta^{13}C$ values range from –26‰ at

the base of the core to –22.5‰ at the top of the core, whereas total carbon gradually decreases from 6% to ~3% towards the top. The C/N ratio shows values ranging from 29.8 at the base of the core to 10.8 at the top. Finally, $CaCO_3$ records higher values at the base of core (~46%), which gradually decrease (~10%) at the top of the core, as does magnetic susceptibility. Sedimentary sequence 2004-804-009 BC consists of a uniform olive-coloured silty clay with dominant silt and clay comprising ~75% and 25% of the sediment, respectively. Stable isotopes analyses indicate relatively constant values along the core with C_{org} content of 2.3%, carbon total of 3%, and $\delta^{13}C$ values of –21.5‰. The C/N ratio is ~11, whereas the $CaCO_3$ content records values of 5%.

1.5.2 Dinocyst assemblages and quantitative reconstruction of sea-surface conditions

Palynomorphs or organic-walled microfossils are abundant throughout the core 2004-804-009 PC except in the lowermost 40 cm where they are absent (Fig. 6). The most abundant palynomorphs are dinocysts, with concentrations ranging from 1766 at the base of the sequence to 15231 cysts/cm^3 (average 8500 cysts/cm^3) between 460 and 400 cm (~ 10 000 to 9500 cal years BP). Dinocyst assemblages reveal low species diversity consistent with previous work in the Canadian Arctic Ocean [*Mudie and Rochon,* 2001]. Indeed, 90% of the assemblages are dominated by four taxa: *Islandinium minutum*, *Brigantedinium* spp., *Spiniferites elongatus/frigidus*, and *Operculodinium centrocarpum*. The ratio of phototrophic to heterotrophic dinocyst taxa (gonyaulacales (G) / peridiniales (P), G/P ratio) records low values in most of the sedimentary sequence, indicating the dominance of non-photosynthetic taxa except between 280 and 100 cm (from ca. 7920 to >3780 cal years BP)

where it reaches values ≥1 indicating an increase in the relative abundance of phototrophic taxa.

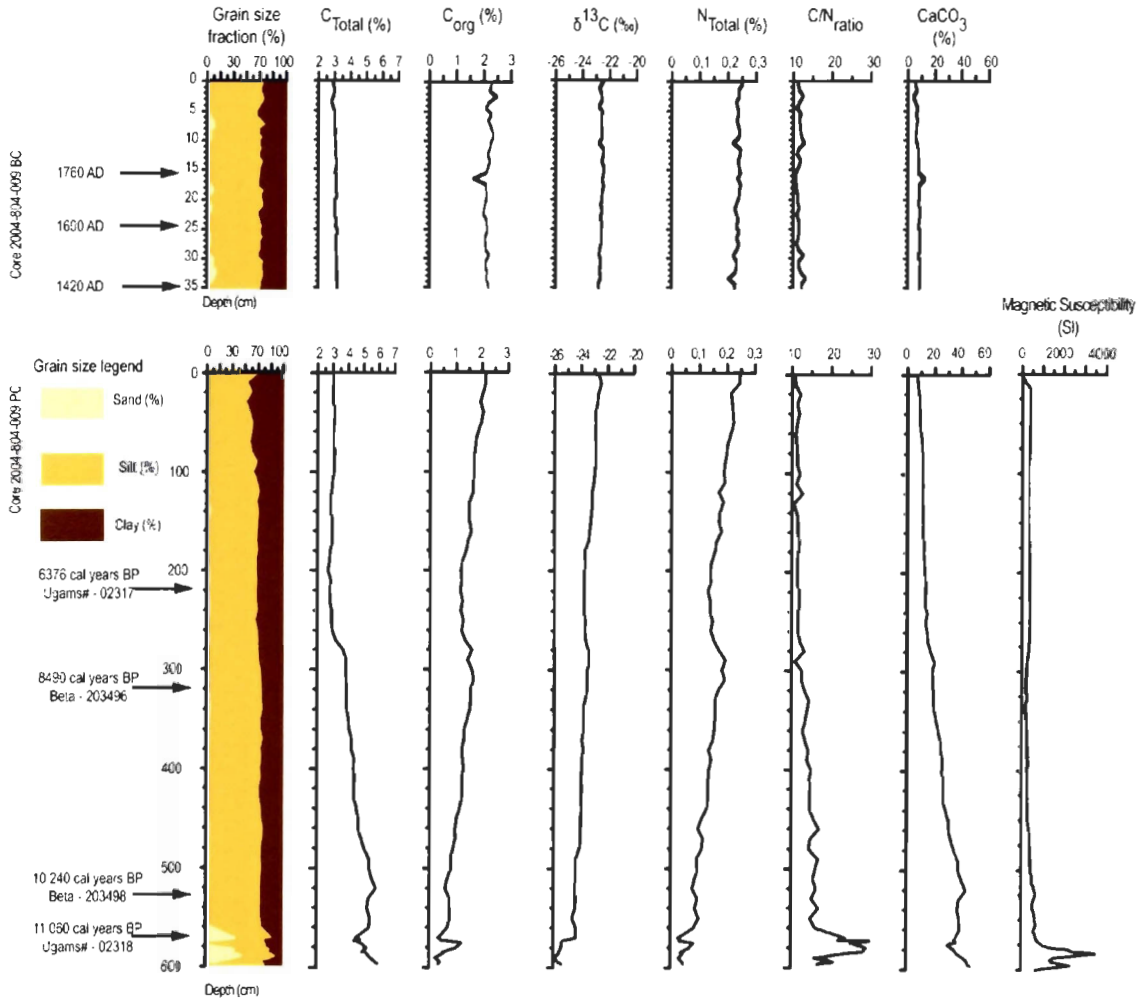

Figure 5. Sedimentological (grain size) and geochemical (stable isotopes) content of cores 2004-804-009 BC and 2004-804-009 PC. The chronology of core 2004-804-009 BC is estimated from ^{210}Pb measurements and expressed in years AD (Fig. 3). The chronology of core 2004-804-009 PC is estimated from accelerator mass spectrometry (AMS) ^{14}C dates on mollusc shells and mixed benthic foraminifers. It is expressed in calibrated years BP (Fig. 4).

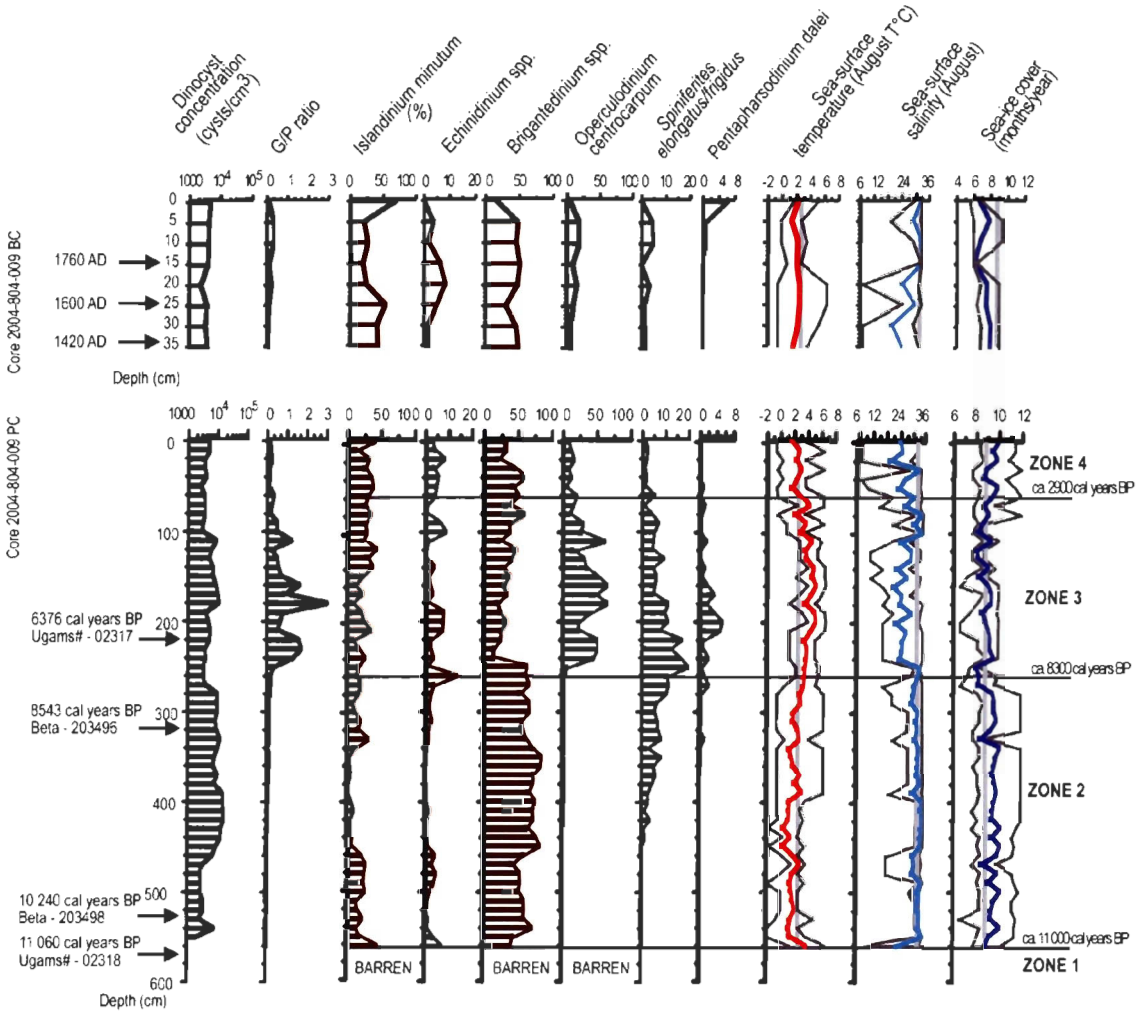

Figure 6. Dinocyst concentration, Gonyaulacales/Peridiniales (G/P ratio), relative abundance of dinocyst taxa, and quantitative estimates of sea-surface conditions based on MAT applied to dinocyst assemblages in cores 2004-804-009 BC and 2004-8004-009 PC. The red, blue and purple lines correspond to the best estimates for the summer temperature and salinity (August) and the duration of sea-ice cover, respectively. The thin black lines correspond to the minimum and maximum values possible according to the set of five analogues. The vertical gray lines indicate the values (means) of modern sea-surface conditions. The chronology of core 2004-804-009 BC is estimated from ^{210}Pb measurements and expressed in years AD (Fig. 3). The chronology of core 2004-804-009 PC is estimated from accelerator mass spectrometry (AMS) ^{14}C dates on mollusc shells and mixed benthic foraminifers. It is expressed in calibrated years BP (Fig. 4).

Palynological analyses show four different zones based on the relative abundance of dinocysts. The first zone, between 600 and 560 cm (from 12 180 to 11 000 cal years BP), is characterized by the absence of dinocyst and other palynomorphs. The second zone, between 560 and 260 cm (from ~11 000 to 7500 cal years BP), is dominated by the heterotrophic taxa *Brigantedinium* spp. (70%) and *I. minutum* (30%). The third zone, between 260 and 60 cm (from ca. 7500 to > 2900 cal years BP), is characterized by an increase in the relative abundance of phototrophic taxa *O. centrocarpum* (50%), *S. elongatus/frigidus* (25%), and *Pentapharsodinium dalei* (5%). Finally, the fourth zone, from 60 cm to the core top, is again dominated by the heterotrophic taxa *Brigantedinium* spp. and *I. minutum*.

The quantitative estimates of past sea-surface conditions reveal important hydrological changes during the Holocene in Lancaster Sound. In zone 2, the application of MAT suggests low summer temperatures of 0 °C on the average, which is ~2°C colder than modern, at least in the lowest part of the zone. This interval is also marked by sea-ice cover of 10 months/year, which is ~1 month/year more than at present. Little or no difference in summer salinity as compared with modern values is suggested by the MAT analysis. Zone 3 is marked by summer temperatures of ~3–4°C, which is slightly warmer than modern values, but with surface salinities of ~25, which is lower than at present. Finally, zone 4 marks the establishment of conditions similar to present.

Core 2004-804-009 BC also shows well-preserved dinocyst assemblages with concentrations ranging from 2220 to 4532 cysts/cm^3 (average 3623 cysts/cm^3). The G/P ratio records low value (>1) indicating the dominance of heterotrophic taxa, mainly

Brigantedinium spp. (40%) and *I. minutum* (40%), whereas phototrophic taxa are represented by *O. centrocarpum* (~15%) and *S. elongatus/frigidus* (~5%). From 25 to 15 cm (~1600 – ~1760 AD), dinocyst assemblages are dominated by the heterotrophic taxa *Brigantedinium* spp. and *Echinidinium* spp. (~50% and ~10%, respectively), whereas the relative abundance of *I. minutum* records a sharp decrease (from ~50% to ~25%). During this interval, phototrophic taxa are mainly represented by *O. centrocarpum* (~10%). These assemblages indicate SST close to modern values, whereas the trend suggests sea-ice cover decrease of ~8–6 months/year accompanied by increased salinity in the upper part of the core spanning the last centuries.

1.6 Discussion

1.6.1 Glaciological instability of the Laurentide-Innuitian ice sheet during the Late Pleistocene

Our palynological, grain-size, geochemical, and magnetic property data provide information on both the past sea-surface conditions and on the changing depositional environment in Lancaster Sound. Between 600 and 560 cm (from 12 180 to 11 000 cal years BP), carbonate content, $CaCO_3$ (detrital), C/N ratio, and magnetic susceptibility are high, whereas C_{org} and $\delta^{13}C$ are low and palynomorph are absent, suggesting an erosive dynamics with high terrigenous inputs. This could have enhanced reduction of the euphotic zone, preventing biological activity in the surface layer. The paleolimnological record of diatoms from Prescott Island (Lake PW03) in the central Canadian Arctic Ocean has shown that diatoms were absent prior to 11 000 cal years BP, but high values of carbon content and magnetic susceptibility were probably owing to high energy glacial outwash

[*Finkelstein and Gajewski,* 2007]. *Bauch et al.* [2001] found high ice-rafted debris (IRD) accumulation in cores from the Greenland-Iceland-Norwegian seas (GIN seas) between 12 000 and 13 000 cal years BP. Similarly, *Scott et al.* [2009] observed an IRD-rich layer at ~12 600 cal years BP in a core from the Amundsen Gulf that is linked to a glaciological instability in this area. Previous work in a fjord from eastern Baffin Island [*Andrews et al.,* 1996] revealed an abrupt increase in detrital carbonate ~12 400 cal years BP related to an ice readvance. A multiproxy study of paleoceanographic and climatic changes in northernmost Baffin Bay [*Knudsen et al.,* 2008] indicates an extensive seasonal sea-ice cover between 12 300 and 11 300 cal years BP. We thus interpret the high percentages of sand and detrital $CaCO_3$ and the peak of magnetic susceptibility as the result of the last stage of the Laurentide–Innuitian ice sheet readvance. The high percentages of detrital $CaCO_3$ at the base of core 2004-804-009 PC might be related to glacial erosion of Paleozoic carbonates from Devon Island [*Bischof and Darby,* 1999] prior to 11 ka.

1.6.2 Holocene large-scale climatic changes: a possible link to the Arctic oscillation at the millennial time scale

The occurrence of dinocysts at 560 cm (ca. 11 000 cal years BP), the increase in C_{org} content, and the decrease in both the C/N ratio and $CaCO_3$ content marks the beginning of biological production in surface waters and hemipelagic sedimentation. It corresponds to the lower part of zone 2 where quantitative reconstructions show cold conditions with low summer temperature (~2°C) and extensive sea-ice cover (close to 10 months/year). These conditions prevailed until ca. 9300 cal years BP when milder conditions prevailed, as suggested by the first occurrence of the phototrophic taxon *S. elongatus/frigidus*. This

warming trend seems to be consistent with the final decay of the Laurentide and Innuitian ice sheets recorded ~10 ka on Devon Island near our sampling site [*England et al.,* 2006]. It also corresponds to the retreat of the Greenland–Ellesmere ice-sheet ~10 ka, which unblocked the Nares Strait, allowing a connection between the Arctic Ocean and the North Atlantic Ocean [*Zreda et al.,* 1999]. Furthermore, recent works based on multiproxy approaches on marine and lake cores [*Lloyd et al.,* 2005; *Andresen et al.,* 2007] from central west and south Greenland indicate colder conditions before 9400 cal years BP followed by a trend towards warmer conditions linked to the gradual strengthening of the relatively warm West Greenland Current. Thus, the extremely cold sea-surface conditions recorded in the lowest part of zone 2 could be due to limited exchange between the Canadian Arctic channels and the North Atlantic Ocean, whereas the trend towards warmer conditions could be the result of the penetration of Atlantic waters in the Canadian Arctic Ocean. The noticeable increase in phototrophic taxa, in particular *S. elongatus/frigidus* at the transition between zones 2 and 3 ~8300 cal years BP, which corresponds to a gradual increase in SST, suggests an increase of exchanges between Arctic and North Atlantic consistent with the findings in the previously mentioned studies. Maximum SSTs are reached in zone 3 around 6 ka when the phototrophic taxa *O. centrocarpum* and *P. dalei* record their maximum abundance, probably as a result of a persistent inflow of warm Atlantic water since 8300 cal years BP. *Duplessy et al.* [2001, 2005], *Hillaire-Marcel et al.* [2004], and *de Vernal et al.* [2005b] have suggested, on the basis of $\delta^{18}O$ data on mesopelagic and benthic foraminifers, a maximum inflow rate of Atlantic water into the Arctic during the early mid-Holocene ~8 ka. Dinocyst assemblages from the Laptev Sea

also suggest an increased contribution of North Atlantic water during the early Holocene [*Polyakova et al.,* 2005]. *Gajewski* [1995] and *Gajewski and Frappier* [2001] found that during this interval pollen concentrations were higher in lakes on Prince of Wales and Somerset islands, suggesting warmer conditions. Therefore, our record of zone 3 seems to be related to a large-scale atmospheric and oceanic reorganization following the last phase of deglaciation in the Arctic and subarctic areas, probably leading to early mid-Holocene thermal maximum as also recorded in Baffin Bay [*Levac et al.,* 2001; *Rochon et al.,* 2006] and West Greenland [*Kaufman et al.,* 2004]. Recently *Vinther et al.* [2009] found an early Holocene climatic optimum with similar millennial-scale evolution east and northwest of the Greeenland ice-sheet based on $\delta^{18}O$ in ice cores from Greenland ice-sheet and adjacent ice caps. This suggests a common climatic forcing in the eastern Arctic during the early-middle Holocene, which could be associated with regional change in solar insolation. However, studies based on lake pollen records in cores from southwest Greenland and eastern Baffin Bay indicate a strong regionalism in climate with a marked east-west gradient [*Fréchette and de Vernal,* 2009]. Dinocyst records from the Reykjanes Ridge and the Faroe-Shetland Channel also suggest contrasted sea-surface climatic trends between the two sites [*Solignac et al.,* 2008]. Therefore, it is possible that change in regional insolation could have triggered some climatic shifts but that large-scale oceanic and atmospheric circulation pattern changes have modulated the amplitude of these shifts.

Under modern climate conditions, the maximum advection of warm Atlantic water to the Arctic corresponds to a positive phase of the AO. This is accompanied by more cyclonic conditions and a doubling of divergence in the eastern Arctic due to Ekman

transport [*Rigor et al.,* 2002]. Strong divergence enhances both more open water and thinner ice but also the upwelling of Atlantic waters, resulting in a positive SST anomaly. During this time, the Beaufort Gyre is weakened, leading to a decrease of freshwater through the CAA [*Proshutinsky et al.,* 2002]. Based on the mineralogy of silt–sand grains in western Arctic cores, *Darby and Bischof* [2004] have suggested a sea-ice drift pattern analogous to the impact of the AO throughout the Holocene. Our zone 3 with maximum SSTs and a trend towards increasing SSS (less freshwater) seems consistent with the impact of positive AO, whereas the decreasing summer temperatures as well as the trend towards reduced salinity in zone 4 could be the result of a shift to negative AO. A trend of decreasing temperature and less advection of Atlantic waters in the Arctic during the late Holocene has been inferred from dinocyst assemblages [*Levac et al.,* 2001], alkenone data [*Calvo et al.,* 2002], faunal and oxygen isotope records of planktonic foraminifera [*Bauch et al.,* 2001], benthic foraminifera [*Ślubowska-Woldengen et al.,* 2007], diatom assemblages [*Wolfe,* 2003], and lake pollen assemblages [*Zabenskie and Gajewski,* 2007]. These data suggest that the neoglacial cooling during the late Holocene could be linked to a shift in the AO at the millennial time scale. Therefore, our records suggest that large-scale atmospheric patterns could have triggered a relatively strong climatic variability over most of the Holocene at least at the millennial time scale.

1.6.3 Historical changes

The most important feature recorded in core 2004-804009 BC is the marked decrease in the relative abundance of the heterotrophic taxon *I. minutum* (from ~50% to ~25%) between 25 and 15 cm (from ~1600 to ~1760 AD) and the limited abundance of

phototropic taxa mainly represented by *O. centrocarpum* (~10%). In contrast, during this interval the relative abundance of the heterotrophic taxa *Brigantedinium* spp. and *Echinidinium* spp. is relatively high (~50% and ~10%, respectively). These are accompanied by a trend towards decreasing sea-ice cover. Based on dinocyst assemblages in Beaufort Sea, *Richerol et al.* [2008b] observed a warming trend between 1400 and 1850 AD.

1.7 Summary and conclusion

Dinocyst assemblages and quantitative reconstructions of sea-surface conditions in the eastern Arctic (Lancaster Sound) reveal climatic changes during the late Pleistocene and the Holocene. Between ~12 180 and 11 000 cal years BP, our records suggest glaciomarine sedimentation with detrital $CaCO_3$ probably originating from the glacial erosion of Devon Island Paleozoic carbonates, which we interpret as the result of the last phase of the Laurentide–Innuitian ice sheet readvance as recorded in eastern Baffin Island [*Andrews et al.,* 1996]. From ~11 000 to 9600 cal years BP, harsh conditions prevailed in Lancaster Sound, suggesting limited connections between the Arctic Ocean and the North Atlantic Ocean, probably due to the presence of the Ellesmere–Greenland ice sheet blocking the Nares Strait until ca. 10 ka [*Zreda et al.,* 1999]. After 9600 cal years BP, a trend toward warmer conditions is recorded, which we associate with a gradual increased of water exchange between the Arctic and the North Atlantic basins resulting in a maximum inflow of Atlantic water. Maximum SSTs were reached ~6 ka, which would constitute the regional thermal optimum of the Holocene. Relatively warm conditions prevailed until the late Holocene, which was marked by a cooling towards conditions similar to present. Such

climatic changes have been also shown in Canadian Arctic lake pollen and diatom records, illustrating linkages between marine and continental climates. In particular, it seems to confirm variability in the meridional advection of atmospheric and oceanic heat flux from the North Atlantic Ocean similar to the effect of the AO.

1.8 Acknowledgements

This work was funded by the ArcticNet Networks of Centres of Excellence and the Natural Sciences and Engineering Research Council (NSERC) of Canada. This is a contribution to the ArcticNet project 1.6, the Polar Climate Stability Network supported by the Canadian Foundation for Climate and Atmospheric Science, and the NSERC International Polar Year project, "Natural climate variability and forcings in Canadian Arctic and Arctic Ocean". We wish to thank the officers and crew of the CCGS *Amundsen* for their help and support during sampling. We also wish to express our gratitude to the following people who helped during the collection and analyse of the samples: Robbie Bennett, Bedford Institute of Oceanography; Trecia Schell, Dalhousie University; and Pierre Simard, Université du Québec à Rimouski. Thanks are due to Bassam Ghaleb and Jean-François Hélie (GEOTOP at UQAM) for geochemical and isotope analyses. We are grateful to the two reviewers, Alwynne B. Beaudoin (Archeological Survey, Provincial Museum of Alberta) and Svend Funder (Geological Museum, University of Copenhagen) for their comments, which helped to improve the manuscript.

CHAPITRE 2

HOLOCENE PALEOCEANOGRAPHY OF THE NORTHWEST PASSAGE, CANADIAN ARCTIC ARCHIPELAGO: THE POSSIBLE ONSET OF AN ARCTIC OSCILLATION CLIMATE MODE

2.1 Abstract/Résumé

Dinoflagellate cyst assemblages, stable isotopes and physical properties were used to assess oceanographic changes during the Holocene from four sediment cores collected in the easternmost and central part of the main axis of the Northwest Passage (cores 2004-804-009 PC/BC, 74°11.2'N/81°11.7'W and cores 2005-804-004 PC/BC, 74°16.1'N/ 91° 05.4'W and 74°16.1N/ 91°4.4'W). The chronology is based on a composite record including calibrated AMS-^{14}C dates and correlation between paleomagnetic secular variations of the geomagnetic field (PSV) and a predicted spherical harmonic model of the geomagnetic field (CALS7K.2). Based on this composite chronology, a new age model to that of *Ledu et al.* [2008] has been constructed for core 009 PC. It suggests that core 009 PC spans the last 11.1 cal. kyr BP with sedimentation rates ranging from 43 to 140 cm/kyr whereas those of core 004 PC indicates sedimentation rates from 15 to 118 cm/kyr over the last 10.8 cal. kyr BP. High terrigenous inputs characterize the interval from 11.1 to 10.8 cal. kyr BP in core 009 PC and 10.8 to 8.5 cal. kyr BP in core 004 PC. We associate the terrigenous input to meltwater outwash deposition during the last Innuitian deglaciation, which was delayed in the central part of the main axis of the Northwest Passage due to maximum ice thickness. Dinocyst assemblages suggest important changes in sea-surface conditions. From 10.8 to 9 cal. kyr BP, core 009 records relatively harsh conditions with summer (August) temperatures 2°C cooler than at present, which are associated with both the presence of active ice-stream in the northernmost Baffin Bay and a weak West Greenland Current. From 8.5 cal. kyr BP to the late Holocene, the two sites show opposite trends, which are marked by warming up to 3°C higher than present in core 009 PC and by a cooling of 3°C in core 004 PC with respect to modern conditions. This is accompanied by a gradual increase in the relative abundance of phototrophic taxa in core 009 PC. These climatic conditions prevailed until 5.5 cal. kyr BP, where a reverse trend is recorded until the late Holocene, with a gradual cooling in core 009 PC and milder conditions in core 004 PC. Climate variability between 8.5 to 5.5 cal. kyr BP, could be the results of large-scale atmospheric pattern such as the Arctic Oscillation in its positive mode, whereas a shift in the AO mode (from AO^+ to AO^-) could characterized climate conditions after 5.5 cal. kyr BP. Comparison of terrestrial ice core $\delta^{18}O$ record from Devon Island Ice Cap and the reconstructed sea-surface temperature from core 009 suggests a strong atmospheric-oceanic coupling throughout the Holocene in this area.

Les assemblages de kystes de dinoflagellés, les isotopes stables ainsi que les propriétés

physiques de quatre carottes sédimentaires échantillonnées au niveau de l'extrémité orientale et de la partie centrale de l'axe principal du passage du Nord-Ouest ont été utilisés afin de documenter les changements océanographiques au cours de l'Holocène (carottes 2004-804-009 PC/BC, 74°11.2'N/81°11.7'W et carottes 2005-804-004 PC/BC, 74° 16.1'N/ 91° 05.4'W et 74°16.1N/ 91°4.4'W). La chronologie des carottes sédimentaires est basée sur un enregistrement composite incluant des âges radiocarbones calibrés et des corrélations entre les variations séculaires du champ géomagnétique terrestre et un modèle du champ géomagnétique basé sur des harmoniques sphériques (CALS7K.2). À partir de ces enregistrements composites, une nouvelle chronologie basée sur celle développée dans *Ledu et al.* [2008] a été construite pour la carotte 009 PC. Les modèles d'âges suggèrent que la carotte 009 couvre les derniers 11,1 ka calibrées avec des taux de sédimentation compris entre 43 et 140 cm/ka tandis que la carotte 004 PC couvrent les derniers 10,8 ka calibrées avec des taux de sédimentation compris entre 15 et 118 cm/ka. Des apports terrigènes importants caractérisent l'intervalle entre 11,1 et 10,8 ka calibrées dans la carotte 009 PC et l'intervalle entre 10,8 et 8,5 ka calibrées dans la carotte 004 PC. Nous associons ces apports terrigènes à une débâcle d'eau de fonte lors de la dernière déglaciation innuitienne, qui dans la partie centrale de l'axe principal du passage du Nord-Ouest a été retardée en raison d'un maximum d'épaisseur de glace. Les assemblages de dinokystes suggèrent des changements importants au niveau des conditions de surface. Durant l'intervalle entre 10,8 et 9 ka calibrées, la carotte 009 enregistre des conditions sévères marquées par des températures d'été (août) de 2°C inférieures aux conditions modernes et qui sont associées à la présence d'un courant de glace actif au niveau de l'extrémité nord de la baie de Baffin, mais aussi à une influence réduite du courant Ouest Groenlandais. L'intervalle compris entre 8,5 ka calibrées et l'Holocène récent se caractérise par des tendances opposées entre les deux sites avec, dans la carotte 009 PC, un réchauffement de plus de 3°C comparé aux conditions présentes, et un refroidissement de 3°C comparé aux conditions modernes dans la carotte 004 PC. Dans la carotte 009 PC, ce réchauffement est accompagné d'une augmentation graduelle de l'abondance relative des taxons phototrophes. Ces conditions climatiques ont persisté jusqu'à 5,5 ka calibrées, où, une tendance inverse, avec un refroidissement graduel dans la carotte 009 PC et des conditions plus chaudes dans la carotte 004 PC, est enregistrée jusqu'à l'Holocène récent. La variabilité climatique entre 8,5 et 5,5 ka calibrées pourrait être liée à des patrons atmosphériques de grande échelle tels que l'oscillation arctique dans son mode positif, tandis qu'un changement de phase de l'OA (OA^+ vers OA^-) pourrait caractériser les conditions climatiques après 5,5 ka calibrées. La comparaison des données de $\delta^{18}O$ d'une carotte de glace prélevée dans le glacier de l'île de Devon et de la température de surface reconstituée de la carotte 009 PC suggère un fort couplage atmosphère-océan durant tout l'Holocène dans cette région.

2.2 Introduction

Several recent studies have documented important hydrographic changes in the Arctic Ocean over the past three decades. Satellite data since 1978 show that the annual average Arctic sea-ice extent has decreased by 2.7% per decade, with larger decrease of 7.4% per decade in summer [*IPCC*, 2007]. A minimum in the Arctic sea-ice extent and area was reached in September 2007, which is ~38% less than the historical climatological average [*Comiso et al.,* 2008]. The decrease of the ice extent was accompanied by a strong thinning of the halocline [*Steele and Boyd,* 1998] and warming of the Atlantic layer, which lies at 200-800 m depth [*Polyakov et al,* 2004]. Most of these changes have been attributed to the impact of the Arctic oscillation (AO), a seesaw pattern of atmospheric mass between the polar regions (Iceland) and mid-latitudes (Azores) and whose index is defined as the leading empirical orthogonal function (EOF) mode of the Northern Hemisphere sea-level pressure (SLP) [*Thompson and Wallace,* 1998]. The AO exerts a dominant role in the wind strength and direction, thus modulating both the location of the transpolar drift (TPD) and the extent of the anticyclonic Beaufort Gyre (BG) [*Proshutinsky et al.,* 2002]. These in turn, affect the sea-ice motion and thickness enhancing changes of both the freshwater circulation pattern and budget in the Arctic Ocean [*Rigor et al.,* 2002]. Atmospheric and oceanic variability in the Arctic on seasonal, interannual and decadal time scale associated with the AO are relatively well established [*Proshuntisky and Johnson,* 1997; *Johnson et al.,* 1999; *Polyakov and Johnson,* 2000; *Venegas and Mysak,* 2000; *Dukhovskoy et al.,* 2004; *Polyakov et al.,* 2004]. Longer time series records are required to better understand the natural climate variability in the Arctic Ocean at centennial to millennial time scale.

Understanding these lower frequencies may be important for predicting future climate changes. Based on marine records, terrestrial data and model experiments, it has been shown that the early Holocene was warmer in the eastern than in the western part of the Arctic Ocean, whereas the late Holocene was marked by the reverse trend [*Vavrus and Harrison,* 2003; *Kaufman et al.,* 2004; *Fischer et al.*, 2006; *Rochon et al.*, 2006; *de Vernal et al.,* 2008; *de Vernal,* 2009], suggesting a longitudinal thermal gradient. In modern conditions a shift of the AO index (from AO^+ to AO^-) creates such sea-ice dipole patterns.

The Canadian Arctic Archipelago (CAA), which represents ~20% of the total shelf area in the Arctic [*Jakobsson,* 2002, 2004] is ideally located to better understand the nature of this thermal gradient because it connects the western and the eastern part of the Arctic Ocean. Moreover, relatively high biogenic flux allows the use of well–preserved biological proxies for the reconstructions of past sea-surface conditions. Holocene climate reconstructions in the CAA have been mostly inferred from paleolimnological data based on chironomidae [*Gajewski et al.,* 2005; *Rolland et al.,* 2008], diatoms [*Finkelstein and Gajewski*, 2007, 2008; *Podritske and Gajewski*, 2007], pollen [*Zabenskie and Gajewski*, 2007] and varved sediments [*Besonen et al.,* 2008]. Qualitative Holocene sea-ice history was also reconstructed based on bowhead bone remains [*Savelle et al.,* 2000; *Dyke and England*, 2003] and driftwoods [*Dyke et al.,* 1997]. Quantitative sea-surface reconstructions are available at the westernmost [*Rochon et al.*, 2006; *Schell et al.,* 2008] easternmost [*Rochon et al.,* 2006; *Ledu et al.,* 2008] and central part [*Ledu et al.,* 2007, 2008; *Vare et al.,* 2009] of the main axis of the Northwest Passage. Poor preservation of biogenic calcium carbonate and biogenic silica in Arctic marine sediments make difficult to use foraminifers

and diatoms to reconstruct sea-surface conditions. In contrast organic-walled microfossils or palynomorphs, in particular the cyst of dinoflagellates (or dinocysts) are composed of highly resistant polymer called dinosporine [*Kokinos et al.*, 1998] and are well preserved in the sediments, allowing their use for the reconstruction of sea-surface parameters.

In order to better understand the nature of the thermal gradient and the natural climate variability in the Arctic during the Holocene, we have collected marine sediment cores during two ArcticNet oceanographic campaigns aboard CCGS *Amundsen* ice breaker in the summer of 2004 in Lancaster Sound (cores 2004-804-009 PC and 2004-804-009 BC) and in the summer of 2005 in Barrow Strait (cores 2005-804-004 PC and 2005-804-004 BC) at the easternmost and central part of the main axis of the Northwest Passage, respectively. These cores show well-preserved dinocyst assemblages, which were used in conjunction with the modern analogue technique (MAT) to reconstruct summer (August) sea-surface temperature (SSTs) and salinity (SSSs) as well as the duration of sea-ice cover over the Holocene.

2.3 Environmental settings

2.3.1 General water mass distribution and major currents in the Arctic Ocean

Typically, the Arctic Ocean contains three distinct water mass. A low density surface layer or Polar Mixed Layer (PML) occupying the upper 50 to 100 m of the water column, which is underlayed by a cold halocline down to ~300 m depth [*Jones et al.*, 2003]. This halocline originates from the Pacific and relates to inflows through the Bering Strait. Summer and winter thermal exchanges at the surface produce two forms of Pacific water that constitute the upper and middle halocline. Finally, the halocline insulates the PML

from the Atlantic water, which can be subdivided in warm intermediate Atlantic layer lying between 200 and 500 m depth and cold bottom Atlantic water below 500 m depth [*McLaughlin et al.,* 2004; *Steele et al.,* 2004]. The Atlantic water enters the Arctic through the Norwegian Atlantic water Current (NwAC), which is the northernmost extension of the North Atlantic Current (NAC). The NwAC consists of two branches (Fig. 1). The Barents Sea branch (BSB) flows eastward through the Barents Sea and the Fram Strait branch (FSB), which forms the West Spitsbergen Current (WSC) flowing poleward through eastern Fram Strait. The WSC divides into the Svalbard branch (SB) flowing northeast and the Yermack branch (YB), flowing northward [*Rudels et al.,* 1994; *Jones*, 2001].

Both the Fram Strait and the Barents Sea branches join in the vicinity of Saint Anna Trough and move eastward along the Eurasian continental slope [*Golubeva and Platov*, 2007]. A strong cyclonic boundary current along the margin of the Ocean Basins enhances a cyclonically movement to this water before recirculation in form of cyclonic gyres within the Canada, Makarov and Nansen basins [*Rudels et al.,* 1994; *Jones*, 2001]. Finally, the Atlantic water exits the Arctic Ocean via Fram Strait through the East Greenland Current (EGC), which flows southward into the Greenland and Norwegian seas. The EGC transports recirculating Atlantic water and the surface/sub-surface Polar Mixed Layer (PML) as well the ice exported from the Arctic Ocean [*Rudels et al.,* 1999; *Woodgate et al.,* 1999]. As it flows through southwest Greenland, the EGC mixed with the warm and salty Irminger Current (IC) to form the West Greenland Current (WGC). This latter follows the Greenland coast and then crosses Baffin Bay and joins water from the CAA and Nares

Figure 1. Map showing polar and Atlantic water masses exchange between the Arctic and North Atlantic Oceans. The North Atlantic water penetrating into the Arctic Ocean at depth ranging from 200 to 1700 m is schematically shown by red arrows, whereas dashed blue arrows correspond to the Arctic surface currents including freshwater export (NAC = North Atlantic Current; IC = Irminger Current; NwAC = Norwegian Atlantic water Current; BSB = Barents Sea branch; FSB = Fram Strait branch; YB = Yermak branch; SB = Svalbard branch; EGC = East Greenland Current; WGC = West Greenland Current; BC = Baffin Current). The EGC and WGC are a mixture of Atlantic water at mid-depth and Arctic surface water. The Arctic freshwater export is accomplished by Jones Sound (J.S), Lancaster Sound (L.S), Nares Strait (N.S) and Fram Strait (F.S).

Strait to form the Baffin Current [*Melling et al.,* 2001], which flows southward to the Labrador Sea. The Arctic freshwater export to the North Atlantic Ocean is accomplished by three major gateways, which are Nares Strait, Fram Strait and the CAA mainly via Lancaster and Jones Sounds [*Dickson et al.,* 2007].

2.3.2 Last glacial conditions and oceanography in the CAA

The CAA is characterized by a large number of narrow channels between islands that were deepened by glacial and fluvial erosion during the Quaternary period. During the Last Glacial Maximum (LGM), most of the CAA was cover by the Innuitian ice sheet (IIS), which was coalescent with the Greenland ice sheet (GIS) along Nares Strait and with the Lautentide ice sheet (LIS) along the 74°N of latitude. Due to this configuration, a zone of maximum ice thickness followed a NE-SW ridge (known as the Innuitian uplift) in the central CAA. Break-up of the IIS progressed from west to east beginning around 11.6 cal. kyr BP but Wellington channel was filled by an ice-stream until 8.5 cal. kyr BP [*Dyke et al.,* 2002; *England et al.,* 2006]. Similarly, the IIS and GIS remained in contact until 8.5 cal. kyr BP feeding several ice-streams in northernmost Baffin Bay [*Dyke*, 1998, 1999, 2008; *England*, 1998, 1999; *Zreda et al.,* 1999; *Dyke et al.,* 2002; *England et al.,* 2000, 2004, 2006; *Atkinsen and England*, 2004; *England and Lajeunesse,* 2004].

As a consequence of this glacial history, about 70% of the CAA is shallower than 500 m (mean depth, 124 m) with a limiting sill at 125 m water depth located in Barrow Strait. Maximum depths are found at the entrance of Lancaster Sound [*Prinsenberg and Bennett,* 1987; *Jakobsson,* 2002, 2004; *McLaughlin et al.,* 2004;]. The main axis of the Northwest Passage (NWP) connects the eastern to the western Arctic through Lancaster Sound,

Barrow, Victoria and Dease straits (Fig. 2). Pack ice persists within the CAA throughout the year and the NWP is generally recovered by heavy multiyear sea-ice. First year sea-ice is also present with freeze up starting in November and minimum sea-ice extent in early September [*Melling,* 2002]. The sea-surface temperature (SST) is about –1.8°C during the period of sea-ice cover to –1.6°C and +5°C in late August-September, whereas the sea-surface salinity (SSS) is 32-33 in winter and ranges from 30-31 in the west to 32-33 in the east during summer [*Mudie and Rochon*, 2001; *Prinsenberg and Hamilton,* 2005].

The mean circulation has an eastward component (Fig. 2) because of steric sea-level effect between the North Pacific and the North Atlantic oceans [*McLaughlin et al.,* 2004; *Steele and Ermold*, 2007]. The inflow of Atlantic water is strongly constrained by the shallow channels and only the entrance of Lancaster Sound received Atlantic water from the deflected WGC [*Prinsenberg and Hamilton,* 2005]. Elsewhere in the main axis of the NWP, the water column consists of a seasonal mixed layer lying on summer and winter Pacific water mass derived from the Canada Basin through M'Clure Strait and Amundsen Gulf [*Jones et al.,* 2003].

Present day conditions in Lancaster Sound are 2°C±1.2°C for the summer (August) SSTs with summer (August) SSS of 31.3±0.98. Sea-ice cover extends for 8.1±0.9 months/year. In Barrow Strait, present summer (August) SSTs is 1.9±1.7°C with SSSs of 30±1.24 and sea-ice cover of 10.2±0.9 months/year [*NODC,* 2001; *NSIDC,* 1953-2000 data].

2.4 Materiel and Methods

2.4.1 Sampling and palynological preparation

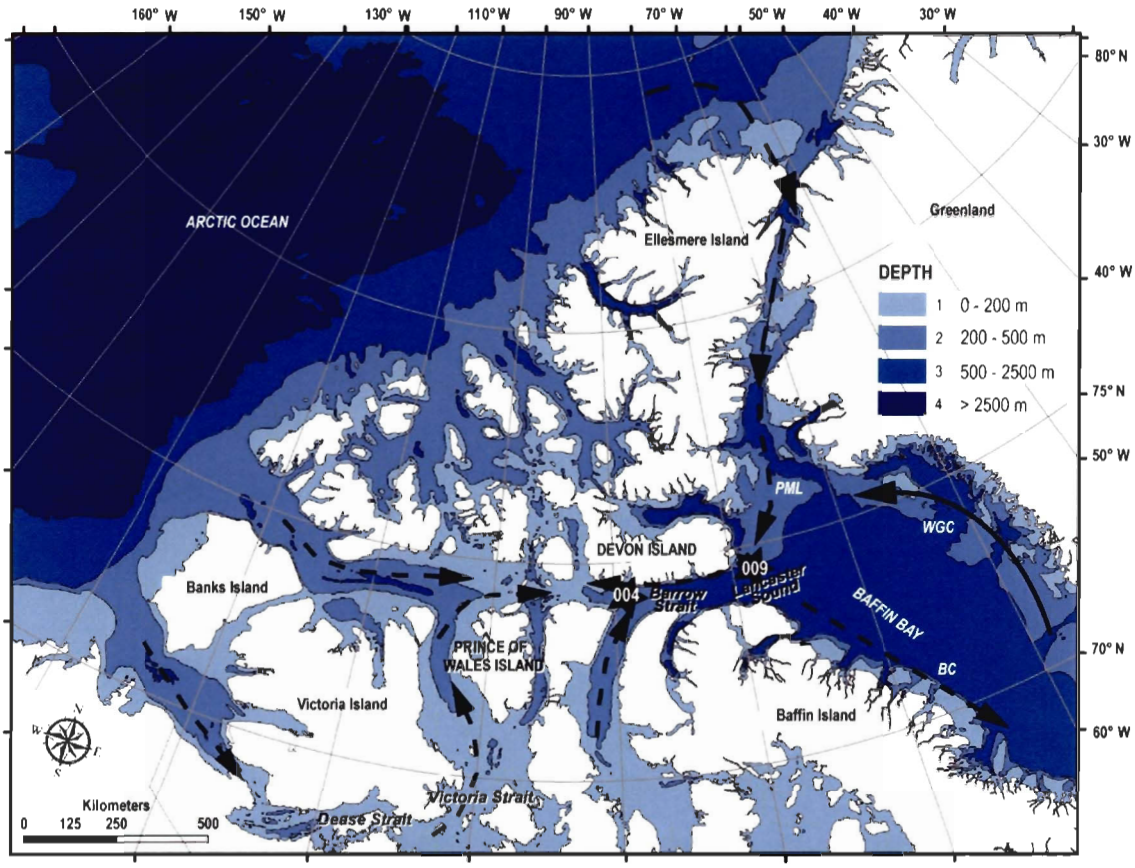

Figure 2. Location of the coring sites at the entrance of the Lancaster Sound and the Barrow Strait (black stars) with major surface currents in the CAA. The circulation in the CAA has an eastward component. Dashed black arrows correspond to the Polar Mixed Layer whereas the black arrow corresponds to the Atlantic water (BC = Baffin Current; WGC = West Greenland Current; PML = Polar Mixed Layer). (Modified from [*Ledu et al.*, 2008]).

Sampling in Lancaster Sound and Barrow Strait (Fig. 2) was respectively carried out in the summer of 2004 and 2005 during legs 9 and 1 of the ArcticNet oceanographic campaigns on board the CCGS *Amundsen* research icebreaker. The sampling sites were selected using a Simrad EM 300 multibeam echosounder and a Simrad 3.5 kHz sub-bottom profiler to avoid disturbed sediment areas (i.e., erosion, mudflows and/or mass movements). Cores 2004-804-009 PC and BC (Lancaster Sound, 74° 11.2'N/ 81° 11.7'W, water depth 781 m, length 6 m and 35 cm respectively, hereinafter referred to as cores 009

PC and 009 BC) and cores 2005-804-004 PC and BC (74°16.1'N/ 91°05.4'W and 74° 16.1'N/ 91°4.4'W, water depth 350 m, length 6,7 m and 35 cm respectively, hereinafter referred to as cores 004 PC and 004 BC) were collected using a piston corer and a box corer. Each core was then sub-sampled every 10 cm (piston cores) and every 5 cm (box cores) for palynological analyses. Sub-samples were processed according to the standard palynological preparation described in *Rochon et al.* [1999]. Five cm^3 of wet sediments were collected by distilled water displacement in a graduate cylinder. A tablet of marker grains (*Lycopodium clavatum* spores, University of Lund, 1984, Batch N° 414831) of known concentration (12 100 ± 1892 spores per tablet) was added to each sample for calculating the concentration of palynomorphs. Sediments were then sieved using Nitex sieves of 100 and 10 µm mesh to eliminate coarse sand, fine silt and clay. The fraction between 100 and 10 µm was then stored in a tube with a few drops of phenol for subsequent chemical treatments.

The chemical processing consists of repeated hot HCl (10%, 4 treatments) alternating with hot HF (49%, 3 treatments) treatments to dissolve carbonate and silicate particles, respectively. The remaining fraction was then rinsed with distilled water to eliminate all traces of acid before a final sieving at 10µm to remove the fluorosilicates and fine particles. Finally, this fraction was mounted in glycerine gel between slide and cover slide. Palynomorphs (dinocysts, pollen grains and spores, acritarchs, organic linings of benthic foraminifers, chlorococcales) were then systematically counted in transmitted light microscopy (Nikon Eclipse 80 – I) at 200 to 400x. A minimum of 300 dinocysts was counted in each sample in order to obtain the suitable statistical representation.

Palynomorphs concentrations were calculated using the marker grain method [*Matthews,* 1969] and expressed in terms of individuals per volume unit (palynomorph/cm^3).

2.4.2 Estimation of past sea-surface conditions

Dinoflagellates are planktonic unicellular organism living in the photic zone of the water column. About half of them are phototrophic (order Gonyaulacales), whereas others are heterotrophic (mainly belonging to the order Peridiniales), mixotrophic, parasitic or symbiotic. During sexual reproduction, some species form a highly resistant cyst composed of a complex biomacromolecular substance, called dinosporine [*Kokinos et al.,* 1998; *Versteegh and Blocker,* 2004].

Many recent studies have shown a close relationship between dinocyst assemblages in surface sediments and sea-surface parameters (see [*Marret and Zonneveld,* 2003 and *de Vernal and Marret,* 2007] for synthesis on the subject). In particular, it has been shown that annual thermal amplitude, salinity and duration of sea-ice cover are determinant factors on the distribution of dinocyst, notably in the North Atlantic [*Rochon and de Vernal,* 1994; *Rochon et al.,* 1999; *de Vernal et al.,* 1994; 1997; 2000], the Canadian Arctic including the Beaufort Sea, the Canadian Archipelago, the Northern Baffin Bay and Hudson Strait [*Mudie and Rochon,* 2001; *Hamel et al.,* 2002; *Richerol et al.,* 2008a], the Laptev Sea [*Kunz-Pirrung,* 2001], the Bering and Chukchi seas [*Radi et al.,* 2001]. The above mentioned studies have led to the development of a surface sediment reference database that is regularly updated [*de Vernal et al.,* 1994, 2001; 2005a; *Rochon et al.,* 1999; *Radi and de Vernal,* 2008]. The database used here contains 1189 reference sites of modern dinocyst spectra (with a total of 60 taxa) and corresponding values of sea-surface

temperature (SST) and salinity (SSS) compiled from the 2001 version of the World Ocean Atlas [*NODC,* 2001]. The seasonal duration of sea-ice cover is expressed as the number of months per year with more than 50% of sea-ice coverage after data from the National Snow and Ice Data Center Climate Data Center [*NSIDC,* 1953-2000 data] in Boulder. Using the software R (http://www.r-project.org/), we applied the modern analogue technique (MAT) for the quantitative estimates of past sea-surface parameters because it required less data manipulation than other techniques with a root mean square error of prediction (RMSEP) among the lowest [*Guiot and de Vernal*, 2007; *de Vernal et al.,* 2005a; *de Vernal*, 2009]. Many studies have used MAT on Holocene Arctic marine cores, including Baffin Bay [*Levac et al.,* 2001; *Rochon et al.,* 2006], Chukchi Sea [*de Vernal et al.,* 2005b; *McKay et al.,* 2008], Beaufort Sea [*Rochon et al.,* 2006; *Richerol et al.,* 2008b], Laptev Sea [*Kunz-Pirrung et al.,* 2001], Barents Sea [*Voronina et al.,* 2001], Nares Strait [*Mudie et al.,* 2006] and the eastern part of the CAA [*Mudie et al.,* 2005; *Ledu et al.,* 2008].

MAT as described by *Guiot and Goeury* [1996] and adapted by *de Vernal et al.* [2001; 2005a] yields good results as indicated by coefficients of correlation (R) greater than 0.93 between estimated and instrumentals hydrographic parameters and RMSEP that are close to the interannual variability recorded from instrumental measurements. The degree of accuracy of the estimated reconstructions (RMSEP) is obtained by the calculation of the standard deviation of the residual (estimated minus observed values), which is ±1.7°C and 1.7 for SSTs and SSSs, respectively and ±1.3 month/year for the duration of sea-ice cover.

2.4.3 Geochemical and isotopic content, grain size and magnetic susceptibility

Organic carbon (C_{org}), nitrogen (N) and inorganic carbon (C_{inorg}) contents were measured using a Carlo-Erba elemental analyser NC 2500 at the Geochemistry and Geodynamics Research Center (GEOTOP). The procedure consists of taking a sediment sample aliquot that is dried, ground and analysed for its total carbon and nitrogen content. A second aliquot is acidified with HCl (1 N) in order to dissolve carbonates, washed and analysed for C_{org} content. C_{inorg} is then calculated by the difference between the two measurements. The $CaCO_3$ content of each sample was determined from the molar weight of $CaCO_3$ (100g) and its content in C_{inorg} (12g) allowing to calculate the calcium carbonate equivalent. The carbon isotopic composition of organic matter ($\delta^{13}C$) was measured on the acidified aliquot by continuous-flow mass spectrometry using a Carlo-Erba elemental analyzer connected to on Isoprime mass spectrometer.

Grain size analysis (0.04 – 2000 μm) was performed at the Institut des sciences de la mer de Rimouski (ISMER) using a Beckman-Coulter LS 13320 laser diffraction grain size analyser. The software Gradistat [*Blott and Pye,* 2001] was used to derive the grain size distribution and statistical parameters (mean and standard deviation). The whole core volumetric magnetic susceptibility was determined at 1 cm intervals for core 009 PC and 2 cm intervals for core 004 PC, using a GEOTEK Multi Sensor Core Logger (MSCL) on board the CCGS *Amundsen.*

2.4.4 Paleomagnetic measurements

Paleomagnetic measurements for cores 009 and 004 PC were carried at the Sedimentary Paleomagnetism Laboratory at ISMER, using a 2-G Enterprises Model SRM-755 cryogenic magnetometer. The natural remanent magnetization (NRM) was measured

on u-channels (rigid u-shaped plastic liners with a square 2 cm cross section and a length of ~1.5 m) at 1 cm intervals. However, due to the finite spatial resolution of the magnetometer's pickup coils, each measurement integrates a stratigraphic interval of 7 cm. In order to eliminate this edge effect, the data from the upper and lower 7 cm of each u-channel were excluded. To isolate the characteristic remanent magnetization (ChRM), the NRM was measured and progressively demagnetized applying peak alternative fields (AF) of 0 to 80 mT at 5 mT increments. The component inclination of the ChRM (ChRM I°) was calculated at 1 cm intervals using a least-square line fitting procedure [*Kirschvink,* 1980]. Using the software developed by *Mazaud* [2005], we also calculated the maximum angular deviation (MAD) to estimate the quality of the directional data.

2.4.5 Color reflectance

Diffuse spectral reflectance was measured with a X-Rite digital swatchbook DTP-22 hand-held spectrophotometer. Reflectance data were then converted in the L* a*b* color space. High values (low values) of L* indicate white (black) color, whereas positive (negative) values of a* indicate red (green) and positive (negative) values of b* correspond to yellow (blue). The L* a* b* data were used to estimate missing sediment due to the piston coring process (Fig. 3).

2.4.6 Initial chronology of the cores

A constant rate supply ^{210}Pb model [*Appleby and Oldfield,* 1983] was used to estimate ages and to determine sedimentation rates in cores 009 BC and 004 BC (Fig. 4a). Data for core 009 BC indicate negligible biological mixing at the top of the sequence and

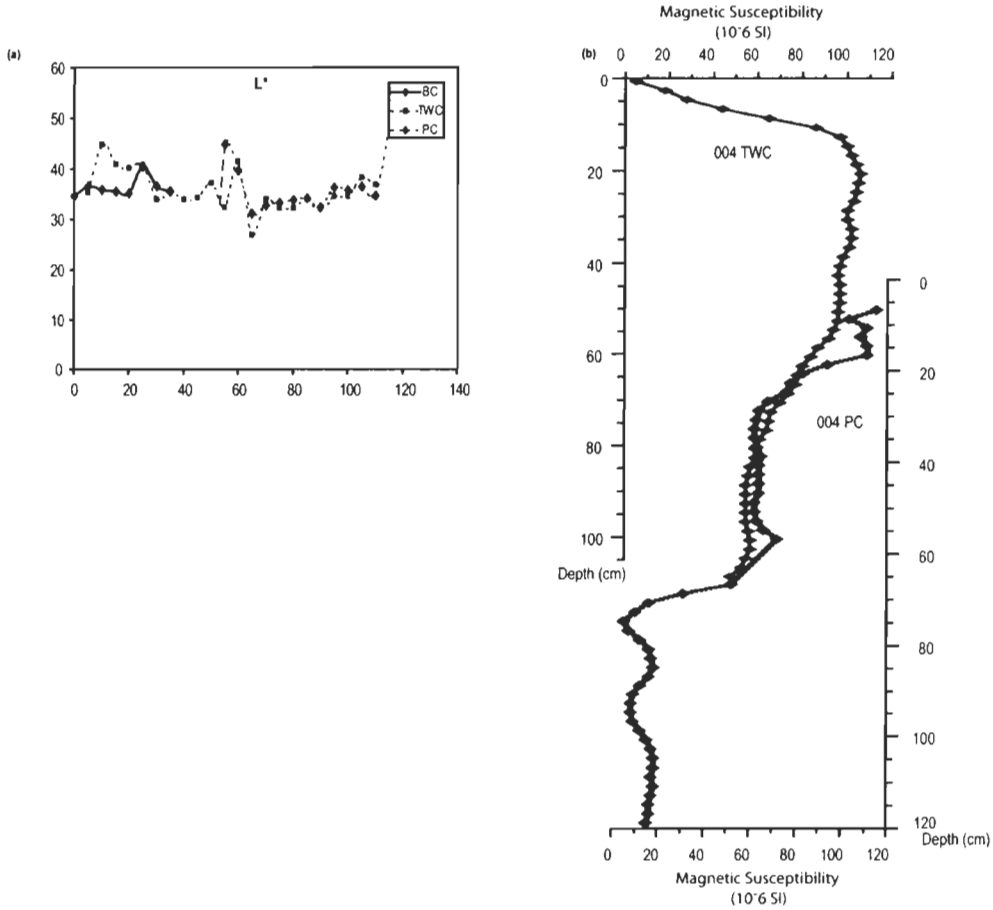

Figure 3. (a) Diagrams showing the color reflectance (L*) for cores 004 PC, TWC and BC, used here to estimate top piston core sediment missing due to piston coring process. (see text for details). (b) Diagram showing the magnetic susceptibility for cores 004 PC and TWC. Diagrams (a) and (b) suggest that about 50 cm of sediment from core 004 PC was lost during coring process.

the ^{210}Pb in excess in the upper 15 cm of the core suggests an average sedimentation rate of about 60 cm/kyr. Assuming a constant sediment accumulation rate from the top to the base of the core, the sequence would cover approximately the last 580 years, from about AD 1420 at the base to the beginning of AD 2000 at the top. In contrast, biological mixing was observed in the uppermost part of the core 004 BC down to ~1.5 cm. The data from this

zone were not used for establishing the chronology using the ^{210}Pb in excess. Apart from the bioturbation mixing zone, the ^{210}Pb in excess in the upper 20 cm indicates sedimentation rates ranging from 212 cm/kyr at the base to the middle part of the core to 33 cm/kyr in the upper part of the core. Using these sediment accumulation rates, and assuming sedimentation rate ranging from 20 cm to 35 cm, we calculated that core 004 BC spans the last 400 years, from about AD 1600 at the base to AD 2000 at the top.

An initial chronostratigraphy for cores 009 and 004 PC was established using calibrated AMS-^{14}C dates on mollusc shells and mixed benthic foraminifers [*Ledu et al.,* 2007, 2008]. All radiocarbon ages were calculated using Libby's half-life (5568 years) and corrected for natural and sputtering fractionation ($\delta^{13}C$ = - 25‰ VPDB). The online Calib V 5.0.2 software was used to convert conventional ^{14}C ages into calendar years using the marine04 calibration curve [*Hughen et al.,* 2004]. In addition to the usual air-sea $^{14}CO_2$ reservoir difference (400 years), a regional correction (ΔR) of 400 years (i.e., total correction of 800 years) has been applied [*Mangerud and Gulliksen,* 1975; *Blake*, 1987; Table 1]. An initial age model based on linear interpolation was constructed for each core assuming constant sedimentation rate between the calibrated age data points. For core 004 PC, this was done using a composite depth scale corrected for missing sediments due to the piston coring process. The comparison of the magnetic susceptibility and the reflectance (L*) data in the piston and trigger weight cores (004 PC and 004 TWC respectively), reveals that about 50 cm of surface sediment was lost during piston coring (Fig. 3). Note that all depths of core 004 PC are expressed in corrected depth, which account for the

missing sediment. In contrast, no estimation of missing sediment has been made for core 009 PC due to the poor recovery of the trigger weight core. The age models indicate that core 009 PC spans about 11 to 2 cal. kyr BP, whereas core 004 PC spans the last 11.4 cal. kyr BP, which represents most of the Holocene. The calculated sedimentation rates ranged

Table 1. Radiocarbon ages used to develop initial age-depth models for cores 2004-804-009 PC and 2005-804-004 PC

Core	Depth (cm)	Material dated	Laboratory numbers	Conventional Radiocarbon Ages (yr BP)[a]	Calibrated Ages (cal. kyr BP)[b]
2004-804-009 PC	217-220	Mixed benthic foraminifers	Ugams# - 02317	6370 ± 30	6.37
2004-804-009 PC	317	Bivalve shell fragments	Beta - 203496	8490 ± 40	8.54
2004-804-009 PC	525	Bivalve shell fragments	Beta - 203498	9770 ± 50	10.24
2004-804-009 PC	571-572	Mixed benthic foraminifers	Ugams# - 02318	10 480 ± 40	11.06
2005-804-004 PC	258 (308*)	Bivalve shell fragments	Beta - 213845	2900 ± 40	2.17
2005-804-004 PC	481 (531*)	Benthic foraminifers	Ugams# -02316	8350 ± 30	8.41
2005-804-004 PC	592 (642*)	Bivalve shell fragments	Beta - 213846	9060 ± 50	9.32
2005-804-004 PC	600 (650*)	Bivalve shell fragments	Beta - 213847	9320 ± 60	9.61

[a]This column lists the AMS -^{14}C ages as reported from the laboratory after normalisation for a δ^{13}C value of -25‰.

[b]Calibrated ages were estimated using the software CALIB 5.0.2 (Stuiver et al. 2005) with Delta R (ΔR) local reservoir effect of 400 years, which means a total correction of 800 years to account for the air-sea reservoir difference. The calibrated ages are computed from the arithmetic average of the calibrated age range, based on two standard deviations (i.e., a confidence interval of 95%).

* Numbers in brackets are the corrected depth due to lost of sediment during piston coring process

from 45 to 122 cm/kyr and from 27 to 141 cm/kyr for core 009 and 004 PC, respectively (Background Data Set, Fig. 4b, appendix 3).

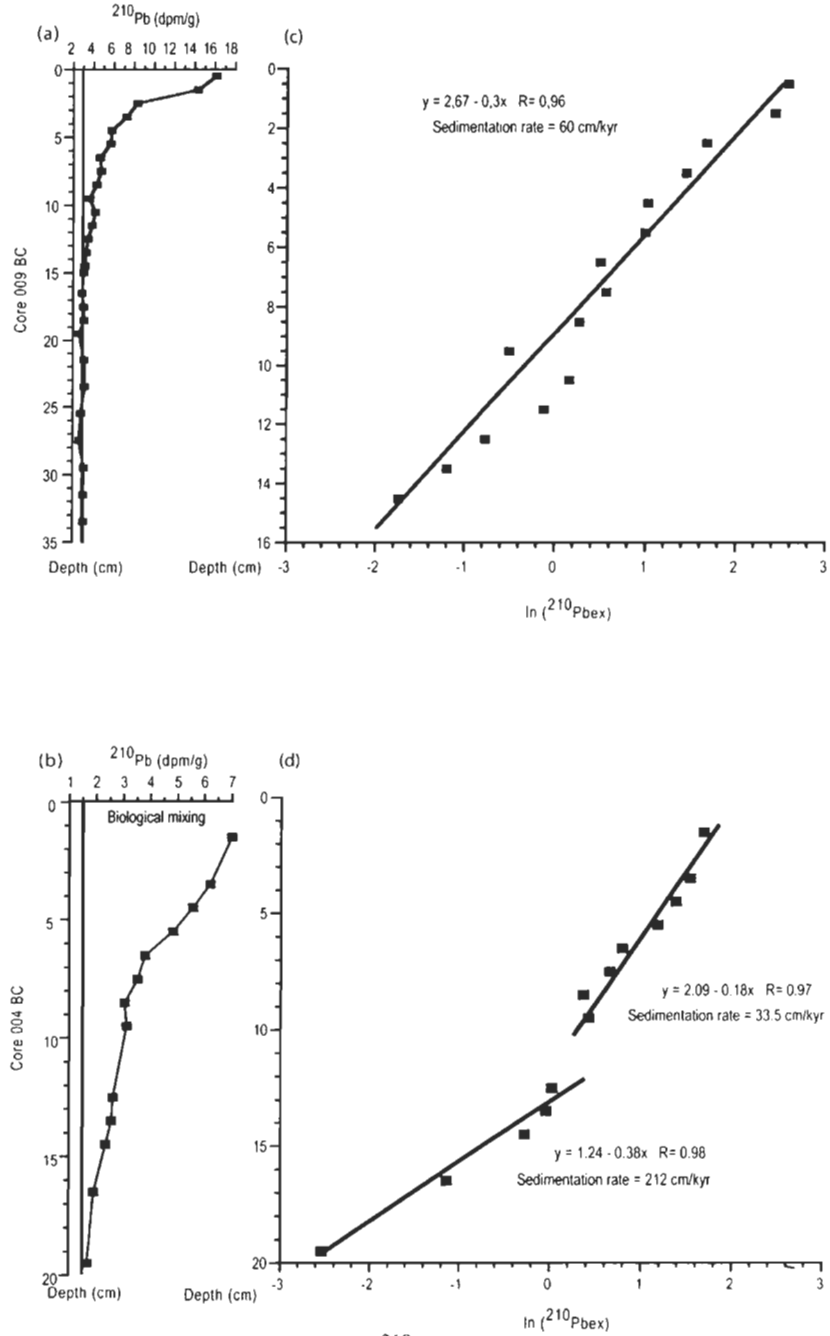

Figure 4a. (a and b) Diagrams showing the ^{210}Pb activity in core 009 and 004 BC. The vertical grey lines (asymptote = 3 for core 009 BC and 1.5 for core 004 BC) correspond to supported ^{210}Pb. (c and d) Diagrams showing the Neperian logarithm of the excess ^{210}Pb, which is used for estimating sedimentation rates. Sedimentation rates are 60 cm/kyr in core 009 BC and ranges from 33.5 to 212 cm/kyr in core 004 BC.

2.4.7 Construction of a composite age-depth model based on paleomagnetic secular variations and harmonic spherical model of the geomagnetic field correlation

Various studies have documented significant directional changes (inclination and declination) of the Earth's magnetic field during the Holocene in high latitudes (Baffin Bay, central Finland, northern Sweden, St Lawrence estuary, Siberia, Russia, Fennoscandia, Iceland, Beaufort and Chukchi seas, Canadian Arctic and Alaskan margins; e.g., *Andrews and Jennings*, 1990; *Saarinen,* 1998; *Snowball and Sandgren,* 2002; *St-Onge et al.,* 2003; *Korte et al.,* 2005; *Korte and Constable,* 2005; *Snowball et al.,* 2007; *Stoner et al.,* 2007; *Barletta et al.,* 2008a; *Besonen et al.,* 2008, *Lisé-Pronovost et al.,* in press]. These geomagnetic directional changes also known as paleomagnetic secular variation (PSV) have been used as a dating method [e.g., *Saarinen,* 1999; *Kotilainen et al.,* 2000; *Breckenridge et al.,* 2004; *St-Onge et al.,* 2003, 2004; *Stoner et al.,* 2007; *Barletta et al.,* 2008b; *Lisé-Pronovost et al.,* in press]. In Arctic sediments where biological remains, such as foraminifers or mollusc shells are generally poorly preserved because of calcium carbonate dissolution, PSV correlation can be useful to improve the chronostratigraphical framework. The paleomagnetic data of core 009 PC shows a strong and stable well-defined component magnetization as indicated by low MAD values (MAD$\leq$2°). In contrast, core 004 PC depicts MAD values above 10° between 460 and 410 cm and between 410 to 150 cm. Such values indicate directional data of low quality [e.g., *Stoner and St-Onge,* 2007]. However, between 50 cm and 150 cm, MAD values are less than 10°, suggesting that the directional paleomagnetic data in the upper part of the core is of better quality (Fig. 5). Nonetheless, between the top of the core and 60 cm, inclination values are relatively shallow compared to the expected values based on a geomagnetic axial dipole model (GAD

= 80°) and were thus excluded. Using the predicted inclinaison data for our coring sites over the last 7000 years derived from the spherical harmonic model of the geomagnetic field, CALS7K.2 model [*Korte et al.,* 2005; *Korte and Constable,* 2005], we correlated the

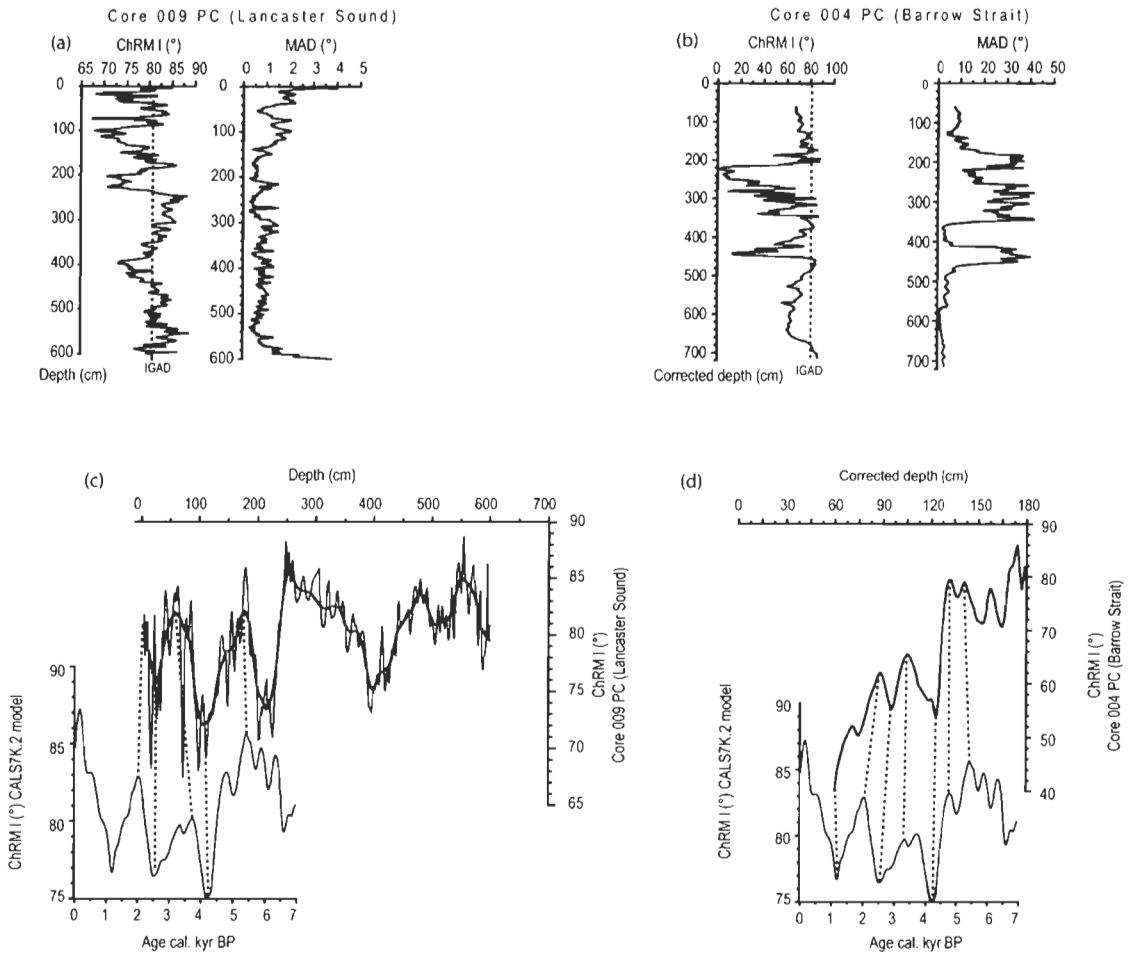

Figure 5. (a and b) Diagrams showing the characteristic remanent magnetisation of the component inclination (ChRM I) and the maximum angular deviation (MAD) values for core 009 and 004 PC. The vertical dashed lines are the value of the geocentric axial dipole (GAD) for the ChRM I at both sites. The grey zones correspond to the zone used for correlation of paleosecular variation of the ChRM I (see text for details).(c and d) ChRM I for core 009 PC and ChRM I for the upper part of core 004 PC and the suggested correlation (dashed lines) with the CALS7K.2 spherical harmonic model [*Korte et al.,* 2005; *Korte and Constable,* 2005] of the predicted ChRM I for both sites. Note that the first correlation in the uppermost part of core 009 PC is only suggested and was not used to construct the age model.

inclination record of the upper part of core 004 PC with the predicted inclinaison calculated using the CALS7K.2 model. Similarly, we correlated the inclination record of core 009 PC with the predicted inclination record derived from the CALS7K.2 model (Fig. 5, Table 2). Recently, *Barletta et al.* [2008a] and *Lisé-Pronovost et al.* [in press] shown a strong consistency between the calculated inclination using the CALS7K.2 spherical harmonic model and inclination records in cores from the Chukchi and Beaufort seas and the Alaskan margin. Due to their proximity to the North Magnetic Pole, cores from the high latitudes have the potential to record higher amplitude directional changes, which are well represented by the CALS7K.2 model at the millennial to centennial time scale [*Barletta et al.*, 2008a].

Table 2. Measured calibrated radiocarbon ages and PSV correlation used to construct new age depth models

Core	Measured calibrated years (cal. kyr BP)	Depth(cm)	CALS7K.2 ages (cal. kyr BP)	Depth equivalence (PSV correlation cm)
2004-804-009 PC	6.37	217-220 (218.5[a])		
	8.54	317	2.5	25
	10.24	525	3.8	60
	11.60	571	4.2	105
			5.4	175
2005-804-004 PC	8.41	531*	1.2	60*
	9.32	642*	2.0	87*
	9.61	650*	2.5	96
			3.25	105*
			4.2	123*
			4.8	132
			5.4	141

*corrected depth for missing sediment due to piston coring processes (see figure 3 and text for details)
a (*mean depth)

This exercise results in five and seven inferred additional ages for cores 009 PC and 004 PC, respectively. A new age model for each core was then constructed using the CALS7K.2 correlation. A second-order polynomial fit was used to derive an age-depth model for core 009 PC, whereas an interpolation fit was used for core 004 PC (Fig. 6). One measured calibrated AMS-^{14}C date in core 004 PC (Beta – 213845) has been excluded from the age model because it appears clearly to be an outlier when compared with the other radiocarbon dates on the PSV correlation probably due to reworking of the mollusc shell fragments in the core. As a result, 9 dates were used for the age model of core 009 PC (5 dates derived from the CALS7K.2 inclination correlation and 4 calibrated AMS-^{14}C dates) and 10 dates for core 004 PC (7 dates from the CALS7K.2 correlation and 3 calibrated AMS-^{14}C dates). In order to test the accuracy of our age models, we compare the magnetic inclination of cores 009 PC and 004 PC based on their new chronology (Fig. 7) with the inclination profiles of Holocene sediment cores from the Arctic (Beaufort and Chukchi seas, [*Barletta et al.,* 2008a]). Major shifts in the magnetic inclination are recorded around 1, 1.5, 2.5, 3.5, 4.5, 5.5 cal. kyr BP and are on average 225±55 yr from those observed in core 009 and 004 PC. These shifts were consistent with the inclination predicted by the CALS7K.2 model but also with the major shifts recorded in lake cores from North America [*Verosub et al.,* 1986; *Geiss and Banerjee*, 2003] and in cores from the Arctic Ocean [*Barletta et al.,* 2008a; *Lisé-Pronovost et al.,* in press]. Even in core 004 PC, where the directional data is more unstable, the shifts are relatively well marked. However, to support our new age model for this core, we also compare the linear interpolation fit used to construct the age-depth relationship with the isostatic emergence

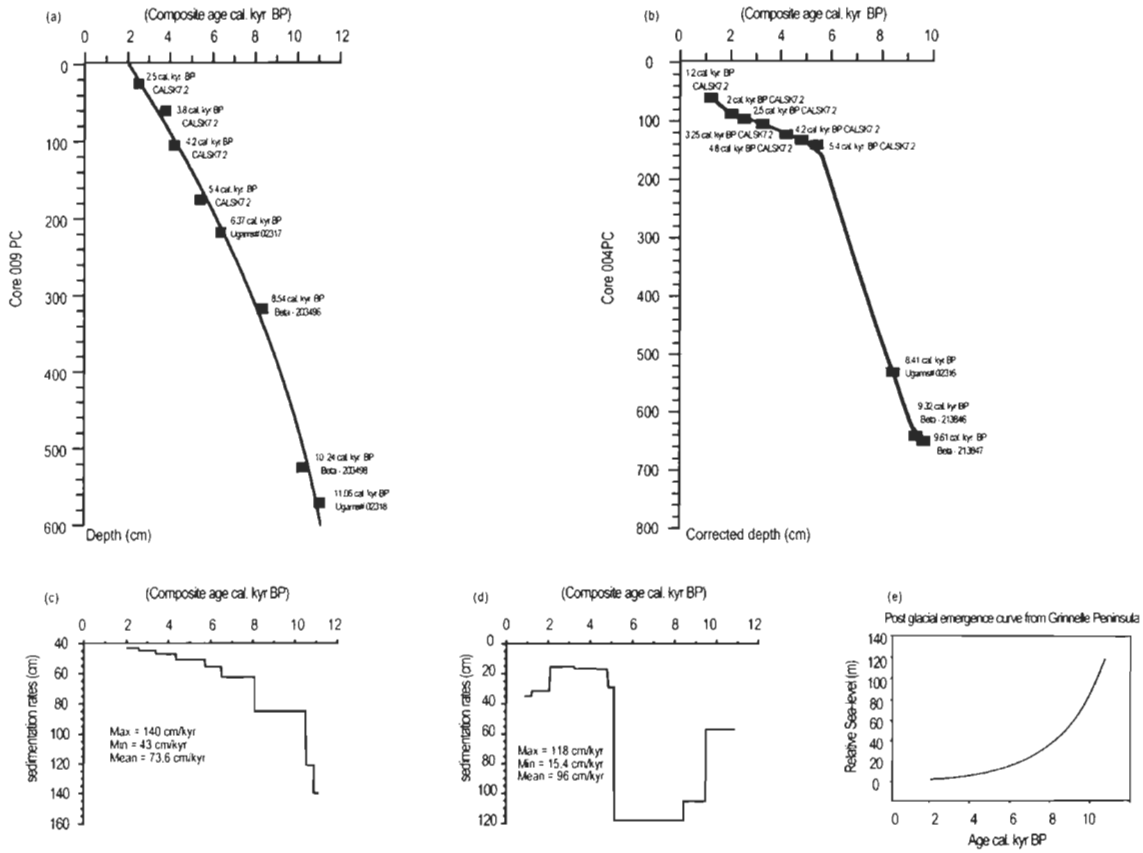

Figure 6. (a and b) Composite age model for cores 009 and 004 PC based on correlations between paleomagnetic secular variations of the geomagnetic field (ChRM I) and the CALS7K.2 predicted inclination for both sites with initial AMS-^{14}C ages (see text and table 2 for details). The age model is based on a 2nd-order polynomial fit for core 009 PC and a linear interpolation fit for core 004 PC.(c and d) Sedimentation rates as suggested by the age models. (e) Post-glacial emergence curve from Grinnelle Peninsula (northeast Barrow Strait), showing a maximum emergence rate between 8.5 and 5 cal. kyr BP, consistent with the high sedimentation rates suggested by the age model of core 004 PC during that interval. (Modified from [*Dyke,* 1998]).

curve near Barrow Strait area [*Dyke,* 1998]. The curve indicates that the maximum emergence rate took place between 8.5 and 5 cal. kyr BP with ~100 m of emergence, which ~80 m have been accomplished in 1500 years (between 8.5 and 7 cal. kyr BP). This

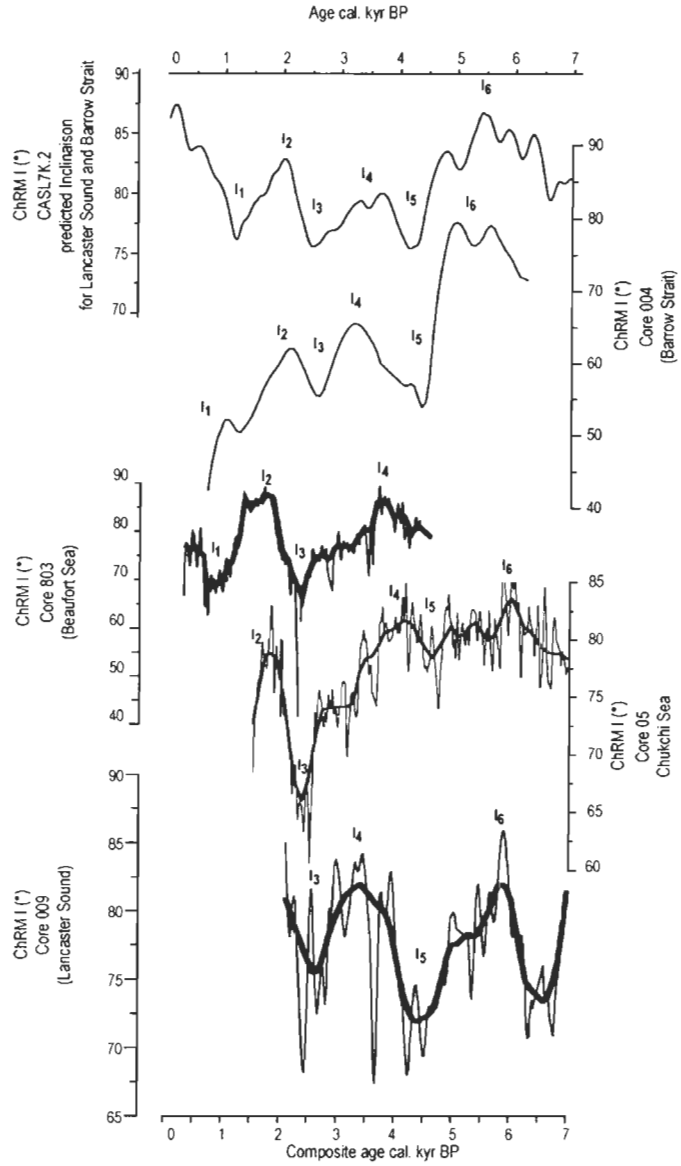

Figure 7. Comparison of the characteristic remanent magnetisation of the component inclination (ChRM I) between cores 009, 004 PC and other cores from the Chukchi and Beaufort seas [*Barletta et al.,* 2008a]. Cores 009 and 004 PC are on their new composite chronology (see text for details). The uppermost diagram corresponds to the CALS7K.2 spherical harmonic model of the predicted magnetic inclination for Lancaster Sound and Barrow Strait [*Korte et al.,* 2005; *Korte and Constable,* 2005]. Major ChRM I shifts observed in all records occurred around 1 (I_1), 1.5 (I_2), 2.5 (I_3), 3.5 (I_4), 4.5 (I_5), 5.5 (I_6) cal. kyr BP.

is also the time interval where the linear interpolation fit for core 004 PC age model indicates maximum sedimentation rates (Fig. 6).

The age models indicate that core 009 PC covers the last 11.1 to 2 cal. kyr BP and core 004 PC covers the last 10.8 to 0.9 cal. kyr BP (Fig. 6). The calculated sedimentation rates range from 43 to 140 cm/kyr and from 15 to 118 cm/kyr for core 009 PC and 004 PC, respectively, allowing for a centennial to millennial time scale resolution.

2.5 Results

2.5.1 Lithology, grain size and magnetic susceptibility

Sediments from 600 and 560 cm in core 009 PC consist of sand mud brown silty clay (2.5Y 5/2, Munsell colour chart). From 560 cm to the top of the core, the sediment consists of olive green silty clay (5Y 4/3) with mottles ranging from 3 to10 μm between 250 and 280 cm. Olive green silty clay (5Y 4/3) is also observed throughout core 009 BC. From 720 to 530 cm, core 004 PC consists of olive brown mud (2.5Y 4/3), whereas from 530 cm to the core top sediment consists in alternating olive grey mud (5GY 4/1) and dark olive brown-black mud (5Y 2/2). Finally, the sediment of core 004 BC consists of olive brown mud (2.5Y 4/3).

Grain size analysis shows that silt and clay are predominant in most part of core 009 PC, representing ~60 and 40% of the grain size fraction, respectively (Fig. 8). Only the lower part of the core records higher percentages of sand (25 to 50%) and coarse silt. Core 004 PC is characterized by an absence of sand and the predominance of silt, representing more than 75% of the grain size fraction (Fig. 9). In core 009 BC silt and clay comprise

about ~75 and 25% of the sediment respectively. Similarly, sediment in core 004 BC is characterized by high percentages of silt (~85%).

Geochemical analyses of core 009 PC indicates that total carbon range from 6% to 3%, with higher values between 11.1 and 10.8 cal. kyr BP (Fig. 8). Organic carbon values ranges from 0.35 to 2% with values increasing gradually from the base to the top of the

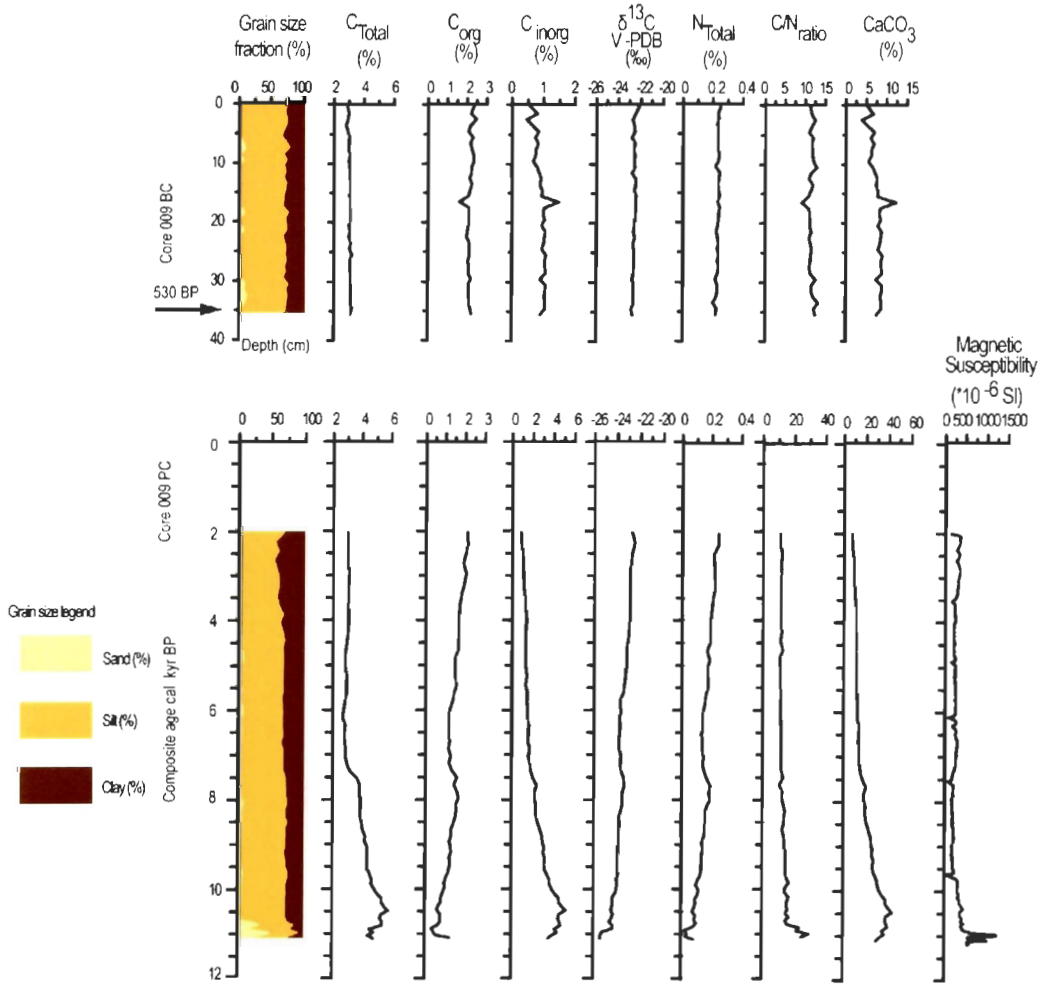

Figure 8. Sedimentological (grain size), geochemical content of cores 009 PC and 009 BC. The chronology of core 009 BC is estimated from ^{210}Pb measurements and was converted from AD to BP ages. (Modified from [*Ledu et al.*, 2008]).

core, whereas inorganic carbon records values of 6% at the base of the sequence (11.1 to 10.8 cal. kyr BP) to 1% at the top. The isotopic composition of organic carbon ($\delta^{13}C$) ranges from -26‰ vs. VPDB at the base of the core (11.1 to 10.8 cal. kyr BP) to -22.5‰ vs. VPDB at the top of the core. The C/N ratio shows values ranging from 30 at the base of

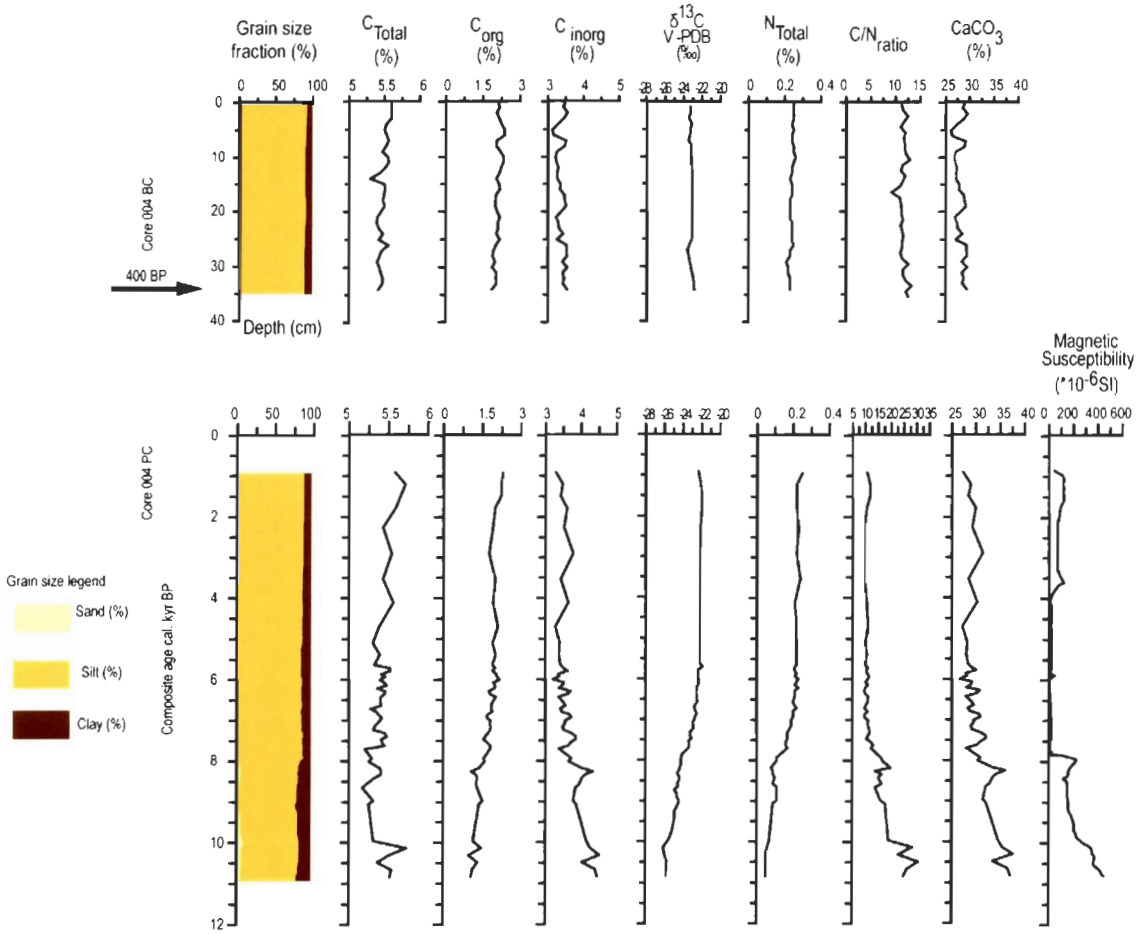

Figure 9. Sedimentological (grain size), geochemical content of cores 004 PC and 004 BC. The chronology of core 004 BC is estimated from ^{210}Pb measurements and was converted from AD to BP ages. (Modified from [*Ledu et al.*, 2008]).

the core (11.1 to 10.8 cal. kyr BP) to 10 at the top. Finally, detrital $CaCO_3$ records higher values at the base of core (~46%), which gradually decreases (~10%) at the top of the core, as does magnetic susceptibility.

Core 004 PC records values of total carbon around 5.5% in the most part of the core (Fig. 9). Organic carbon values ranges from 1% to 2.3% with values increasing from the base to the top of the sequence. Inorganic carbon records values of 3% in most of the sequence and $\delta^{13}C$ depicts its lowest values at the base of the core (from -26‰ to –25.5‰ vs. VPDB during the interval 10.8 to 8.5 cal. kyr BP). In contrast, the C/N ratio is relatively high at the base of the core (10.8 and 8.5 cal. kyr BP) with values around 30, and gradually decreases toward the top of the core reaching 10. Similarly magnetic susceptibility records relatively high values from 10.8 to 8.5 cal. kyr BP. Finally detrital $CaCO_3$ shows values around 30% in the most part of the sequence.

Geochemical analyses in core 009 BC indicate relatively constant values along the core with total carbon of 3%, C_{org} content of 2%, C_{inorg} values of 0.5% and $\delta^{13}C$ values of –22.5‰ (Fig. 8). The C/N ratio is about 11, whereas the $CaCO_3$ records values of 5%. Core 004 BC records also relatively constant values with total carbon of 5.5%, C_{org} content around 2% and C_{inorg} values of 3.5%, whereas C/N ratio is about 10 and $CaCO_3$ around 30% (Fig. 9).

2.5.2 Dinocyst assemblages and quantitative estimates of past sea-surface parameters

Cores 009 and 004 PC show well-preserved dinocyst throughout the sequence (Figs. 10 and 11), except in the lowermost part of core 009 PC, between 11.1 to 10.8 cal. kyr BP, where they are absent. Dinocyst assemblages reveal low species diversity, which is

consistent with previous work in the CAA [*Mudie and Rochon*, 2001]. Indeed, core 009 PC is dominated by four taxa that make up 90% of the assemblage: *Brigantedinium* spp., *Islandinium minutum*, *Spiniferites elongatus/frigidus* and *Operculodinium centrocarpum*. In core 004 PC, 90% of the assemblages are dominated by two taxa: *Brigantedinium* spp. and *Islandinium minutum*.

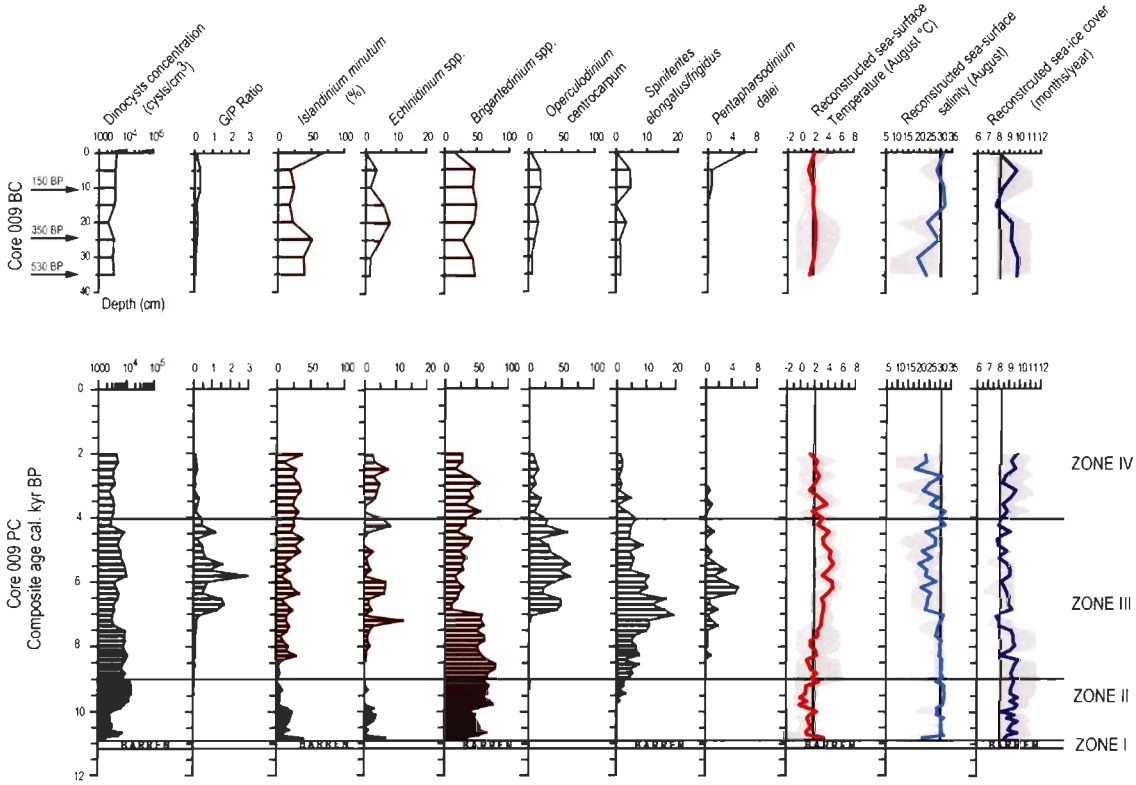

Figure 10. Diagram of dinocyst concentration, Gonyaulacales/Peridiniales (G/P ratio), relative abundance of dinocyst taxa and quantitative estimates of sea-surface conditions based on modern analogue technique (MAT) applied to dinocyst assemblages in cores 009 BC and 009 PC. The red, blue and purple lines correspond to the best estimates for the summer temperature and salinity (August) and the duration of sea-ice cover, respectively. The grey zones correspond to the minimum and maximum values possible according to the set of five best analogues. The vertical black lines indicate the values of modern sea-surface conditions. The chronology of core 009 BC is estimated from ^{210}Pb measurements and was converted from AD to BP ages. (Modified from [*Ledu et al.*, 2008]).

The ratio of phototrophic to heterotrophic dinocyst taxa (G/P ratio) records low values in the most part of core 009 PC, indicating the dominance of non-phototrophic taxa,

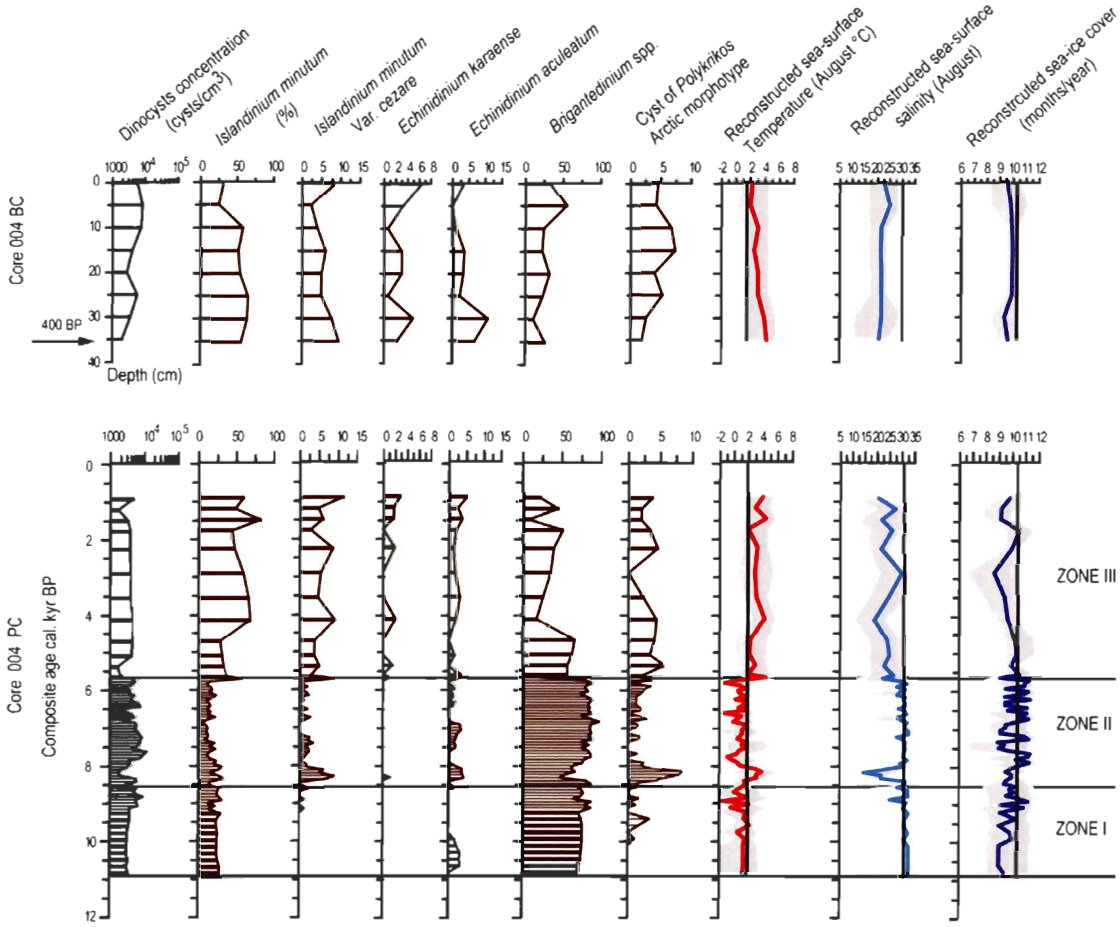

Figure 11. Diagram of dinocyst concentration, relative abundance of dinocyst taxa and quantitative estimates of sea-surface conditions based on modern analogue technique (MAT) applied to dinocyst assemblages in cores 004 BC and 004 PC. The red, blue and purple lines correspond to the best estimates for the summer temperature and salinity (August) and the duration of sea-ice cover, respectively. The grey zones correspond to the minimum and maximum values possible according to the set of five best analogues. The vertical black lines indicate the values of modern sea-surface conditions. The chronology of core 004 BC is estimated from ^{210}Pb measurements and was converted from AD to BP ages.

except between 8.5 and 4 cal. kyr BP, where it reaches values ≥1. In contrast, photosynthetic taxa are absent throughout the length of core 004 PC. Dinocyst concentrations range from 1766 to 15230 cysts/cm^3 (average 6378 cysts/cm^3) and from 1634 to 12407 cysts/cm^3 (average 4739 cysts/cm^3), in core 009 and 004 PC, respectively.

Based on the relative abundance of dinocyst taxa, core 009 PC shows four different zones (Fig. 10). The first zone (from 11.1 to 10.8 cal. kyr BP) is characterized by the absence of dinocysts. The second zone (from 10.8 to 9 cal. kyr BP) is dominated by the heterotrophic taxa *Brigantedinium* spp. and *Islandinium minutum*, representing 75 and 20% of the assemblages, respectively. Quantitative estimates of past sea-surface conditions suggest low SSTs (August) of 0°C on average, which is about 2°C colder than modern values, accompanied with sea-ice cover of 10 months/year, which is about 1 month/year more that at present. The third zone (from 9 to 4 cal. kyr BP) is marked by an increase in the relative abundance of the phototrophic taxa *Operculodinium centrocarpum* (50%), *Spiniferites elongatus/frigidus* (20%) and *Pentapharsodinium dalei* (5%). Sea-surface reconstructions suggest SSTs (August) reaching about 4.5°C, which is 3°C warmer than modern conditions, but with SSSs of about 25, which is lower than at present. Finally, the fourth zone (after 4 cal. kyr BP) is again dominated by *Brigantedinium* spp. and *Islandinium minutum* marking the establishment of modern conditions.

Based on dinocyst assemblages, core 004 PC shows three different zones (Fig 11). The first zone (from 10.8 to 8.5 cal. kyr BP) is dominated by the heterotrophic taxa *Brigantedinium* spp. (70%) and *Islandinium minutum* (25%). The reconstructed sea-surface parameters indicate relatively low SSTs (August, on average 1°C) and sea-ice cover of

about 9 months/year, which is about 1.5 month/year less than modern conditions. The second zone (from 8.5 to 5.5 cal. kyr BP) is also marked by the dominance of *Brigantedinium* spp. and *Islandinium minutum* but with an increase of dinocyst diversity as shown by the presence of *Islandinium minutum* var. *cezare* (10%), *Echinidinium aculeatum* (5%), *Echinidinium karaense* (3%) and the cyst of *Polykrikos* Arctic morphotype (10%), reaching their maximum relative abundance around 8.5 cal. kyr BP. Quantitative estimates of past sea-surface conditions suggest warmer (~3°C) SSTs (August) than modern around 8.5 cal. kyr BP, decreasing SSSs (minimum around 15) and sea-ice cover (1.5 months/year lower than modern conditions). After this interval, relatively harsh conditions prevailed, with lower SSTs (August, 0°C on average) and variation of sea-ice cover (minimum of 9 and maximum of 11 months/year). Finally, the third zone (after ~5.5 cal. kyr BP) is also characterized by an increase of dinocyst species diversity but more pronounced than in zone II reflecting a general trend towards warmer conditions as suggested both by the reconstructed SSTs (August, 3°C warmer than modern) and the reconstructed sea-ice cover (2 months/year lower than modern conditions).

Core 009 BC also shows well-preserved dinocyst assemblages (Fig. 10) with concentrations ranging from 2220 to 4532 cysts/cm^3 (average 3623 cysts/cm3). The G/P ratio records low values (<1), indicating the dominance of heterotrophic taxa, mainly *Brigantedinium* spp. (40%) and *Islandinium minutum* (40%), whereas phototrophic taxa are represented by *Operculodinium centrocarpum* (~15%) and *Spiniferites frigidus/elongatus* (~5%). From 25 to 10 cm (~1600 to ~1800 AD) dinocyst assemblages are dominated by the heterotrophic taxa *Brigantedinium* spp and *Echinidinium* spp. (~50 and ~10%,

respectively), whereas the relative abundance of *Islandinium minutum* records a sharp decrease (from ~50% to ~25%). During this interval phototrophic taxa are mainly represented by *Operculodinium centrocarpum* (~10%). These assemblages indicate SSTs (August) close to modern values, whereas the trend suggests a sea-ice cover decrease from 9.5 to 8 months/year accompanied by increased SSSs in the upper part of the core spanning the last two centuries.

Core 004 BC records dinocyst concentrations (Fig. 11) ranging from 1986 to 8066 cysts/cm^3 (average 4872 cysts/cm^3) with the dominance of the two heterotrophic taxa *Brigantedinium* spp. (25%). and *Islandinium minutum* (50%) accompanied by other taxa (*Islandinium minutum* var. *cezare*, *Echinidinium aculeatum*, *Echinidium karaense*, cyst of *Polykrikos* Arctic morphotype). The reconstructed SSTs (August) show a trend towards modern values that is reaches at the top of the core.

2.6 Discussion

2.6.1 The gradual break-up of the IIS in the east and central part of the main axis of the NWP

The absence of dinocysts together with high $CaCO_3$ (detrital) content, high magnetic susceptibility, high C/N ratio and low $\delta^{13}C$ values at the base of core 009 PC, between 11.1 and 10.8 cal. kyr BP (Zone I) indicates that Lancaster Sound site has recorded large terrigenous inputs related to an erosive dynamic during this time interval. Stable isotopes, $CaCO_3$ content and magnetic susceptibility from core 004 PC reveal the same pattern from 10.8 cal. kyr BP until 8.5 cal. kyr BP.

The paleolimnological record of diatoms from Prescott Island in the central CAA has shown that diatoms remained absent until 11 cal. kyr BP, but that high values of carbon content and magnetic susceptibility were probably due to high energy glacial outwash [*Finkelstein and Gajewski,* 2007]. *Andrews et al.* [1995, 1996, 1998], *Dyke* [2008] and *Parnell et al.* [2007] have reported detrital carbonate layers in cores from the northern Baffin Bay, the Labrador Sea and the northern North Atlantic around 11 cal. kyr BP. Similarly *Scott et al.* [2009] observed an IRD rich layer prior to 11 cal. kyr BP, in a core from the Amundsen Gulf in the western CAA. Recently, *Darby and Zimmerman* [2008] found in cores from the Fram Strait, central Arctic and Chukchi Borderland six or seven sequences of IRD peaks dated from 36 to 11 cal. kyr BP, which they associate to ice calving and discharge events in the Arctic. The last IRD sequence recorded took place around 11.5 cal. kyr BP. This timing is closely related to the first stage of the IIS decay as suggested by *England et al.* [2000, 2006]. Therefore, we associate the large terrigenous inputs at the base of cores 009 and 004 PC to the final collapse of the IIS in the CAA. The high $CaCO_3$ content at the base of both cores probably originates from glacial erosion on Devon Island and Ellesmere islands. The bedrock of this area consists of a Precambrian crystalline basement, overlain by a lower Paleozoic succession dominated by shallow marine platform carbonates [*Bischof and Darby,* 1999; *Parnell et al.,* 2007]. The fact that the central CAA was the center of the maximum Innuitian uplift (maximum former ice thickness reaching more than 1 km) probably explains why Barrow Strait site recorded the Innuitian deglaciation over a much longer time interval.

The occurrence of dinocysts at 10.8 cal. kyr BP together with a gradual increase of the C_{org} content and a gradual decrease of both the C/N ratio and detrital carbonate content marked the onset of the biological activity in surface waters and the beginning of hemipelagic sedimentation in core 009 PC. It corresponds to zone II, dated between 10.8 and 9 cal. kyr BP, in which quantitative estimates of past sea-surface parameters suggest low SSTs (August) and sea-ice cover for 10 months/year. The harsh reconstructed climatic conditions between 10.8 and 9 cal. kyr BP are consistent with records based on dinocysts, diatoms and foraminifers from northernmost Baffin Bay [*Levac et al.,* 2001; *Knudsen et al.,* 2008]. However, it contradicts results based on bowhead bone remains [*Dyke et al.,* 1996] indicating less sea-ice cover in the CAA from 10.6 to 8.5 cal. kyr BP. Less sea-ice cover (~1.5 months/year lower than modern conditions) is also indicated by our records from central CAA (Barrow Strait) during that time interval. Recently, *Vare et al.* [2009], based on the biomarker IP_{25} also found less sea-ice in the central CAA during that time. We associate the reduced ice cover in Barrow Strait with glacial outwash related to the last step of the Innuitian deglaciation triggering high terrigenous inputs as suggested by high magnetic susceptibility values and high detrital carbonate content as well as high C/N ratio. In contrast, the reconstructed harsh sea-surface conditions in Lancaster Sound and northernmost Baffin Bay could be due to the presence of an ice-stream fed by the coalescence of the IIS and GIS [*Blake et al.,* 1992b; *Kelly et al.,* 1999; *Zreda et al.,* 1999; *England et al.,* 2000, 2006]. Recently, *Dyke* [2008] shown that the area of Baffin Bay was marked by active ice-streams between ~10 and 9 cal. kyr BP. Cooler conditions in Lancaster Sound could also be due to limited exchange between the North Atlantic Ocean

and Baffin Bay during that time. In modern conditions, the WGC transports polar surface water of EGC origin, whereas relatively warm and salty intermediate Atlantic water, originating from the IC, is found between ~200 and 500 m water depth [*Cunny et al.*, 2002]. Several works in northern and central Baffin Bay have shown that the PML is affected by this warm intermediate Atlantic water through turbulent mixing and upwelling [*Melling et al.*, 2001; *Ingram et al.*, 2002; *Gratton et al.*, 2003; *Dunlap and Tang*, 2006; *Knudsen et al.*, 2008; *Zweng and Munchow*, 2006]. Based on diatoms, foraminifers and the physical properties of sediments in cores from western Greenland, *Lloyd et al.* [2005] and *Ren et al.* [2009] found a weaker WGC before 9 cal. kyr BP. Therefore the reconstructed harsh conditions in Lancaster Sound between 10.8 and 9 cal. kyr BP could be linked to the presence of an ice-stream, a reduced influence of the warm Atlantic water in the area of Baffin Bay or both.

2.6.2 The early to middle Holocene in the NWP: major oceanographic changes and the possible gradual onset of an Arctic Oscillation-like climate mode

The first occurrence of the phototrophic taxon *Spiniferites elongatus/frigidus* around 9 cal. kyr BP in core 009 PC at the transition between zone II and zone III marks the establishment of a gradual warming as suggested by the reconstructed SSTs (August). Maximum SSTs (August, 3°C above present) were reached between 6 and 5 cal. kyr BP in zone III, when the phototrophic taxa *Operculodinium centrocarpum* and *Pentapharsodinium dalei* record their maximum abundance. Based on dinocyst assemblages in cores from Baffin Bay, the Laptev Sea and southwest Greenland, *Levac et al.* [2001], *Rochon et al.* [2006], *Polyakova et al.* [2005] and *de Vernal* and *Hillaire-Marcel*

[2006] found warmer conditions during the early-middle Holocene. Similarly, diatom assemblages in cores from the Reykjanes Ridge in the subpolar North Atlantic, Greenland-Iceland-Norwegian seas (GIN seas) and the northern shelf of Iceland indicate an increase influence of warm Atlantic water in the upper water column during the early-middle Holocene [*Koç and Jansen,* 2002; *Andersen et al.,* 2004a,b; *Justwan et al.,* 2008]. Several studies based on mesopelagic and benthic foraminifers in cores from the Barents and Chukchi seas reported a maximum inflow rate of Atlantic water during the early Holocene around 8 cal. kyr BP [*Duplessy et al.,* 2001, 2005; *Hillaire-Marcel et al.,* 2004; *de Vernal et al.,* 2005b]. Recently, *Ślubowska-Woldengen et al.* [2008] using benthic foraminifers also found an increasing inflow of the warm Atlantic water in the Barents Sea, Svalbard shelf and Iceland shelf accompanied by a strengthening of both the WSC and IC. These are consistent with benthic foraminifers records from west Greenland, which suggest a strengthening of the warm WGC since 9 cal. kyr BP [*Lloyd et al.,* 2005]. A strengthening of both the IC and WGC indicates an increase influence of the warm intermediate Atlantic water [*Ślubowska-Woldengen et al.,* 2008]. Positive SST anomalies during the early-middle Holocene were found along the main axis of the NAC and NwAC [*de Vernal and Hillaire-Marcel,* 2006] suggesting a strong influence of the warm intermediate Atlantic water in the upper water column.

Warmer conditions in the eastern Arctic during the early-middle Holocene were also reported from continental records. Based on diatom assemblages from northeast Ellesmere island lakes, *Smith* [2002] reported warmer conditions in the early/middle Holocene. Data on stable isotopes from southwestern Greenland [*Anderson and Leng,* 2004] indicate

negative precipitation/evaporation balance during this time interval. Pollen assemblages and concentrations in cores from Baffin Island lakes suggest warmer conditions around 6 cal. kyr BP [*Kerwin et al.,* 2004]. Similarly, chironomids from lakes in Baffin Island suggest milder conditions during the middle Holocene [*Miller et al.,* 2005; *Francis et al.,* 2006]. $\delta^{18}O$ data in ice core from Devon Island Ice Cap also indicate warmer conditions during the early-middle Holocene [*Fisher,* 1976, 1979; *Fisher and Koerner,* 1980; *Fisher et al.,* 1983].

In contrast, our records from the central CAA (Barrow Strait) show an opposite trend between 8 and 5.5 cal. kyr BP with minimum reconstructed SSTs (August, 3°C lower than present) and variation of sea-ice cover (from 9 to 11 months/year). *Dyke et al.* [1996] have shown that bowhead whales were excluded in the central channels of the CAA between 8.5 and 5 cal. kyr BP because of sea-ice conditions more severe than those of historical times. Records based on dinocyst assemblages in cores from the Beaufort and Chukchi seas also indicate extensive sea-ice cover during the early-middle Holocene but with a maximum inflow of warm intermediate Atlantic water [*Hillaire-Marcel et al.,* 2004; *de Vernal et al.,* 2005b; *Rochon et al.,* 2006; *McKay et al.,* 2008]. This strong decoupling in the western Arctic between surface layer and the intermediate Atlantic water mass could be due to an increase of Eurasian river runoff enhancing a sharp halocline, which promoted the formation of sea-ice. Water in the central CAA is mainly derived from the Canada Basin through M'Clure Strait. The inflow of this low salinity water into the central CAA is consistent with both the decrease of the reconstructed SSSs (August) around 8.5 cal. kyr BP and the final collapse of the Wellington channel ice-stream, which blocked the full

penetration of the Sea until 8.5 cal. kyr BP [*Dyke et al.,* 2002; *England et al.,* 2006]. Strong emergence between 8.5 and 7 cal. kyr BP [*Dyke,* 1998] due to isostatic rebound (~80 m in 1500 years) has also probably triggered variations of the sea-ice cover. Such processes, probably explain the relatively harsh conditions and variations of sea-ice cover recorded in Barrow Strait between 8 and 5.5 cal. kyr BP.

Therefore, our records in the eastern and central CAA during the early-middle Holocene (Zone III, Lancaster Sound; Zone II, Barrow Strait) seems to be related to a large-scale atmospheric and oceanic reorganization following the last phase of the deglaciation in the Arctic and subarctic areas. In the eastern Arctic, this reorganization was marked by a strong influence of the warm intermediate Atlantic water mass in the upper water column along or near sites influencing by the NAC, NwAC, IC and WGC. The northern Baffin Bay recorded this influence much latter probably due to the gradual strengthening of the WGC after 9 cal. kyr BP that is consistent with major oceanographic changes in the northwestern Atlantic during the early-middle Holocene [*Hillaire-Marcel et al.,* 2001; *Knudsen et al.,* 2008; *Ren et al.,* 2009]. These includes a gradual strengthening of both the IC and the WGC as well as the development of an active site of intermediate Labrador Sea-water formation [*Hillaire- Marcel et al.,* 2001; *Lloyd et al.,* 2005; *Knudsen et al.,* 2008; *Ren et al.,* 2009]. In the central and western Arctic, a sharp halocline has promoted the formation of a relatively extensive sea-ice cover. This sharp halocline is probably the result of an increase of Eurasian river runoff, which fed the Canada Basin. The inflow of this low salinity water into the central CAA following the last step of the Innuitian deglaciation has probably enhanced harsh conditions. The opposition in marine

records between the eastern and western Arctic together with the simultaneous increase in temperatures over land suggests a strong coupling of the ocean-atmosphere system during this interval. In modern conditions, such dipole pattern in the Arctic marine realm between the east and west is related to the positive mode of the AO. These include strong divergence in the eastern Arctic leading to positive SST and less summer sea-ice. In western Arctic, strong convergence results in negative SST [*Rigor et al.,* 2002] and relatively extensive sea-ice cover accompanied by an increase in Eurasian river discharge due to storm tracks [*Dickson et al.,* 2000; *Peterson et al.,* 2002; *Steele and Ermold,* 2004].

2.6.3 Reverse trend in sea-surface conditions during the middle to late Holocene: a possible shift in the AO mode at the millennial time scale

From 5.5 cal. kyr BP to the late Holocene, dinocyst assemblages in core 009 PC show a general decrease in the relative abundance of phototrophic taxa corresponding to the upper part of zone III and zone IV. These are accompanied by a general trend towards relatively low SSTs (August) with values reaching modern conditions (~2°C) and extensive sea-ice cover (10 months/year). Based on dinocyst, diatom assemblages and planktonic foraminifers in cores from northernmost Baffin Bay and western Greenland, *Levac et al.* [2001], *Knudsen et al.* [2008] and *Seidenkrantz et al.* [2007, 2008] found cooler conditions in surface water associated with an increasing influence of Arctic water mass during the late Holocene. Similarly, *Justwan et al.* [2008] and *Ran et al.* [2008] based on diatom assemblages in core from the North Iceland shelf reported cooler conditions that they associate with a decreasing influence of the warm intermediate Atlantic water in the upper water column together with a reinforcement of the polar water in the EGC during the late

Holocene. The increasing influence of polar waters in the EGC has also been proposed by *Jennings et al.* [2002] on the basis of stable isotopes, benthic foraminifers and IRD fluxes in cores from east Greenland shelf to explain the SST cooling trend during the late Holocene. A similar decrease in SST was also inferred from alkenones in cores from the North Icelandic shelf [*Bendle and Rosell-Melé*, 2007] and the Norwegian Sea [*Calvo et al.,* 2002]. Based on benthic foraminifers, *Lloyd et al.* [2007] reported a cooling from 3.5 cal. kyr BP to the late Holocene in west Greenland. Neoglacial cooling with decreasing Atlantic water influence has been recognized in southwest Greenland on the basis of benthic foraminifers [*Lassen et al.,* 2004; *Lloyd et al.,* 2007]. Neoglacial cooling in the eastern Arctic has been also found in many terrestrial records in cores from Ellesmere and Baffin islands and the eastern Arctic as a whole [*Joynt and Wolfe,* 2002; *Wolfe,* 2002; *Kaufman et al.,* 2004; *Michelutti et al.,* 2006]. A reduction of marine aerosol content and decreasing $\delta^{18}O$ in ice core from Devon Island Ice Cap suggest increased sea-ice cover and cooling since 3.5 cal. kyr BP in this area [*Fisher,* 1976, 1979; *Fisher and Koerner,* 1980; *Fisher et al.,* 1983, 1995; *Bradley,* 1990].

In contrast, dinocyst assemblages from Barrow Strait show an increase in species diversity from 5.5 cal. kyr BP to the late Holocene. It corresponds to zone III, where quantitative estimates of past sea-surface conditions suggest warmer SSTs (August, ~3°C warmer than modern conditions) with both a decrease of SSSs and sea-ice cover. *Rochon et al.* [2006], on the basis of dinocyst assemblages in a sediment core from the Beaufort Sea, found that heterotrophic dinocyst species were gradually replaced by phototrophic taxa, indicating a decrease in sea-ice cover from the middle to late Holocene. Similarly, *McKay*

et al. [2006, 2008] and *de Vernal et al.* [2005b] based on dinocyst assemblages in cores from the Chukchi Sea also argued for less sea-ice cover during the late Holocene. However, *Vare et al.* [2009] found an increase in the abundance of the biomarker IP_{25} in a nearby core from Barrow Strait during the last 5 cal. kyr BP, which suggests an increase of sea-ice occurrence. This biomarker is though to be produced by sea-ice algae belonging to the diatom genera *Haslea*, which is a minor component of sea-ice diatom assemblages in the Arctic [*Riedel et al.,* 2003; *Belt et al.,* 2007, 2008]. Comparison between the abundance of IP_{25} and diatom-based sea-surface temperature reconstructions in core from the Northwest Iceland shelf during the late Holocene indicates that both records are consistent [*Massé et al.,* 2008; *Andrews et al.,* 2009]. Therefore, the discrepancy between our record and that of *Vare et al.* [2009] is difficult to explain. Nevertheless, it is noteworthy that dinocyst-based reconstructions are related to the duration of the sea-ice cover expressed as the number of months/year, whereas IP_{25} is related to a qualitative assessment expressed as presence or absence of sea-ice. Furthermore, relatively little is known about the ecology of *Haslea* spp. [*Belt et al.,* 2007] and it is possible that the production of IP_{25} might be related, in some cases, to factors other than sea-ice. Indeed, *Parrish and Wangersky* [1987] and *Parrish et al.* [1998] found that the production of triglycerides and ketones in some marine diatoms was most likely due to nitrogen limitation rather than the abundance of sea-ice cover. Therefore, the production of IP_{25} could be linked to nutrient limitation that may occur during periods of peak production in the bottom ice. In any case, further studies are needed to better understand factors that affect the production of IP_{25} and it potential linkage with nutrients availability. Comparative studies on both proxies from the same samples are also

needed for intercalibration purposes. On the other hand, dinoflagellate cyst-based reconstructions rely on the cyst production by dinoflagellate populations in the upper part of the water column, the distribution of which is dependant upon the presence of nutrients, but also on environmental parameters, in particular the presence of sea-ice [*Taylor,* 1987; *de Vernal et al.,* 2001; 2005b; 2008]. Therefore, our dinocyst-based reconstructions during the middle to late Holocene with opposite trend between Lancaster Sound and Barrow Strait seems consistent with change in large-scale atmospheric pattern such as the AO. Under modern climate conditions, the AO creates sea-ice dipole pattern between the eastern and western Arctic on annual to decadal time scale. In particular a strong negative mode of the AO enhances less advection of Atlantic water in the Arctic Ocean. This is accompanied by more anticyclonic conditions triggering eastward displacement of the Pacific/Atlantic water front and westward displacement of the transpolar drift along northern Greenland, whereas the Beaufort Gyre is strengthened allowing higher freshwater flux through the CAA [*Proshutinsky et al.,* 2002]. During AO^-, divergence in eastern Arctic is reduced resulting in negative SST anomalies. Recently, *Darby and Bischof* [2004], based on the mineralogy of silt-sand grains from western Arctic cores, have suggested a sea-ice drift pattern analogous to the impact of the AO throughout the Holocene. Therefore, our records from the middle to late Holocene with opposite trends in sea-surface conditions (colder at Lancaster Sound and warmer at Barrow Strait), and marked decreasing SSSs in Barrow Strait (increasing influence of the Beaufort Gyre) could be the result of a shift of the AO mode (from AO^+ in early-middle Holocene to AO^- in middle-late Holocene). Based on driftwood records, *Dyke et al.* [1997] and *Tremblay et al.* [1997] found a major switch in

the path of the TPD at the onset of middle-late Holocene, which corroborates a change of the AO mode. Comparison of ice core $\delta^{18}O$ record from Devon Island Ice Cap and the reconstructed SSTs (August) from core 009 suggests a strong atmospheric/oceanic coupling throughout the Holocene in this area (Fig. 12) consistent with the impact of large-scale atmospheric pattern such as the Arctic Oscillation operating at the millennial time scale.

2.6.4 Historical climate changes

Dinocyst assemblages in core 009 BC are dominated by the two heterotrophic taxa *Islandinium minutum* and *Brigantedinium* spp. throughout the sequence. However, between 25 and 10 cm (from ~1600 to AD ~1800), the relative abundance of *Islandinium minutum* records a sharp decrease (from 50 to 25%). This is accompanied by an increase in the relative abundance of the heterotrophic taxon *Echinidinium* spp. (from 2% to 10%) suggesting more open water. During this time interval, quantitative estimates of past sea-surface conditions indicate a trend towards decreasing sea-ice cover (from about 9.5 to 8 months/year) with SSTs (August) slightly warmer than present conditions. From 10 cm to the top of the core (from ~AD 1800 to the beginning of AD 2000), the relative abundance of *Islandinium minutum* increases (from 25% to a maximum value of 75%). The reconstructed SSTs (August) suggest a slight cooling towards modern values. Based on dinocyst assemblages in cores from the Beaufort Sea, *Richerol et al.* [2008b] also argued for a warming trend from AD 1600 to 1800, whereas *Levac et al.* [2001] suggest a slight cooling of the SSTs during the last 200 years consistent with our records.

Core 004 BC spans approximately the last 400 years, from AD 1600 at the base to the beginning of AD 2000 at the top of the sequence. Dinocyst assemblages are dominated by *Islandinium minutum* and *Brigantedinium* spp. but include occurrence of other taxa such as *Islandinium* var. *cezare*, *Echinidinium karaense*, *Echinidinium aculeatum* and the cyst of *Polykrikos* Arctic morphotype. Quantitative estimates of past sea-surface conditions

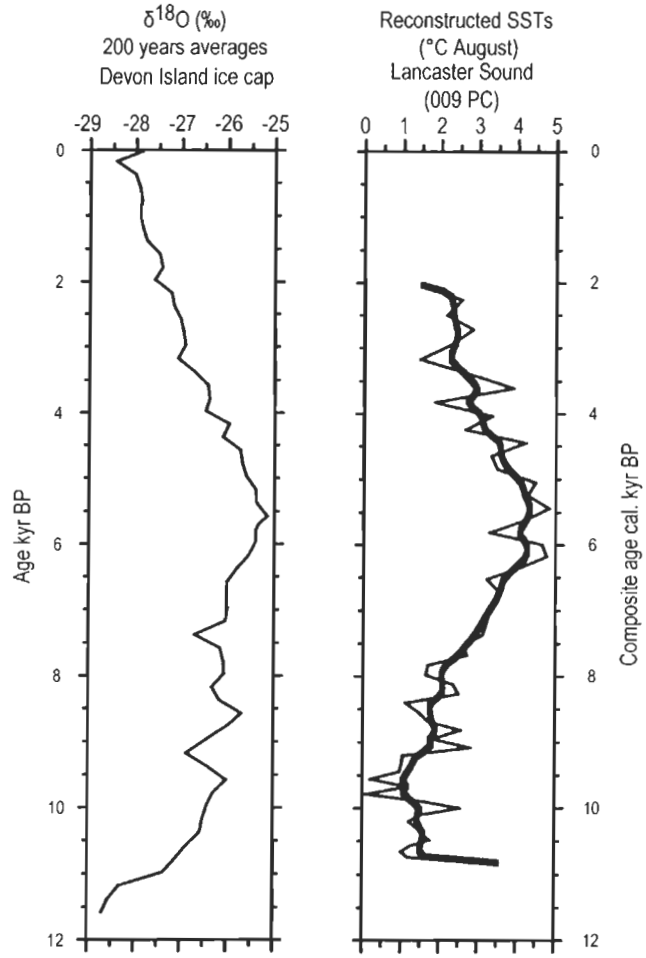

Fig. 12. Holocene ice core $\delta^{18}O$ records from Devon Island ice cap (200 years average) vs quantitative estimates of SSTs (August) from Lancaster Sound (core 009 PC). The thicker black line corresponds to a smoothing curve (10 pts) of the reconstructed SST. The comparison of the two diagrams shows the same trend suggesting a strong oceanic/atmospheric coupling throughout the Holocene in this area.

suggest warmer SSTs (August) throughout the sequence with maximum values of 4°C, which is about 2.5°C higher than present, at the base of the core (i.e., around AD 1600). A general trend of decreasing temperatures towards modern values is recorded in the uppermost part of the core.

2.7 Summary and Conclusion

Dinocyst assemblages and quantitative estimates of past-surface conditions reveal important climatic change throughout the Holocene in the easternmost and central part of the main axis of the Northwest Passage. During the early Holocene, both sites records high terrigenous inputs as suggested by high C/N ratio, high magnetic susceptibility and high detrital $CaCO_3$ content. This is accompanied in Lancaster Sound by an absence of dinocyst, whereas in Barrow Strait dinocyst assemblages are characterized by low species diversity, *Islandinium minutum* and *Brigantedinium* spp. making up more than 90% of the assemblages. We associate this dynamics with the last stage of the Innuitian deglaciation in this area, which is recorded during ~300 years in Lancaster Sound (from 11.1 to 10.8 cal. kyr BP) and during ~2000 years in Barrow Strait (from 10.8 to 8.5 cal. kyr BP). We explain this delay between the two sites by the presence of the main axis of the Innuitian uplift (zone of maximum thicker ice) following a NE/SW ridge [*England et al.*, 2006] in the north central CAA.

The first occurrence of dinocysts at 10.8 cal. kyr BP in Lancaster Sound marked the beginning of the biological productivity in surface waters. From 10.8 to 9 cal. kyr BP dinocyst assemblages were dominated by heterotrophic taxa (*Islandinium minutum* and *Brigantedinium* spp.). This is accompanied by relatively harsh conditions as suggested by

quantitative estimates of past sea-surface conditions indicating low SSTs (August) and extensive sea-ice cover (10 months/year). During this time interval, several ice-streams were active in northernmost Baffin Bay, Smith Sound and Kane basins and the WGC and IC were not yet fully established [*Zreda et al.,* 1999; *Lloyd et al.,* 2005; *England et al.,* 2006; *Olafsdottir et al.,* 2006; *Dyke,* 2008; *Ren et al.,* 2009]. Thus, the reconstructed harsh conditions in Lancaster Sound from 10.8 to 9 cal. kyr BP are most likely due to the presence of an active ice-stream together with a limited or absence of influence of the warm intermediate Atlantic water mass.

After 8.5 cal. kyr BP, both sites recorded opposite trends with maximum reconstructed SSTs reached between 6 and 5 cal. kyr BP (~3°C more than modern conditions) in Lancaster Sound and minimum SSTs in Barrow Strait around 6 cal. kyr BP (~3°C lower than modern conditions). These are accompanied by an increase in the relative abundance of phototrophic taxa in Lancaster Sound. We associate the warmer trend in Lancaster Sound with a gradual increase in the influence of the warm intermediate Atlantic water in the upper water column due to the gradual establishment of the WGC. Maximum sea-surface temperatures were also found in cores along or near the WGC, IC, NAC and NwAC [*Levac et al.,* 2001; *de Vernal and Hillaire-Marcel,* 2006; *Ren et al.,* 2009] during the early-middle Holocene. This was associated with a maximum inflow rate of Atlantic water into the Arctic but with a strong decoupling between the surface layer and the Atlantic water mass in the western Arctic promoting the formation of sea-ice [*Hillaire Marcel et al.,* 2004; *de Vernal et al.,* 2005b]. This sharp halocline in the western Arctic is probably due to an increase of Eurasian rivers runoff, which fed the Canada Basin. The

inflow of this low salinity water from the Canada Basin into the central CAA through M'Clure Strait is consistent with the marked decreased of the reconstructed SSSs (August) and the final collapse of the Wellington channel ice-stream around 8.5 cal kyr BP [*Dyke et al.,* 2002; *England et al.,* 2006]. In modern conditions, such a sea-ice dipole pattern between the eastern and western Arctic accompanied by a maximum inflow of Atlantic water and an increase of Eurasian rivers runoff is closely related to the positive mode of the AO [*Dickson et al.,* 2000; *Peterson et al.,* 2002; *Rigor et al.,* 2002; *Steele and Ermold,* 2004].

During the late Holocene, the reconstructed sea-surface conditions indicate cooler conditions in Lancaster Sound and warmer conditions in Barrow Strait, suggesting a possible shift of the AO mode (from AO^+ to AO^-) consistent with decreasing SSSs in core 004 PC and changes in driftwood delivered in the CAA [*Dyke et al.,* 1997]. At the scale of the Holocene, our records in the central and eastern part of the main axis of the Northwest Passage indicate major oceanographic changes after 8.5 cal. kyr BP. These major changes are marked by the gradual establishment of the WGC consistent with the onset of an active site of intermediate water formation in the Labrador Sea [*Hillaire-Marcel et al.,* 2001]. This large oceanic reorganization following the last deglaciation could have enhanced a strong oceanic/atmospheric coupling as suggested by the comparison of SSTs (August) in Lancaster Sound and $\delta^{18}O$ record from Devon Island Ice Cap. Therefore, our records seem to confirm the strong coupling between the atmosphere and the ocean in the meridional advection of heat flux from the North Atlantic Ocean to the Arctic Ocean similar to the effect of the Arctic Oscillation.

2.8 Acknowledgements

This work was funded by the ArcticNet Network of Centres of Excellence and the Natural Science and Engineering Research Council (NSERC) of Canada. This is a contribution to the ArcticNet project 1.6, the Polar Climate Stability Network (PCSN) supported by the Canadian Foundation for Climate and Atmospheric Science (CFCAS), and the NSERC-IPY project "International Polar Year: Natural climate variability and forcings in Canadian Arctic and Arctic Ocean".

We wish to thank the officers and crew of the CCGS *Amundsen* for their help and support during sampling. We also wish to express our gratitude to the following people who helped during the collection and analysis of the samples (Robbie Bennett, Bedford Institute of Oceanography; Trecia Schell, Dalhousie University; Sylvain Leblanc, Pierre Simard and Guillaume Auclair, UQAR). Thanks are due to Bassam Ghaleb and Jean-François Hélie (GEOTOP) for geochemical and isotope analyses. Discussions with Francesco Barletta (ISMER-GEOTOP) improved this research. We also wish to thank Monika Korte for the CALS7K.2 inclination data for cores 009 and 004 PC. We are grateful to the two anonymous reviewers for their comments, which helped to improve the manuscript.

CHAPITRE 3

HOLOCENE SEA-ICE HISTORY AND CLIMATE VARIABILITY ALONG THE MAIN AXIS OF THE NORTHWEST PASSAGE, CANADIAN ARCTIC

3.1 Abstract/Résumé

Palynological, geochemical and physical records were used to document Holocene paleoceanographic changes in marine sediment cores from Dease Strait in the western part of the main axis of the Northwest Passage (core 2005-804-006 PC/BC, latitude 68°59.5N, longitude106°34.4W and latitude 68°N, longitude 106°34.5W). Quantitative estimates of past sea-surface were inferred from the modern analogue technique applied to dinoflagellate cyst assemblages. The chronology of core 2005-804-006 PC is based on a combined used of the paleomagnetic secular variation records and the CALS7K.2 time-varying spherical harmonic model of the geomagnetic field. The age-depth model indicates that the core spans the last ~7700 cal years B.P., with a sedimentation rate of 61 cm kyr^{-1}. The reconstructed sea-surface parameters were compared with those from Barrow Strait and Lancaster Sound (core 2005-804-004 PC/BC and core 2004-804-009 PC/BC, respectively), which allowed us to draw a millennial scale Holocene sea-ice history along the main axis of the Northwest Passage (MANWP). Overall, our data are in good agreement with previous studies based on bowhead whale remains. However, dinoflagellate sea-surface based reconstructions suggest several new features. The presence of dinoflagellate cysts in the three cores for most of the Holocene indicates that the MANWP was partially ice-free over the last 10 000 years. This suggests that the recent warming observed in the MANWP could be part of the natural climate variability at the millennial time scale, whereas anthropogenic forcing could have accelerated the warming over the past decades. We associate Holocene climate variability in the MANWP with large-scale atmospheric pattern, such as the Arctic Oscillation, which may have operated since the early Holocene. Nevertheless, more local conditions such as the presence of coastal current, the halocline structure or the proximity of an ice-cap were of major influence on the sea-ice cover and created strong regionalism. This highlights the need to further develop regional investigations in the Arctic to provide realistic boundary conditions for climatic simulations.

Des traceurs palynologiques, géochimiques et physiques de sédiments marins prélevés dans le détroit de Dease, dans la partie occidentale de l'axe principal du passage du Nord-Ouest (carotte 2005-804-006 PC/BC, latitude 68°59.5N, longitude 106°34.4W et latitude 68°N, longitude 106°34.5W), ont été utilisés afin de documenter les changements paléocéanographiques au cours de l'Holocène. La technique des analogues modernes a été

appliquée aux assemblages de kystes de dinoflagellés afin d'obtenir des estimations quantitatives des conditions de surface au cours de l'Holocène. La chronologie de la carotte 2005-804-006 PC est basée sur l'utilisation combinée des enregistrements des variations paléomagnétiques séculaires et du modèle harmonique sphérique temporellement variable du champ géomagnétique, CALS7K.2. Le modèle d'âge indique que la carotte couvre les derniers 7 700 années calibrées B.P. avec un taux de sédimentation de 61 cm/ka. Les paramètres de surface reconstruits ont été comparés avec ceux des sites des détroits de Barrow et de Lancaster (carotte 2005-804-004 PC/BC et carotte 2004-804-009 PC/BC, respectivement) nous permettant de dégager une histoire du couvert de glace à l'échelle millénaire le long de l'axe principal du passage du Nord-Ouest (APPNO). Nos données sont généralement cohérentes avec les études antérieures basées sur les restes de baleines à bosse. Cependant, les reconstitutions réalisées à partir des assemblages de kystes de dinoflagellés suggèrent plusieurs nouveaux éléments. La présence de kystes de dinoflagellés dans les trois carottes durant la majeure partie de l'Holocène indique que l'APPNO était partiellement ouvert et libre de glace durant les 10 000 dernières années. Cela suggère que le réchauffement actuel observé dans l'APPNO pourrait être dû à une variabilité climatique naturelle à l'échelle millénaire, tandis que les facteurs anthropiques pourraient avoir accéléré le réchauffement au cours des dernières décennies. Nous associons la variabilité climatique au cours de l'Holocène dans l'APPNO avec des patrons atmosphériques de grandes échelles, comme l'oscillation arctique, qui pourrait avoir agit depuis le début de l'Holocène. Néanmoins, des conditions locales comme la présence de courants de côte, la structure de l'halocline ou la proximité de glaciers ont été d'une influence majeure sur le couvert de glace, et ont crée un régionalisme marqué. Cette étude souligne l'importance de développer des recherches au niveau régional dans l'Arctique pour fournir des conditions réalistes aux simulations climatiques.

3.2 Introduction

Major hydrographical changes took place in the Arctic over the past few decades. The decline of sea-ice cover extent, which began in the late 1970s, has accelerated since 1998 reaching a historical record low in the summer of 2007 [*Comiso et al.,* 2008; *Deser and Teng*, 2008; *Stroeve et al.,* 2008]. This minimum was 25% lower than the previous summer 2005 record and 40% lower than the 1979-2006 average based on satellite measurements [*Schweiger et al.*, 2008]. This reduction in sea-ice has occurred mainly in the western sector of the Arctic Ocean and on the Russian shelves. Satellite-derived summer mean sea-surface temperature (SST) anomalies since 2000 reveal warm anomalies during 2002-2005 over the Bering Strait, the Beaufort and the eastern Siberian seas [*Steele et al.,* 2008]. This "Arctic warm period" [*Overland et al.*, 2008] has been mostly associated with changes in the atmospheric circulation identified as the Northern Annular Mode (NAM), also known as the Arctic Oscillation (AO) [*Thompson and Wallace*, 1998] or the closely related North Atlantic Oscillation (NAO) [*Deser et al.,* 2000; *Dickson et al.*, 2000; *Hurrell and James,* 2003; *Hurrell and Deser*, in press]. The AO creates a marked SST and sea-ice dipole pattern between the eastern and western Arctic [*Rigor et al.,* 2002; *Zhang et al.*, 2003; *Vavrus and Harrison*, 2003]. Dinoflagellate cyst assemblages in cores from the Labrador Sea [*de Vernal et al.*, 2001], Baffin Bay and Hudson Strait [*Levac et al.,* 2001; *Rochon et al.,* 2006] suggest a reduced sea-ice cover during the early Holocene, whereas cores from the Beaufort and Chukchi seas indicate a steady decrease of sea-ice cover from the early to late Holocene [*de Vernal et al.,* 2005a; *Rochon et al.,* 2006; *McKay et* al., 2008]. Similarly, *Ledu et al.* [2008a,b, submitted] reconstructed an opposite trend between the easternmost

(Lancaster Sound) and central (Barrow Strait) part of the MANWP during the same interval. The dipolar character of sea-surface parameters has also been inferred from dinoflagellate cyst assemblages in the northern North Atlantic during the Holocene [*Solignac et al.*, 2004; *de Vernal* and *Hillaire-Marcel*, 2006].

The main objective of this paper is to better understand the spatial character of this dipolar structure in the Arctic Ocean, i.e. to spatially define the east-west thermal gradient, and to better understand the mechanism(s) behind its potential variability at the millennial time scale. For this purpose, marine sediment cores in the westernmost (Dease Strait), central (Barrow Strait) and easternmost (Lancaster Sound) part of the MANWP were collected during the ArcticNet oceanographic campaigns of summer 2004 and 2005. Due to their strong relationship with sea-surface parameters in the Arctic and sub-arctic seas [*Rochon and de Vernal,* 1994; *de Vernal et al.,* 2001, 2005b; *Kunz-Pirrung,* 2001; *Mudie and Rochon*, 2001; *Radi et al.,* 2001; *Matthiessen et al.,* 2005; *Richerol et al.,* 2008a,b; *de Vernal and Marret*, 2007], their relatively high species diversity and good preservation in polar sediments [*Kokinos et al.,* 1998; *de Vernal et al.,* 2001; *Rochon,* 2009], dinoflagellate cysts were used as tracer of past sea-surface conditions. Quantitative estimates of the duration of sea-ice cover (months/year) as well as summer sea-surface temperature (SSTs) and salinity (SSSs) were derived from the modern analogue technique [*de Vernal et al.*, 2001, 2005b]. This method yields one of the lowest root mean square errors of prediction (RMSEP) among transfer function techniques [*Guiot and de Vernal*, 2007]. Here we present the new results from Dease Strait and we compare sea-surface reconstructions with

those from cores recovered from Barrow Strait and Lancaster Sound [*Ledu et al.*, 2008a, submitted].

3.3 Environmental settings

3.3.1 Hydrography of the western Arctic

The MANWP connects the eastern and western Arctic across the Canadian Arctic Archipelago (CAA), which is one of the largest continental shelves in the Arctic Ocean [*Jakobsson*, 2002, 2004]. With the exception of the area of Lancaster Sound in the easternmost part of the MANWP, where major rift structures formed during the early Cretaceous [*Okulitch and Trettin*, 1991] reach depths of more than 500 m, nearly all the channels of the CAA were deepened by glacial and fluvial erosion during the Quaternary. As a result, about 70% of the channels in the CAA are shallower than 500 m depth and become deeper toward the eastern side of Barrow Strait. The mean depth in the western part of the MANWP was estimated at ~125 m [*Jakobsson*, 2004; *McLaughlin et al.*, 2004]. The flow through the MANWP has an eastward component related to the sea-level elevation difference across the CAA between the Arctic Ocean and Baffin Bay [*Kliem and Greenberg*, 2003]. Water in the western part of the MANWP is derived from the Canada Basin through Amundsen Gulf and M'Clure Strait. This flow is strongly associated with the Beaufort Gyre (BG) and the transpolar drift (TPD), which both contribute to sea-ice and freshwater export from the western to the eastern Arctic. The stratification in the Canada Basin is relatively complex because of multiple layers that composed the halocline. The upper 50 to ~100 m of the water column is occupied by a cold low salinity mixed layer (ML), which is influenced in summer by sea-ice melt, river plume spreading and by brine

rejection during sea-ice formation in winter. The strong halocline between 40-50 m to ~200 m is characterized by a reverse thermocline and three major layers, which are mainly of Pacific origin. The upper halocline (between 40-50 m and 125 m) is composed of summer Pacific water including both the relatively warm and fresh Alaskan Coastal Current water (ACCW, $31<S<32$ and $1°C<T°<6°C$) and the relatively colder and saltier summer Bering Sea water (sBSW, $32<S<33$ and $0°C<T°<2°C$). The middle and lower halocline (between 125 and 200 m) are composed of the winter Bering Sea water (wBSW) near the freezing point with salinity ranging from 32.5 to 33.1. The respective importance and mixing of these water masses varies in time and space within the Canada Basin [*Steele et al.,* 2004]. In the northern BG, the ACCW overlies the summer Bering Sea water, which flows above the winter Bering Sea water. In contrast, in the southern BG the ACCW overlies wBSW [*Steele et al.,* 2004]. The warm (up to 3°C) and salty (~34.5) intermediate Atlantic water flows between 200 and 800 m [*Shimada et al.,* 2001; *McLaughlin et al.,* 2004; *Steele et al.,* 2004]. Below 800 m, only the deep-water masses of Atlantic-origin are found [*Carmack et al.,* 2008; *Steele et al.,* 2004]. As a consequence almost all the water flowing from the Canada Basin to the MANWP is of Pacific origin [*Jones et al.,* 2003]. Therefore, the CAA appears as a major gateway for low salinity water export from the western Arctic to the northern North Atlantic via Baffin Bay and Labrador Sea. Its contribution to this export has been estimated to ~100 mSv, which is about the same order of the total annual runoff in the Arctic Ocean [*Melling,* 2004; *Prinsenberg and Hamilton, 2005*; *Dickson et al., 2007*]. Nevertheless, it has been shown that both the low salinity water content of the Canada Basin and its export into the CAA as well as the flux from the CAA to the North Atlantic

Ocean were strongly influenced by the state of the AO mode [*Dickson et al.,* 2000; *Proshutinsky et al.,* 2002; *Steele et al.,* 2004; *Prinsenberg and Hamilton*, 2005]. During the negative mode of the AO, wind conditions are more anticyclonic and the BG is largely expanded, whereas the transpolar drift (TPD) is deflected toward Russian shelves enhancing a decrease of water transport (including sea-ice) through Fram Strait and an increase throughout the CAA. During positive mode of the AO the reverse trend is observed. Instrumental data reveal that this alternating wind-driven system has operated at annual and decadal time scales over the past 40 years across the Arctic Ocean [*Proshuntisky and Johnson,* 1997; *Johnson et al.,* 1999; *Polyakov and Johnson,* 2000; *Venegas and Mysak,* 2000; *Dukhovskoy et al.,* 2004; *Polyakov et al.,* 2004]. Recent studies suggest that it could have operated since the early Holocene [*Darby and Bischof*, 2004; *de Vernal et al.,* 2005a; *Ledu et al.,* 2008a, submitted; *McKay et al.,* 2008; *Fréchette and de Vernal*, 2009]. Although the chronological resolution of Holocene sedimentary records in the Arctic generally does not permit inference on annual to decadal frequency of positive and negative AO modes, it may serve to document what has been the dominant mode.

3.4 Material and methods

3.4.1 Coring site and palynological preparation

Sampling in the MANWP was carried out in the summers of 2004 and 2005, during leg 9 and leg 1 of the ArcticNet oceanographic campaigns aboard the CCGS *Amundsen*. The sampling sites were selected using a Simrad EM 300 multibeam echosounder and a Simrad 3.5 kHz sub-bottom profiler to avoid disturbed sediment areas (i.e., erosion, mudflows and/or mass movements). Cores from Dease Strait, Barrow Strait and Lancaster

Sound were collected using a piston and box corer (hereinafter, referred to as cores 006 PC/BC, 004 PC/BC and 009 PC/BC, respectively (for details see Table 1 and Fig 1).

Table 1. Geographic coordinates of the coring sites in Dease Strait (core 2005-804-006), Barrow Strait (core 2005-804-004) and Lancaster Sound (core 2004-804-009). The length of the cores and the water depth are also indicated

Cores ID	Latitude N	Longitude W	Length of the core (cm)	Water depth (m)
2005-804-006 PC	68°59.5	106°34.4	400	118
2005-804-006 BC	68°	106°34.5	35	117
2005-804-004 PC	74° 16.1	91° 05.4	670	350
2005-804-004 BC	74° 16.1	91° 04.4	35	350
2004-804-009 PC	74° 11.2	81° 11.7	600	781
2004-804-009 BC	74° 11.2	81° 11.7	600	781

Sampling for palynological analyses was performed at a 10 cm sampling interval for the piston cores and 5 cm for the box cores. Each sub-sample was then processed according to the standard palynological preparation technique described in *Rochon et al.* [1999]. In summary, a first sieving on 5 cm^3 of wet sediment is made at 100 and 10 µm to remove coarse sand, fine silt and clay, respectively. The 10-100 µm fraction was then subjected to chemical treatments consisting of repeated hot HCl (10%, 4 treatments) and hot HF (49%, 3 treatments) acid attack to dissolve carbonates and silicates, respectively. The remaining fraction was then rinsed with distilled water to eliminate all traces of acid before a final sieving at 10 µm to remove the fluorosilicates and fine particles. Finally this fraction was mounted in glycerine gel between slide and cover slide. Palynomorphs (dinocysts, pollen grains and spores, acritarchs, organic lining of benthic foraminifers, chlorococcales) were then systematically counted using transmitted light microscopy (Nikon Eclipse 80 – I) at

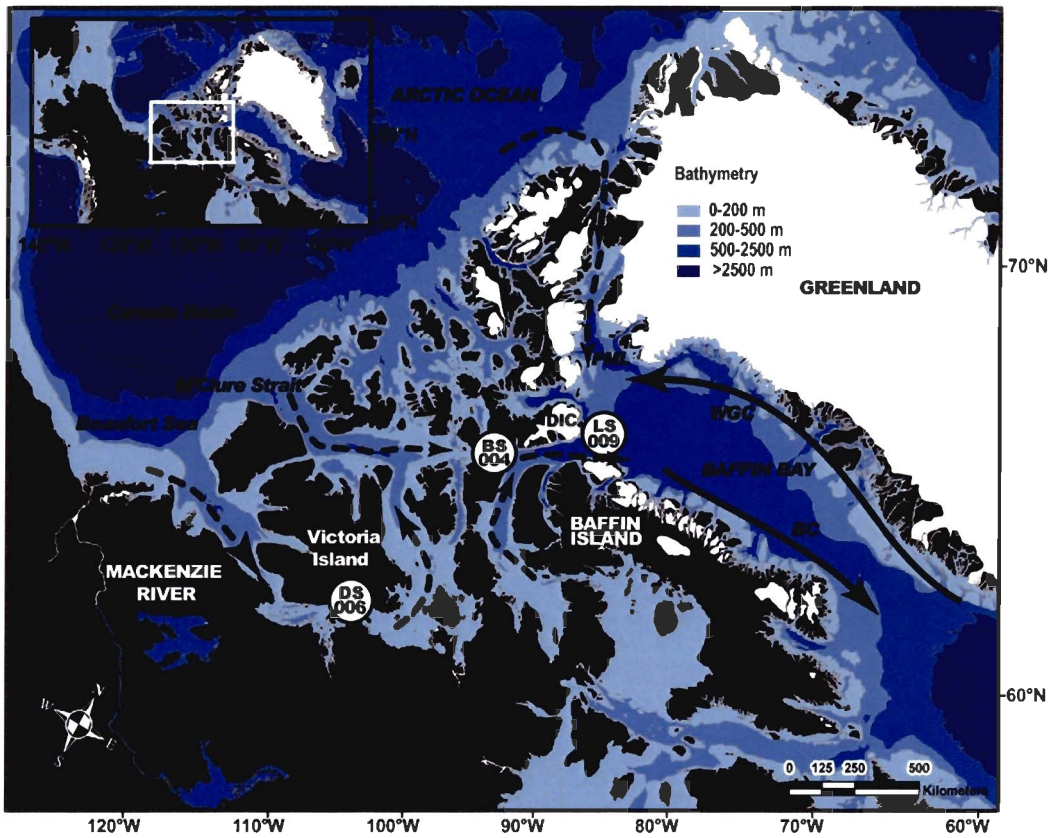

Figure 1. Location of the coring sites (white circles) at Dease Strait (DS 006), Barrow Strait (BS 004) and Lancaster Sound (LS 009) with major surface currents in the CAA. Modern ice caps are also shown (white coverage, DIC = Devon Island Ice Cap). The circulation in the CAA has an eastward component. Dashed black arrows correspond to the Polar Mixed Layer whereas the black arrows correspond to the Atlantic water (BC = Baffin Current; WGC = West Greenland Current; PML = Polar Mixed Layer).

200 to 400x. A minimum of 300 dinocysts was counted in each sample in order to obtain the best statistical representation. The addition of a marker spore tablet (*Lycopodium clavatum*, University of Lund, 1984, Batch N° 414831) of known concentration (12 100 ±1892 spores per tablet) before the first sieving allowed us to calculate the palynomorph concentration [*Matthews*, 1969].

3.4.2 Quantitative estimates of past sea-surface conditions

Quantitative estimates of past-sea surface conditions were made using the modern analogue technique (MAT) and the software R. MAT was applied to dinocyst assemblages following the procedures described in *de Vernal et al.* [2005b]. The method consists of comparing fossil assemblage samples with modern assemblages from a reference database. Here, we used the updated reference dinocyst database, which includes 64 taxa and 1189 sites from the North Atlantic, North Pacific, Arctic Ocean and sub-polar seas [*de Vernal et al.,* 1997, 2001, 2005b; *Radi and de Vernal,* 2008]. The distance or degree of dissimilarity between the fossil spectrum to be analysed and the spectra in the reference database is calculated after logarithmic transformation of percentage data. The modern spectra with the lowest distance then permit identifying the best modern analogues. Here, we used a set of five modern analogues from which hydrographic parameters (SSTs and SSSs and the duration of sea-ice cover expressed as the number of months per year with sea-ice concentration greater than 50%) were averaged after weighting inversely to the distance of the analogues. This average constitutes the most probable estimates. The hydrographic data are compiled using the 2001 version of the World Ocean Atlas [*NODC*, 2001], in addition to the duration of sea-ice cover which is derived from the 1953-2000 dataset provided by the National Snow and Ice Data Center [*NSIDC*], in Boulder, Colorado.

Quantitative estimates of sea-surface conditions using MAT yields good results as indicated by coefficients of correlation greater than 0.93 between estimated and instrumental hydrographic parameters. The degree of accuracy of the estimated reconstructions is obtained by the calculation of the standard deviation of the residual

(estimated minus observed values), which is ±1.5°C for the SSTs, ±1.8 for the SSSs and ±1.1 months/year for the duration of sea-ice cover. Modern conditions in Dease Strait are 8.5±1.3 months/year for the sea-ice cover, 3.9±2°C and 25±3 for the August SSTs and SSSs, respectively [*NSIDC*, 1953-2000; *NODC*, 2001].

3.4.3 Carbon and nitrogen stable isotopes

Geochemical analyses (organic carbon and total nitrogen) were performed at the Geochemistry and Geodynamics Research Center (GEOTOP), Montréal. The procedure consists of taking a sediment sample aliquot that is dried, ground and analysed for its total carbon and nitrogen content. A second aliquot is acidified with HCl in order to dissolve carbonates, washed and analysed for the C_{org} content. C_{inorg} is then calculated by the difference between the two measurements. The $CaCO_3$ content of each sample was determined from the molar weight of $CaCO_3$ (100g) and its content in C_{org} (12g) allowing to calculate the calcium carbonate equivalent. The carbon isotopic composition of organic matter ($\delta^{13}C$) was measured on the acidified aliquot by continuous-flow mass spectrometry using a Carlo-Erba elemental analyzer connected to an Isoprime mass spectrometer. It is expressed in standard notation δ versus VPDB. The error, which is based on replicate analyses, is ± 0.004% for N, ±0.015% for C and ±0.1‰ for the $\delta^{13}C$.

Grain size measurements (fraction between 0.04 – 2000 μm) were performed at the Institut des sciences de la mer de Rimouski (ISMER) using a Beckman-Coulter LS 13320 laser diffraction grain size analyser. Grain size distribution and statistical parameters (mean and standard deviations) were derived from the Gradistat software [*Blott and Pye* 2001]. The whole core low field volumetric magnetic susceptibility (k_{LF}) of the sediment was

determined at 2 cm intervals using a GEOTEK multi sensor core logger (MSCL) on board the CCGS *Amundsen*. k_{LF}, depends mainly to the concentration of ferromagnetic minerals (e.g., magnetite) but is also grain size dependent [*e.g.*, *Dunlop and Özdemir* 1997].

3.4.4 Color reflectance

Diffuse spectral reflectance was measured with a X-Rite digital swatchbook DTP-22 hand-held spectrophotometer on board the CCGS *Amundsen*. Reflectance data were then converted in the L*a*b* color space. High values (low values) of L* indicate white (black) color, whereas positive (negative) values of a* indicate red (green) and positive (negative) values of b* correspond to yellow (blue). The L*a*b* data were used to estimate missing sediment due to the piston coring process (Fig 2).

3.4.5 Paleomagnetic measurements

Paleomagnetic measurements for the piston cores were performed at the Sedimentary Paleomagnetism Laboratory at ISMER, using a 2-G Enterprises Model SRM-755 cryogenic magnetometer. The natural remanent magnetization (NRM) was measured on u-channels (rigid u-shaped plastic liners with a 2 cm square cross section and a length of ~1.5 m) at 1 cm intervals. However, due to the finite spatial resolution of the magnetometer's pickup coils, each measurement integrates a stratigraphic interval of 5 cm [*Weeks et al.*, 1993]. In order to eliminate this edge effect, the data from the upper and lower 5 cm of each u-channel were excluded. To isolate the characteristic remanent magnetization (ChRM), the NRM was measured and progressively demagnetized applying peak alternative fields (AF)

of 0 to 80 mT at 5 mT increments. The component inclination of the ChRM (ChRM I) was calculated using a least-square line fitting procedure [*Kirschvink*, 1980]. In addition, the

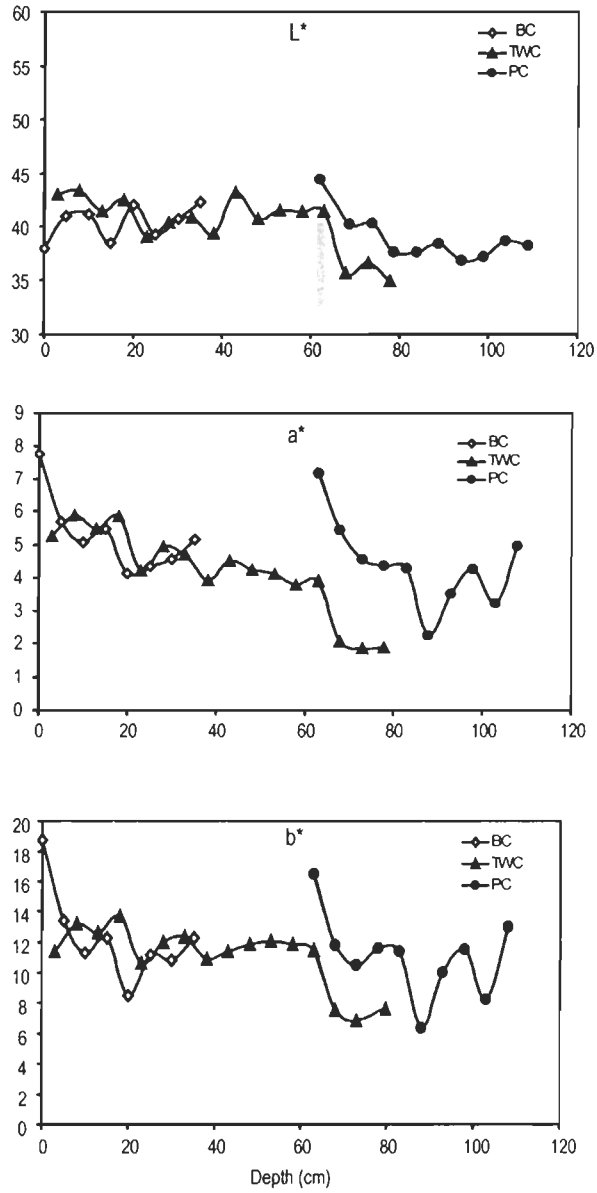

Figure 2. Diagrams showing the color reflectance (L*a*b*) for cores 006 PC, TWC and BC, used here to estimate top piston core sediment missing due to piston coring process. (see text for details). The grey line indicates that about 63 cm of sediment from core 006 PC was lost during coring process. Note that only the upper 110 cm of core 006 PC is shown.

precision of the best-fit procedure was estimated by the maximum angular deviation (MAD) [*Kirschvink,* 1980]. Lastly, the median destructive field of the NRM (MDF_{NRM}, the value of the peak AF field necessary to reduce the NRM intensity to half of its initial value) was derived in order to characterize changes in magnetic grain size and mineralogy.

3.4.6 Chronology of the cores

In the study core, biogenic carbonate was too rare for accelerator mass spectrometry (AMS) ^{14}C measurements and the chronostratigraphy is based on geomagnetic directional changes, also known as paleomagnetic secular variations (PSV). Arctic Holocene magnetic inclination and declination profiles have been correlated from distant as well as proximate sites [*Lund,* 1996; *Andrews and Jennings,* 1990; *Stoner et al.,* 2007; *Barletta et al.,* 2008a, b; *Besonen et al.,* 2008; *Lisé-Pronovost et al.,* in press; *Ledu et al.,* submitted]. Significant Holocene geomagnetic directional changes have been documented in high latitude environments (Baffin Bay, central Finland, northern Sweden, St Lawrence Estuary, Siberia, Russia, Fennoscandia, Iceland, Beaufort and Chukchi seas, Canadian Arctic and Alaskan margins and main axis of the Northwest Passage ([e.g., *Andrews and Jennings*, 1990; *Saarinen,* 1998; *Snowball and Sandgren*, 2002; *St-Onge et al.,* 2003; *Korte et al.,* 2005; *Korte and Constable,* 2005; *Snowball et al.,* 2007; *Stoner et al.,* 2007; *Barletta et al.,* 2008a; *Besonen et al.,* 2008, *Lisé-Pronovost et al.,* in press; *Ledu et al.,* submitted]). These PSV records have been used as a relative dating method [*Saarinen,* 1999; *Kotilainen et al.,* 2000; *St-Onge et al.,* 2003, 2004; *Breckenridge et al.,* 2004; *Stoner et al.,* 2007; *Barletta et al.,* 2008b; *Lisé-Pronovost et al.,* in press; *Ledu et al.,* submitted]. Recently, *Barletta et al.* [2008b], *Lisé-Pronovost et al.* [in press] and *Ledu et al.* [submitted] found a strong

consistency between the Holocene inclination data in cores from the Chukchi and Beaufort seas, the Alaskan margin, the MANWP and the calculated inclination using the CALS7K.2 time-varying spherical harmonic model of *Korte and Constable* [2005]. Due to their proximity to the north magnetic pole, cores from high latitudes have the potential to record higher amplitude directional changes, which are well represented by the CALS7K.2 model at the millennial to centennial time scale [*Barletta et al.,* 2008a; *Lisé-Pronovost et al.*, in press; *Ledu et al.,* submitted].

Here, we present a chronology for core 006 PC based on the combined used of PSV records (here the magnetic inclination) and the CALS7K.2 model [*Korte and Constable*, 2005].

3.5 Results

3.5.1. Lithological description and missing sediment

Core 006 PC is composed of two lithological units (see Fig 3). The first unit between 463 and 323 cm consists of olive gray mud (5Y 4/1, Munsell color chart) and is overlained by the second unit between 323 cm and the top of the core, which consists of reddish brown mud (5YR 5/4). Variable degree of bioturbation appears along the entire core but it is mostly developped in the upper lithological unit. Core 006 BC also consists of reddish brown mud (5YR 5/4) with traces of bioturbation between 10 and 20 cm. The comparison based on the L*a*b* color space between the trigger weight (TWC) and the piston cores (PC) indicate that about 63 cm was lost during the coring process (Fig 2). Note that all depths of core 006 PC are expressed in corrected depth, which account for the missing sediment.

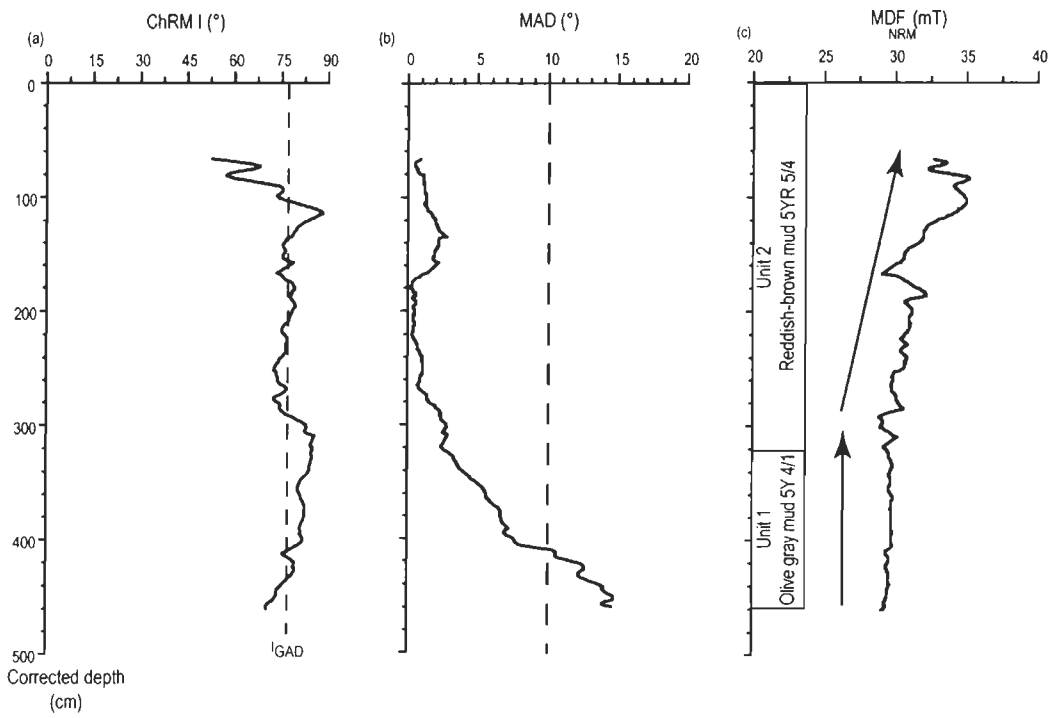

Figure 3. (a and b) Diagrams showing the characteristic remanent magnetization of the component inclination (ChRM I) and the maximum angular deviation (MAD) values for core 006 PC. The vertical dashed line is the value of the geocentric axial dipole (GAD) for the ChRM I at Dease Strait site. (c) Diagram showing the median destructive field of the NRM (MDF_{NRM}, see text for details) and the lithological units of core 006 PC. Note the two distinct trends in the MDF_{NRM} parameter (as indicated by arrows) associated with the gradual change in color sediment (colors are given according to the Munsell soil color charts)

3.5.2 Paleomagnetic secular variation records and composite age-depth model

The AF demagnetization behaviour of the NRM of core 006 PC reveals the presence of two magnetic components: a low-coercivity magnetic component (viscous magnetization) easily removed in the 0-15 mT AF range and a stable, well-defined, magnetic component in the 20-80 mT AF range (Fig 4). Aside from the last 50 cm where the ChRM is less well defined (MAD>10°), MAD values are generally lower than 5°,

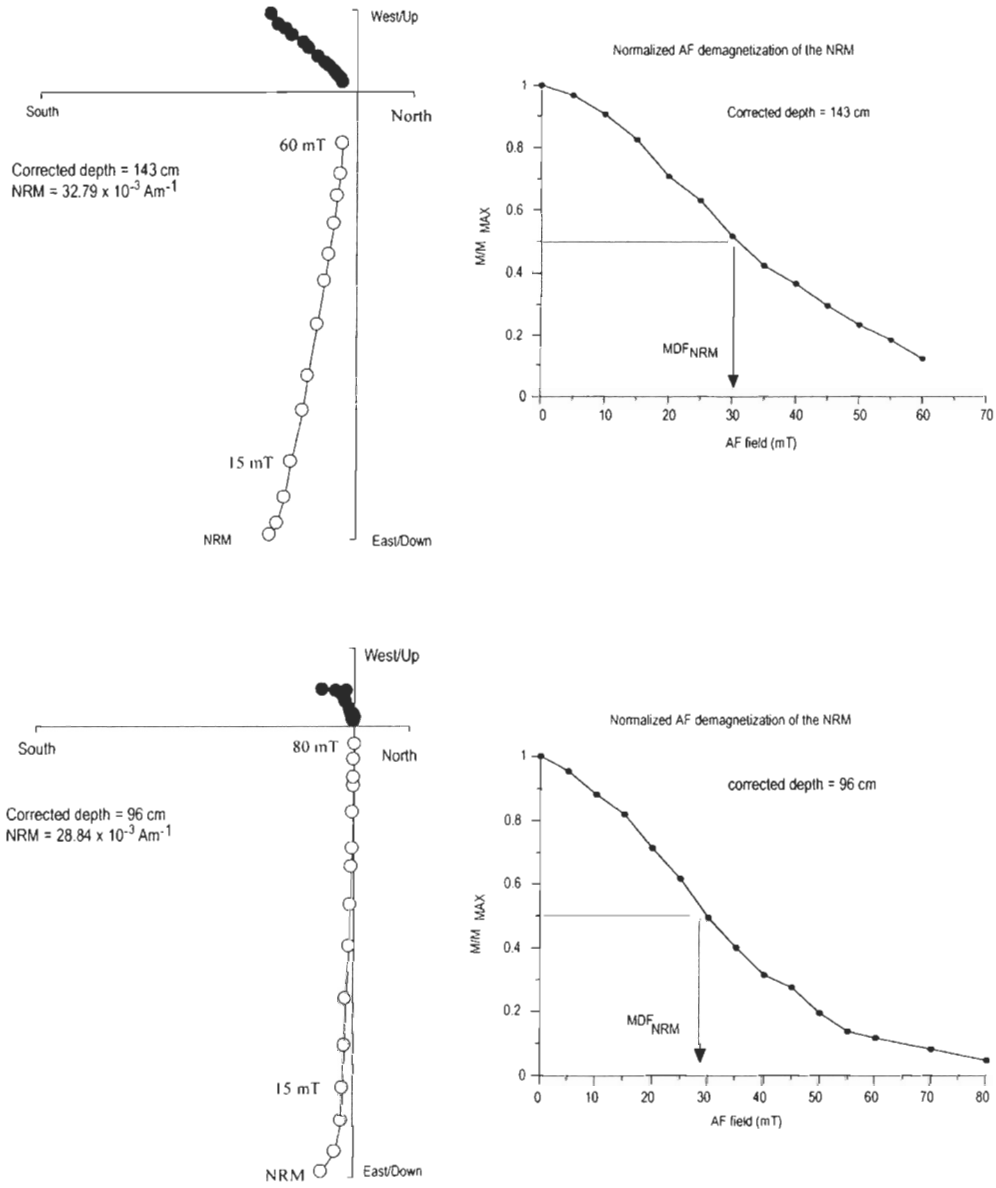

Figure 4. Typical vector end-point orthogonal projection diagrams [*Zijderveld*, 1967] at two selected depths (left diagrams). Solid data points indicate vector end-points projected onto the horizontal plane; open data points indicate vector end-points projected onto the vertical plane; numbers adjacent to data points are the AF demagnetization steps. In the right diagrams, the normalized AF demagnetization curves for the NRM are shown. At the 60 mT AF demagnetization step, only ~10% of the initial NRM is still present supporting the absence of high-coercivity magnetic components.

while the ChRM I fluctuate around the expected inclination value for a geocentric axial dipole model (I_{GAD} = 77°; [e.g., *Butler*, 1992]). Relatively uniform magnetic grain-size assemblage variations in the down-core MDF_{NRM} parameters are generally ascribed to changes in the coercivity of the magnetic minerals [*e.g. Stoner and St-Onge* 2007]. As revealed in Figure 4, the transitional change in color sediment is clearly associated with an increase of the MDF_{NRM}. In addition, red minerals are often associated with the presence of high-coercivity minerals (e.g., titanohematites; [*Dunlop and Özdemir* 1997]). Accordingly, variations in the MDF_{NRM} profile are probably due to change in magnetic mineralogy. According to *Stoner and St-Onge* [2007] titanomagnetites are the primary remanence carrier for high-quality PSV records. It is possible that high-coercivity minerals could affect the quality of the PSV record (i.e., the ChRM I). However, as revealed by the analysis of the Zijderveld diagrams (Fig 3), an extremely stable and well-defined (MAD <5°) magnetic component in the low-medium coercivity spectrum has been isolated. Based on these results, a possible effect of high-coercivity mineral(s) on the PSV record is negligible.

Furthermore, the MDF_{NRM} varies between 28.9 and 35.2 mT supporting the presence of a low-coercivity ferrimagnetic mineral (most likely magnetite) as principal carrier of the isolated ChRM (Figure 4). Accordingly, the magnetic properties of core 006 PC meet all the criteria necessary to have a reliable PSV record [e.g., *Stoner and St-Onge*, 2007].

Using the predicted magnetic inclination for our coring site over the last 7000 cal years B.P. computed from the CALS7K.2 model and the magnetic inclination of core 006 PC, we constructed an age-depth relationship based on 8 paleomagnetic tie-points that result from the comparison of both records (Fig 5 and Table 2). The age-depth model was

constructed using a linear fit between ages on a composite depth scale corrected for missing sediment due to the piston coring process (Figure 2 and Fig 6). In order to test

Table 2. Paleomagnetic tie-points used to construct the age-depth relationship for core 006 PC (see text for details)

Core	CALS7K.2 Age (cal years B.P.)	Depths equivalence (cm) (PSV correlation) *
2005-804-006 PC	1200	63
	2000	117
	2530	155
	3265	190
	3655	225
	4100	250
	5000	280
	5500	325

* Note that all the depths equivalence are expressed in a corrected depth, which accounts for missing sediment due to piston coring processes (see text for details)

the reliability of our age-depth model, we compared the magnetic inclination record of core 006 PC based on its new chronology with other Holocene PSV records from the western Canadian Arctic [*Barletta et al.,* 2008a; *Lisé-Pronovost et al.,* in press], and the western northern America (Fish Lake, Oregon, USA; [*Verosub et al.,* 1986]). Major shifts of the magnetic inclination are observed in all cores around 1000, 2000, 2500, 3500, 4500 and 5500 cal years B.P. and are on average 150±40 years from those recorded in core 006 PC (Figure 7a). Theses shifts are also well recorded by the CALS7K.2 model output and all paleomagnetic inclination records indicate a shallowing trend between ~6000 and ~2500 cal years B.P. (Fig 7a). The age-depth model indicates that core 006 PC spans the last 7730 cal years B.P, with a constant sedimentation rate of 61 cm kyr^{-1} (Fig 6). Chronologies for cores 009 PC and 004 PC are also based on a composite records between

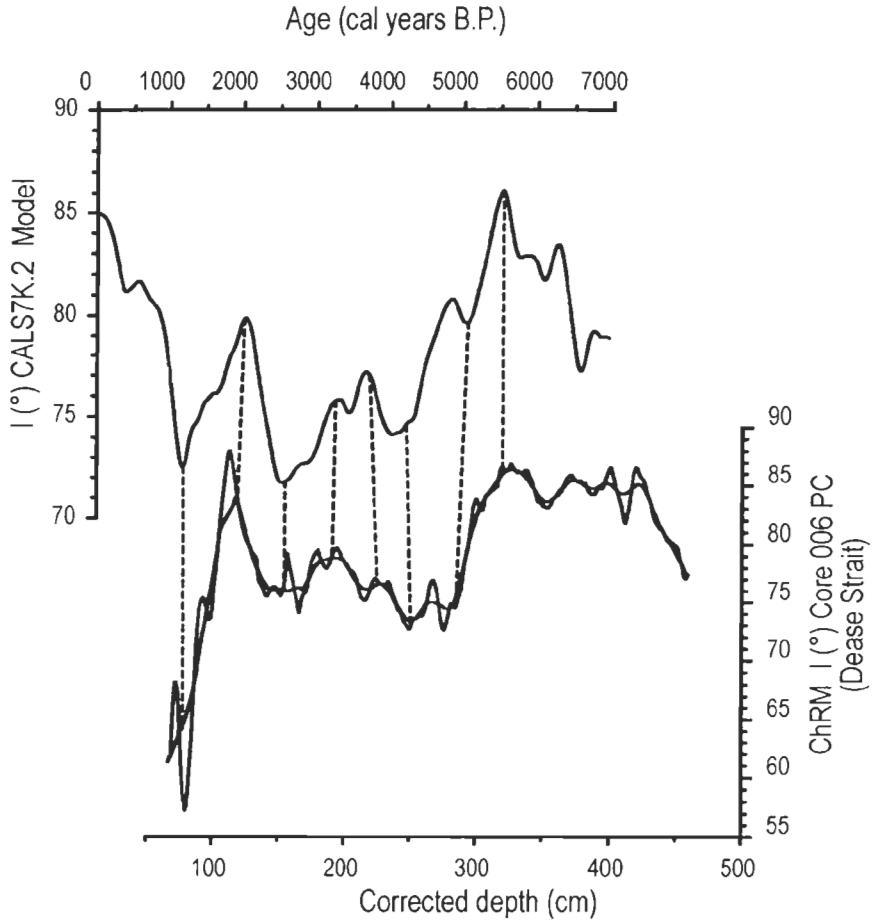

Figure 5. ChRM I for core 006 PC and magnetic inclination I (°) for Dease Strait inferred from the CALS7K.2 model. The dashed lines are the suggested correlations with the CALS7K.2 model [*Korte and Constable*, 2005].

the magnetic inclination and the predicted inclination for both sites derived from the CALS7K.2 (background data set, Fig 7b, appendix 4) [*Ledu et al.*, submitted]. The age depth models indicate that core 009 PC and 004 PC span approximately the last 11, 000 years. The calculated sedimentation rates range from 43 to 140 cm kyr^{-1} and from 15 to 118 cm kyr^{-1} for cores 009 and 004 PC, respectively (background data set, Fig 7b, appendix 4) Based on these sedimentation rates and the sampling interval, we can achieve a centennial to millennial time scale resolution.

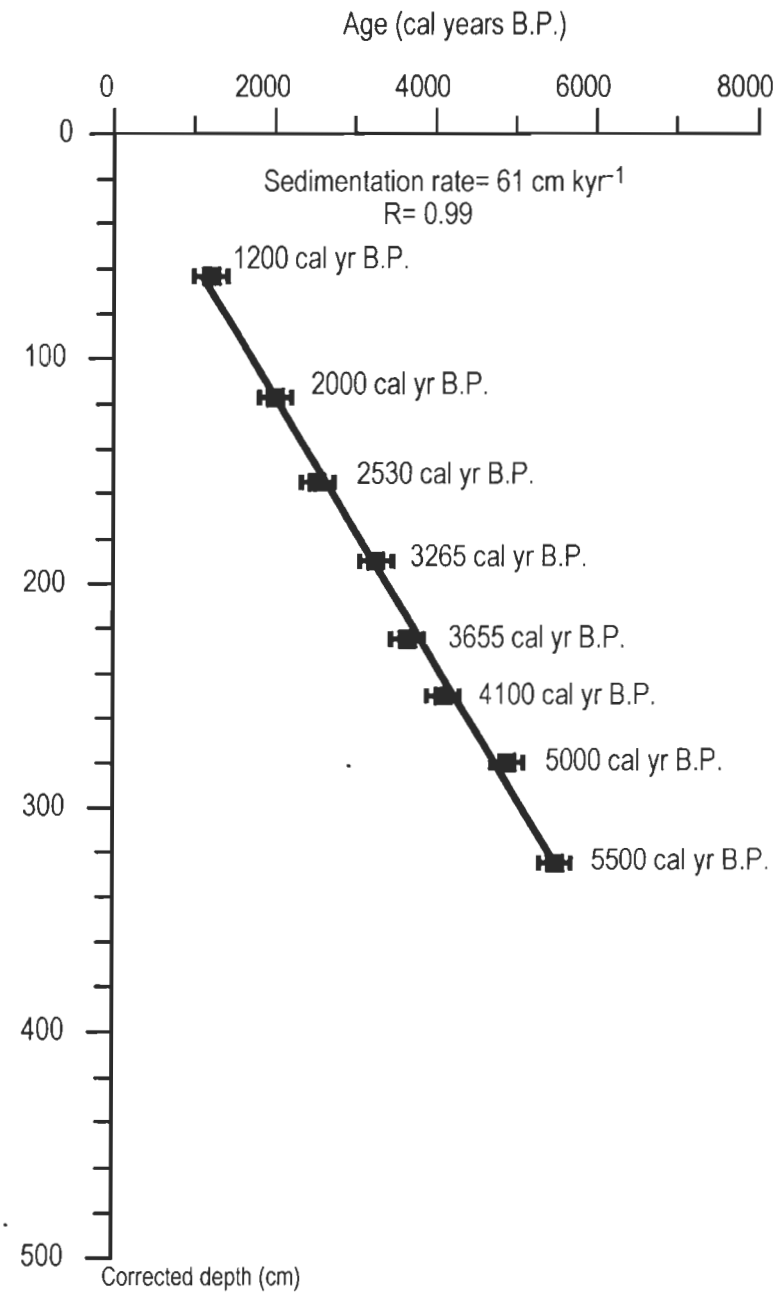

Figure 6. Age-depth model for core 006 PC based on correlations between PSV records (ChRM I) and the CALS7K.2 predicted inclination for Dease Strait. A linear fit was used to construct the age depth relationship (R = 0.99) and an error bar of ± 200 years was assigned to each age on the profil.

3.5.3 Grain size and stable isotopes

Grain size analyses (Fig 8) show the dominant silt (more than 75%) and clay fractions in cores 006 PC and BC. Geochemical data (Fig 8) indicate that carbon and nitrogen

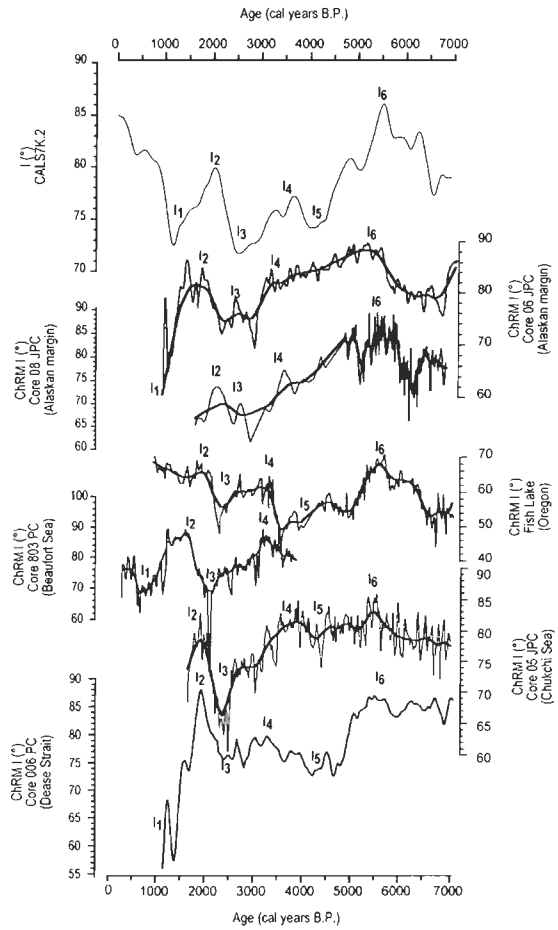

Figure 7a. Comparison of the characteristic remanent magnetisation of the component inclination (ChRM I) between cores 006 PC and other cores from the Chukchi and Beaufort seas [*Barletta et al.*, 2008a], North America (Fish Lake, Oregon, USA [*Verosub et al.*, 1986]), and the Alaskan margin [*Lisé-Pronovost et al.*, in press]. Core 006 PC is on its new composite chronology (see text for details). The uppermost diagram corresponds to the CALS7K.2 model of the predicted magnetic inclination for Dease Strait [*Korte and Constable*, 2005]. Major ChRM I shifts observed in all records occurred around 1000 (I_1), 2000 (I_2), 2500 (I_3), 3500 (I_4), 4500 (I_5), 5500 (I_6) cal years B.P. Note the shallow magnetic inclination, which is marked in all records between 6000 and 2500 cal years B.P.

content are relatively constant along the cores, except in the lower part of core 006 PC, between 6000 and 5000 cal years B.P. During this interval, the organic carbon content

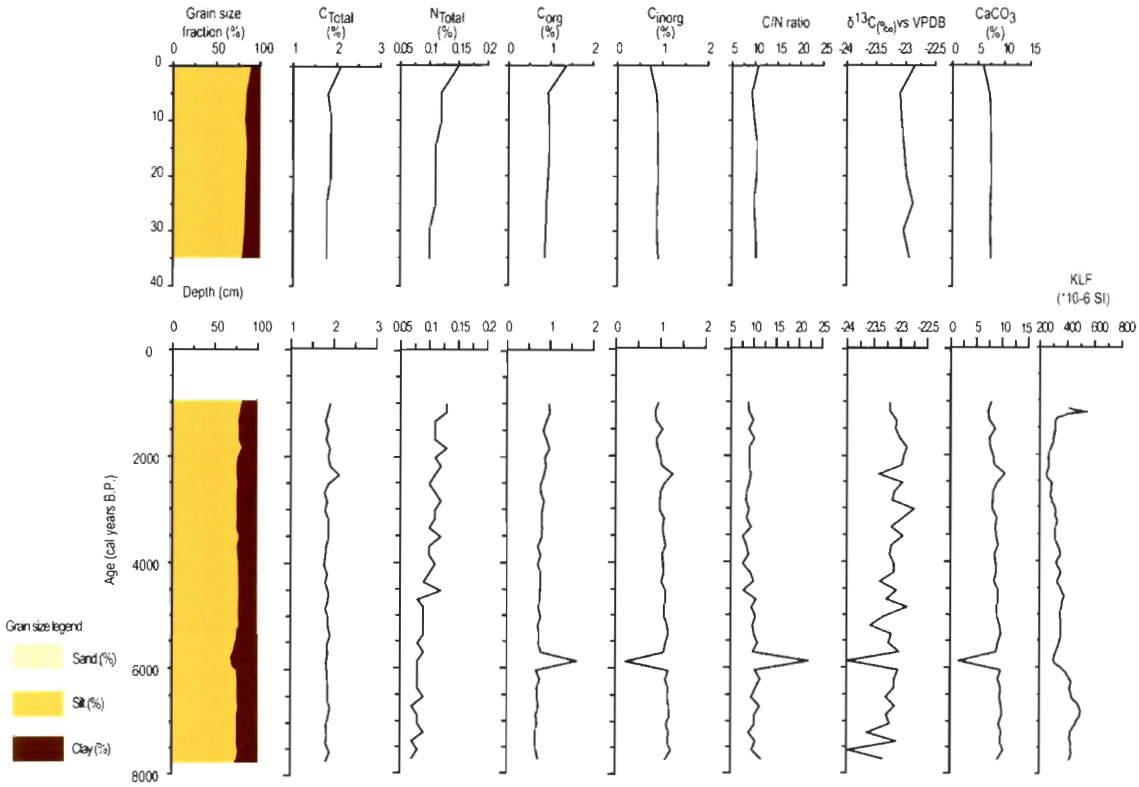

Figure 8. Grain size, carbon and nitrogen stable isotopes content of cores 006 BC and 006 PC. The magnetic susceptibility is also shown for core 006 PC.

(C_{org}) records its highest values (1.63%, core average 0.8%), whereas the inorganic carbon content (C_{inorg}) and $CaCO_3$ display their lowest values (0.2% and 1.6%, core average 1.05% and 9%, respectively). This is accompanied by high value of the C/N ratio (22, core average 9.8). During this time, the $\delta^{13}C$ depicts its lowest values (-23.9‰, core average –23.1‰ vs VPDB).

3.5.4 Dinocyst assemblages and reconstruction of sea-surface parameters

Well-preserved dinocysts are present throughout the core 006 PC with concentrations ranging from 950 to 10 930 cysts/cm^3 (mean 1935 cysts/cm^3) and maximum values were observed between 6000 and 5500 cal years B.P. (Fig 9). This corresponds to fluxes of 667

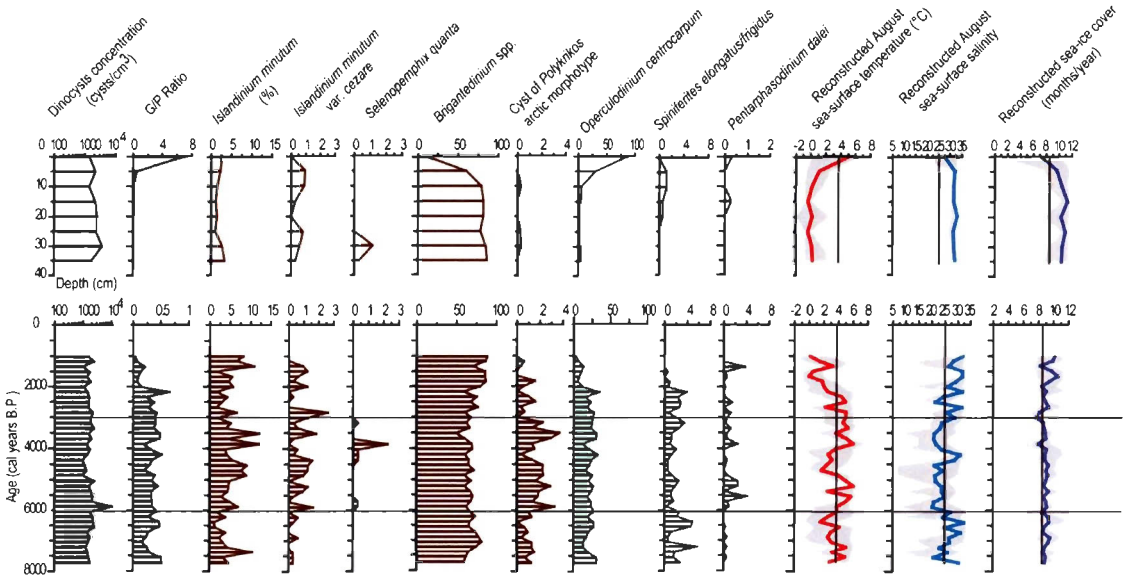

Figure 9. Diagram of dinocyst concentration, Gonyaulacales/Peridiniales (G/P ratio), relative abundance of dinocyst taxa and quantitative estimates of sea-surface conditions based on modern analogue technique (MAT) applied to dinocyst assemblages in cores 006 BC and 006 PC. The red, blue and purple lines correspond to the best estimates for the summer temperature and salinity (August) and the duration of sea-ice cover, respectively. The grey zones correspond to the minimum and maximum values possible according to the set of five best analogues. The vertical black lines indicate the values of modern sea-surface conditions and the horizontal grey lines are the different zones based on dinocyst assemblages (see text for details).

cysts/cm^2 year^{-1}, which reflect a high productivity. The ratio of phototrophic to heterotrophic dinocyst taxa (Gonyaulacales (G) / Peridiniales (P), G/P ratio) records values ranging from 0.03 to 0.66 (mean 0.32) indicating the dominance of heterotrophic taxa although photosynthetic taxa occur in significant number. Dinocyst assemblages are characterized by low species diversity, which is consistent with previous studies from the CAA [*Mudie and Rochon*, 2001; *Ledu et al.*; 2008a, submitted]. Core 006 PC is dominated

by three taxa that make up 90% of the assemblages: *Brigantedinium* spp., *Operculodinium centrocarpum* and *Islandinium minutum*. It is noticeable that the relative abundance of the heterotrophic taxon *Brigantedinium* spp. is higher than 50% throughout the core. Its maximum abundance in the Canadian Arctic has been associated with the Mackenzie freshwater plume in the Beaufort Sea or more generally with nutrient-rich area [*Mudie and Rochon,* 2001; *Richerol et al.,* 2008a,b] or polynyas [*Hamel et al.,* 2002].

Based on the relative abundance of dinocyst taxa, core 006 PC shows three different zones (Fig 9). The first zone, between 7730 and ~6000 cal years B.P. is dominated by *Brigantedinium* spp. and the phototrophic taxon *Operculodinium centrocarpum* (~15-20%). Other taxa of the assemblages are the heterotrophic taxa *Islandinium minutum* (5-10%), *Islandinium minutum* var. *cezare* (1%), the cyst of *Polykrikos* Arctic morphotype (1%) and the phototrophic taxon *Spiniferites elongatus/frigidus* (2-4%). Quantitative estimates of past sea-surface conditions suggest a sea-ice cover slightly above modern conditions (up to 1 month/year) with SSTs (August) that fluctuate around modern values but with a general decreasing trend. Minimum SSTs (August, 1°C) is reached around 6500 cal years B.P., which is 2.5° C cooler compared to modern conditions. This is accompanied by a general increase in SSSs (August).

The second zone between 6000 and 3000 cal years B.P. is also characterized by the dominance of *Brigantedinium* spp. (more than 50%) and *Operculodinium centrocarpum* (~ 25%) but it is marked by the occurrence of the phototrophic taxon *Pentapharsodinium dalei* and of the heterotrophic taxon *Selenophemphix quanta*. These are also marked by an increase in the relative abundance of *Islandinium minutum* var. *cezare* and the maximum

abundance of the cyst of *Polykrikos* Arctic morphotype. The reconstructed SSTs and SSSs (August) fluctuate around modern conditions. Maximum SSTs (August) are reached at ~5500, 5200 and 4000 cal years B.P. and corresponds to an increase of 2.5°C with regards to modern conditions whereas minimum values are reached around 4700 cal years B.P. (2.5°C lower than modern). Sea–ice cover is rather stable and similar to that of the first zone.

The third zone, between 3000 and 1000 cal years B.P. is marked by both the gradual increase dominance of *Brigantedinium* spp. and the gradual decrease in the relative abundance of *Operculodinum centrocarpum.* In the uppermost part of the zone, the relative abundance of *Brigantedinium* spp. reaches 88%, whereas that of *Operculodinium centrocarpum* is around 10%. These are also accompanied by the disappearance of *Selenopemphix quanta* and *Spiniferites elongatus/frigidus.* Quantitative estimates of past sea-surface parameters indicate a general cooling trend with minimum values of 0°C in August at 1500 and 1000 cal years B.P., which is 3.5°C lower than modern conditions. The cooling trend is accompanied by SSSs (August) and sea-ice cover increase. Maximum sea-ice cover is reached at 1500 and 1000 cal years B.P. with values ~1.5 months/year more than present conditions.

Core 006 BC also shows well-preserved dinocyst with concentrations ranging from 1377 to 3635 cysts/cm^3 (average 2148 cysts/cm^3). Dinocyst assemblages are strongly dominated by *Brigantedinium* spp., which makes up more than 75% of the assemblages in most of the sequence (Figure 8). Quantitative estimates indicate low summer SSTs (August, on average 3°C lower than modern conditions) and extensive sea-ice cover (up to

2 months/year with respect to modern conditions) accompanied by SSSs (August) around 30. The most salient features are the strong decrease of the relative abundance of *Brigantedinium* spp (from ~75 to ~10%) and the strong increase in the relative abundance of *Operculodinium centrocarpum* (from ~5 to ~90%) in the uppermost part of the core. This is marked by relatively abrupt changes in sea-surface conditions. The reconstructed SSTs (August) indicate a maximum values of ~5°C, which corresponds to a thermal amplitude of 4°C compared with the August average SSTs of the middle and down core. Similarly, sea-ice cover indicates a decrease (from 10 to 7 months/year, which is 1.5 months lower than modern conditions). This is accompanied by a decrease of the SSSs (August) from 30 to 27.

3.5.5 Other palynomorph concentrations

Other organic-walled microfossils show relatively low concentrations throughout the length of cores 006 PC and 006 BC. However, between 6000 and 5500 cal years B.P., core 006 PC depicts a strong increase of the pollen, spores, brackish water algae *Halodinium*, pre-Quaternary reworked palynomorphs and organic linings of foraminifers (OL) concentrations (Figure 10). Maximum values are reached during that time with pollen concentration of 605 grains/cm^3 (average 79 grains/cm^3) and spores concentration of 213 individuals/cm^3 (average 30 spores/cm^3). Pre-Quaternary reworked palynomorphs (average 48 individuals/cm^3), *Halodinium* (average 213 individuals/cm^3), and organic linings of foraminifers (average 234 individuals/cm^3) also indicate maximum concentration with values of 533, 213, 1601 individuals/cm^3, respectively. The pollen/dinocyst ratio (P/D ratio, average 0.04) shows a slight increase during that time (from 0.02 to 0.05).

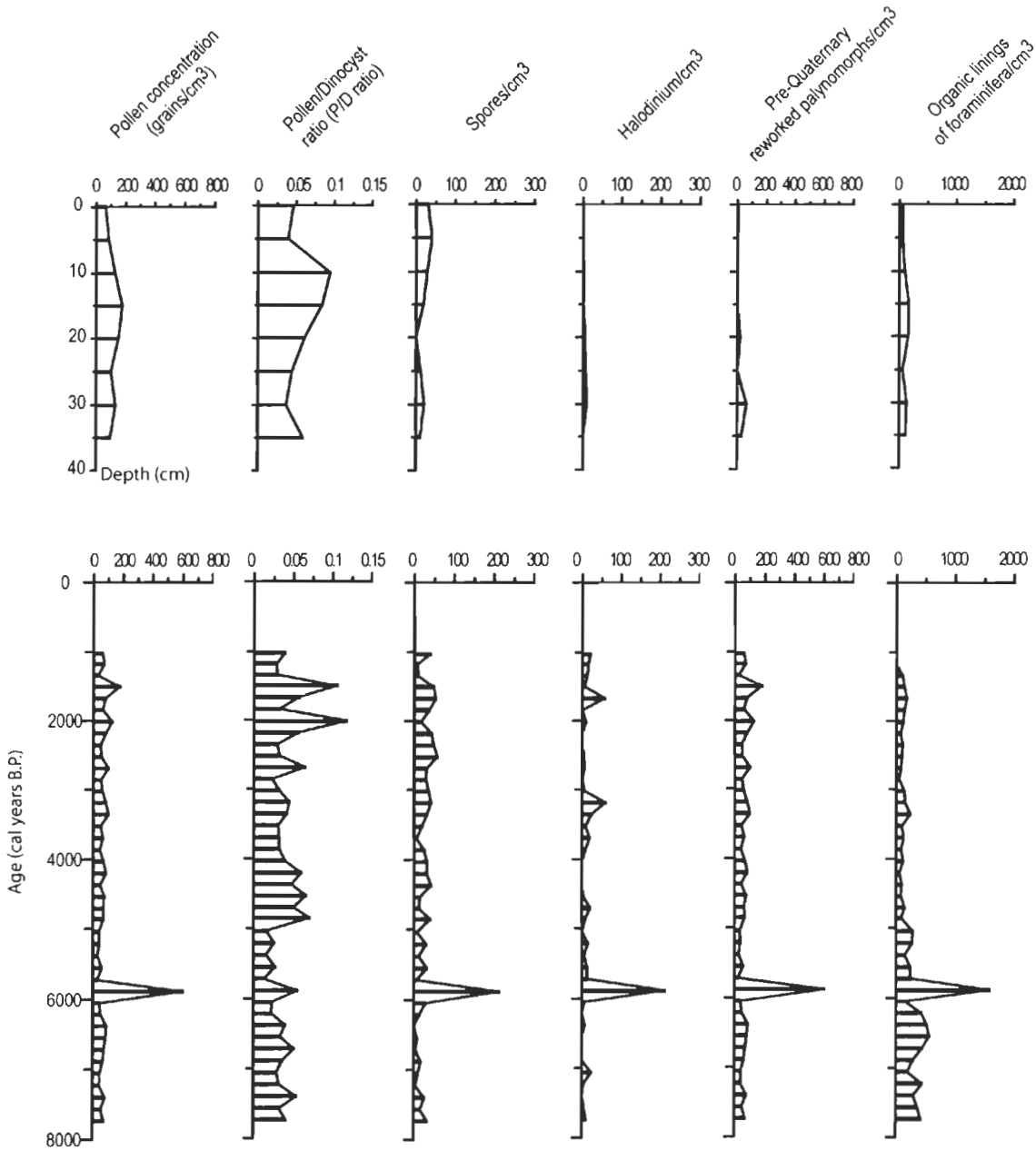

Figure 10. Diagram of pollen, spores, *Halodinium*, Pre-quaternary reworked palynomorphs and organic linings of foraminifera concentrations. The pollen/dinocyst ratio (P/D ratio) is also shown.

3.6 Discussion

3.6.1 The early-middle Holocene in the main axis of the Northwest Passage

Quantitative estimates of past sea-surface conditions (Figs 9 and 11) suggest relatively harsh conditions in Dease Strait during the early to middle Holocene (from ca 7730 to 6000 cal years B.P.). It corresponds to the zone I, where the reconstructed SSTs (August) are relatively low (2.5°C lower than modern conditions around 6500 cal years B.P.). This is accompanied by little sea-ice change with respect to modern conditions and a general increase of the reconstructed SSSs (August, maximum of 32 reached around 6500 cal years B.P.). Similarly, paleoceanographic records based on dinocyst assemblages in core 004 PC (Barrow Strait, Fig 11) also indicate low SSTs (August, on average 1°C, modern conditions 1.9°C) with sea-ice cover, which fluctuates around present conditions (maximum of 11.3 months/year, minimum of 9 months/year, present conditions of 10.2 months/year). Records based on dinocyst assemblages, mesopelagic and benthic foraminifers from the Chukchi Sea [*de Vernal et al.*, 2005a; *McKay et al.*, 2008] also indicate relatively harsh conditions with a sharp halocline promoting an extensive sea-ice cover. These differ from marine records from the Eastern Arctic, which rather indicate warmer conditions in the early-middle Holocene. Dinocyst assemblages in core 009 PC (Lancaster Sound, Fig 11), and from northernmost Baffin Bay indicate an increase in the relative abundance of phototrophic taxa beginning around 8500 cal years B.P., accompanied by a general trend towards warmer SSTs [*Levac et al.*, 2001; *Rochon et al.*, 2006; *Ledu et al.*, 2008b, submitted]. These opposite climatic trends between the eastern and western Arctic indicate that higher regional summer insolation was not the only mechanism explaining the climate variability during the early-middle Holocene. During this interval, change in the relative sea-level (RSL) due to strong emergence (~80 m between 8500 and 7000 cal years B.P.

northeast Barrow Strait, for details see *Dyke*, [1998] and *England et al.,* [2006]) could have explained climate variability in the central channels of the CAA. *Williams et al.* [1995] hypothesized that the flow of intermediate Atlantic water could have been prevented in the central CAA as the channels became shallower due to isostatic rebound. In modern conditions, the flow of this water mass is severely constrained by the shallow sill (125 m) in Barrow Strait. This sill is located at the western side of core 004 PC, which indicates that the only source of intermediate Atlantic water could be through the easternmost part of the CAA through Lancaster Sound. However, the flow of this water mass through this pathway does not penetrate as far as Barrow Strait [*Prinsenberg and Bennett,* 1987; *Jones et al.,* 2003]. Therefore, early-middle Holocene climate changes in Barrow Strait associated with RSL were probably related to variations in the inflow of Pacific water rather than changes in the inflow of intermediate Atlantic water. This could have enhanced fluctuations of the sea-ice cover as indicated by our records from core 004 PC. However, the spatial pattern of sea-surface conditions in the MANWP and in the Arctic as a whole during this interval suggests intensified cyclonic circulation resulting in a stronger Trans Polar Drift. In modern conditions, the positive mode of the AO creates such climatic conditions between the eastern and western Arctic. These include an increase advection of Atlantic water into the Arctic Ocean with strong divergence in the eastern Arctic resulting in positive SST anomalies, whereas convergence in the western Arctic enhanced negative SST anomalies accompanied by an extensive sea-ice cover, but with little variations [*Dickson et al.,* 2000; *Rigor et al.,* 2002; *Zhang et al.,* 2003]. These are consistent with a maximum inflow of Atlantic water recorded by mesopelagic and benthic foraminifers in cores from the Barents,

Chukchi and Beaufort seas, west Greenland, Svalbard and Iceland shelves around 8000 cal years B.P. [*Duplessy et al.*, 2001, 2005; *Andrews and Dunhill*, 2004; *Hillaire-Marcel et al.*, 2004; *de Vernal et al.*, 2005a; *Lloyd et al.*, 2005; *Ślubowska-Woldengen et al.*, 2008]. Maximum SST was found from sites along or near the North Atlantic Current and its components from the early to middle Holocene [*de Vernal and Hillaire-Marcel*, 2006]. In modern conditions, the positive mode of the AO is associated with more northward position of the jet stream, which enhanced an increase of Eurasian river discharge with a more eastward component along the East Siberian seas and the Canada Basin [*Johnson and Polyakov*, 2001; *Peterson et al.*, 2002; *Schlosser et al.*, 2002; *Steele et al.*, 2004]. These processes create a negative sea-surface salinity anomaly in most of the Canada Basin [*Steele and Ermold*, 2004], which enhances a strong stratification promoting the formation of sea-ice. Therefore, we associate the relatively harsh conditions in the westernmost/central (Dease/Barrow straits) as well as the milder conditions in the easternmost part of the MANWP (Lancaster Sound) with a positive mode of the AO, which creates such a dipole pattern in the Arctic marine realm. In the eastern Arctic, this was accompanied by major oceanographic changes, including the gradual strengthening of the Irminger and West Greenland currents as well as the onset of intermediate Labrador Sea water formation [*Hillaire-Marcel et al.*, 2001; *Knudsen et al.*, 2008; *Ren et al.*, 2009].

3.6.2 The middle Holocene in the MANWP: major oceanographic and atmospheric changes

Dinocyst assemblages, other palynomorph concentrations, quantitative estimates of past sea-surface and stable isotopes suggest that the middle Holocene corresponds to a time

of important changes in Dease Strait (Figs 9, 10 and 11). Maximum SSTs (~6°C, 2°C warmer than modern conditions) are reached around 5500 cal years B.P., in the lowermost zone II and are 4.5°C greater than those of the uppermost zone I. During the same interval,

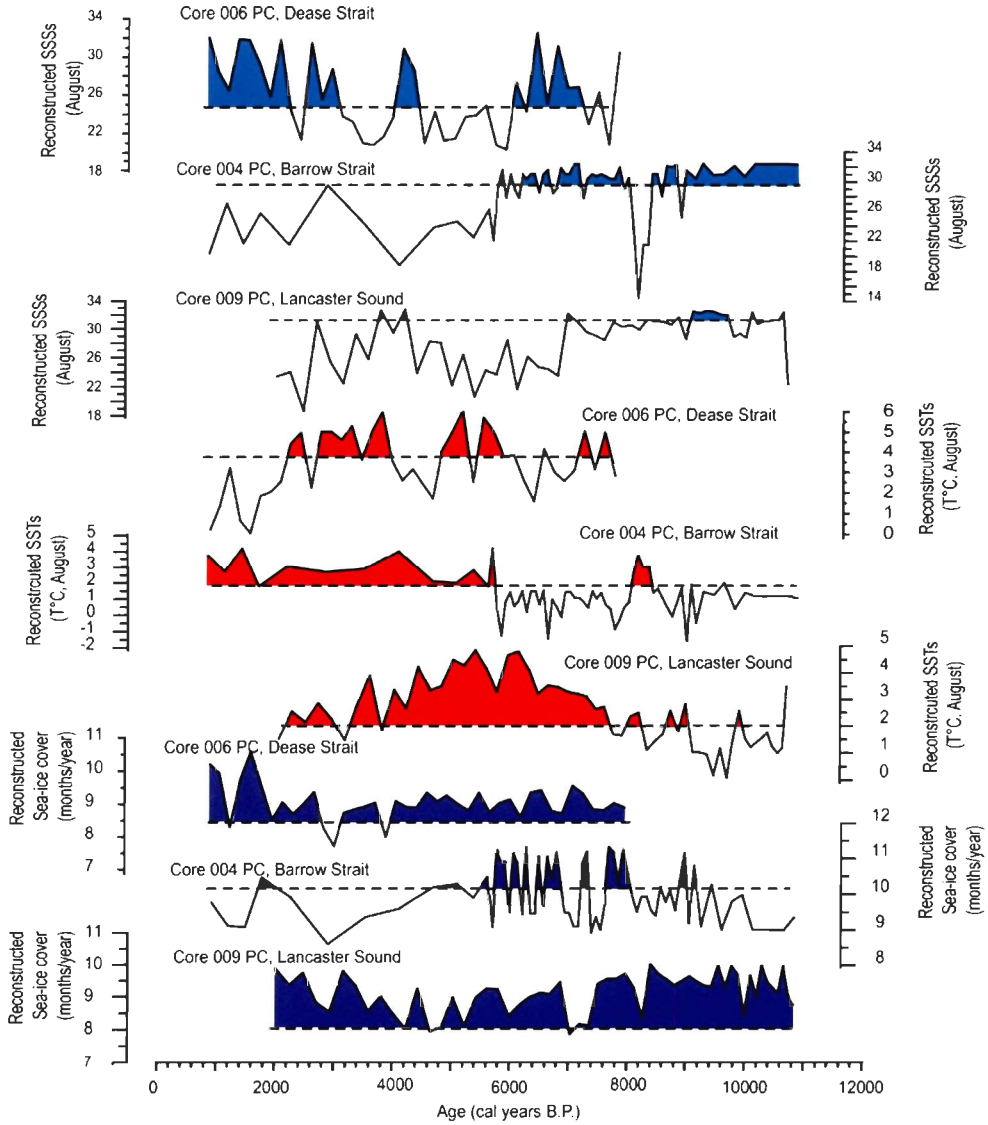

Figure 11. Reconstructed sea-surface parameters for cores 009 PC (Lancaster Sound), 004 PC (Barrow Strait), and 006 PC (Dease Strait). The dash lines correspond to the modern sea-surface conditions for each site. The purple zones are the reconstructed sea-ice cover with values higher than modern conditions. The red zones are the reconstructed SSTs (August) with values warmer than modern conditions. The blue zones are the reconstructed SSSs (August) with values higher than modern conditions. (see text for details).

the reconstructed SSSs (August) also indicate a strong amplitude between the uppermost zone I (value of ~32) and the lowermost zone II (value of ~20). These are also marked by the first occurrence of the heterotrophic taxon *Selenopemphix quanta*. Most important is the abrupt and strong increase of the dinocyst concentrations (from 1800 to 10900 cysts/cm^3) as well as pollen, spores and pre-Quaternary reworked palynomorph concentrations between 6000 and 5500 cal years B.P. (Figs 8, 9 and 10). The relatively high pollen and spore concentrations during this time interval (605 and 213 individuals/cm^3) indicate important continental inputs. The increased concentration of the brackish water algae, *Halodinium* (from ~5 to 213 individuals/cm^3), suggests that hydrodynamic transport through river runoff was the main source of the terrestrial palynomorphs. The concentration of organic linings of foraminifers also records a strong increase, which suggests relatively important benthic productivity. This indicates an efficient transfer of organic matter from the surface to the seafloor, probably in a low energy environment. The pollen:dinocyst ratio (P/D ratio) also indicates that sea-surface production was important despite both a marked increase of the C/N ratio and a strong decrease of the $\delta^{13}C$, which suggest dominant continental contribution to the organic matter content. The $CaCO_3$ content also depicts a decrease, consistent with low values of the C_{inorg}. Stable isotopes records in core from the eastern Chukchi Sea indicate a decrease of the terrestrial organic matter, which began in the middle Holocene and related to a possible more eastward component of the Mackenzie discharge [*McKay et al.,* 2008]. Based on driftwood records, *Dyke and Savelle* [2000], found no wood in the western CAA (northwestern Victoria Island) before 4700 cal years B.P. These authors proposed that during the early Holocene, the Mackenzie Current (in

modern conditions, the Mackenzie Current is an eastward-flowing current on the inner Mackenzie continental shelf) was not active or was deflected toward the western Beaufort shelf by the BG. However, we argued for a positive mode of the AO in the early Holocene, which is not consistent with an extended BG. Furthermore, in modern conditions, the BG does not affect the inner shelf of the Beaufort Sea. However, strong Eurasian river discharge during the early to middle Holocene could have abnormally pushed the TPD toward North America. This in turn could have pushed the BG against the Beaufort Sea inner shelf, deflecting the Mackenzie Current toward the west. These are consistent with a possible strong positive mode of the AO during the early Holocene. This mechanism could have operated until the middle Holocene, where more anticyclonic conditions may have reduced the influence of TPD toward North America, allowing the eastward implementation of the Mackenzie Current. Thus, our record in Dease Strait is most likely due to an increase influence of the Mackenzie Current into the western CAA. *Millot et al.* [2003] shown that the southeastern (Slave Province) part of the Mackenzie watershed was undersaturated with respect to calcite. An increase contribution of this sector in the Mackenzie River discharge may explain the decreasing $CaCO_3$ content recorded in core 006 PC. *Naidu et al.* [2000] estimated that ~30 to 50% of the organic matter in nearshore and shelf sediments of the Beaufort Sea is of terrigenous origin consistent with the low $\delta^{13}C$. Based on organic petrology, *Carrie et al.* [2009] found that the Mackenzie River carries abundant spores and pollen. Therefore, the middle Holocene in Dease Strait is probably marked by the implementation of the modern Mackenzie Current as suggested by the lower reconstructed SSSs. This major oceanographic change in the westernmost part of the

MANWP was synchronous with important changes in the central and easternmost part of the MANWP (Barrow Strait and Lancaster Sound). Quantitative estimates of SSTs and SSSs (August) in core 004 PC (Barrow Strait) also indicate large amplitude change of temperatures (5°C) and salinity (from 32 to 22) between ~6500 and 6000 cal years B.P., followed by a gradual trend toward warmer conditions (Figure 11). Paleoceanographic records from core 009 PC (Lancaster Sound) suggest a trend toward cooler conditions beginning around 5000 cal years B.P. (Fig 11), which is also recorded by the $\delta^{18}O$ data from the Devon Island Ice cap (Fig 12) [*Fisher*, 1976, 1979; *Fisher and Koerner*, 1980; *Fisher et al.*, 1983]. We associate our records in the MANWP in the middle Holocene to major changes in the atmospheric circulation following the early Holocene large-scale oceanic reorganization, which could correspond to a shift toward more anticyclonic conditions (i.e., from AO^+ to AO^-).

3.6.3 The middle to late Holocene and a possible impact of the negative mode of the AO

Quantitative estimates of past sea-surface conditions in Dease Strait indicate a cooling trend beginning around 4000 cal years B.P. (Figs 9 and 11). The reconstructed SSTs (August) record minimum values of 0°C (around 2000 cal years B.P.), which is ~4°C lower than modern conditions. These are accompanied by a general increase of both the SSSs (August, maximum of 32) and the sea-ice cover (maximum of 10.5 months/year, which is 2 months/year more than modern conditions). This cooling trend corresponds to the uppermost zone II and zone I, where a gradual increase in the relative abundance of

Brigantedinium spp. and a decrease of the cyst of *Polykrikos* Arctic morphotype is observed. These are also accompanied by the complete disappearance of *Selenopemphix*

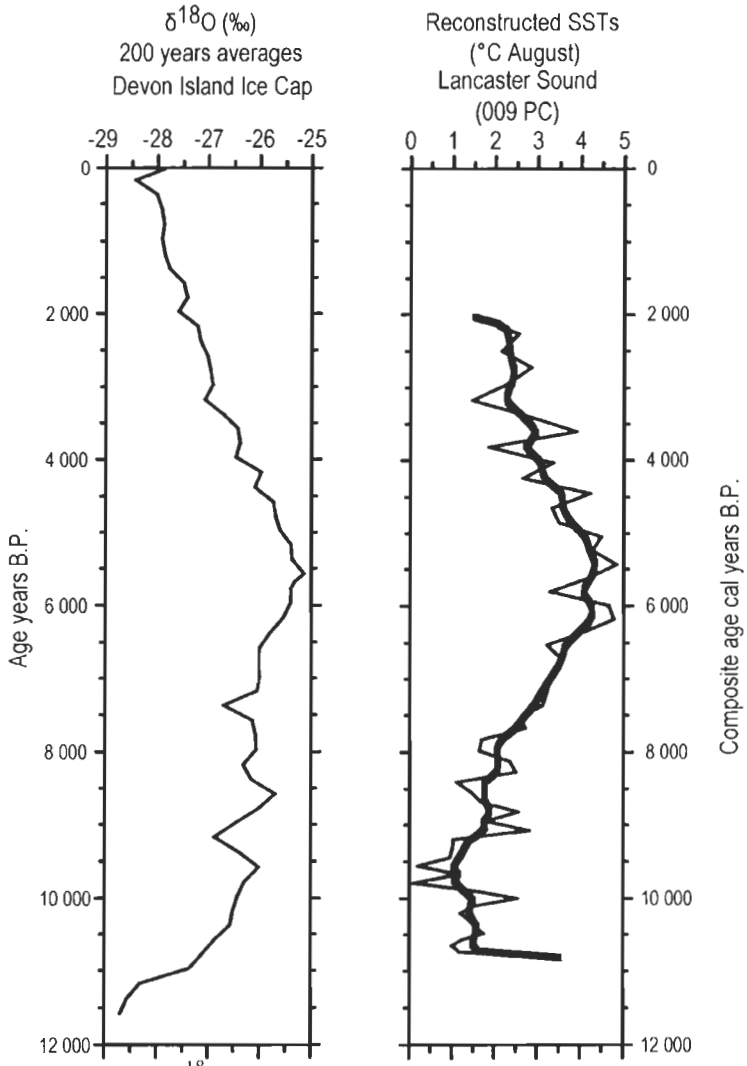

Figure 12. Holocene ice core $\delta^{18}O$ records from Devon Island ice cap (200 years average) vs quantitative estimates of SSTs (August) from Lancaster Sound (core 009 PC). The thicker black line corresponds to a smoothing curve (10 pts) of the reconstructed SST. The comparison of the two diagrams shows the same trend suggesting a strong oceanic/atmospheric coupling throughout the Holocene in this area. (Modified from [*Ledu et al.*, submitted]).

quanta and the gradual decrease of *Operculodinium centrocarpum* and *Spiniferites elongatus/frigidus* in the uppermost Zone I. This cooling trend during the late Holocene in

Dease Strait contradicts results from other marine records from the western Arctic. Quantitative estimates of past sea-surface conditions based on dinocyst assemblages in cores from the Beaufort Sea [*Rochon et al.,* 2006], the eastern and western Chukchi seas [*McKay et al.,* 2008; *de Vernal et al.,* 2005a] indicate a general trend toward increasing both SSTs and SSSs as well as decreasing sea-ice cover. Similarly, records from core 004 PC (Barrow Strait, Fig 11) suggest warmer conditions with an increase of the reconstructed SSTs (August) accompanied by both a decrease SSSs (August) and sea-ice cover [*Ledu et al.,* 2008a, submitted]. Under modern conditions, the negative mode of the AO implied less precipitation over the Siberian watershed (because the jet-stream is further south) as well as more advection of Pacific water in the Arctic Ocean [*McLaughlin et al.,* 1996, 2002; *Proshutinsky et al.,* 2002; *Hakkinen and Proshutinsky*, 2004; *Steele et al.,* 2004; *Steele and Ermold*, 2004; *Swift et al.,* 2005]. In the western Canadian Arctic, the strong northeasterlies reinforced the anticyclonic BG and enhance upwelling of deep water along the shelf [*Carmack and MacDonald*, 2002]. Taken together, these processes create both a relative salinification in the western Arctic with positive SST anomalies. Several studies based on pollen, radiocarbon dated fossils, diatoms, aquatic palynomorphs and foraminifers have documented a decrease of freshwater content in the Russian Arctic seas during the middle to late Holocene. [*Polyak et al.,* 2000, 2002a,b; *Bauch and Polyakova*, 2003; *Prange and Lohman*, 2003; *Polyakova et al.,* 2005]. These have been associated with a decrease in precipitation over the Northern Eurasia [*Andreev and Klimanov*, 2000; *MacDonald et al.,* 2000]. During the negative mode of the AO, storm tracks tend to be over the central Arctic rather than over northern Eurasia [*Dickson et al.,* 2000; *Serreze and Barrett*, 2008]

consistent with both increase Canadian river and decrease Eurasian river discharge [*Peterson et al.*, 2002, 2006; *Déry and Wood*, 2005; *McClelland et al.*, 2006].

Therefore, the trend toward increasing SSSs recorded in cores from the Chukchi Sea [*de Vernal et al.*, 2005a; *McKay et al.*, 2008] between the middle to late Holocene is probably due to a decrease of Russian river discharge together with an increase inflow of Pacific water, which triggered a relative salinification of the surface layer in this area. The sea-surface conditions recorded in core 006 PC (Dease Strait) with both the low SSTs (August) and increase reconstructed SSSs (August) is most likely due to vertical mixing between the ACCW (upper summer Pacific halocline) and the wBSW (winter Pacific halocline), which constitute the halocline in this area [*Jones et al.*, 2003; *Steele et al.*, 2004]. In modern conditions, strong upwelling events have been reported around Cape Bathurst and in Amundsen Gulf as well as in the inner Beaufort Shelf [*Carmack and MacDonald*, 2002; *Williams and Carmack*, 2008; *Mundy et al.*, 2009]. The mix of the ACCW with the relatively cold saline nutrient-rich wBSW could have promoted a high abundance of diatoms, which can grow under variable light conditions in cold water [*Wassmann et al.*, 1999; *Agusti and Duarte*, 2000; *von Quillfeldt*, 2000; *Lovejoy et al.*, 2002]. This could explain the gradual decrease in the relative abundance of the phototrophic dinoflagellate and the gradual increase in the relative abundance of the opportunistic heterotrophic taxon *Brigantedium* spp.

The decreased SSSs (August) and sea-ice cover in core 004 PC (Barrow Strait) could be due to the storms track during the negative mode of the AO. In modern conditions, prominent reduction of sea-ice concentration in the central Arctic has been linked with

well-developed cyclone pattern [*Barry and Maslanik*, 1989; *Serreze et al.*, 1989, 2003; *Serreze and Barrett*, 2008]. Increase in Arctic cyclone activity from 7000 cal years B.P. has been inferred from pollen records [*Fréchette and de Vernal*, 2009]. The impact of the negative mode of the AO during the middle to late Holocene is further supported by records from the eastern Arctic. Data from core 009 PC (Lancaster Sound, Fig 11) and northernmost Baffin Bay [*Levac et al.*, 2001; *Rochon et al.*, 2006; *Ledu et al.*, 2008a, submitted] indicate higher SSTs than modern conditions but with a cooling trend. Similarly, a general cooling in the eastern Arctic has been documented on the basis of alkenones, diatom assemblages and planktonic foraminifers [*Calvo et al.*, 2002; *Bendle and Rosell-Melé*, 2007; *Seidenkrantz et al.*, 2007, 2008; *Knudsen et al.*, 2008; *Justwan et al.*, 2008; *Ran et al.*, 2008].

Continental data based on pollen concentrations and diatom assemblages in lake cores from the western and central CAA indicate cool conditions in the late Holocene [*Finkelstein and Gajewski*, 2007, 2008; *Zabenski and Gajewski*, 2007; *Peros and Gajewski*, 2008]. Neoglacial cooling in the eastern Arctic has also been reported in cores from Ellesmere and Baffin islands and the eastern Arctic as a whole [*Joynt and Wolfe*, 2002; *Wolfe*, 2002; *Kaufman et al.*, 2004; *Michelutti et al.*, 2006]. Therefore, we associate our record in the MANWP during the middle to late Holocene to the negative mode of the AO operating at the millennial time scale.

3.6.4 Historical changes

The most salient feature of core 006 BC is the marked decrease in the relative abundance of the heterotrophic taxon *Brigantedinium* spp. (from 75 to 10%) in the

uppermost part of the core (Figure 9). This is accompanied by the strong increase of the phototrophic taxa *Operculodinium centrocarpum* (from 5 to 90%). These records must be interpreted with caution because of possible taphonomic processes (processes affecting an organism after death and that results in its fossilization), which could have affected dinocyst assemblages [*Zonneveld et al.,* 2007]. However, the good preservation of protoperidinoid cysts indicates that the records can be interpreted as a paleoclimatic signal. The harsh conditions recorded in most of the core are then replaced by milder conditions as suggested by the increase SSTs (August, from a minimum of ~0°C to a maximum values of ~5°C). This is also accompanied by a decrease of sea-ice cover and SSSs (August), from ~11 to 7 months/year and from 30 to 27, respectively. Geochemical data also indicate changes in the uppermost part of core 006 BC with both the increase of the $\delta^{13}C$ and C_{org}. Such conditions could correspond to the implementation of modern conditions in Dease Strait. The strong dominance of the phototrophic taxa *Operculodinium centrocarpum* is characteristic of modern dinocyst assemblages from Amundsen Gulf [*Richerol et al.,* 2008a]. During the last 600 years, dinoflagellate cyst assemblages in cores from the Beaufort Sea shelf (Mackenzie Trough) indicate the gradual replacement of heterotrophic taxa by phototrophic taxa accompanied by both increase SSTs toward modern values and decrease sea-ice cover and SSSs. Based on foraminifers records in cores from Amundsen Gulf, *Schell et al.* [2008] also found milder conditions with a gradual decrease of sea-ice over the last two centuries. In contrast core 004 BC (Barrow Strait) indicate a general trend toward cooler conditions over the last ~450 years. Records from core 009 PC (Lancaster Sound) suggest a general trend toward reduced sea-ice during the last ~500 years (Fig 13).

Such climatic conditions along the MANWP could be due to the gradual return to a more positive mode of the AO at the millennial time scale. This is consistent with a decrease of Pacific water extent observed in the last decades as well as the increase influence of the intermediate Atlantic water [*McLaughlin et al.,* 2004; *Shimada et al.,* 2004; *Steele et al.,* 2008].

3.6.5 Holocene climate changes in the MANWP: comparison between previous studies and dinocyst-based reconstruction

3.6.5.1 Holocene sea-ice history in the MANWP: the qualitative approach

Reconstruction of Holocene sea-ice history in the MANWP has been mostly inferred from both raised beach bowhead whale and walrus bone remains and driftwood incursions [*Dyke et al.,* 1996, 1997, 2005; *Tremblay et al.,* 1997; *Dyke,* 1999; *Dyke and Savelle*, 2000, 2001; *Savelle et al.,* 2000; *Dyke and England*, 2003]. Recently, *Vare et al.* [2009] have also proposed a qualitative reconstruction of Holocene sea-ice history for the central part of the CAA (Barrow Strait) based on the biomarker IP_{25}. Overall, these studies indicate that the early Holocene in the MANWP (from ~10 500 to ~8500 cal years B.P.) was the warmest interval of the last 10 000 years, except in Viscount Melville Sound (central northwest), where sea-ice is though to have been a permanent feature throughout the Holocene [*Dyke et al.,* 2005]. Faunal records suggest an abrupt cooling from 8500 to 5500 cal years B.P., preventing the penetration of bowhead whales in most of the CAA, whereas bowhead whales is though to have re-expanded their ranges in the central and eastern part of the CAA from 5500 to 3500 cal years B.P. [*Dyke et al.,* 1996, 1997, 2005]. *Dyke and Savelle* [2001] found that no whales reached southwestern Victoria Island from 8500 to 1500 cal

years B.P., which suggests an extensive sea-ice cover in the westernmost part of the MANWP for most of the Holocene. Finally, after 3000 cal year B.P., extensive sea-ice cover is suggested for most of the CAA [*Dyke et al.*, 2005; *Vare et al.*, 2009].

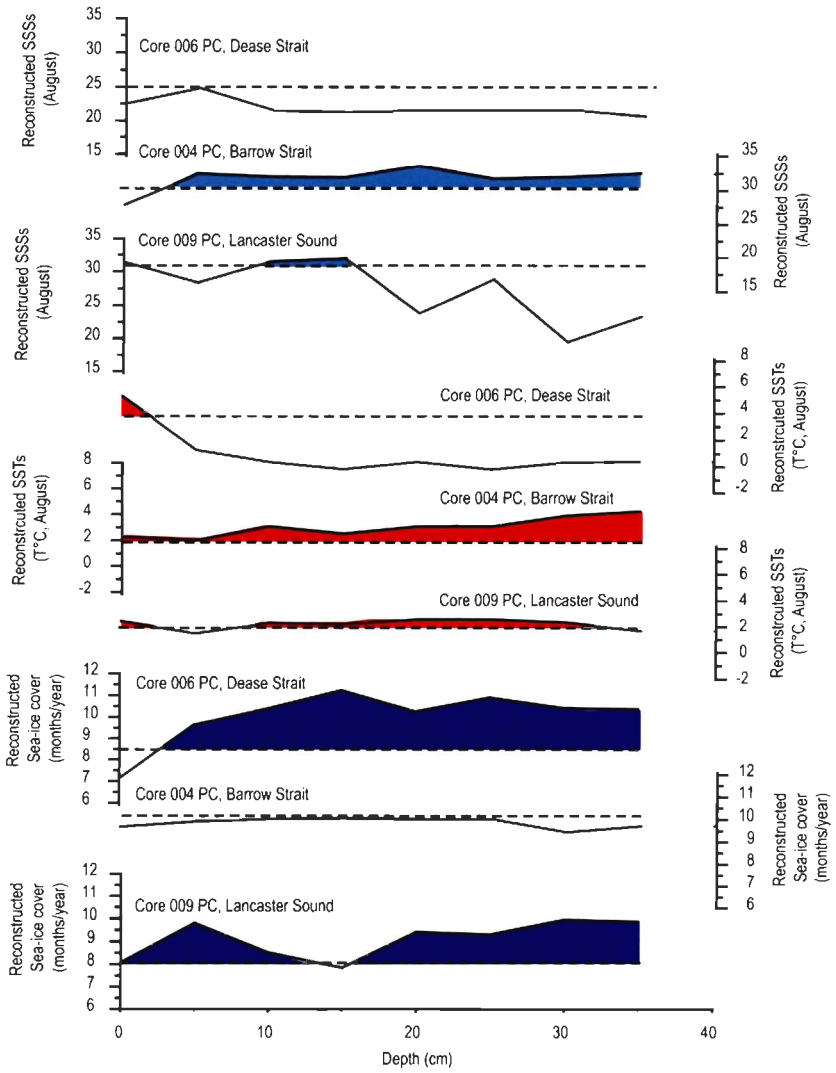

Figure 13. Reconstructed sea-surface parameters for cores 009 BC (Lancaster Sound), 004 BC (Barrow Strait), 006 BC (Dease Strait). The dash lines correspond to the modern sea-surface conditions for each site. The purple zones are the reconstructed sea-ice cover with values higher than modern conditions. The red zones are the reconstructed SSTs (August) with values warmer than modern conditions. The blue zones are the reconstructed SSSs (August) with values higher than modern conditions (see text for details).

3.6.5.2 A new Holocene sea-ice history for the MANWP: a synthesis between qualitative and quantitative dinocyst approaches

Overall, our records based on dinocyst assemblages are in relative good agreement with sea-ice history in the CAA inferred from bowhead whale remains (Table 3). However, our dinocyst-based sea-surface reconstructions show several important new features concerning the Holocene sea-ice history in the MANWP. The presence of dinocyst throughout the Holocene in cores from Lancaster Sound, Barrow and Dease straits suggests that the MANWP has already been ice free during the summer over the last 10 000 years. We also found an extensive sea-ice cover in the eastern part of the MANWP (Lancaster Sound) for most of the Holocene (Fig 11), whereas bowhead whale remains indicate less sea-ice cover from 10 500 to 8500 cal years B.P. and from 5000 to 3000 cal years B.P. [*Dyke et al.,* 1996, 2005]. Our sampling site in Lancaster Sound is located at the southeasternmost part of Devon Island. The comparison between the $\delta^{18}O$ in ice core from Devon Ice Cap and the reconstructed SSTs (August) from core 009 PC suggests a strong oceanic and atmospheric coupling throughout the Holocene (Fig 12). Although, our record indicates a gradual cooling (SSTs) from the middle to late Holocene, we found that SSTs were warmer than modern conditions over most of the Holocene. We associate the discrepancy between bowhead whale remains and dinocyst sea-ice based reconstructions in the easternmost part of the MANWP to the gradual input of local freshwater from the eastern part of the Devon Island Ice Cap as suggested by the low reconstructed SSSs (August). This local low surface water salinity has probably promoted the formation of a

local extensive sea-ice cover from most of the Holocene. In modern conditions, the western part of the Devon Island Ice Cap terminates entirely on land but the eastern part is

Table 3. Comparison between Holocene sea-ice bowhead remains based reconstructions and Holocene dinocyst sea-surface based reconstructions in the CAA. The first number is the average for each time interval, and the numbers in brackets are the minimum and maximum values records. Note that, the dinocyst quantitative reconstructions are based on the best estimates, which are the averages of hydrographic parameters weighted inversely to the distance for the five best modern analogues

			Bowhead remains-based reconstructions	Dinocyst-based reconstructions		
Epoch	Interval cal years B.P.	MANWP zone	sea-ice cover vs modern conditions	Sea-ice cover vs modern conditions (months/year) average (Min/Max)	SSTs vs modern conditions (T°C) average (Min/Max)	SSSs vs modern conditions average (Min/Max)
Modern conditions		Eastern		8.1	2	31.3
		Central		10.2	1.9	30
		Western		8.5	3.9	25
Historical changes	~ last 500 years	Eastern	More	Higher 9.0 (7.8-9.9)**	Slightly lower 1.9 (1.2/2.3)	Lower 27.3 (19.5-31.9)
		Central	More	Lower 9.7 (9.3-9.9)	Higher 2.9 (1.9/4.1)**	Lower 21.9 (20.6/24.8)
		Western	More	Higher 10.0 (7.1-11.2)	Lower 0.7 (-0.3/5.1)	Higher 31.3 (27.5/33.1)
Middle-late Holocene	After ca 6000	Eastern	Less	Higher 8.9 (7.9-9.8)	Higher 3.1 (1.4/4.8)**	Lower 25.9 (18.6-32.7)
		Central	Less	Lower 9.9 (8.6-11.2)	Higher 2.3 (-1.2/4.0)	Lower 24.7 (18.8/31.6)
		Western	more	Higher 9.0 (7.7-10.5)	Lower 3.4 (0.0/6.0)	Slightly higher 25.4 (20.3/32)
Early- middle Holocene	ca 8500 to 6000	Eastern	more	Higher 8.9 (7.8-10.0)	Higher 2.9 (1.1/4.7)	Lower 28.2 (21.6-32.1)
		Central	more	Slightly Lower 10.1 (8.9-11.3)*	Lower 1.0 (-1.4/3.6)	Lower 29.2 (14.4/32.3)
		Western	more	Slightly higher 9.0 (8.6-9.5)	Lower 3.3 (1.5/5.0)	Slightly higher 26.2 (20.3/32.5)
Pleistocene Holocene transition	ca 10,800 to 8500	Eastern	Less	Higher 9.4 (8.4-9.9)	Lower 1.5 (0.0/3.5)	Lower 30.7 (22.3/32.5)
		Central	Less	Lower 9.6 (8.9-11.1)	Lower 0.9 (-1.5/2.0)	Higher 31.1 (25.1/32.4)
		Western	Less	No records	No records	No records

*With large fluctuations, ** with a general cooling trend (see text for details)

connected to the sea [*Burgess and Sharp*, 2004, 2008; *Burgess et al.*, 2005]. The southeasternmost part of the Ice Cap is known to be one of the most sensitive to air temperature [*Dowdeswell et al.*, 2004; *Burgess and Sharp*, 2008; *Colgan et al.*, 2008]. Extensive sea-ice cover in the early Holocene is also probably due to the presence of active ice streams in the northernmost Baffin Bay until 8500 cal years B.P. [*England et al.*, 2006; *Dyke*, 2008; *Ledu et al.*, submitted].

The bowhead whales remains and dinocyst-based Holocene sea-ice reconstructions in the MANNWP may indicate the following conditions:

(1) Less sea-ice cover than modern conditions in most of the MANWP during the late early Holocene transition (from 10 800 to ~8500 cal years B.P.) but with more sea-ice in few areas (e.g., Lancaster Sound), which indicate a more pronounced regionalism than previously reported.

(2) More sea-ice cover than modern conditions in the easternmost part of the MANWP but with millennial scale sea-ice fluctuations in the central part of the MANWP during the early-middle Holocene (from ~8500 to ~6000 cal years B.P.). The westernmost part of the MANWP indicates little changes with respect to modern conditions.

(3) More sea-ice cover than modern conditions in the easternmost part of the MANWP from the middle to late Holocene (after ~6000 cal years B.P.). In contrast, a decrease of the sea-ice cover is recorded in the central part of the MANWP with respect to modern conditions. The record in the westernmost part of the MANWP suggests little changes from 6000 to 4000 cal years B.P. A slight increase of the sea-ice cover is indicated after 4000 cal years B.P.

3.7 Summary and conclusion

Cores 006, 004 and 009 provide the first quantitative records of sea-surface conditions in the MANWP for most of the Holocene. The early Holocene (from ~11 000 to ~8500 cal years B.P.) is characterized by strong terrigenous inputs in the easternmost and central part of the MANWP (for details see *Ledu et al.*, 2008a,b, submitted). We associate

this time interval with important meltwater outwash related to the last phase of the Innuitian deglaciation. During this time interval, several ice-streams, which were active in the northernmost Baffin Bay, Smith Sound and Kane Basin, promoted an extensive sea-ice cover in Lancaster Sound. Maximum ice thickness in the central north CAA together with the presence of the Wellington Channel ice-stream have probably created more unstable conditions in Barrow Strait [*Ledu et al.,* submitted]. The early-middle Holocene (from ~8000 to ~6000 cal years B.P.) was marked by opposite trends between the western-central and eastern part of the MANWP. Maximum influence of the warm intermediate Atlantic water was recorded along or near the North Atlantic Current and its components [*de Vernal and Hillaire-Marcel*, 2006]. However, in the easternmost part of the MANWP (Lancaster Sound), this influence was limited to the SST. Increase in air temperatures, as suggested by the $\delta^{18}O$ record from Devon Island Ice Cap have probably promoted terrestrial ice melt, which triggered local freshwater input as suggested by the low reconstructed SSSs in core 009 PC. This led to a relatively extensive sea-ice cover in Lancaster Sound. The western Arctic was marked by a sharp halocline promoting the formation of sea-ice [*de Vernal et al.,* 2005a; *McKay et al.,* 2008]. We associate, the climate variability in the MANWP during the early-middle Holocene to a strong positive mode of the AO operating at the millennial time scale. This is consistent with a strong divergence in the eastern Arctic, which triggered positive SST anomalies and a marked convergence with increased Eurasian river runoff, which enhanced negative SST anomalies and extensive sea-ice cover in the western Arctic. This was accompanied by major oceanographic changes, including the gradual implementation of the modern West Greenland and Irminger currents as well as the

development of an active site of intermediate Labrador Sea water formation [*Hillaire-Marcel et al.,* 2001; *Knudsen et al.,* 2008; *Ren et al.,* 2009]. The middle Holocene (around 6000 cal years B.P.) in the westernmost and central part of the MANWP (Dease and Barrow straits) is marked by a thermal amplitude as much as ~5°C (from ~ –1.5 to +3.5°C). Records from the easternmost part of the MANWP (Lancaster Sound) indicate the onset of a trend toward cooler conditions. In Dease Strait, this was probably accompanied by the implementation of the modern Mackenzie Current in a low energy environment. We associate the climate variability in the MANWP during the middle Holocene to a change in atmospheric circulation marked by more anticyclonic conditions related to a shift of the AO (from AO^+ to AO^-). The middle to late Holocene (after ~6000 cal years B.P.) is characterized by harsh conditions in the westernmost part of the MANWP, whereas records from the Chukchi Sea [*McKay et al.,* 2008; *de Vernal et al.,* 2005a] and the central part of the MANWP (Barrow Strait) [*Ledu et al.,* 2008b, submitted] indicate warmer conditions. We associate these conditions with vertical mixing between the summer and cold nutrient-rich winter Pacific water. This has probably promoted a large abundance of diatoms, which can grow under more variable light conditions and are more competitive than phototrophic dinoflagellate. Records from the easternmost part of the MANWP (Lancaster Sound) indicate a gradual cooling, which highlighted the dipolar structure between the eastern and western Arctic similar to the impact of the AO. Therefore, climate variability in the MANWP during the middle-late Holocene is associated with the dominance of negative AO mode accompanied by northeasterly winds inducing upwelling along the western coast of the CAA.

At the scale of the Holocene, our records suggest that the climate variability in the MANWP is strongly influenced by large-scale atmospheric patterns, such as the AO, operating at the millennial time scale. However, local conditions may create a marked regionalism highlighting the strong heterogeneity of the Arctic Ocean.

3.8 Acknowledgements

This work was funded by the ArcticNet Network of Centres of Excellence and the Natural Science and Engineering Research Council (NSERC) of Canada. This is a contribution to the ArcticNet project 1.6 (The Opening NW Passage: Resources, Navigation, Sovereignty & Security), the Polar Climate Stability Network (PCSN) supported by the Canadian Foundation for Climate and Atmospheric Science (CFCAS), and the NSERC-IPY project "International Polar Year: Natural climate variability and forcings in Canadian Arctic and Arctic Ocean".

We wish to thank the officers and crew of the CCGS *Amundsen* for their help and support during sampling. We also wish to express our gratitude to the following people who helped during the collection and analysis of the samples (Robbie Bennett, Bedford Institute of Oceanography; Trecia Schell, Dalhousie University; Sylvain Leblanc, Pierre Simard and Guillaume Auclair, UQAR). Thanks are due to Bassam Ghaleb and Jean-François Hélie (GEOTOP) for geochemical and isotope analyses. We also wish to thank Monika Korte for the CALS7K.2 inclination data at the sites of cores 006, 004 and 009 PC. Finally, we are grateful to the two anonymous reviewers for their comments, which helped to improve the manuscript.

CONCLUSION GÉNÉRALE

L'application de la technique des analogues modernes aux assemblages de dinokystes de trois carottes sédimentaires a permis de caractériser la variabilité climatique naturelle des 10 000 dernières années le long de l'APPNO. Les données climatiques quantitatives issues de cette étude indiquent que l'évolution paléocéanographique des conditions hydrographiques de surface le long de l'APPNO a été caractérisée par la mise en place progressive d'un gradient climatique Est-Ouest. Après les derniers stades de la déglaciation innuitienne autour de 8.5 ka calibrées BP, des anomalies positives du couvert de glace ont persisté aux extrémités Est et Ouest de l'APPNO jusqu'à l'Holocène récent. Entre 8 et ~6 ka calibrées BP, l'existence d'un gradient climatique Est-Ouest semble avoir été fortement liée aux fluctuations importantes du couvert de glace dans le centre de l'APPNO. À partir de ~6 ka calibrées BP jusqu'à l'Holocène récent, une diminution marquée du couvert de glace dans le centre de l'APPNO entretient un gradient climatique persistent le long de l'APPNO. L'existence d'un gradient climatique entre la baie de Baffin et la mer de Beaufort et plus généralement entre l'Est et l'Ouest de l'Arctique avait déjà été enregistrée au cours de l'Holocène [*de Vernal et al.*, 2005b; *Rochon et al.*, 2006; *McKay et al.*, 2008]. Cependant, aucune étude n'avait documenté ni caractérisé l'existence d'un tel gradient dans l'AAC et dans l'AAPNO sur une base quantitative. Ainsi, la variabilité climatique au cours de l'Holocène dans l'océan Arctique semble fortement marquée par la présence d'oppositions climatiques. De telles oppositions pourraient être liées à des forts couplages atmosphère/océan de type oscillation Arctique opérant à l'échelle millénaire. Dans cette perspective l'Holocène moyen apparaît comme une période de transition importante le long

de l'APPNO et pourrait correspondre à un changement de phase de l'oscillation Arctique (de OA^+ à l'Holocène ancien à moyen vers OA^- de l'Holocène moyen à récent). Cependant, les facteurs locaux semblent agir comme des boucles de rétroactions positives ou négatives, amplifiant, atténuant ou renversant le signal climatique de ce type de forçage hémisphérique. Les résultats de cette thèse suggèrent, en effet, que la variabilité climatique au cours de l'Holocène dans l'Arctique se caractérise par un régionalisme prononcé. Par conséquent la variabilité climatique Holocène dans l'Arctique ne peut plus être abordée comme une simple opposition dipolaire entre l'Est et l'Ouest de l'Arctique mais plutôt comme une mosaïque de gradients climatiques suivant des transects régionaux Est-Ouest. La présence de dinokystes dans les trois carottes sédimentaires durant la quasi-totalité de l'Holocène indique également que l'axe principal du passage du Nord-Ouest a été libre de glace sur une base saisonnière au cours des 10 000 dernières années. Cependant les reconstitutions quantitatives révèlent une variabilité climatique prononcée des paramètres hydrographiques de surface le long de l'APPNO durant cet intervalle.

Ainsi, les résultats du chapitre 1 indiquent que le détroit de Lancaster a été marqué, au cours de l'Holocène, par des changements climatiques importants à l'échelle millénaire confirmant ainsi l'hypothèse de recherche. La transition Pleistocène-Holocène se caractérise par une absence de dinokystes accompagnée d'importants apports terrigènes associés à la dernière déglaciation inuitienne. Le début de l'Holocène est marqué par des conditions relativement froides par rapport aux conditions modernes probablement en raison d'échanges limités entre l'océan Atlantique et l'océan Arctique. Après cet intervalle, une tendance graduelle vers des températures (août) plus chaudes que les conditions

modernes s'installent dans le détroit de Lancaster, tandis que le couvert de glace reste proche des valeurs modernes avec de faibles valeurs de salinité. Les assemblages de dinokystes indiquent une nette augmentation de l'abondance relative des taxons phototrophes synchrone avec l'augmentation graduelle des températures (août). Les températures maximums sont atteintes à l'Holocène moyen, et sont également enregistrées dans la baie de Baffin [*Levac et al.,* 2001; *Rochon et al.,* 2006]. Cet intervalle est associé à une augmentation graduelle de l'influence de l'eau Atlantique intermédiaire dans la partie supérieure de la colonne d'eau. Cet optimum thermique régional est suivi d'une tendance au refroidissement accompagnée par une diminution graduelle de l'abondance relative des taxons phototrophes jusqu'à l'Holocène récent. Cette tendance climatique a également été enregistrée dans l'est de l'Arctique, et est associée à une diminution de l'influence de l'eau Atlantique intermédiaire dans la partie supérieure de la colonne d'eau. Cette étude suggère que durant la majeure partie de l'Holocène, la variabilité climatique dans la région du détroit de Lancaster, et plus généralement dans la baie de Baffin, pourrait être fortement liée aux changements dans l'advection méridionale du flux de chaleur. En particulier, des mécanismes atmosphériques à grandes échelles tels que l'oscillation arctique pourrait agir à l'échelle millénaire depuis le début de l'Holocène.

La définition d'un cadre chronostratigraphique pour les détroits de Lancaster et de Barrow a permis de comparer les résultats des deux sites au cours de l'Holocène. Ces résultats présentés dans le chapitre 2 indiquent qu'après les dernières phases de la déglaciation inuitienne, marquées par d'importants apports terrigènes et des températures de surface relativement froides, les deux sites enregistrent des tendances climatiques

opposées confirmant l'hypothèse de recherche de ce chapitre. L'Holocène ancien à moyen (de 8,5 à 5,5 ka calibrées BP) est marqué par des conditions plus chaudes que les conditions modernes dans le détroit de Lancaster mais plus froides dans le détroit de Barrow. La tendance inverse est enregistrée de l'Holocène moyen à récent (après 5,5 ka calibrées BP). Cette structure climatique dipolaire a également été enregistrée durant les mêmes intervalles entre la baie de Baffin, la mer de Beaufort et la mer de Chukchi [*de Vernal et al.*, 2005b; *Rochon et al.*, 2006; *McKay et al.*, 2008]. Les résultats du chapitre 2 confirment l'existence d'un gradient climatique est-ouest durant la majeure partie de l'Holocène qui suggère la mise en place de mécanismes atmosphériques tels que l'oscillation arctique opérant à l'échelle millénaire depuis environ 8,5 ka calibrées BP. Des changements océanographiques majeurs tels que la mise en place du courant de Irminger, du courant Ouest Groenlandais et le développement d'un site actif de formation d'eau intermédiaire dans la mer du Labrador [*Hillaire-Marcel et al.*, 2001] sont synchrones avec le début d'un mode climatique de type oscillation arctique.

L'inversion des tendances climatiques à l'Holocène moyen entre les détroits de Lancaster et de Barrow pourrait être due à un changement de phase de l'oscillation arctique (OA^+ vers OA^-). Dans les conditions modernes, un tel changement de phase s'accompagne d'une diminution des flux méridionaux de chaleur de l'océan Atlantique vers l'océan Arctique.

Les résultats présentés dans le chapitre 3 semblent confirmer, d'une part, l'existence de changements importants dans l'APPNO au cours de l'Holocène moyen et, d'autre part, le rôle d'un mode climatique de type oscillation arctique depuis le début de l'Holocène. Les

enregistrements du détroit de Dease suggèrent la mise en place du courant du Mackenzie dans sa configuration moderne aux alentours de 5,8 ka calibrées BP. Durant cet intervalle, des changements importants des conditions de surface sont enregistrés de manière synchrone dans les détroits de Lancaster, de Barrow et de Dease. Ces changements océanographiques sont associés à un changement de phase de l'oscillation arctique (OA^+ vers OA^-) cohérent avec les conclusions du second chapitre. La comparaison des reconstitutions quantitatives du couvert de glace basée sur les assemblages de dinokystes avec les reconstitutions qualitatives déduites des restes de baleines à bosse est relativement cohérente au cours de l'Holocène. Cependant, les données du chapitre 3 indiquent que les extrémités est et ouest (détroit de Lancaster et Dease respectivement) ont enregistré un couvert de glace plus extensif que les conditions modernes durant la quasi-totalité de l'Holocène. Ces résultats indiquent que le gradient climatique est-ouest dans l'Arctique est plus complexe qu'une simple opposition dipolaire, et nuance l'hypothèse de recherche générale. Si un mode climatique de type oscillation arctique semble fortement impliqué dans la variabilité climatique de l'Holocène dans l'APPNO, des facteurs locaux comme la proximité d'un glacier, la structure de l'halocline ou la présence d'un courant de côte ont une influence majeure sur les conditions de surface.

La connaissance de la réponse de ces facteurs à des forçages supra-régionaux, mais aussi la manière dont cette réponse amplifie, atténue ou renverse la tendance climatique imprimée par ces forçages, apparaît fondamentale dans la compréhension de la variabilité climatique naturelle de l'océan Arctique. En particulier, les études futures dans l'archipel arctique canadien, mais aussi plus généralement dans l'Arctique, devront se développer

dans des sites où des conditions locales sont susceptibles d'interagir avec des forçages supra-régionaux de type oscillation arctique. Dans l'archipel arctique canadien, le détroit de M'Clure, situé entre les îles de Melville et Banks, serait un site très intéressant pour de futures investigations paléocéanographiques. En effet, c'est par ce détroit que s'écoule une partie des eaux du bassin du Canada alimentant ainsi l'axe central du passage du Nord-Ouest. Des données paléocéanographiques basées sur l'utilisation conjointe des assemblages de dinokystes et de foraminifères méso-pélagiques et benthique pourraient révéler la variabilité des conditions de la colonne d'eau au cours de l'Holocène. Dans ce secteur, cela permettrait de documenter la variabilité de l'halocline particulièrement influencée par les entrées d'eau Pacifique qui sont elles mêmes, dans les conditions modernes, dépendantes des phases de l'oscillation arctique [*Jones et al.*, 2003; *Steele et al.*, 2008]. Enfin, des données hautes résolutions sur les sites des détroits de Lancaster, Barrow et Dease permettraient d'accéder à une résolution temporelle décennale à sub-décennale. En complément des données micropaléontologiques, certaines analyses des propriétés physiques des sédiments permettraient d'obtenir des données très haute résolution. Par exemple, l'analyse des données au scanner Itrax fournirait une résolution d'environ 100 µm pour chaque carotte sédimentaire permettant ainsi d'identifier des zones propices à un échantillonnage haute résolution en vue d'analyses micropaléontologiques.

RÉFÉRENCES

Agusti, S.; Duarte, C. M. 2000. «Experimental induction of a large phytoplankton bloom in Antarctic coastal waters». **Marine Ecology Progress series**, vol. 206, pp 73-85.

Andresen, C.S.; Björck, S.; Jessen, C.; Rundgren, M. 2007. «Early Holocene terrestrial climatic variability along a North Atlantic Island transect: paleoceanographic implications». **Quaternary Science Reviews**, vol. 26, n° 15-16, pp. 1989–1998.

Andersen, C.; Koç, N.; Jennings, A.; Andrews, J.T. 2004a. «Non uniform response of the major surface currents in the Nordic Seas to insolation forcing: implications for the Holocene climate variability». **Paleoceanography,** vol. 19, PA2003, doi:10.1029/2002PA000873.

Andersen, C.; Koç, N.; Moros, M.; 2004b. «A highly unstable Holocene climate in the subpolar North Atlantic: evidence from diatoms». **Quaternary Science Reviews,** vol. 23, n° 20-22 pp. 2155-2166.

Anderson, N. J.; Leng, M. J. 2004. «Increased aridity during the early Holocene in West Greenland inferred from stable isotopes in laminated-lake sediments». **Quaternary Science Reviews**, vol. 23, n° 7-8 (Special Issue), pp. 841-849.

Andreev, A. A.; Klimanov, V. A. 2000. «Quantitative Holocene climatic reconstruction from Arctic Russia». **Journal of Paleolimnology**, vol. 24, n°1, pp. 81-91.

Andrews, J. T.; Jennings, A. E., 1990. «Geomagnetic Secular Variations (Inclination) of High-Latitude Fjord Cores - Eastern Canadian Arctic». **Polar Research**, vol. 8, n° 2, pp. 245-259.

Andrews, J. T.; Maclean, B.; Kerwin, M.; Manley, W.; Jennings, A. E.; Hall, F. 1995. «Final stages in the collapse of the laurentide ice sheet, Hudson Strait, Canada, NWT: 14C- AMS dates, seismics stratigraphy, and magnetic susceptibility logs». **Quaternary Science Reviews**, vol. 14, n° 10, pp. 983-1004.

Andrews, J. T.; Osterman, L. E.; Jennings, A. E.; Syvitski, J. P. M.; Miller, G. H.; Weiner, N.; 1996. «Abrupt changes in marine conditions, Sunneshine Fiord, eastern Baffin Island, NWT during the last deglacial transition: Younger Dryas and H-0 events». Dans **Late Quaternary Palaeoceanography of the North Atlantic Margins.** Préparé par Andrews, J.T.; Austin, W. E. N.; Bergsten, H.; Jennings, A. E. Geological Society Special Publications no.111, Geological Society, pp. 11-27.

Andrews, J. T.; Kirby, M. E.; Aksu, A.; Barber, D. C.; Meese, D. 1998. «Late quaternary detrital carbonate (DC) layers in Baffin bay marine sediments (67°-74°N): correlation with heinrich events in the North Atlantic?». **Quaternary Science Reviews**, vol. 17, n° 12, pp. 1125-1137.

Andrews, J.T.; Dunhill, G. 2004. «Early to mid-Holocene Atlantic water influx and deglacial meltwater events, Beaufort Sea slope, Arctic Ocean». **Quaternary Research,** vol. 61, pp 14-21.

Andrews, J.T.; Belt, S.T.; Olafsdottir, S.; Massé, G.; Vare, L.L. 2009. «Sea ice and marine climate variability for NW Iceland/Denmark Strait over the last 2000 cal. yr BP». **The Holocene,** vol. 19, pp. 775-784.

Appleby, P. G.; Oldfield, F. 1983. «The assessment of 210Pb data from sites with varying sediment accumulation rates». **Hydrobiologia**, vol. 103, n° 1, pp. 29-35.

Atkinson, N.; England, J. 2004. «Postglacial emergence of Amund and Ellef Ringnes islands, Nunavut: Implications for the northwest sector of the Innuitian Ice Sheet». **Canadian Journal of Earth Sciences,** vol. 41, n°3, pp. 271-283.

Atkinson, D. E.; Brown, R.; Alt, B.; Agnew, T.; Bourgeois, J.; Burgess, M.; Duguay, C.; Henry, G.; Jeffers, S.; Koerner, R.; Lewkowicz, A. G.; McCourt, S.; Melling, H.; Sharp, M.; Smith, S.; Walker, A.; Wilson, K.; Wolfe, S.; Woo, M. K.; Young, K. L. 2006. «Canadian cryospheric response to an anomalous warm summer: A synthesis of the climate change action fund project "The state of the arctic cryosphere during the extreme warm summer of 1998"». **Atmosphere-Ocean**, vol. 44, n°4, pp. 347-375.

Barletta, F.; St-Onge, G.; Channell, J.E.T.; Rochon, A.; Polyak, L.; Darby, D.A. 2008a. «High-resolution paleomagnetic secular variation and relative paleointensity records from the western Canadian Arctic : implication for Holocene stratigraphy and geomagnetic field behaviour». **Canadian Journal of Earth Sciences,** vol. 45, n°11, pp. 1265-1281.

Barletta, F; St-Onge G.; Rochon, A. 2008b. «Paleomagnetic dating of Holocene Western Canadian Arctic sediments: combined use of secular variation and time-varing spherical harmonic model of the geomagnetic field». Dans **Arctic Change 2008 Conference Programme and Abstracts**, Arctic change 2008, Québec, p.177

Barry, R.G.; Maslanik, J.A. 1989. «Arctic sea ice characteristics and associated atmosphere-ice interactions in summer inferred from SMMR data and drifting buoys: 1979 to 1985». **Geo Journal**, vol. 18, n°1, pp. 35-44.

Bauch, H.A.; Erlenkeuser, H.; Spielhagen, R.F.; Struck, U.; Matthiessen, J.; Thiede, J.; Heinemeier, J. 2001. «A multiproxy reconstruction of the evolution of deep and surfaces waters in the subarctic Nordic seas over the last 30,000 yr». **Quaternary Science Reviews**, vol. 20, n°4, pp. 659–678.

Bauch, H. A.; Polyakova, Y. I. 2003. «Diatom-inferred salinity records from the Arctic Siberian Margin: Implications for fluvial runoff patterns during the Holocene». **Paleoceanography**, vol. 18, n°2, 1027, doi:10.1029/2002PA000847.

Belt, S.T.; Massé, G.; Rowland, S.J.; Poulin, M.; Michel, C.; Leblanc, B. 2007. «A novel chemical fossil of paleo sea ice: IP25». **Organic Geochemistry,** vol. 38, pp. 16-27.

Belt, S.T.; Massé, G.; Vare L.L.; Rowland, S.J.; Poulin, M.; Sicre, M. A.; Sampei, M.; Fortier, L. 2008. «Distinctive C-13 isotopic signature distinguishes a novel sea ice biomarker in Arctic sediments and sediments traps». **Marine Chemistry,** vol. 12, pp. 158-167.

Bendle, J.A.P.; Rosell-Melé, A. 2007. «High-resolution alkenone sea-surface temperature variability on the North Icelandic Shelf: implications for Nordic Seas palaeoclimatic development during the Holocene». **The Holocene,** vol. 17, n°1, pp. 9-24.

Besonen, M. R.; Patridge, W.; Bradley, R. S.; Francus, P.; Stoner, J. S.; Abbott, M. B. 2008. «A record of climate over the last millennium based on varved lake sediments from the Canadian High Arctic». **The Holocene**, vol.18, n°1, pp. 169-180.

Bischof, J. F.; Darby, D. A. 1999. «Quaternary ice transport in the canadian arctic and extent of Late Wisconsinan Glaciation in the Queen Elizabeth Islands». **Canadian Journal of Earth Sciences,** vol. 36, n°12, pp. 2007-2022.

Blake, W. J., 1987. «Geological Survey of Canada radiocarbon dates XXVI». **Geological Survey of Canada**, Paper 86-7, 60 p.

Blake,W. J. 1992b. «Shell-bearing till along Smith Sound, Ellesmere Island-Greenland: age and significance». Dans **Quaternary Stratigraphy, Glacial Morphology and Environmental Change**. Préparé par Robertson, A-M.; Ring-berg, B.; Miller, U.; Brunnberg, L. Sveriges Geologiska Undersokning, vol. 81, pp. 51–58.

Blott, S.J.; Pye, K. 2001. «GRADISTAT. A grain size distribution and statistics package for the analysis of unconsolidated sediments». **Earth and Surface Processes and Landforms**, vol. 26, n°11, pp. 1237-1248.

Bradley, R. S., 1990. «Holocene paleoclimatology of the Queen Elizabeth Islands, Canadian High Arctic». **Quaternary Science Reviews**, vol. 9, n°4 , pp. 365-384.

Breckenridge, A.; Johnson, T. C.; Beske-Diehl, S.; Mothersill, J. S. 2004. «The timing of regional Lateglacial events and post-glacial sedimentation rates from Lake Superior». **Quaternary Science Reviews**, vol.23, n°23-24, pp. 2355-2367.

Burgess, D. O.; Sharp, M. J. 2004. «Recent changes in areal extent of the Devon Ice Cap, Nunavut, Canada». **Arctic Antarctic and Alpine Research**, vol. 36, n°2, pp. 261-271.

Burgess, D. O.; Sharp, M. J.; Mair, D. W. F.; Dowdeswell, J. A.; Benham, T. J. 2005. «Flow dynamics and iceberg calving rates of Devon Ice Cap, Nunavut, Canada». **Journal of Glaciology**, vol. 51, n°173, pp. 219-230.

Burgess, D.; Sharp, M. J. 2008. «Recent changes in thickness of the Devon Island ice cap, Canada». **Journal of Geophysical Research Solid Earth**, vol. 113, B07204, doi:10.1029/2007JB005238.

Butler, R.F.1992. **Paleomagnetism: Magnetic Domains to Geologic Terranes**. Blackwell, Oxford, 319p.

Calvo, E.; Grimalt, J.; Jansen, E. 2002. «High resolution UK'37sea surface temperature reconstruction in the Norwegian Sea during the Holocene». **Quaternary Science Reviews**, vol. 21, n°12-13, pp. 1385-1394.

Carmack E.C.; MacDonald, R.W. 2002. «Oceanography of the Canadian Shelf of the Beaufort Sea: A Setting for Marine Life». **Arctic,** vol. 55, n°1, pp. 29-45.

Carmack, E.; McLaughlin, F.; Yamamoto-Kawai, M.; Itoh, M.; Shimada, K.; Krishfield, R.; Proshutinsky, A. 2008. «Freshwater storage in the Northern Ocean and the special role of the Beaufort Gyre». Dans **Arctic-Subarctic Ocean Fluxes: Defining the Role of the Northern Seas in Climate**. Préparé par Dickson, R. R. ; Meincke, J.; Rhines, P.; Springer Netherlands, pp. 145-169.

Carrie, J.; Sanei, H.; Goodarzi, F.; Stern, G.; Wang, F. Y. 2009. «Characterization of organic matter in surface sediments of the Mackenzie River Basin, Canada». **International Journal of Coal Geology**, vol. 77, n°3-4, pp. 416-423.

Colgan, W.; Davis, J.; Sharp, M. 2008. «Is the high-elevation region of Devon Ice Cap thickening?» **Journal of Glaciology**, vol. 54, n°186, pp. 428-436.

Comiso, J.C. 2002. «A rapidly declining perennial sea-ice cover in the Arctic». **Geophysical Research Letters**, vol. 29, n°20, pp. 1956.

Comiso, J.C. 2006. «Abrupt decline in the Arctic winter sea-ice cover». **Geophysical Research Letters**, vol. 33, L18504. doi:10.1029/ 2006GL027341.

Comiso, J. C.; Parkinson, C. L.; Gersten, R.; Stock, L. 2008. «Accelerated decline in the Arctic Sea-ice cover». **Geophysical Research Letters,** vol. 35, L01703, doi:10.1029/2007GL031972.

Cuny, J.; Rhines, R.B.; Niiler, P.P.; Bacon, S. 2002. «Labrador Sea boundary currents and the fate of the Irminger Sea Water». **Journal of Physical Oceanography**, vol. 32, n°2, pp. 627–647.

Darby, D. A.; Bischof, J. F. 2004. «A Holocene record of changing Arctic Ocean ice drift analogous to the effects of the Arctic Oscillation». **Paleoceanography**, vol.19, PA1027, doi:10.1029/2003PA000961.

Darby, D. A.; Zimmerman, P. 2008. «Ice-rafted detritus events in the Arctic during the last glacial interval, and the timing of the Innuitian and Laurentide Ice Sheet calving events». **Polar Research**, vol.27, n°2, pp. 114-127.

Déry, S. J.; Wood, E. F. 2005. «Decreasing river discharge in northern Canada». **Geophysical Research Letters**, vol. 32, L10401, doi:10.1029/2005GL022845.

Deser, C.; Walsh, J. E.; Timlin, M. S. 2000. «Arctic sea ice variability in the context of recent atmospheric circulation trends». **Journal of Climate**, vol. 13, n°3, pp. 617-633.

Deser, C.; Teng, H. 2008. «Evolution of Arctic sea ice concentration trends and the role of atmospheric circulation forcing, 1979-2007». **Geophysical Reearch Letters**, vol. 35, n°2, pp. 5.

de Vernal, A.; Turon, J.-L.; Guiot, J. 1994. «Dinoflagellate cyst distribution in high latitude marine environments and quantitative reconstruction of sea-surface temperature, salinity and seasonality». **Canadian Journal of Earth Sciences**, vol. 31, n°1, pp. 48–62.

de Vernal, A.; Rochon, A.; Turon, J.L.; and Matthiessen, J. 1997. «Organic-walled dinoflagellate cysts: Palynological tracers of sea-surface conditions in middle to high latitude marine environments». **Geobios**, vol. 30, n°7, pp. 905–920.

de Vernal, A.; Hillaire-Marcel, C.; Turon, J. L.; Matthiessen, J. 2000. «Reconstruction of sea-surface temperature, salinity, and sea-ice cover in the northern North Atlantic during the last glacial maximum based on dinocyst assemblages». **Canadian Journal of Earth Sciences**, vol. 37, n°5, pp.725-750.

de Vernal, A.; Henry, M.; Matthiessen, J.; Mudie, P. J.; Rochon, A.; Boessenkool, K. P.; Eynaud, F.; Grosfjeld, K.; Guiot, J.; Hamel, D.; Harland, R.; Head, M. J.; Kunz-Pirrung, M.; Levac, E.; Loucheur, V.; Peyron, O.; Pospelova, V.; Radi, T.; Turon, J. L.; Voronina, E. 2001. «Dinoflagellate cyst assemblages as tracers of sea-surface conditions in the northern North Atlantic, Arctic and sub-Arctic seas: the new 'n=677' data base and its application for quantitative palaeoceanographic reconstruction». **Journal of Quaternary Science**, vol. 16, n°7, pp. 681-698.

de Vernal, A.; Eynaud, F.; Henry, M.; Hillaire-Marcel, C.; Londeix, L.; Mangin, S.; Matthiessen, J.; Marret, F.; Radi, T.; Rochon, A.; Solignac, S.; Turon, J. L. 2005a. «Reconstruction of sea-surface conditions at middle to high latitudes of the Northern Hemisphere during the Last Glacial Maximum (LGM) based on dinoflagellate cyst assemblages». **Quaternary Science Reviews,** vol. 24, n° 7-9, pp. 897-924.

de Vernal, A.; Hillaire-Marcel, C.; Darby, D. A. 2005b. «Variability of sea-ice cover in the Chukchi Sea (western Arctic Ocean) during the Holocene». **Paleoceanography**, vol. 20, PA4018, doi:10.1029/2005PA001157.

de Vernal, A.; Hillaire-Marcel., C. 2006. «Provincialism in trends and high frequency changes in the northwest North Atlantic during the Holocene». **Global and Planetary Change**, vol. 54, n°3-4, pp. 263–290.

de Vernal, A.; Marret, F. 2007. «Organic-walled dinoflagellates : tracers of sea-surface conditions». Dans **Proxies in Late Cenozoic Paleoceanography**. Préparé par Hillaire-Marcel, C; de Vernal, A. Elsevier, pp. 371-408.

de Vernal, A.; Hillaire-Marcel, C.; Solignac, S. ; Radi, T. ; Rochon, A. 2008. «Reconstructing Sea Ice Conditions in the Arctic and Sub-Arctic Prior to Human Observations». Dans **Arctic Sea Ice Decline: Observations, Projections, Mechanisms, and Implications**. Préparé par DeWeaver, E.T.; Bitz, C. M.; Tremblay, L-B. Geophysical Monograph Series 180, American Geophysical Union, 350pp.

de Vernal., A. (2009). «Marine Palynology and its use for studying nearshore environments. From Deep-sea to Coastal Zones: Methods and Techniques for Studying Paleoenvironments». **IOP Conference Series: Earth and Environmental Sciences,** vol. 5, 012002, doi:10.1088/1755-1307/5/1/012002.

de Vernal, A.; Hillaire-Marcel, C.; Rochon, A.; Radi, T.; Ledu, D.; Bonnet, S. 2009. «Holocene variations of sea-ice cover and sea-surface temperature in the western Arctic, from the Fram Strait to the Chukchi Sea». Dans **APEX meeting**, Copenhagen, pp. 85.

Dickson, R. R.; Osborn, T. J.; Hurrell, J. W.; Meincke, J.; Blindheim, J.; Adlandsvik, B.; Vinje, T.; Alekseev, G.; Maslows ,W. 2000. «The Arctic Ocean response to the North Atlantic Oscillation». **Journal of Climate**, vol. 13, n°15, pp. 2671-2696.

Dickson, R.; Rudels, B.; Dye, S.; Karcher, M.; Meincke, J.; Yashayaev, I. 2007. «Current estimates of freshwater flux through Arctic and subarctic seas». **Progress in Oceanography,** vol. 73, n°3-4, pp. 210-230.

Dowdeswell, J. A.; Benham, T. J.; Gorman, M. R.; Burgess, D.; Sharp, M. J. 2004. «Form and flow of the Devon Island Ice Cap, Canadian Arctic». **Journal of Geophysical Research Earth Surface**, F02002, doi:10.1029/2003JF000095.

Drobot, S.; Stroeve, J.; Maslanik, J.; Emery, W.; Fowler, C.; Kay, J. 2008. «Evolution of the 2007-2008 Arctic sea ice cover and prospects for a new record in 2008». **Geophyical Research Letters**, vol. 35, L19501, doi:10.1029/2008GL035316.

Dukhovskoy, D. S.; Johnson, M. A.;Proshutinsky, A. 2004. «Arctic decadal variability: An auto-oscillatory system of heat and fresh water exchange». **Geophysical Research Letters**, vol. 31, L03302, doi:10.1029/2003GL019023.

Dunlap, E.; Tang, C.L. 2006. «Modelling the Mean Circulation of Baffin Bay». **Atmosphere-Ocean**, vol. 44, n°1, pp. 99-110.

Dunlop, D. J.; Özdemir, Ö. 1997. **Rock Magnetism. Fundamentals and Frontiers. Cambridge Studies in Magnetism Series XXI**. Cambridge University Press, Cambridge, New York, Port Chester, Melbourne, Sydney, 573 pp.

Duplessy, J. C.; Ivanova, E.; Murdmaa, I., Paterne, M.; Labeyrie, L. 2001. «Holocene paleoceanography of the northern Barents Sea and variations of the northward heat transport by the Atlantic Ocean». **Boreas**, vol. 30, n°1, pp. 2-16.

Duplessy, J. C.; Cortijo, E.; Ivanova, E.; Khusid, T.; Labeyrie, L.; Levitan, M.; Murdmaa, I.; Paterne, M. 2005. «Paleoceanography of the Barents Sea during the Holocene». **Paleoceanography**, vol. 20, PA4004, doi:10.1029/2004PA001116.

Dyke, A. S.; Hooper, J.; Savelle, J. M. 1996. «A history of sea-ice in the Canadian Arctic Archipelago based on postglacial remains of the bowhead whale (Balaena mysticetus)». **Arctic**, vol. 49, n°3 , pp. 235-255.

Dyke, A. S.; England, J.; Reimnitz, E.; Jette, H. 1997. «Changes in driftwood delivery to the Canadian arctic archipelago: The hypothesis of postglacial oscillations of the transpolar drift». **Arctic**, vol. 50, n°1, pp. 1-16.

Dyke, A. S. 1998. «Holocene delevelling of Devon Island, Arctic Canada: implications for ice sheet geometry and crustal response». **Canadian Journal of Earth Sciences**, vol. 35, n°8, pp. 885-904.

Dyke, A. S. 1999. «Last Glacial Maximum and deglaciation of Devon Island, Arctic Canada: support for an Innuitian Ice Sheet». **Quaternary Science Reviews**, vol. 18, n°3 , pp. 393-420.

Dyke, A. S.; Savelle, J. M. 2000. «Holocene driftwood incursion to southwestern Victoria Island, Canadian Arctic Archipelago, and its significance to paleoceanography and archaeology». **Quaternary Research**, vol. 54, n°1, pp. 113-120.

Dyke, A. S.; Savelle, J. M. 2001. «Holocene history of the Bering Sea bowhead whale Balaena mysticetus in its Beaufort Sea summer grounds off southwestern Victoria Island, western Canadian Arctic». **Quaternary Research**, vol. 55, n°3, pp. 371-379.

Dyke, A. S.; Andrews, J. T.; Clark, P. U.; England, J. H.; Miller, G. H.; Shaw, J.; Veillette, J. J. 2002. «The Laurentide and Innuitian ice sheets during the Last Glacial Maximum». **Quaternary Science Reviews**, vol. 21, n°1-3, pp. 9-31.

Dyke, A. S.; England, J. 2003. «Canada's most northerly postglacial bowhead whales (Balaena mysticetus): Holocene sea-ice conditions and polynya development». **Arctic**, vol. 56, n°1, pp. 14-20.

Dyke. A.S.; Savelle, J.M.; Hodgson, D.A. 2005. «Environmental history and archaeology along the Northwest Passage. Water, Ice, And Life: The Quaternary Interface». Dans **Canadian Quaternary Association Conference**, University of Manitoba, Winnipeg, Manitoba, pp. A21.

Dyke, A. S. 2008. «The Steensby Inlet Ice-Stream in the context of the deglaciation of Northern Baffin Island, Eastern Arctic Canada». **Earth Surface Processes and Landforms**, vol. 33, n°4, pp. 573-592.

England, J. 1998. «Support for the Innuitian Ice Sheet in the Canadian High Arctic during the Last Glacial Maximum». **Journal of Quaternary Science**, vol. 13, n°3 , pp. 275-280.

England, J. 1999. «Coalescent Greenland and Innuitian ice during the Last Glacial Maximum: revising the Quaternary of the Canadian High Arctic». **Quaternary Science Reviews**, vol. 18, n°3 , pp. 421-456.

England, J.; Smith, I. R.; Evans, D. J. A. 2000. «The last glaciation of east-central Ellesmere Island, Nunavut: ice dynamics, deglacial chronology, and sea level change». **Canadian Journal of Earth Sciences**, vol. 37, n°10, pp. 1355-1371.

England, J.; Dyke, A.S., McNeely, R. 2003. «Inter-species, radiocarbon age comparisons on subfossil molluscs from Arctic Canada: the Portlandia arctica problem». Dans **33rd International Annual Arctic Workshop**, Program with Abstracts, Polar Environmental Centre, Tromsø, Norway, p. 66.

England, J.; Atkinson, N.; Dyke, A.; Evans, D.; Zreda, M. 2004. «Late wisconsinan buildup and wastage of the innuitian Ice Sheet across southern Ellesmere Island, Nunavut». **Canadian Journal of Earth Sciences**, vol. 41, n°1 , pp. 39-61.

England, J.; Lajeunesse, P. 2004. «Overview of the Innuitian ice sheet and new perspectives on episodic ice shelves on the NW Laurentide ice sheet». **Joint Annual Meeting, Geological Association of Canada**, Abstracts vol. 29, St. Catherines, Canada, p. 41.

England, J.; Atkinson, N.; Bednarski, J.; Dyke, A. S.; Hodgson, D. A.; Cofaigh, C. O. 2006. «The Innuitian Ice Sheet: configuration, dynamics and chronology». **Quaternary Science Reviews,** vol. 25, n°7-8, pp. 689-703.

Fensome, R.A.; Taylor, F.J.R.; Norris, G.; Sarjeant, W.A.S.; Wharton, D.I; and Williams, G.L. 1993. «**A Classification of Living and Fossil Dinoflagellates. Micropaleontology, Special Publication Number 7**». American Museum of Natural History, New York, 351p.

Finkelstein, S. A.; Gajewski, K. 2007. «A palaeolimnological record of diatom-community dynamics and late-Holocene climatic changes from Prescott Island, Nunavut, central Canadian Arctic». **The Holocene**, vol. 17, n°26, pp. 803-812.

Finkelstein, S. A.; Gajewski, K. 2008. «Responses of Fragilarioid-dominated diatom assemblages in a small Arctic lake to Holocene climatic changes, Russell Island, Nunavut, Canada». **Journal of Paleolimnology**, vol. 40, n°4, pp. 1079-1095.

Fisher, D. A., 1976. «A study of two O-18 records from Devon Ice cap, Canada, and comparison of them to Camp Century O-18 record, Greenland». Thèse de doctorat, University of Copenhagen, 278 pp.

Fisher, D. A., 1979. «Comparison of 105 years of oxygen isotope and insoluble impurity profiles from the Devon Island and Camp Century ice cores». **Quaternary Research**, vol. 11, n°3 , pp. 299-305.

Fisher, D. A.; Koerner, R.M. 1980. «Some aspects of climatic change in the High Arctic during the Holocene as deduced from ice cores». Dans **Quaternary Climatic Change Symposium**. Préparé par Mahaney, W.C. York University, Toronto, pp. 349-371.

Fisher, D. A.; Koerner, R. M.; Paterson, W. S. B.; Dansgaard, W.; Gundestrup, N.; Reeh, N. 1983. «Effect of wind scouring on climatic records from ice-core oxygen-isotope profiles». **Nature**, vol. 301, n° 5897, pp. 205-209.

Fisher, D. A.; Koerner, R. M.; Reeh, N. 1995. «Holocene Climatic Records from Agassiz Ice Cap, Ellesmere Island, Nwt, Canada». **The Holocene**, vol. 5, n°1, pp.19-24.

Fisher, D.; Dyke, A.; Koerner, R.; Bourgeois, J.; Kinnard, C.; Zdanowicz, C; de Vernal, A.; Hillaire-Marcel, C.; Savelle, J.; Rochon, A. 2006. «Natural Variability of Arctic Sea-ice Over the Holocene». **Eos, Transactions American Geophysical Union**, vol. 87, n°28, pp. 273-275.

Francis, D. R.; Wolfe, A. P.;Walker, I. R.; Miller, G. H. 2006. «Interglacial and Holocene temperature reconstructions based on midge remains in sediments of two lakes from Baffin Island, Nunavut, Arctic Canada». **Palaeogeography, Palaeoclimatology, Palaeoecology**, vol. 236, n°1-2, pp. 107-124.

Fréchette, B.; de Vernal, A. 2009. «Relationship between Holocene climate variations over southern Greenland and eastern Baffin Island and synoptic circulation pattern». **Climate of the Past Discussions**, vol. 5, n°2, pp. 879-910.

Gajewski, K. 1995. «Modern and Holocene pollen assemblages from some small Arctic lakes on Somerset Island, NWT, Canada». **Quaternary Research**, vol. 44, n°2, pp. 228–236.

Gajewski, K.; Frappier, M. 2001. «A Holocene Lacustrine record of environmental change in northeastern Prince of Wales Island, Nunavut, Canada». **Boreas**, vol. 30, n°4 , pp. 285–289.

Geiss, C.E.; Banerjee, S.K. 2003. «A Holocene-Late Pleistocene geomagnetic inclination record from Grandfather Lake, SW Alaska». **Geophysic Journal International**, vol.153, n°2, pp. 497-507.

Golubeva, E.N.; Platov, G.A., 2007. «On improving the simulation of Atlantic water circulation in the Arctic ocean». **Journal of Geophysical Research**, vol. 112, C04S05, doi:10.1029/2006JC003734.

Goosse, H.; Fichefet, T.; Campin, J. M. 1997. «The effects of the water flow through the Canadian Archipelago in a global ice-ocean model» **Geophysical Research Letters**, vol. 24, n°12, pp. 1507-1510.

Gratton, Y.; Melling, H.; Ingram, R.G.; Rail, M.E. 2003. «Circulation and formation of the North Water Polynya, Baffin Bay». **Geophysical Research Abstracts**, vol. 5, 08068. http://www.cosis.net/abstracts/EAE03/08068/EAE03-J-08068.pdf

Guiot, J.; Goeury, C. 1996. «PPPBase, a software for statistical analysis of paleoecological and paleoclimatological data». **Dendrochronologia**, vol. 14, pp. 295-300.

Guiot, J.; de Vernal, A. 2007. «Transfer functions: methods for quantitative paleoceanography based on microfossils». Dans **Proxies in Late Cenozoic Paleoceanography**. Préparé par Hillaire-Marcel, C.; de Vernal, A. Elsevier, pp.523-563.

Haak, H.; Jungclaus, J.H.; Koenigk, T.; Sein, D.; Mikolajewicz, U. 2005. «Arctic Ocean freshwater budget variability». Arctic / Subarctic Ocean Fluxes (ASOF) Newsletter, vol. 3, pp. 6-9.

Hakkinen, S.; Proshutinsky, A. 2004. «Freshwater content variability in the Arctic Ocean». **Journal of Geophysical Research – Oceans**, vol. 109, C03051, doi:10.1029/2003JC001940.

Hamel, D.; de Vernal, A.; Gosselin, M.; Hillaire-Marcel, C. 2002. «Organic-walled microfossils and geochemical tracers: sedimentary indicators of productivity changes in the North Water and northern Baffin Bay during the last centuries». **Deep-Sea Research Part II-Topical Studies in Oceanography**, vol. 49, n°22-23, pp. 5277-5295.

Head, M.J.; Harland, R.; Matthiessen, J. 2001. «Cold marine indicators of the late Quaternary: the new dinoflagellate cyst genus Islandinium and related morphotypes». **Journal of Quaternary Science**, vol. 16, n°7 , pp. 621–636.

Hillaire-Marcel, C.; de Vernal, A.; Bilodeau, G.; Weaver, A.J. 2001. «Absence of deep-water formation in the Labrador Sea during the last interglacial period». **Nature**, vol. 410, pp. 1073–1077.

Hillaire-Marcel, C.; de Vernal, A.; Polyak, L.; Darby, D. 2004. «Size-dependent isotopic composition of planktic foraminifers from Chukchi Sea vs. NW Atlantic sediments - implications for the Holocene paleoceanography of the western Arctic». **Quaternary Science Reviews**, vol. 23, n°3-4, pp. 245-260.

Holland, M. M.; Finnis, J.; Serreze, M. C. 2006. «Simulated Arctic Ocean freshwater budgets in the twentieth and twenty-first centuries». **Journal of Climate**, vol. 19, n°23, pp. 6221-6242.

Howell, S. E. L.; Tivy, A.; Yackel, J. J.; McCourt, S. 2008. «Multi-year sea-ice conditions in the western Canadian Arctic Archipelago region of the Northwest Passage: 1968-2006». **Atmosphere-Ocean**, vol. 46, n°2, 229–242.

Hughen, K. A.; Baillie, M. G. L.; Bard, E.; Bayliss, A.; Beck, J. W.; Blackwell, P. G.; Buck, C. E.; Burr, G. S.; Cutler, K. B.; Damon, P. E.; Edwards, R. L.; Fairbanks, R. G.; Friedrich, M.; Guilderson, T. P.; Herring, C.; Kromer, B.; McCormac, F. G.; Manning, S. W.; Ramsey, C. B.; Reimer, P. J.; Reimer, R. W.; Remmele, S.; Southon, J. R.; Stuiver, M.; Talamo, S.; Taylor, F. W.; van der Plicht, J.; Weyhenmeyer, C. E. 2004. «Marine04 Marine radiocarbon age calibration, 26 - 0 ka BP». **Radiocarbon**, vol. 46, n°3, pp. 1059-1086.

Hurrell, J. W. 1995. «Decadal Trends in the North-Atlantic Oscillation : Regional Temperatures and Precipitation». **Science**, vol. 269, n°5224, pp. 676-679.

Hurrell, J. W.; Deser, C. Sous-presse. «North Atlantic climate variability: The role of the North Atlantic Oscillation». **Journal of Marine Systems**, Épreuve corrigée.

Hurrell, J. W.; James, R. H. 2003. «CLIMATE VARIABILITY | North Atlantic and Arctic Oscillation» Dans **Encyclopedia of Atmospheric Sciences**. Préparé Holton, J.; Pyle, J.; Curry J., Academic Press, Oxford, pp. 439-445.

Ingram, R.G.; Bâcle, J.; Barber, D.G.; Gratton, Y.; Melling, H. 2002. «An overview of physical processes in the North Water». **Deep-Sea Research. Part II. Topical studies in oceanography**, vol. 49, n°22-23, pp. 4893–4906.

Intergovernmental Panel on Climate Change. 2007. «Climate Change 2007: Synthesis Report». **Contribution of Working Groups I, II and III to the Fourth Assessment Report of the Intergovernmental Panel on Climate Change.** Préparé par Pachauri, R.K.; Reisinger, A. IPCC, Geneva, Switzerland, 104 p.

Jakobsson, M. 2002. «Hypsometry and volume of the Arctic Ocean and its constituent seas». **Geochemistry Geophysics Geosystems**, vol. 3, n°5, 1028, doi:10.1029/2001GC000302.

Jakobsson, M. 2004. «Correction to "Hypsometry and volume of the Arctic Ocean and its constituentseas"». **Geochemistry Geophysics Geosystems**, vol. 5, Q02005, doi:10.1029/2004GC000694.

Jennings, A.E.; Knudsen, K.L.; Hald, M.; Hansen, C.V.; Andrews, J.T. 2002. «A mid-Holocene shift in Arctic sea-ice variability on the East Greenland Shelf». **The Holocene**, vol. 12, n°1, pp. 49-58.

Johannessen, O. M.; Bengtsson, L.; Miles, M. W.; Kuzmina, S. I.; Semenov, V. A.; Alekseev, G. V.; Nagurnyi, A. P.; Zakharov, V. F.; Bobylev, L. P.; Pettersson, L. H.; Hasselmann, K.; Cattle, H. P. 2004. «Arctic climate change: observed and modelled temperature and sea-ice variability (vol 56A, pg 328, 2004)», **Tellus**, vol. 56A, pp. 559-560.

Johnson, M. A.; Proshutinsky, A. Y.; Polyakov, I. V. 1999. «Atmospheric patterns forcing two regimes of arctic circulation: A return to anticyclonic conditions?» **Geophysical Research Letters**, vol. 26, n°11, pp. 1621-1624.

Johnson, M. A.; Polyakov, I. V. 2001. «The Laptev Sea as a source for recent Arctic Ocean salinity changes». **Geophysical Research Letters**, vol. 28, n°10, pp. 2017-2020.

Jones, E. P. 2001. «Circulation in the Arctic Ocean». **Polar Reasearch**, vol. 20, n°2, pp. 139-146.

Jones, E. P.; Swift, J. H.; Anderson, L. G.; Lipizer, M.; Civitarese, G.; Falkner, K. K.; Kattner, G.; McLaughlin, F. 2003. «Tracing Pacific water in the North Atlantic Ocean». **Journal of Geophysical Research-Oceans**, vol. 108, C4, 3116, doi:10.1029/2001JC001141.

Joynt, E. H.; Wolfe A. P. 2001. «Paleoenvironmental inference models from sediment diatom assemblages in Baffin Island lakes (Nunavut, Canada) and reconstruction of summer water temperature». **Canadian Journal of Fisheries and Aquatic Sciences**, vol. 58, n°6, pp. 1222–1243.

Justwan, A.; Koc, N.; Jennings, A. E. 2008. «Evolution of the Irminger and East Icelandic Current systems through the Holocene, revealed by diatom-based sea-surface temperature reconstructions». **Quaternary Science Reviews**, vol. 27, n°15-16, pp. 1571-1582.

Karl, T. R.; Trenberth, K. E. 2003. «Modern global climate change». **Science**, vol. 302, n°5651, pp. 1719-1723.

Kaufman, D. S.; Ager, T. A.; Anderson, N. J.; Anderson, P. M.; Andrews, J. T.; Bartlein, P. J.; Brubaker, L. B.; Coats, L. L.; Cwynar, L. C.; Duvall, M. L.; Dyke, A. S.; Edwards, M. E.; Eisner, W. R.; Gajewski, K.; Geirsdóttir, A.; Hu, F. S.; Jennings, A. E.; Kaplan, M. R.; Kerwin, M. W.; Lozhkin, A. V.; MacDonald, G. M.; Miller, G. H.; Mock, C. J.; Oswald, W. W.; Otto-Bliesner, B. L.; Porinchu, D. F.; Rühland, K.; Smol, J. P.; Steig, E. J.; Wolfe, B. B. 2004. «Holocene thermal maximum in the western Arctic (0-180°W)». **Quaternary Science Reviews**, vol. 23, n°5-6, pp. 529-560.

Kay, J. E.; L'Ecuyer, T.; Gettelman, A.; Stephens, G.; O'Dell, C. 2008. «The contribution of cloud and radiation anomalies to the 2007 Arctic sea ice extent minimum». **Geophysical Research Letters,** vol. 35, L08503, doi:10.1029/2008GL033451.

Kelly, M.; Funder, S.; Houmark-Nielsen M.; Knudsen, K. L.; Kronborg, C.; Landvik, J.; Sorby, L. 1999. «Quaternary glacial and marine environmental history of northwest Greenland: a review and reappraisal». **Quaternary Science Reviews**, vol. 18, n°3, pp. 373-392.

Kerwin, M. W.; Overpeck, J. T.; Webb, R. S.; Anderson, K. H. 2004. «Pollen-based summer temperature reconstructions for the eastern Canadian boreal forest, subarctic, and Arctic». **Quaternary Science Reviews**, vol. 23, n°18-19, pp. 1901-1924.

Kirschvink, J. L. 1980. «The least-squares line and plane and the analysis of paleomagnetic data». **Geophysical Journal of the Royal Astronomical Society**, vol. 62, pp. 699-718.

Kliem, N.; Greenberg, D. A. 2003. «Diagnostic simulations of the summer circulation in the Canadian Arctic Archipelago». **Atmosphere - ocean**, vol. 41, n°4, 273-289.

Klyuvitkina, T. S.; Bauch, H. A. 2006. «Hydrological changes in the Laptev Sea during the Holocene inferred from the studies of aquatic palynomorphs». **Oceanology**, vol. 46, n°6, pp. 859-868.

Knudsen, K. L.; Stabell, B.; Seidenkrantz, M.-S.; Eiríksson, J.; Blake, W. Jr. 2008. «Deglacial and Holocene conditions in northernmost Baffin Bay: sediments, foraminifera, diatoms and stable isotopes». **Boreas**, vol. 37, n°3, pp. 346–376.

Koç, N.; Jansen, E. 2002. «Holocene climate evolution of the North Atlantic Ocean and the Nordic Seas – a synthesis of new results». Dans **Climate development and History in the North Atlantic Realm**. Préparé par Wefer, G.; Berger, W.H.; Behre, K.-E.; Jansen, E. Springer-Verlag Berlin Heidelberg, New York, pp. 165-173.

Koenigk, T.; Mikolajewicz, U.; Haak, H.; Jungclaus, J. 2007. «Arctic freshwater export in the 20th and 21st centuries». **Journal of Geophysical Research Biogeoscience**, vol. 112, G04S41, doi:10.1029/2006JG000274.

Kokinos, J. P.; Eglinton, T. I.; Goni, M. A.; Boon, J. J.; Martoglio, P. A.; Anderson, D. M. 1998. «Characterization of a highly resistant biomacromolecular material in the cell wall of a marine dinoflagellate resting cyst». **Organic Geochemistry**, vol. 28, n°5, pp. 265-288.

Korte, M.; Constable, C. G. 2005. «Continuous geomagnetic field models for the past 7 millennia: 2. CALS7K». **Geochemistry Geophysics Geosystems**, vol. 6, Q02H16, doi:10.1029/2004GC000801.

Korte, M.; Genevey, A.; Constable, C. G.; Frank, U.; Schnepp, E. 2005. «Continuous geomagnetic field models for the past 7 millennia: 1. A new global data compilation». **Geochemistry Geophysics Geosystems**, vol. 6, Q02H15, doi:10.1029/2004GC000800.

Kotilainen, A. T.; Saarinen, T.; Winterhalter, B. 2000. «High-resolution paleomagnetic dating of sediments deposited in the central Baltic Sea during the last 3000 years». **Marine Geology**, vol. 166, n°1-4, pp. 51-64.

Kunz-Pirrung, M. 2001. «Dinoflagellate cyst assemblages in surface sediments of the Laptev Sea region (Arctic Ocean) and their relationship to hydrographic conditions». **Journal of Quaternary Science**, vol. 16, n°7, pp. 637-649.

Kunz-Pirrung, M.; Matthiessen, J.; de Vernal, A. 2001. «Late Holocene dinoflagellate cysts as indicators for short-term climate variability in the eastern Laptev Sea (Arctic Ocean)». **Journal of Quaternary Science**, vol. 16, n°7, pp. 711-716.

Kwok, R. 2000. «Recent changes in Arctic Ocean sea ice motion associated with the North Atlantic Oscillation». **Geophysical Research Letters**, vol. 27, n°6, pp. 775-778.

Lassen, S. J.; Kuijpers, A.; Kunzendorf, H.; Hoffmann-Wieck, G.; Mikkelsen, N.; Konradi, P. 2004. «Late-Holocene Atlantic bottom-water variability in Igaliku Fjord, South Greenland, reconstructed from foraminifera faunas». **Holocene**, vol. 14, n°2, pp. 165-171.

Ledu, D.; Rochon, A.; de Vernal, A.; St-Onge, G. Accepté. «Holocene paleoceanography of the Northwest Passage, Canadian Arctic Archipelago: the possible onset of an Arctic Oscillation climate mode». **Quaternary Science Reviews**

Ledu, D.; Rochon, A.; de Vernal, A.; St-Onge, G. 2008a. «Palynological Evidence of Holocene Climate Change in the Eastern Arctic: a Possible shift in the Arctic Oscillation at the Millennial Time Scale». **Canadian Journal of Earth Science**, vol. 45, n°11, pp. 1363-1375.

Ledu, D.; Rochon, A.; de Vernal, A.; St-Onge, G. 2008b. «Holocene climate changes in the main axis of the Northwest Passage inferred from dinocyst assemblages: a possible influence of the Arctic Oscillation at the millennial time scale». Dans **Conference Programme and Abstracts, International Arctic Change 2008 Conference. December 9-12, 2008**. Québec, Québec, pp. 110-111.

Levac, E.; de Vernal, A.; Blake, W. 2001. «Sea-surface conditions in northernmost Baffin Bay during the Holocene: palynological evidence». **Journal of Quaternary Science**, vol.16, n°4, pp. 353-363.

Lindsay, R. W.; Zhang, J. 2005. «The thinning of Arctic sea ice, 1988-2003: Have we passed a tipping point?» **Journal of Climate**, vol. 18, n°22, pp. 4879-4894.

Lisé-Pronovost, A.; St-Onge, G.; Brachfeld, S.; Bareletta, F.; Darby, D. Sous presse. Paleomagnetic constraints on the Holocene stratigraphy of the Arctic Alaskan margin. **Global and Planetary Change**.

Lloyd, J.M.; Park, L.A.; Kuijpers, A.; Moros, M. 2005. «Early Holocene palaeoceanography and deglacial chronology of Disko Bugt, West Greenland». **Quaternary Science Reviews**, vol. 24, n°14-15, pp. 1741-1755.

Lloyd, J. M.; Kuijpers, A.; Long, A.; Moros, M.; Park, L. A. 2007. «Foraminiferal reconstruction of mid- to late-Holocene ocean circulation and climate variability in Disko Bugt, West Greenland». **The Holocene**, vol.17, n°8, pp.1079-1091.

Lovejoy, C.; Legendre, L.; Price, N. M. 2002. «Prolonged diatom blooms and microbial food web dynamics: experimental results from an Arctic polynya». **Aquatic microbial ecology**, vol. 29, n°3, pp. 267-278.

Lund, S.P. 1996. «A comparison of Holocene paleomagnetic secular variation records from North America». **Journal of Geophysical Research Solid Earth**, 101(B4), 8007–8024.

Massé, G.; Rowland, S.J.; Sicre, M.A.; Jacob, J.; Jansen, E.; Belt, S.T. 2008. «Abrupt climate changes for Iceland during the last millennium: Evidence from high resolution sea ice reconstructions». **Earth and Planetary Science Letters,** vol. 269, pp. 564-568.

MacDonald, G.; Felzer, B.; Finney, B.; Forman, S. 2000. «Holocene lake sediment records of Arctic hydrology». **Journal of Paleolimnology**, vol. 24, n°3, pp. 1-14.

McClelland, J. W.; Déry, S. J.; Peterson, B. J.; Holmes, R. M.; Wood, E. F. 2006. «A pan-arctic evaluation of changes in river discharge during the latter half of the 20th century». **Geophysical Research Letters**, 33, L06715, doi:10.1029/2006GL025753.

McKay, J. L.; Hillaire-Marcel, C.; de Vernal, A.; Polyak, L.; Darby, D. 2006. «Holocene Paleoceanography of the Chukchi Sea / Alaskan Margin, Western Arctic Ocean». **Eos Tranactions AGU, Fall Meeting Supplement,** vol. 8, n°52, Abstract OS53B-1101.

McKay, J.L; de Vernal, A.; Hillaire-Marcel, C.; Not C.; Polyak, L.; Darby, D. 2008. «Holocene fluctuations in Arctic sea-ice cover: dinocyst-based reconstructions for the eastern Chukchi Sea». **Canadian Journal of Earth Science**, vol. 45, n°11, pp. 1377-1397.

McLaughlin, F. A.; Carmack, E. C.; MacDonald, R. W.; Bishop, J. K. B. 1996. «Physical and geochemical properties across the Atlantic Pacific water mass front in the southern Canadian Basin». **Journal of Geophysical Research Oceans**, 101, n°C1, pp. 1183–1197.

McLaughlin, F.A.; Carmack, E.; Mcdonald, R.; Weaver, A.; and Smith, J. 2002. «The Canada Basin 1989–1995: upstream events and far-field effects of the Barents Sea Branch». **Journal of Geophysical Research**, vol. 107, C7, 3082, doi:10.1029/ 2001JC000904.

McLaughlin, F. A.; Carmack, E. C.; Macdonald, R. W.; Melling, H.; Swift, J. H.; Wheeler, P. A.; Sherr, B. F.; Sherr, E. B. 2004. «The joint roles of Pacific and Atlantic-origin waters in the

Canada Basin, 1997-1998». **Deep-Sea Research Part 1. Oceanographic Research Papers**, vol. 51, n°1, pp. 107-128.

Mangerud, J.; Gulliksen, S. 1975. «Apparent radioacarbon ages of recent marine shells from Norway, Spitsbergen and Arctic Canada». **Quaternary Research**, vol. 5, n°2, pp. 263-273.

Marret, F.; Zonneveld, K. A. F. 2003. «Atlas of modern organic-walled dinoflagellate cyst distribution». **Review of Palaeobotany and Palynology**, vol. 125, n°1-2, pp. 1-200.

Matthews, J. 1969. «The assessment of a method for the determination of absolute pollen frequencies». **New Phytologist**, vol. 68, n°1, pp. 161-166.

Matthiessen, J.; de Vernal, A.; Head, M.; Okolodkov, Y.; Zonneveld, K.; Harland, R. 2005. «Modern organic-walled dinoflagellate cysts in Arctic marine environments and their paleo- environmental significance». Paläontologische Zeitschrift, vol. 79, n°1, pp. 3-51.

Mazaud, A. 2005. «User-friendly software for vector analysis of the magnetization of long sediment cores». **Geochemistry Geophysics Geosystems**, vol. 6, Q12006, doi:10.1029/2005GC001036.

Melling, H. 2000. «Exchanges of freshwater through the shallow straits of the North American Arctic». Dans **The freshwater budget of the Arctic Ocean**. Publié par Lewis, E.L.; Jones, P., Lemke, P., Prowse, T.D.; Wadhams, P. Kluwer Academic Publishers, Dordrecht, pp. 479–502.

Melling, H.; Gratton, Y.; Ingram G. 2001. «Ocean circulation within the North Water Polynya of Baffin Bay». **Atmosphere-Ocean**, vol. 39, n°3, pp. 301-325.

Melling, H. 2002. «Sea ice of the northern Canadian Arctic Archipelago». **Journal of Geophysical Research-Oceans**, vol. 107, C11, 3181, doi:10.1029/2001JC001102

Melling, H. 2004. «Fluxes through the Northern Canadian Arctic Archipelago». **ASOF Newsletter**, vol. 2, pp. 3-13.

Michel, C.; Ingram, R. G.; Harris, L. R. 2006. «Variability in oceanographic and ecological processes in the Canadian Arctic Archipelago». **Progress in Oceanography**, vol. 71, n°2-4, pp. 379-401.

Michelutti, N.; Douglas, M. S. V.; Wolfe, A. P.; Smol, J. P. 2006. «Heightened sensitivity of a poorly buffered high arctic lake to late-Holocene climatic change». **Quaternary Research**, vol. 65, n°3, pp. 421-430.

Miller, G. H.; Wolfe, A. P.; Briner, J. P.; Sauer, P. E.; Nesje, A. 2005. «Holocene glaciation and climate evolution of Baffin Island, Arctic Canada». **Quaternary Science Reviews**, vol. 24, n°14-15, pp. 1703-1721.

Millot, R.; Gaillardet, J.; Dupre, B.; Allegre, C. J. 2003. «Northern latitude chemical weathering rates: Clues from the Mackenzie River Basin, Canada». **Geochimica et cosmochimica acta**, ol. 67, n°7, pp. 1305-1329.

Mudie, P. J.; Rochon, A. 2001. «Distribution of dinoflagellate cysts in the Canadian Arctic marine region». **Journal of Quaternary Science**, vol. 16, n°7, pp. 603-620.

Mudie, P. J.; Rochon, A.; Levac, E. 2005. «Decadal-scale sea-ice changes in the Canadian Arctic and their impacts on humans during the past 4000 years». **Environmental Archeologist**, vol. 10, pp. 113-126.

Mudie, P. J.; Rochon, A.; Prins, M.A.; Soenarjo, D.; Troelstra, S.R.; Levac, E.; Scott, D.B.; Roncaglia, L.; Kuijpers, A. 2006. «Late Pleistocene-Holocene marine geology of Nares Strait region: Paleoceanography from foraminifera and dinoflagellate cysts, sedimentology and stable isotopes». **Polarforschung**, vol. 74, n°1-3, pp. 169-183.

Mundy, C.J.; Gosselin, M.; Ehn, J.; Gratton, Y.; Rossnagel, A.; Barber, D.G.; Martin, J.; Tremblay, J.E.; Palmer, M.; Arrigo, K.R.; Darnis, G.; Fortier, L.; Else, B.; Papakyriakou, T. 2009. «Contribution of under-ice primary production to an ice-edge upwelling phytoplankton bloom in the Canadian Beaufort Sea. **Geophysical Research Letters,** vol. 36, L17601, doi: 10. 1029/2009GL38837.

Naidu, A. S.; Cooper, L. W.; Finney, B. P.; MacDonald, R. W.; Alexander, C.; Semiletov, I. P. 2000. «Organic carbon isotope ratios delta C-13 of Arctic Amerasian Continental shelf sediments». **International Journal of Earth Sciences**, vol. 89, n°3, pp. 522-532.

National Oceanography Data Center (NODC). Page consultée en janvier 2009. **World Ocean Atlas, 2001. National Oceanic and Atmospheric Administration (NOAA)**. [En ligne]. Adresse URL : http://www.nodc.noaa.gov/OC5/WOD01/pr_wod01.html.

National Snow and Ice Data Center (NSIDC). (Page consultée en septembre 2008). Sea-ice extent 1953-2000 [En ligne]. Adresse URL : http://nsidc.org.

Okulitch, A.V.; Trettin, H.P. 1991. «Late Cretaceaous to Early Tertiary deformation, Aretie Islands». Dans **Geology of the Innuitian Orogen and Aretie Platform of Canada and Greenland**. Préparé par Trettin, H.P. Geological Survey of Canada, Ottawa, 3, 469-489.

Olafsdottir, S.; Geirsdottir, A.; Jennings, A.E.; Stoner, J.S.; Miller, G.H. 2006. «High- resolution Holocene Paleoceanographic and Paleoclimatic Records from Iceland: Land Sea Correlation». **EOS Transactions AGU, Fall Meeting supplement**, vol. 87, n°52, abstract PP43A-1222.

Olyunina, O. S.; Polyakova, E. I.; Romanenko, F. A. 2008. «Diatom assemblages from Holocene sediments of the Kola Peninsula». **Doklady Earth Sciences**, vol. 423, n°2, pp. 1343-1347.

Overland, J. E.; Wang, M.; Salo, S. 2008. «The recent Arctic warm period». **Tellus**, vol. 60A, pp. 589-597.

Parkinson, C. L.; Cavalieri, D. J.; Gloersen, P.; Zwally, H. J.; Comiso, J. C. 1999. «Arctic sea ice extents, areas, and trends, 1978-1996». **Journal of Geophysical Research**, vol. 104, n°C9, pp. 20837-20856.

Parkinson, C. L.; Cavalieri, D. J. 2002. «A 21 year record of Arctic sea-ice extents and their regional, seasonal and monthly variability and trends». **Annals of Glaciology**, vol.34, pp.441-446

Parkinson, C. L.; Cavalieri, D. J. 2008. «Arctic sea ice variability and trends, 1979-2006». **Journal of Geophysical Research Oceans**, vol. 113, pp. 28.

Parnell, J.; Bowden, S.; Andrews, J. T.; Taylor, C. 2007.« Biomarker determination as a provenance tool for detrital carbonate events (Heinrich events?): Fingerprinting Quaternary glacial sources into Baffin Bay». **Earth and Planetary Science Letters**, vol. 257, n°1-2, pp. 71-82.

Parrish, C.C.; Wangersky, P.J. 1987. «Particulate and dissolved lipid classes in cultures of *Phaeodactylum tricornutum* grown in cage culture turbidostats with a range of nitrogen supply rates». **Marine Ecology-Progress Series,** vol. 35, pp. 119-128.

Parrish, C.C.;Wells, J.S.;Yang, Z.; Dabinett, P. 1998.«Growth and lipid composition of scallop juveniles, *Placopecten magellanicus*, fed the fagellate *Isochrysis galbana* with varying lipid composition and the diatom *Chaetoceros muelleri*». **Marine Biology**, vol. 133, pp. 461-471.

Peros, M. C.; Gajewski, K. 2008. «Holocene climate and vegetation change on Victoria Island, western Canadian Arctic». **Quaternary Science Reviews**, vol. 27, n°3-4, pp. 235-249.

Peterson, B.J.; Holmes R.M.; McClelland, J.W.; Vörösmarty, C.J.; Lammers, R.B.; Shiklomanov, A.I.; Shoklimanov, I.A.; Rahmstorf, S. 2002. «Increasing River Discharge to the Arctic Ocean». **Science**, vol. 298, n°5601, pp. 2171-2173.

Peterson, B. J.; McClelland, J.; Curry, R.; Holmes, R. M.; Walsh, J. E.; Aagaard, K. 2006. «Trajectory shifts in the Arctic and subarctic freshwater cycle». **Science**, vol. 313, n°5790, pp. 1061-1066.

Podritske, B.; Gajewski, K. 2007. «Diatom community response to multiple scales of Holocene climate variability in a small lake on Victoria Island, NWT, Canada». **Quaternary Science Reviews**, vol. 26, n°25-28, pp. 3179-3196.

Polyak, L.; Levitan, M.; Gataullin, V.; Khusid, T.; Mikhailov, V.; Mukhina, V. 2000. «The impact of glaciation, river-discharge and sea-level change on Late Quaternary

environments in the southwestern Kara Sea». **International Journal of Earth Sciences**, vol. 89, n°3, pp. 550-562.

Polyak, L.; Levitan, M.; Khusid, T.; Merklin, L.; Mukhina, V. 2002a. «Variations in the influence of riverine discharge on the Kara Sea during the last deglaciation and the Holocene», **Global and Planetary Change**, vol. 32, n°4, pp. 291-309.

Polyak, L.; Korsun, S.; Febo, L. A.; Stanovoy, V.; Khusid, T.; Hald, M.; Paulsen, B. E.; Lubinski, D. J. 2002b. «Benthic foraminiferal assemblages from the southern Kara Sea, a river-influenced Arctic marine environment». **Journal of Foraminiferal Research**, vol. 32, n°3, pp. 252-273.

Polyakov, I. V.; Johnson, M. A. 2000. «Arctic decadal and interdecadal variability». **Geophysical Research Letters**, vol. 27, n°24, pp. 4097-4100.

Polyakov, I. V.; Alekseev, G. V.; Timokhov, L. A.; Bhatt, U. S.; Colony, R. L.; Simmons, H. L.; Walsh, D.; Walsh, J. E.; Zakharov, V. F. 2004. «Variability of the intermediate Atlantic water of the Arctic Ocean over the last 100 years». **Journal of Climate**, vol. 17, n°23, pp. 4485-4497.

Polyakova, Y. I.; Bauch, H. A.; Klyuvitkina, T. S. 2005. «Early to middle Holocene changes in Laptev Sea water masses deduced from diatom and aquatic palynomorph assemblages». **Global and Planetary Change**, vol. 48, n°1-3, pp. 208-222.

Prange, M.; Lohmann, G. 2003. «Effects of mid-Holocene river runoff on the Arctic ocean/sea-ice system: a numerical model study». **The Holocene**, vol. 13, n°3, pp. 335-342.

Prinsenberg, S. J.; Bennett, E. B. 1987. «Mixing and transports in Barrow Strait, the central part of the Northwest passage». **Continental Shelf Research**, vol. 7, n°8, pp. 913-935.

Prinsenberg, S. J.; Hamilton, J. 2005. «Monitoring the volume, freshwater and heat fluxes passing through Lancaster Sound in the Canadian Arctic Archipelago». **Atmosphere-Ocean**, vol. 43, n°1, pp. 1-22.

Proshutinsky, A. Y.; Johnson, M. A. 1997. «Two circulation regimes of the wind driven Arctic Ocean». **Journal of Geophysical Research-Oceans**, vol. 102, n°C6, pp. 12 493-12 514.

Proshutinsky, A.; Bourke, R. H.; McLaughlin, F. A. 2002. «The role of the Beaufort Gyre in Arctic climate variability: Seasonal to decadal climate scales». **Geophysical Research Letters**, vol. 29, n°23, 2100, doi:10.1029/2002GL015847.

Radi, T.; de Vernal, A.; Peyron, O. 2001. «Relationships between dinoflagellate cyst assemblages in surface sediment and hydrographic conditions in the Bering and Chukchi seas». **Journal of Quaternary Science**, vol. 16, n°7, pp. 667-680.

Radi, T.; de Vernal, A. 2008. «Dinocysts as proxy of primary productivity in mid-high latitudes of the Northern Hemisphere». **Marine Micropaleontology**, vol. 68, n°1-2, pp. 84-114.

Ran, L.; Jiang, H.; Knudsen, K.L.; Eiríksson J. 2008. «The mid to late Holocene paleoceanographic changes in the northern North Atlantic». **Frontiers of Earth Science in China**, vol. 2, n°4, pp. 449-457.

Ren, J.; Jiang, H.; Seideinkrantz, M, S.; Kuijpers, A. 2009. «A diatom-based reconstruction of Early Holocene hydrographic and climatic change in a southwest Greenland fjord». **Marine Micropaleontology**, vol. 70, n°3-4, pp. 166-176.

Richerol, T.; Rochon, A.; Blasco, S.; Scott, D. B.; Schell, T. M.; Bennett, R. J. 2008a. «Distribution of dinoflagellate cysts in surface sediments of the Mackenzie Shelf and Amundsen Gulf, Beaufort Sea (Canada)». **Journal of Marine Systems**, vol. 74, n°3-4, pp. 825-839.

Richerol, T.; Rochon, A.; Blasco, S.; Scott, D. B.; Schell, T. M.; Bennett, R. J. 2008b. «Evolution of paleo sea-surface conditions over the last 600 years in the Mackenzie Trough, Beaufort Sea (Canada)». **Marine Micropaleontology**, vol. 68, n°1-2, pp. 6-20.

Riedel, A.; Michel, C.; Poulin, M.; Lessard, S. 2003. «Taxonomy and abundance of microalgae and protists at a first-year sea ice station near Resolute Bay, Nunavut, spring to early summer 2001». **Canadian Data Report of Hydrography and Ocean Science,** vol.159, pp. 54.

Rigor, I. G.; Wallace, J. M.; Colony, R. L. 2002. «Response of sea-ice to the Arctic oscillation». **Journal of Climate**, vol. 15, n°18, pp. 2648-2663.

Rigor, I. G.; Wallace, J. M. 2004. «Variations in the age of Arctic sea-ice and summer sea-ice extent». Geophysical Research Letters, vol. 31, L09401, doi:10.1029/2004GL019492.

Rochon, A.; de Vernal, A. 1994. «Palynomorph distribution in Recent sediments from the Labrador Sea». **Canadian Journal of Earth Sciences**, vol. 31, n°1, pp. 115-127.

Rochon, A.; de Vernal, A.; Turon, J-L.; Matthiessen, J.; Head, M.J. 1999. «Distribution of recent dinoflagellate cysts in surface sediments from the North Atlantic and adjacent seas, and quantitative reconstruction of sea-surface parameters». **American Association of Stratigraphic Palynologists, Contribution Series**, vol. 35, 150 p.

Rochon, A., et les participants à board. 2004. **CASES 2004, Leg 9 and ArcticNet Preliminary Cruise Report, CCGS Amundsen**, 05 August to 25 August 2004, 59 p.

Rochon, A.; Scott, D.B.; Schell, T.M.; Blasco, S.; Bennett, R.; Mudie, P. 2006. «Evolution of sea-surface Conditions During the Holocene : Comparison Between Eastern (Baffin Bay

and Hudson Strait) and Western (Beaufort Sea) Canadian Arctic». **EOS Transactions AGU, Fall Meeting supplement**, vol. 87, n°52, abstract U43B-0867.

Rochon, A. 2009. «The ecology and biological affinity of Arctic dinoflagellates and their paleoceanographical signifiance in the Canadian High Arctic». **From Deep-sea to Coastal Zones: Methods and Techniques for Studying Paleoenvironments. IOP Conference Series; Earth and Environmental Sciences**, vol. 5, 012003, doi;10.1088/1755-1307/5/1/012003.

Rolland, N.; Larocque, I.; Francus, P.; Pienitz, R.; Laperriere, L. 2008. «Holocene climate inferred from biological (Diptera : Chironomidae) analyses in a Southampton island (Nunavut, Canada) lake». **The Holocene**, vol. 18, n°2, pp. 229-241.

Rudels, B.; Jones, E. P.; Anderson, L. G.; Kattner, G. 1994. «On the intermediate depth waters of the Arctic Ocean». Dans "**The role of polar oceans in shaping the global climate.**" Préparé par Johannessen, O.M.; Muench, R.D.; Overland, J.E., American Geophysical Union, Washington, D.C., pp. 33-46.

Rudels, B.; Friedrich, H.J.; Quadfasel D. 1999. «The arctic circumpolar boundary current». **Deep-Sea Research Part II: Topical studies in oceanography**, vol. 46, n°6-7, pp. 1023-1062

Saarinen, T. 1998. «High-resolution palaeosecular variation in northern Europe during the last 3200 years». **Physics of The Earth and Planetary Interiors**, vol. 106, n°3-4, pp. 299-309.

Saarinen, T. 1999. «Palaeomagnetic dating of Late Holocene sediments in Fennoscandia». **Quaternary Science Reviews**, vol. 18, n°7, pp. 889-897.

Savelle, J. M.; Dyke, A. S.; McCartney, A. P. 2000. «Holocene bowhead whale (*Balaena mysticetus*) mortality patterns in the Canadian Arctic Archipelago». **Arctic**, vol. 53, n°4, pp. 414-421

Schell, T. M.; Moss, T. J.; Scott, D. B.; Rochon, A. 2008. «Paleo-sea-ice conditions of the Amundsen Gulf, Canadian Arctic Archipelago: Implications from the foraminiferal record of the last 200 years». **Journal of Geophysical Research-Oceans**, vol. 113, C03S02, doi:10.1029/2007JC004202.

Schlosser, P.; Newton, R.; Ekwurzel, B.; Khatiwala, S.; Mortlock, R.; Fairbanks, R. 2002. «Decrease of river runoff in the upper waters of the Eurasian Basin, Arctic Ocean, between 1991 and 1996: Evidence from delta δ18O data». **Geophysical Research Letters**, vol. 29, 1289, doi:10.1029/2001GL013135.

Schweiger, A. J.; Lindsay, R. W.; Vavrus, S.; Francis, J. A. 2008. «Relationships between Arctic sea ice and clouds during autumn». **Journal of Climate**, vol. 21, n°18, pp. 4799-4810.

Scott, D.B.; Schell, T.; St-Onge, G.; Rochon, A.; Blasco, S. 2009. «Foraminiferal assemblage changes over the last 15,000 years on the Mackenzie/Beaufort Sea slope and Amundsen Gulf, Canada: implication for past sea-ice conditions», **Paleoceanography**,vol. 24, PA2219, doi:10.1029/2007PA001575.

Seidenkrantz, M. S.; Aagaard-Sørensen, S.; Sulsbrück , H.; Kuijpers, A.; Jensen, K. G.; Kunzendorf, H. 2007. «Hydrography and climate of the last 4400 years in a SW Greenland fjord: implications for Labrador Sea palaeoceanography». **The Holocene**, vol. 17, n°3, pp. 387-401.

Seidenkrantz, M.-S.; Roncaglia, L.; Fischel, A.; Heilmann-Clausen, C.; Kuijpers, A.; Moros, M. 2008. «Variable North Atlantic climate seesaw patterns documented by a late Holocene marine record from Disko Bugt, West Greenland». **Marine Micropaleontology**, vol. 68, n°1-2, pp. 66-83.

Serreze, M. C.; Barry, R. G.; McLaren, A. S. 1989. «Seasonal variations in sea ice motion and effects on sea ice concentration in the Canada Basin». **Journal of Geophysical Research**, vol. 94, n°C8, pp. 10 955– 10 970.

Serreze, M.C.; Maslanik, J.A.; Scambos, T.A.; Fetterer, F.; Stroeve, J.; Knowles, K.; Fowler, C.; Drobot, S.; Barry, R.G.; Haran, T.M. 2003. « A record minimum arctic sea ice extent and area in 2002». **Geophysical Research Letters**, vol. 30, n°3, 1110, doi:10.1029/2002GL016406.

Serreze, M. C.; Barrett, A. P.; Slater, A. G.; Woodgate, R. A.; Aagaard, K.; Lammers, R. B.; Steele, M.; Moritz, R.; Meredith, M.; Lee, C. M. 2006. «The large-scale freshwater cycle of the Arctic». **Journal of geophysical research**, vol. 111, n°C11, pp. 19.

Serreze, M. C.; Barrett, A. P.; Slater, A. G.; Steele, M.; Zhang, J. L.; Trenberth, K. 2007. «The large-scale energy budget of the Arctic». **Journal of Geophysical Research Atmospheres**, vol. 112, D11122, doi:10.1029/2006JD008230.

Serreze, M. C.; Barrett, A. P. 2008. «The summer cyclone maximum over the central Arctic Ocean». **Journal of Climate**, vol. 21, n°5, 1048-1065.

Shimada, K.; Carmack, E. C.; Hatakeyama, K.; Takizawa, T. 2001. «Varieties of shallow temperature maximum waters in the Western Canadian Basin of the Arctic Ocean». **Geophysical Research Letters**, vol. 28, n°18, pp. 3441-3444.

Shimada, K.; McLaughlin, F.; Carmack, E.; Proshutinsky, A.; Nishino, S.; Itoh, M. 2004. «Penetration of the 1990s warm temperature anomaly of Atlantic Water in the Canada Basin». **Geophysical Research Letters**, vol. 31, L20301, doi:10.1029/2004GL020860.

Ślubowska-Woldengen, M.; Koç, N.; Rasmussen, T. L.; Klitgaard-Kristensen, D.; Hald, M.; Jennings, A. E. 2008. «Time-slice reconstructions of ocean circulation changes on the

continental shelf in the Nordic and Barents Seas during the last 16,000 cal yr BP». **Quaternary Science Reviews**, vol. 27, n°15-16, pp. 1476-1492.

Smith, I. R. 2002. «Diatom-based holocene paleoenvironmental records from continental sites on northeastern Ellesmere Island, high Arctic, Canada». **Journal of Paleolimnology**, vol. 27, n°1, pp. 9-28.

Snowball, I.; Sandgren, P. 2002. «Geomagnetic field variations in northern Sweden during the Holocene quantified from varved lake sediments and their implications for cosmogenic nuclide production rates». **Holocene**, vol. 12, n°5, pp. 517-530.

Snowball, I.; Zillén, L.; Ojala, A.; Saarinen, T.; Sandgren, P. 2007. «FENNOSTACK and FENNORPIS: Varve dated Holocene palaeomagnetic secular variation and relative palaeointensity stacks for Fennoscandia». **Earth and Planetary Science Letters**, vol. 255, n°1-2, pp. 106-116.

Solignac, S.; de Vernal, A.; Hillaire-Marcel, C. 2004. «Holocene sea-surface conditions in the North Atlantic - contrasted trends and regimes in the western and eastern sectors Labrador Sea vs. Iceland Basin». **Quaternary Science Reviews**, vol. 23, n°3-4, pp. 319-334.

Solignac, S.; Grelaud, M.; de Vernal, A.; Giraudeau, J.; Moros, M.; Mc Cave, I.N.; Hoogakker, B. 2008. «Reorganization of the upper ocean circulation in the mid-Holocene in the northeastern Atlantic». **Canadian Journal of Earth Sciences,** vol. 45, pp. 1417-1433.

Steele, M.; Boyd, T. 1998. «Retreat of the cold halocline layer in the Arctic Ocean». **Journal of Geophysical Research-Oceans**, vol. 103, n°C5, pp. 10419-10435.

Steele, M.; Ermold, W. 2004. «Salinity trends on the Siberain shelves». **Geophysical Research Letters**, vol. 31, L24308, doi:10.1029/2004GL021302.

Steele, M.; Morison, J.; Ermold, W.; Rigor, I.; Ortmeyer, M.; Shimada, K. 2004. «Circulation of summer Pacific halocline water in the Arctic Ocean». **Journal of Geophysical Research-Oceans**, vol. 109, C02027, doi:10.1029/2003JC002009.

Steele, M.; Ermold, W. 2007. «Steric sea level change in the Northern Seas». **Journal of Climate**, vol. 20, n°3, pp. 403-417.

Steele, M.; Ermold, W.; Zhang, J. L. 2008. «Arctic Ocean surface warming trends over the past 100 years». **Geophysical Research Letters**, vol. 35, L02614, doi:10.1029/2007GL031651.

Stoner, J.S.; St-Onge, G. 2007. «Magnetic stratigraphy in paleoceanography: reversals, excursions, paleointensity and secular variation». Dans **Proxies in Late Cenozoic Paleoceanography**. Édité par Hillaire-Marcel, C.; *de Vernal*, A., Elsevier, pp. 99-137.

Stoner, J. S.; Jennings, A.; Kristjansdottir, G. B.; Dunhill, G.; Andrews, J. T.; Hardardottir, J. 2007. «A paleomagnetic approach toward refining Holocene radiocarbon-based chronologies: Paleoceanographic records from the north Iceland (MD99-2269) and east Greenland (MD99-2322) margins». **Paleoceanography**, vol. 22, PA1209, doi:10.1029/2006PA001285.

St-Onge, G.; Stoner, J. S.; Hillaire-Marcel, C. 2003. «Holocene paleomagnetic records from the St. Lawrence Estuary, eastern Canada: centennial- to millennial-scale geomagnetic modulation of cosmogenic isotopes». **Earth and Planetary Science Letters**, vol. 209, n°1-2, pp. 113-130.

St-Onge, G.; Mulder, T.; Piper, D. J. W.; Hillaire-Marcel, C.; Stoner, J. S. 2004. «Earthquake and flood-induced turbidites in the Saguenay Fjord (Québec): a Holocene paleoseismicity record». **Quaternary Science Reviews**, vol. 23, n°3-4, pp. 283-294.

Stroeve, J.; Serreze, M.; Drobot, S.; Gearhead, S.; Holland, M.; Maslanik, J.; Meier, W.; Scambo, T. S. 2008. «Arctic sea ice extent plummets in 2007». **Eos Transactions AGU**, vol. *89*, n°2, pp.13.

Stuiver, M.; Reimer, P. J.; Reimer, R. W. (Page consultée en 2005). **CALIB 5.0 [WWW program and documentation]**. [En ligne] Adresse URL : http://calib.qub.ac.uk/calib/.

Swift, J. H.; Aagaard, K.; Timokhov, L.; Nikiforov, E. G. 2005. «Long-term variability of Arctic Ocean waters: Evidence from a reanalysis of the EWG data set». **Journal of Geophysical Research Oceans**, 110, C03012, doi:10.1029/2004JC002312.

Taylor, F.J.R. 1987. «**The Biology of Dinoflagellates. Botanical Monographs, Volume 21**». Blackwell Sciences Inc., Oxford, 785p.

Thompson, D. W. J.; Wallace, J. M. 1998. «The Arctic Oscillation signature in the wintertime geopotential height and temperature fields». **Geophysical Research Letters**, vol. 25, n°9, pp. 1297-1300.

Tremblay, L. B.; Mysak, L. A.; Dyke, A. S. 1997. «Evidence from driftwood records for century-to-millennial scale variations of the high latitude atmospheric circulation during the Holocene». **Geophysical Research Letters**, vol. 24, n°16, pp. 2027-2030.

Vare, L. L.; Massé, G.; Gregory, T. R.; Smart, C. W.; Belt, S. T. 2009 «Sea ice variations in the central Canadian Arctic Archipelago during the Holocene». **Quaternary Science Reviews**, vol. 28, n°13-14, pp. 1354-1366.

Vavrus, S.; Harrison, S. P. 2003. «The impact of sea-ice dynamics on the Arctic climate system». **Climate Dynamics**, vol. 20, n°7-8, pp. 741-757.

Venegas, S. A.; Mysak, L. A. 2000. «Is there a dominant timescale of natural climate variability in the Arctic?» **Journal of climate**, vol. 13, n°19, pp. 3412-3434.

Verosub, K.L.; Mehringer, P.J; Waterstraat, P. 1986. «Holocene secular variation in Western North America: Paleomagnetic record from Fish Lake, Harney County, Oregon». **Journal of Geophysical Research**, 91, n°B3, pp. 3609-3624.

Versteegh, G. J. M.; Blokker, P. 2004. Resistant macromolecules of extant and fossil microalgae. **Phycological Research**, vol.50, n°4, pp. 325-339.

Vinnikov, K. Y.; Robock, A.; Stouffer, R. J.; Walsh, J. E.; Parkinson, C. L.; Cavalieri, D. J.; Mitchell, J. F. B.; Garrett, D.; Zakharov, V. F. 1999. «Global warming and Northern Hemisphere sea ice extent». **Science**, vol.286, n°5446, pp. 1934-1937.

Vinogradov, M. E.; Vedernikov, V. I.; Romankevich, E. A.; Vetrov, A. A. 2000. «Components of the carbon cycle in the Russian Arctic Seas: Primary production and flux of C-org from the photic layer». **Oceanology**, vol. 40, n°2, pp. 204-215.

Vinther, B.M.; Buchardt, S.L.; Clausen, H.B.; Dahl-Jensen, D.; Johnsen, S.J.; Fisher, D.A.; Koerner, R.M.; Raynaud, D.; Lipenkov, V.; Andersen, K.K.; Blunier, T.; Rasmussen, S.O.; Steffensen, J.P.; Svensson, A.M. 2009. «Holocene thinning of the Greenland ice sheet». **Nature,** vol. 461, pp. 385-388.

von Quillfeldt, C. H. 2000. «Common diatom species in arctic spring blooms: Their distribution and abundance». **Botanica Marina**, vol. 43, n°6., pp. 499-516.

Voronina, E.; Polyak, L.; de Vernal, A.; Peyron, O. 2001. «Holocene variations of sea-surface conditions in the southeastern Barents Sea, reconstructed from dinoflagellate cyst assemblages». **Journal of Quaternary Science**, vol. 16, n°7, pp. 717-726.

Wadley, M. R.; Bigg, G. R. 2002. «Impact of flow through the Canadian Archipelago and Bering Strait on the north Atlantic and Arctic circulation: An ocean modelling study». **Quarterly Journal of the Royal Meteorological Society**, 128A, n°585, pp. 2187-2203.

Wallace, J. M.; Thompson, D. W. J. 2002. «The Pacific center of action of the Northern Hemisphere annular mode: Real or artifact?» **Journal of Climate**, vol. 15, n°14, pp. 1987-1991.

Wang, M. Y.; Overland, J. E. 2009. «A sea ice free summer Arctic within 30 years?» **Geophysical Research Letters**, vol. 36, L07502, doi:10.1029/2009GL037820.

Wassmann, P.; Ratkova, T.; Andreassen, I.; Vernet, M.; Pedersen, C.; Rey, F. 1999. «Spring bloom development in the marginal ice zone and the central Barents Sea». **Marine Ecology**, vol. 20, n°3-4, pp. 321-346.

Weeks, R.; Laj, C.; Endignoux, L.; Fuller, M.; Roberts, A.; Manganne, R.; Blanchard, E.; Goree, W. 1993. «Improvements in Long-Core Measurement Techniques - Applications in Paleomagnetism and Paleoceanography». **Geophysical Journal International**, vol. 114, n°3, pp. 651-662.

Williams, K, M.; Short, K.S.; Andrews, J.T., Jennings, A.E.; Mode, N.W., Syvitski, P.M.J. 1995. The Eastern Canadian Arctic at ca.6 ka BP: A Time of Transition. **Géographie Physique et Quaternaire**, vol, 49, n°1, pp 13-27.

Williams, J.; Carmack, E.C. 2008. «Combined effect of wind-forcing and isobath divergence on upwelling at Cape Batthurst, Beaufort Sea». **Journal of Marine Research,** vol. 66, n°5, pp. 645-663.

Wolfe, A. P. 2002. «Climate modulates the acidity of Arctic lakes on millennial time scales». **Geology**, vol. 30, n°3, pp. 215-218.

Wolfe, A.P. 2003. «Diatom community responses to late-Holocene climatic variability, Baffin Island, Canada: a comparison of numerical approaches». **The Holocene**, vol. 13, n°1, pp. 29–37.

Woodgate, R.A.; Fahrbach, E.; Rohardt, G. 1999. «Structure and transport of the East Greenland Current at 75°N from moored current meters». **Journal of Geophysical Research**, vol. 104, n°C8, pp. 18059-18072.

Zabenskie, S.; Gajewski, K. 2007. «Post-glacial climatic change on boothia peninsula, Nunavut, Canada». **Quaternary Research**, vol. 68, n°2, pp. 261-270.

Zhang, X. D.; Ikeda, M.; Walsh, J. E. 2003. «Arctic sea ice and freshwater changes driven by the atmospheric leading mode in a coupled sea ice-ocean model». **Journal of Climate**, vol.16, n°2, pp. 2159-2177.

Zhang, X. D.; Walsh, J. E. 2006. «Toward a seasonally ice-covered Arctic Ocean: Scenarios from the IPCC AR4 model simulations». **Journal of Climate**, vol.19, n°9, pp. 1730-1747.

Zijderveld, J.D. 1967. «Demagnetization of Rocks: analysis of results. Dans **Methods in paleomagnetism**. Préparé par Collinson, D.W.; Creer, K.M.; Runcorn, S.K., Elsevier, Amsterdam, pp. 254-286.

Zonneveld, K. A. F.; Bockelmann, F.; Holzwarth, U. 2007. «Selective preservation of organic-walled dinoflagellate cysts as a tool to quantify past net primary production and bottom water oxygen concentrations». **Marine Geology**, vol. 237, n°3-4, pp. 109-126.

Zreda, M.; England, J.; Phillips, F.; Elmore, D.; Sharma, P. 1999. «Unblocking of the Nares Strait by Greenland and Ellesmere ice-sheet retreat 10,000 years ago». **Nature**, vol. 398, n°6723 pp. 139-142.

Zweng, M.M.; Munchow, A. 2006. «Warming and freshening of Baffin Bay, 1916–2003». **Journal of Geophysical Research**, vol. 111, C07016, doi:10.1029/2005JC003093.

APPENDICE 1

LISTE DES TAXONS UTILISÉS DANS CETTE ÉTUDE AVEC LES ABBRÉVIATIONS ET LES LIMITES BIOGÉOGRAPHIQUES. LES TAXONS HÉTÉROTROPHES SONT SIGNALÉS PAR UN ASTÉRISQUE (*).

Taxa name	Abreviation	Notes	Occurrence
Achomosphaera spp.	ACHO		Atlantic
Ataxiodinium choane	ATAX		Arctic, Atlantic, Pacific
Bitectatodinium spongium	BSPO		Pacific
Bitectatodinium tepikiense	BTEP		Arctic, Atlantic, Pacific
Brigantedinium cariacoense*	BCAR	Grouped with Brigantedinium spp.	Arctic, Atlantic, Pacific
Brigantedinium simplex*	BSIM	Grouped with Brigantedinium spp.	Arctic, Atlantic, Pacific
Brigantedinium spp.*	BSPP		Arctic, Atlantic, Pacific
Cyst A*	CYSA		Pacific
Cyst of cf. Scrippsiella trifida	ALEX		Arctic, Atlantic, Pacific
Cyst of Pentapharsodinium dalei	PDAL		Arctic, Atlantic, Pacific
Cyst of Polykrikos cf. kofoidii*	PCFK		Pacific
Cyst of Polykrikos kofoidii*	PKOF		Arctic, Atlantic, Pacific
Cyst of Polykrikos schwartzii*	PSCH		Arctic, Atlantic, Pacific
Cyst of Polykrikos spp.—Arctic morphotype *	PARC		Arctic, Atlantic
Cyst of Polykrikos spp.—quadrangular morphotype*	PQUA	Grouped with cyst of Polykrikos spp. Arctic morphotype	Arctic, Atlantic
Cyst of Protoperidinium americanum*	PAME		Arctic, Atlantic, Pacific
Cyst of Protoperidinium nudum*	PNUD	Grouped with S. quanta	Arctic, Atlantic, Pacific
Dubridinium spp.*	DUBR		Atlantic, Pacific
Echinidinium aculeatum*	EACU		Pacific
Echinidinium cf. karaense*	EKAR		Arctic, Atlantic
Echinidinium delecatum*	EDEL		Pacific
Echinidinium granulatum*	EGRA		Atlantic, Pacific
Echinidinium spp.*	ESPP		Arctic, Atlantic, Pacific
Gymnodinium catenatum*	GCAT		Atlantic
Gymnodinium nolleri*	GNOL		Atlantic
Impagidinium aculeatum	IACU		Atlantic, Pacific
Impagidinium pallidum	IPAL		Arctic, Atlantic, Pacific
Impagidinium paradoxum	IPAR		Arctic, Atlantic, Pacific
Impagidinium patulum	IPAT		Arctic, Atlantic, Pacific
Impagidinium plicatum	IPLI		Atlantic, Pacific
Impagidinium sphaericum	ISPH		Arctic, Atlantic, Pacific
Impagidinium spp.	ISPP		Arctic, Atlantic, Pacific
Impagidinium strialatum	ISTR		Atlantic, Pacific
Impagidinium velorum	IVEL		Atlantic, Pacific
Islandinium brevispinosum*	IBRE		Atlantic, Pacific
Islandinium minutum*	IMIN		Arctic, Atlantic, Pacific
Islandinium? Cesare*	IMIC		Arctic, Atlantic, Pacific
Lejeunecysta oliva*	LOLI	Grouped with Lejeunecysta spp.	Arctic, Atlantic, Pacific
Lejeunecysta sabrina*	LSAB	Grouped with Lejeunecysta spp.	Atlantic, Pacific
Lejeunecysta spp.*	LSSP		Arctic, Atlantic, Pacific
Lingulodinium machaerophorum	LMAC		Arctic, Atlantic, Pacific
Nematosphaeropsis labyrinthus	NLAB		Arctic, Atlantic, Pacific
O. centrocarpum sensu Wall & Dale 1966—short processes	OCSS	Grouped with O. centrocarpum sensu Wall & Dale 1966	Arctic, Atlantic, Pacific
Operculodinium centrocarpum sensu Wall & Dale 1966	OCEN		Arctic, Atlantic, Pacific
Operculodinium centrocarpum—Arctic morphotype	OARC	Grouped with O. centrocarpum sensu Wall & Dale 1966	Arctic, Atlantic, Pacific
Operculodinium centrocarpum—morphotype cezare	OCEZ	Grouped with O. centrocarpum sensu Wall & Dale 1966	Arctic, Atlantic, Pacific
Operculodinium cf. janduchenei	OJAN		Arctic, Atlantic, Pacific
Operculodinium israelianum	OISR		Atlantic, Pacific
Polysphaeridium zoharyi	PZOH		Atlantic, Pacific
Protoperidinioids*	PERI		Arctic, Atlantic, Pacific
Protoperidinium stellatum*	PSTE		Atlantic, Pacific
Pyxidinopsis reticulata	PRET		Arctic, Atlantic, Pacific
Quinquecuspis concreta*	QCON		Arctic, Atlantic, Pacific
Selenopemphix nephroides*	SNEP		Arctic, Atlantic, Pacific
Selenopemphix quanta*	SQUA		Arctic, Atlantic, Pacific
Spiniferites belerius	SBEL	Grouped with S. membranaceus	Arctic, Atlantic, Pacific
Spiniferites bentorii	SBEN		Atlantic, Pacific
Spiniferites bulloideus	SBUL	Grouped with S. ramosus	Arctic, Atlantic, Pacific
Spiniferites delicatus	SDEL		Arctic, Atlantic, Pacific
Spiniferites elongatus	SELO		Arctic, Atlantic, Pacific
Spiniferites frigidus	SFRI	Grouped with S. elongatus	Arctic, Atlantic, Pacific
Spiniferites lazus	SLAZ		Arctic, Atlantic
Spiniferites membranaceus	SMEM		Arctic, Atlantic, Pacific
Spiniferites mirabilis-hyperacanthus	SMIR		Arctic, Atlantic, Pacific
Spiniferites ramosus	SRAM		Arctic, Atlantic, Pacific
Spiniferites ramosus type granosus	SGRA		Atlantic
Spiniferites spp.	SSPP		Arctic, Atlantic, Pacific
Stelladinium sp.*	STSP		Pacific
Tectatodinium pellitum	TPEL		Atlantic, Pacific
Trinovantedinium applanatum*	TAPP		Arctic, Atlantic, Pacific
Trinovantedinium variabile*	TVAR		Pacific
Votadinium calvum*	VCAL		Arctic, Atlantic, Pacific
Votadinium spinosum*	VSPI		Atlantic, Pacific
Xandarodinium xanthum*	XAND		Atlantic

APPENDICE 2

PRÉCISION DE LA TECHNIQUE DES ANALOGUES MODERNES (MAT) APPLIQUÉE AUX ASSEMBLAGES DE DINOKYSTES

Précision de la technique des analogues modernes (MAT)

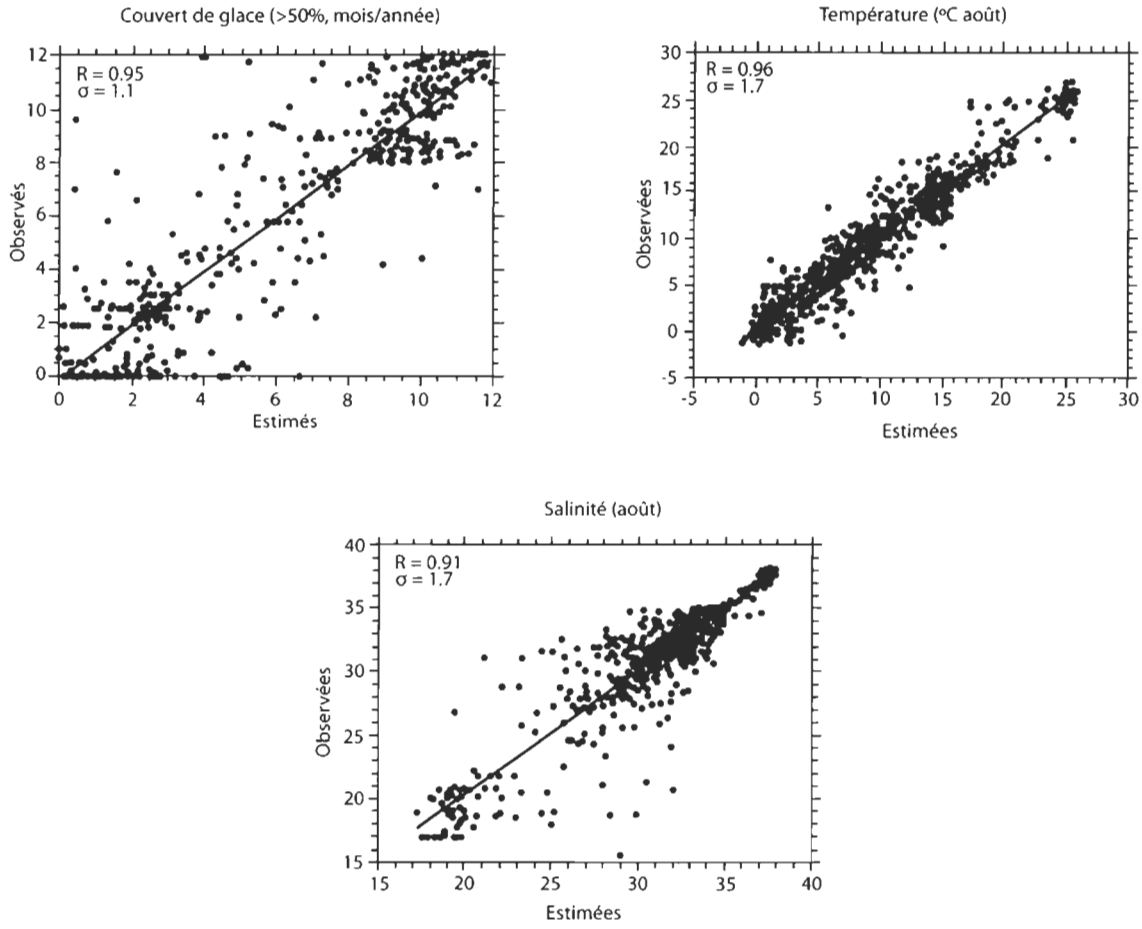

Illustration de la précision de la technique des analogues modernes (MAT) appliquée aux dinokystes pour la reconstitution de l'étendue du couvert de glace, de la température et de la salinité. Les données observées correspondent à la moyenne des paramètres hydrographiques sur la période 1953-2000 AD. Les coefficients de corrélations et les écarts-types expriment la différence entre les reconstitutions et les observations (RMSEP) et fournissent la précision des reconstitutions.

APPENDICE 3

CHAPITRE 2 HOLOCENE PALEOCEANOGRAPHY OF THE NORTHWEST PASSAGE, CANADIAN ARCTIC ARCHIPELAGO: THE POSSIBLE ONSET OF AN ARCTIC OSCILLATION CLIMATE MODE

Background data set Figure 4b

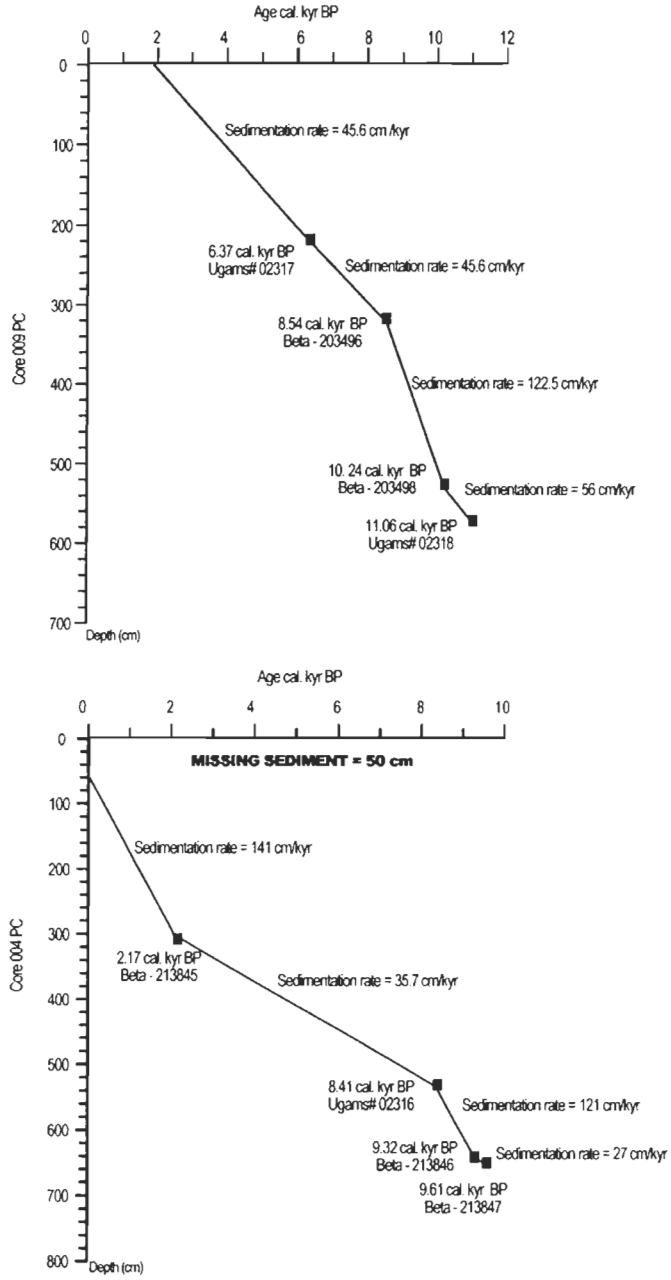

Figure 4b. (background data set). Initial age-depth model for cores 009 and 004 PC, respectively. Both age models are based on linear interpolation fit between calibrated AMS-^{14}C and indicate sedimentation rates ranging from 45 to 122 cm/kyr and from 27 to 141 cm/kyr for cores 009 and 004 PC respectively. The grey zone corresponds to the missing sediment due to piston coring process.

APPENDICE 4

CHAPITRE 3 HOLOCENE SEA-ICE HISTORY AND CLIMATE VARIABILITY ALONG THE MAIN AXIS OF THE NORTHWEST PASSAGE, CANADIAN ARCTIC

Background data set Figure 7b

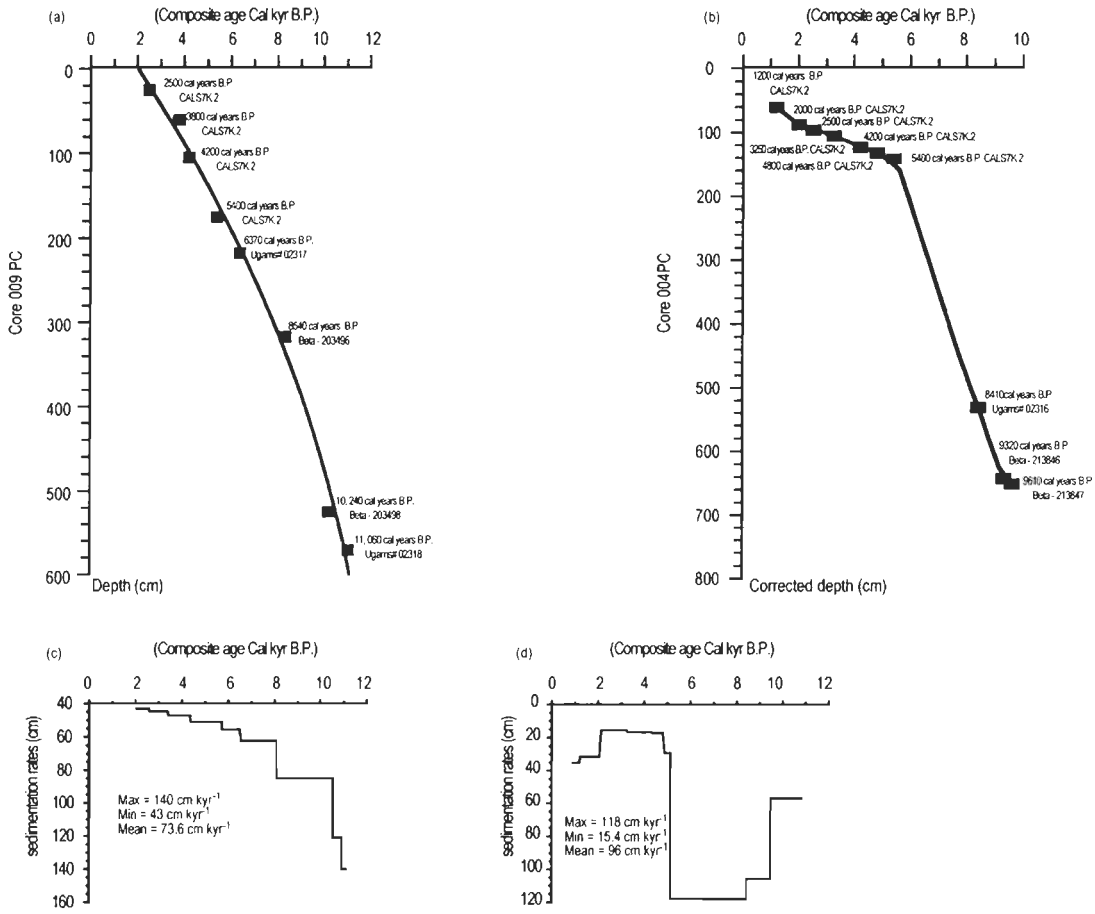

Figure 7b (background data set). (a and b) Composite age model for cores 009 and 004 PC based on correlations between PSV records (ChRM I) and the CALS7K.2 predicted inclination for both sites with initial AMS-^{14}C ages (see text and table 2 for details). The age model is based on a 2nd-order polynomial fit for core 009 PC and a linear interpolation fit for core 004 PC. (c and d) Sedimentation rates as suggested by the age models.

APPENDICE 5

DÉNOMBREMENT DES DINOKYSTES DANS LES CAROTTES À BOÎTES

Dénombrement des dinokystes dans les carottes à boîtes

Carotte	Profondeur (cm)	Somme grains marqueurs	Somme des dinokystes	OCEN	SELO	SSPP	PDAL	IMIN	IMIC	IPAL	BSPP	PARC	ESPP
009	0-1	165	309	12	0	0	19	213	20	0	45	0	0
009	5-6	186	307	56	12	2	2	60	13	4	145	2	11
009	10-11	192	316	59	15	0	2	80	12	3	140	0	5
009	15-16	192	300	27	0	0	0	56	46	2	150	0	18
009	20-21	328	301	45	8	2	0	70	1	0	140	11	24
009	25-26	206	311	30	4	0	0	160	0	0	93	9	15
009	30-31	231	305	17	4	1	0	120	20	0	135	3	5
009	35-36	215	322	20	5	0	0	130	5	0	155	2	5

Carotte	Profondeur (cm)	Somme grains marqueurs	Somme des dinokystes	IMIN	IMIC	IBRE*	EKAR	BSPP	PARC	EACU
004	0-1	133	310	98	28	37	20	102	14	11
004	5-6	93	310	77	7	37	10	166	13	0
004	10-11	103	315	179	12	22	2	76	21	3
004	15-16	182	302	155	18	20	9	68	22	10
004	20-21	270	302	160	15	2	9	95	12	9
004	25-26	131	305	197	15	0	2	69	16	6
004	30-31	210	306	191	23	3	15	34	8	32
004	35-36	380	312	170	29	0	7	80	6	20

* Non utilisé dans les reconstitutions (*Islandinium brevispinosum* cf)

Carotte	Profondeur (cm)	Somme grains marqueurs	Somme des dinokystes	OCEN	SELO	SSPP	PDAL	IMIN	IMIC	BSPP	SQUA	PARC	EACU
006	0-1	567	324	283	0	0	1	8	0	32	0	0	0
006	5-6	367	316	102	0	4	0	7	3	200	0	0	0
006	10-11	615	309	20	1	1	0	5	3	275	0	1	3
006	15-16	390	305	15	1	2	1	4	1	280	0	0	1
006	20-21	349	303	6	0	0	0	5	0	292	0	0	0
006	25-26	406	316	9	2	0	0	4	3	297	0	1	0
006	30-31	235	320	15	1	0	0	0	2	296	4	1	1
006	35-36	470	303	15	0	0	0	10	1	276	1	0	0

APPENDICE 6

DÉNOMBREMENT DES DINOKYSTES DANS LA CAROTTE 009 PC

Dénombrement des dinokystes 009 PC

Profondeur non corrigée (cm)	Modèle d'âge	Somme grains marqueurs	Somme des dinokystes	OCEN	SELO	SSPP	PDAL	PERI	IMIN	IMIC	IPAL	BSPP	PARC	ESPP
0-1	2034.70	483	301	20	4	2	0	48	113	7	0	87	12	8
10-11	2268.20	151	304	30	6	1	0	132	29	2	0	88	6	10
20-21	2499.10	357	301	44	5	2	0	57	87	24	0	53	6	23
30-31	2727.10	186	301	19	2	0	0	76	71	0	0	123	1	9
40-41	2952.30	145	301	19	4	1	0	62	101	3	2	93	1	15
50-51	3174.90	238	304	4	3	4	2	38	108	4	2	119	7	13
60-61	3394.50	169	302	49	15	5	0	0	83	0	0	139	0	11
70-71	3611.50	165	300	42	0	5	3	69	71	1	4	97	7	1
80-81	3825.50	169	304	18	11	0	1	0	97	0	0	175	0	0
90-91	4036.80	195	311	80	21	0	0	6	76	0	0	107	2	18
100-101	4245.40	213	301	78	15	0	0	0	78	1	0	104	0	25
110-111	4451.00	72	301	146	14	0	4	0	63	7	0	60	4	3
120-121	4654.10	98	310	32	13	0	0	0	123	4	0	136	0	0
130-131	4854.10	113	310	73	28	0	0	0	83	5	0	121	0	0
140-141	5051.50	87	307	90	13	1	3	5	106	0	0	76	4	9
150-151	5246.10	100	337	114	20	0	1	0	72	8	0	119	0	3
160-161	5437.80	72	322	173	16	5	5	0	33	1	0	85	0	4
170-171	5626.90	54	314	117	14	0	10	0	63	3	0	94	6	7
180-181	5812.90	52	308	191	36	0	4	0	19	0	0	58	0	0
190-191	5996.40	150	315	96	30	0	10	23	63	2	0	68	0	22
200-201	6177.00	123	307	68	33	2	16	0	71	0	0	96	0	21
210-211	6354.80	96	319	67	22	0	15	12	106	0	0	76	0	21
220-221	6529.90	107	300	130	51	0	2	23	23	0	0	66	0	5
230-231	6702.10	167	302	152	36	0	2	23	45	0	0	38	1	5
240-241	6871.60	132	301	114	49	0	6	14	72	0	0	37	1	8
250-251	7038.20	155	300	9	59	0	1	0	45	1	0	185	0	0
260-261	7202.10	159	303	7	33	0	3	0	43	2	0	176	1	38
270-271	7363.20	136	300	3	34	0	6	0	58	0	0	190	0	9
280-281	7521.40	60	322	1	33	5	1	61	51	0	0	163	1	6
290-291	7677.10	67	326	1	20	7	1	62	21	0	0	208	2	4
300-301	7829.60	58	310	1	16	9	1	47	33	0	0	199	0	4
310-311	7979.60	72	333	1	22	2	1	61	59	0	0	175	5	7
320-321	8126.70	70	323	2	22	7	0	64	47	0	0	175	3	3
330-331	8271.00	49	312	3	25	0	3	0	92	0	0	184	2	3
340-341	8412.60	57	306	2	6	2	0	58	28	0	0	208	0	2
350-351	8551.30	72	300	1	24	4	0	16	9	0	0	246	0	0
360-361	8687.40	79	306	3	15	4	0	21	12	0	3	248	0	0
370-371	8820.40	53	307	5	17	1	0	53	15	0	0	214	1	0
380-381	8950.80	70	303	2	13	0	0	74	6	0	0	207	1	0
390-391	9078.50	39	326	6	8	1	0	98	4	0	0	205	3	1
400-401	9203.20	35	315	3	8	0	0	61	18	0	0	224	0	1
410-411	9325.40	33	303	3	3	0	0	58	28	0	0	206	1	4
420-421	9444.40	32	302	2	10	0	0	68	14	0	0	208	0	0
430-431	9560.90	42	312	2	1	0	0	105	16	0	0	188	0	0
440-441	9674.60	46	320	2	4	0	0	65	15	0	0	232	2	0
450-451	9785.40	59	303	0	0	0	0	56	10	0	0	236	0	1
460-461	9893.60	73	303	0	0	0	0	75	51	0	0	165	2	10
470-471	9998.70	160	304	1	1	0	0	107	72	0	0	117	1	5
480-481	10101.00	205	316	0	0	0	0	74	70	0	0	158	2	12
490-491	10201.00	180	300	0	0	0	0	57	72	0	0	160	1	10
500-501	10298.00	195	300	0	0	0	0	60	48	0	0	180	1	11
510-511	10392.00	158	300	0	0	0	0	57	50	0	0	180	1	12
520-521	10483.00	158	312	0	0	0	0	96	38	0	0	175	3	0
530-531	10572.00	232	308	1	0	0	0	66	60	8	0	169	0	4
540-541	10657.00	64	311	0	0	0	0	67	30	0	0	210	2	2
550-551	10740.00	103	300	0	0	0	0	95	30	1	0	172	0	2
560-561	10821.00	272	300	0	1	1	0	33	121	13	0	108	2	21

APPENDICE 7

DÉNOMBREMENT DES DINOKYSTES DANS LA CAROTTE 004 PC

Dénombrement des dinokystes 004 PC

Profondeur non corrigée (cm)	Modèle d'âge	Somme grains marqueurs	Somme des dinokystes	IMIN	IMIC	EKAR	BSPP	PARC	EACU
0-1	914.02	148	305	175	33	8	63	11	15
10-11	1200.00	159	304	141	14	5	131	6	7
20-21	1486.00	446	310	247	18	5	20	6	11
30-31	1772.00	221	302	129	8	1	148	10	6
40-41	2252.70	202	315	145	26	6	119	14	4
50-51	2898.10	200	305	175	16	3	104	1	5
60-61	3538.20	190	311	200	14	3	76	7	9
70-71	4118.60	192	307	204	27	6	50	13	6
80-81	4699.00	157	301	83	11	1	193	12	1
90-91	5095.00	170	307	92	11	2	187	10	5
100-101	5380.40	175	309	99	15	5	170	17	2
110-111	5630.80	450	304	109	8	2	167	7	9
120-121	5706.40	361	306	192	28	4	65	5	10
130-131	5781.90	152	302	47	4	0	236	11	3
140-141	5854.60	139	308	32	3	0	268	3	2
150-151	5926.10	178	309	47	6	0	240	11	4
160-161	5997.50	301	311	53	2	0	243	8	5
170-171	6068.70	194	309	41	5	0	251	7	3
180-181	6139.90	214	315	71	7	1	226	6	4
190-191	6211.30	159	336	58	3	0	266	4	4
200-201	6282.90	174	302	29	3	1	264	4	1
210-211	6354.70	181	325	43	2	0	271	4	5
220-221	6426.80	110	307	45	3	0	251	4	4
230-231	6499.00	94	306	33	6	2	256	6	3
240-241	6571.80	397	306	46	3	1	249	6	1
250-251	6644.60	Absent	304	34	2	0	263	2	3
260-261	6717.80	177	331	71	9	2	241	6	2
270-271	6791.40	148	309	32	4	0	263	9	1
280-281	6865.10	314	305	10	2	0	291	1	1
290-291	6939.40	135	316	31	2	0	269	5	9
300-301	7013.80	125	310	35	2	0	260	4	9
310-311	7088.60	145	315	30	3	0	265	2	10
320-321	7163.90	120	305	35	0	0	260	3	7
330-331	7239.10	108	325	38	8	1	266	6	6
340-341	7315.10	87	314	24	6	0	274	5	5
350-351	7391.10	105	323	66	11	2	237	3	4
360-361	7467.60	99	306	42	4	0	253	2	5
370-371	7544.40	124	317	68	7	0	234	3	5
380-381	7621.40	175	308	44	7	1	251	1	3
390-391	7699.00	63	323	34	5	3	273	5	2
400-401	7776.70	80	302	40	3	0	256	1	2
410-411	7854.90	100	329	74	3	0	249	0	3
420-421	7933.40	215	321	62	5	3	239	8	2
430-431	8012.00	193	315	95	6	0	199	6	5
440-441	8091.30	225	301	78	18	0	181	11	10
450-451	8170.60	338	302	44	15	1	197	25	10
460-461	8250.50	411	307	80	27	0	160	24	11
470-471	8330.70	385	309	101	21	4	144	17	12
480-481	8411.00	134	309	44	3	0	242	13	2
490-491	8491.60	134	335	43	0	0	285	4	1
500-501	8572.30	256	316	81	8	0	215	6	5
510-511	8653.00	125	321	79	1	0	235	2	3
520-521	8733.70	154	310	72	0	0	234	1	1
530-531	8814.40	138	310	80	0	0	225	2	1
540-541	8895.10	81	310	94	4	0	197	5	1
550-551	8975.80	130	308	37	0	0	263	3	3
560-561	9056.60	139	347	73	0	1	267	4	1
570-571	9137.40	111	302	39	4	0	257	0	0
580-581	9261.10	205	308	87	3	0	213	2	2
590-591	9435.60	199	305	69	2	0	222	10	2
600-601	9610.00	200	305	70	2	0	226	5	2
610-611	9784.40	210	305	75	0	0	225	3	2
620-630	9958.90	228	300	70	0	0	222	3	5
630-640	10133.00	230	306	72	0	0	225	2	7
640-650	10308.00	240	302	70	0	0	220	2	10
650-660	10482.00	250	316	78	0	0	228	0	10
660-670	10657.00	210	300	80	0	0	210	0	10

APPENDICE 8

DÉNOMBREMENT DES DINOKYSTES DANS LA CAROTTE 006 PC

Dénombrement des dinokystes 006 PC

Profondeur non corrigée (cm)	Modèle d'âge	Somme grains marqueurs	Somme des dinokystes	OCEN	SELO	PDAL	IMIN	IMIC	EKAR	BSPP	SQUA	PARC
0-1	1023.6	480	311	10	0	0	25	0	1	275	0	0
10-11	1174.9	302	312	20	0	0	20	0	0	270	0	2
20-21	1343	780	311	42	0	12	33	3	0	220	0	1
30-31	1511.1	454	321	34	2	1	5	4	0	275	0	0
40-41	1679.2	540	315	24	0	2	17	2	0	270	0	0
50-51	1847.3	392	312	18	3	0	14	1	0	271	0	5
60-61	2015.4	724	321	39	2	1	18	4	0	255	0	2
70-71	2183.5	505	304	109	12	0	5	0	0	178	0	0
80-81	2351.6	448	309	50	7	1	13	1	0	234	0	3
90-91	2519.7	458	309	73	9	5	9	0	0	208	0	5
100-101	2687.8	475	307	55	8	0	5	0	1	237	0	1
110-111	2855.9	332	308	87	2	4	20	8	0	185	0	2
120-121	3024	404	315	82	7	2	6	4	0	214	0	0
130-131	3192.1	404	313	80	11	1	16	1	0	196	1	7
140-141	3360.2	306	313	74	8	4	12	2	0	209	0	4
150-151	3528.3	502	326	102	4	2	40	6	0	160	0	12
160-161	3696.4	375	314	96	4	2	13	1	0	189	0	9
170-171	3864.5	564	310	37	3	8	37	0	0	214	7	4
180-181	4032.6	450	330	72	7	0	12	2	0	231	1	5
190-191	4200.7	531	314	104	4	0	13	1	0	190	1	1
200-201	4368.8	795	317	77	2	2	17	5	2	207	1	4
210-211	4536.9	659	314	68	2	1	28	4	0	204	0	7
220-221	4705	574	320	51	2	0	24	4	1	231	0	7
230-231	4856.3	784	308	80	4	2	27	3	2	183	0	7
240-241	5041.2	304	319	64	8	8	15	0	0	219	0	5
250-251	5209.3	468	310	83	6	8	14	4	0	186	0	9
260-261	5377.4	410	322	79	4	0	14	3	0	216	0	6
270-271	5545.5	367	331	61	4	14	9	1	2	234	0	6
280-281	5713.6	370	311	73	5	2	15	0	0	211	1	4
290-291	5881.7	68	307	75	1	3	21	5	0	191	1	10
300-301	6049.8	410	305	86	8	0	5	0	0	203	0	3
310-311	6217.9	343	310	56	7	0	12	2	0	229	0	4
320-321	6386	320	301	82	15	0	3	1	0	200	0	0
330-331	6554.1	287	301	83	14	1	4	0	0	197	0	2
340-341	6722.2	531	311	63	4	0	12	0	0	229	0	3
350-351	6890.3	413	305	54	2	2	7	2	0	237	0	1
360-361	7058.4	495	310	40	2	0	10	0	0	254	0	4
370-371	7226.5	581	310	41	18	2	13	0	0	232	0	4
380-381	7394.6	547	332	68	6	0	35	1	0	217	0	5
390-391	7562.7	467	311	99	5	2	10	1	0	192	0	2
400-401	7730.8	440	321	101	9	0	15	1	0	191	0	4

APPENDICE 9

ANALOGUES CHOISIS POUR LES CAROTTES À BOÎTES

Analogues choisis pour les carottes à boîtes

Carotte	Profondeur (cm)	Analogue 1	Analogue 2	Analogue 3	Analogue 4	Analogue 5
009	0-1	F1231	Y691	P571	H1118	Y690
009	5-6	Z502	Z503	B256	B257	F1258
009	10-11	B256	B257	Z502	P579	Y692
009	15-16	P577	P566	P568	P576	Z507
009	20-21	Z730	F993	Z584	Z495	Z523
009	25-26	Z730	Z726	F993	Y696	Z495
009	30-31	Z584	Z523	Z531	Z495	Z598
009	35-36	Z523	Z730	Z584	Z495	P570
004	0-1	H1120	Z467	Z462	Z479	Z453
004	5-6	H1120	Z723	Z722	Z721	Z453
004	10-11	Z453	Z462	Z471	Z479	Z483
004	15-16	Z453	Z462	Z479	Z483	Z471
004	20-21	Z462	Z453	Z471	H1120	Z479
004	25-26	Z453	Z462	Z471	Z479	Z483
004	30-31	H1120	Z471	Z586	Z462	Z483
004	35-36	Z471	Z462	Z586	Z470	P569
006	0-1	F1003	Z806	P1226	Z810	Z809
006	5-6	Y375	Z806	Y687	Y688	Y372
006	10-11	Z806	Y377	Z730	Y372	Z507
006	15-16	Z806	Y375	Y372	Y377	A816
006	20-21	Z806	Y377	Z802	Z707	Y373
006	25-26	Z806	Y377	Y372	Z507	Z730
006	30-31	Z806	Y377	Z730	Y372	Z507
006	35-36	Z806	Y377	Y372	Z707	J290

APPENDICE 10

ANALOGUES CHOISIS POUR LA CAROTTE 009 PC

Analogues choisis pour la carotte 009 PC

Profondeur non corrigée (cm)	Modèle d'âge	Analogue 1	Analogue 2	Analogue 3	Analogue 4	Analogue 5
0-1	2034.70	Z584	Z730	Z495	Z523	Z531
10-11	2268.20	F993	Z730	Z584	Z495	Z523
20-21	2499.10	Z584	Z531	Z523	Z601	Z504
30-31	2727.10	Y696	Z707	Z730	Y375	Z806
40-41	2952.30	Y686	P570	Z523	Z584	P578
50-51	3174.90	Z601	Y688	Z495	Z498	Z523
60-61	3394.50	Y375	Y696	F993	F997	Z810
70-71	3611.50	Y693	F1003	Y688	F996	F993
80-81	3825.50	Y696	Y691	Y375	Z810	Z809
90-91	4036.80	Y696	F993	Z810	F997	Z730
100-101	4245.40	Y696	Z810	Y686	P570	P578
110-111	4451.00	F1251	F1255	P579	F1258	F1256
120-121	4654.10	Y686	P570	Y696	P575	P578
130-131	4854.10	Y696	Z598	Y686	P579	P575
140-141	5051.50	F997	F1001	F993	F999	F1002
150-151	5246.10	P579	Y691	Z598	Y696	Y686
160-161	5437.80	F1002	F997	F1261	F1001	Z556
170-171	5626.90	F1251	F1242	F1256	F1255	F998
180-181	5812.90	F1002	Z809	F995	F1001	Y696
190-191	5996.40	F1251	Z547	P579	H130	F1002
200-201	6177.00	F1002	Z556	F997	F1001	O756
210-211	6354.80	F1002	F1251	Z556	Z809	Z547
220-221	6529.90	Y696	F1002	Z809	F1001	F995
230-231	6702.10	F1001	Y696	F997	F1002	Z809
240-241	6871.60	F997	F1001	F1002	F1251	Y696
250-251	7038.20	Y696	P579	B256	Y691	H130
260-261	7202.10	F1251	Y691	B256	H132	P579
270-271	7363.20	Z811	Y696	Y691	Z556	G039
280-281	7521.40	Y375	Z811	F993	F997	Y696
290-291	7677.10	Y375	F993	Z811	F997	Y694
300-301	7829.60	Y375	Z811	Y694	F993	Z714
310-311	7979.60	Z811	F993	Y375	Z730	Z495
320-321	8126.70	Y375	F993	Z811	Z730	Y693
330-331	8271.00	Y696	Z811	F997	Z730	Y691
340-341	8412.60	Y375	Z811	Y694	Z806	Z802
350-351	8551.30	Y375	Z811	F993	Y694	Z806
360-361	8687.40	Y375	Z811	F993	B256	Y693
370-371	8820.40	Y375	F993	Y696	Z811	Z730
380-381	8950.80	Z811	Z806	Y375	F993	Y696
390-391	9078.50	F993	Y375	Z806	Z730	Z811
400-401	9203.20	Z811	Z806	Y375	Y696	Y694
410-411	9325.40	Z806	Z811	Z707	Y375	Z730
420-421	9444.40	Z811	Z806	Y375	Y694	Z802
430-431	9560.90	Z806	Z802	Z707	Y377	Z811
440-441	9674.60	Z811	Z806	Z730	Z728	Z717
450-451	9785.40	Z802	J348	Z705	Z706	Z806
460-461	9893.60	Z717	Z716	Z728	Z802	Z477
470-471	9998.70	Z707	Z705	Z717	Z802	Z706
480-481	10101.00	Z717	Z716	Z728	Z477	Z802
490-491	10201.00	Z802	Z705	Z706	Z254	Z708
500-501	10298.00	Z802	Z705	Z706	Z254	Z708
510-511	10392.00	Z802	Z705	Z707	Z706	Z254
520-521	10483.00	Z717	Z716	Z728	Z727	Z721
530-531	10572.00	J348	Z255	Y689	H1116	P572
540-541	10657.00	Z717	Z716	Z728	Z802	Z727
550-551	10740.00	Z802	Z705	Z811	Z706	Z254
560-561	10821.00	P569	Z591	P574	Z543	Z546

APPENDICE 11

ANALOGUES CHOISIS POUR LA CAROTTE 004 PC

Analogues choisis pour la carotte 004 PC

Profondeur non corrigée (cm)	Modèle d'âge	Analogue 1	Analogue 2	Analogue 3	Analogue 4	Analogue 5
0-1	914.02	Z471	Z462	Z483	Z586	Z479
10 11	1200.00	Z462	Z546	P569	H1120	Z471
20-21	1486.00	Z492	Z471	Z586	P569	P574
30-31	1772.00	Z723	Z453	Z546	Z462	Z722
40-41	2252.70	Z462	Z453	Z479	Z471	Z483
50-51	2898.10	Z255	P572	Y689	H1116	Z461
60-61	3538.20	Z462	Z471	P569	Z453	Z546
70-71	4118.60	Z471	Z462	Z483	Z453	Z586
80-81	4699.00	Z453	Z462	Z479	Z546	Z723
90-91	5095.00	Z453	Z462	Z546	Z723	Z479
100-101	5380.40	Z453	Z462	Z479	Z546	Z471
110-111	5630.80	Z723	Z546	Z453	Z462	Z721
120-121	5706.40	Z471	Z586	Z462	Z470	P569
130-131	5781.90	Z723	Z721	Z722	Z546	Z453
140-141	5854.60	Z802	Z705	Z706	Z254	Z708
150-151	5926.10	Z723	Z721	Z722	Z546	Z453
160-161	5997.50	Z728	Z717	Z716	Z727	Z731
170-171	6068.70	Z723	Z721	Z722	Z546	Z453
180-181	6139.90	Z723	Z721	Z546	Z722	P569
190-191	6211.30	Z717	Z716	Z728	Z727	Z731
200-201	6282.90	Z723	Z721	Z722	J348	Z728
210-211	6354.70	Z717	Z728	Z716	Z727	Z731
220-221	6426.80	Z717	Z728	Z716	Z727	Z731
230-231	6499.00	Z723	Z721	Z546	Z722	Z453
240-241	6571.80	Z728	Z717	Z716	Z727	Z731
250-251	6644.60	Z802	Z705	Z706	Z254	Z708
260-261	6717.80	Z723	Z546	Z721	P569	Z453
270-271	6791.40	Z721	Z723	Z722	Z546	Z453
280-281	6865.10	Z802	J348	Z705	Z706	Z806
290-291	6939.40	Z728	Z717	Z716	Z727	Z731
300-301	7013.80	Z717	Z728	Z716	Z727	Z731
310-311	7088.60	Z802	Z705	Z706	Z254	Z708
320-321	7163.90	Z802	Z705	Z706	Z254	Z708
330-331	7239.10	Z723	Z721	Z546	Z722	Z453
340-341	7315.10	Z723	Z721	Z546	Z722	Z543
350-351	7391.10	Z255	J348	H1116	Y689	P572
360-361	7467.60	J348	Y689	Z255	H1116	Y377
370-371	7544.40	J348	Y689	Z255	H1116	P572
380-381	7621.40	J348	Z255	H1116	Y689	Y377
390-391	7699.00	Z723	Z721	Z722	Z546	Z543
400-401	7776.70	J348	Y689	Y377	Z802	Y694
410-411	7854.90	Z802	Z705	Z706	Z254	Z708
420-421	7933.40	Z723	Z721	Z722	Z546	Z453
430-431	8012.00	Z723	Z721	Z546	P574	Z722
440-441	8091.30	Z453	Z479	Z462	Z546	Z471
450-451	8170.60	Z591	Z590	Z601	Z495	Z453
460-461	8250.50	Z453	Z479	Z462	Z483	Z471
470-471	8330.70	Z453	Z479	Z462	Z471	Z483
480-481	8411.00	Z728	Z727	Z731	Z717	Z716
490-491	8491.60	Z717	Z728	Z716	Z727	Z731
500-501	8572.30	Z723	Z546	Z721	P569	Z453
510-511	8653.00	Z802	Z705	Z706	Z254	Z708
520-521	8733.70	Z802	Z705	Z706	Z254	Z708
530-531	8814.40	Z802	Z705	Z706	Z254	Z708
540-541	8895.10	Z591	Z495	Z723	Y694	Z721
550-551	8975.80	Z802	Z705	Z706	Z254	Z708
560-561	9056.60	Z717	Z716	Z728	Z727	Z721
570-571	9137.40	J348	Y689	H1116	Z255	Y377
580-581	9261.10	Z705	Z802	Z706	Z254	Z708
590-591	9435.60	Z728	Z717	Z727	Z716	Z731
600-601	9610.00	Z717	Z716	Z728	Z727	Z725
610-611	9784.40	Z802	Z705	Z706	Z254	Z708
620-630	9958.90	Z717	Z716	Z728	Z727	Z721
630-640	10133.00	Z802	Z705	Z706	Z254	Z708
640-650	10308.00	Z802	Z705	Z706	Z254	Z708
650-660	10482.00	Z802	Z705	Z706	Z254	Z708
660-670	10657.00	Z802	Z705	Z706	Z254	Z708

APPENDICE 12

ANALOGUES CHOISIS POUR LA CAROTTE 006 PC

Analogues choisis pour la carotte 006 PC

Profondeur non corrigée (cm)	Modèle d'âge	Analogue 1	Analogue 2	Analogue 3	Analogue 4	Analogue 5
0-1	1023.6	Z806	Z707	Y377	Y378	Z802
10-11	1174.9	Z806	Z707	Z726	Y377	F1003
20-21	1343	F1003	Y691	F1231	F1229	H1118
30-31	1511.1	Y372	Z806	Y691	B256	Y377
40-41	1679.2	Y372	Z806	Y377	Y691	J289
50-51	1847.3	Z730	F993	Z495	Z806	Z523
60-61	2015.4	Z730	Y691	Z584	Z523	B256
70-71	2183.5	Z810	Y696	B082	Y375	F993
80-81	2351.6	F993	Z730	F997	F998	F1001
90-91	2519.7	F994	F997	F1001	F998	F1003
100-101	2687.8	F993	Z810	Y696	Z806	Y375
110-111	2855.9	Y691	H132	F1255	F998	F1257
120-121	3024	Z547	Y691	H132	H130	H131
130-131	3192.1	F998	F993	F997	F1001	Z730
140-141	3360.2	F998	F994	F997	F1001	F1234
150-151	3528.3	Z584	F998	Z730	F1255	Z504
160-161	3696.4	F994	F998	F1003	F997	F1001
170-171	3864.5	F998	Z438	E008	F1003	F994
180-181	4032.6	F993	Z730	Z502	Z584	F998
190-191	4200.7	Z810	Y696	F993	Z730	Z502
200-201	4368.8	F998	Z435	H1120	Y691	Z730
210-211	4536.9	Z730	Z584	Z504	F1003	Z523
220-221	4705	Z730	H1120	Z584	Z504	Z523
230-231	4856.3	F998	Z435	Z730	F1003	Z584
240-241	5041.2	F994	F997	F1001	F998	F1003
250-251	5209.3	F998	F1255	F1256	F1234	F994
260-261	5377.4	Z730	Z584	F993	Z502	Z523
270-271	5545.5	F994	F998	F1234	F1238	F997
280-281	5713.6	F997	F998	F994	F1003	F1001
290-291	5881.7	F998	F1003	Z504	Z730	Z584
300-301	6049.8	F993	Z810	Y696	F1001	F997
310-311	6217.9	Z730	F993	Z502	Z584	Z523
320-321	6386	Z810	Y696	Z806	B082	Y375
330-331	6554.1	F1001	F997	F993	Z810	F994
340-341	6722.2	F993	Z810	Y696	Z730	Z806
350-351	6890.3	Y691	Y372	F1003	F998	Z806
360-361	7058.4	F993	Z806	Z730	F1003	Z726
370-371	7226.5	F997	F1001	F993	F994	F998
380-381	7394.6	Z730	F993	Y696	Z584	Z495
390-391	7562.7	F997	F998	F994	F1001	F1003
400-401	7730.8	F993	Z730	Y696	Z810	Z502

APPENDICE 13

CARTE DES ANALOGUES CHOISIS POUR LES CAROTTES 009 BC/PC, 004 BC/PC ET 006 BC/PC

Carte des analogues

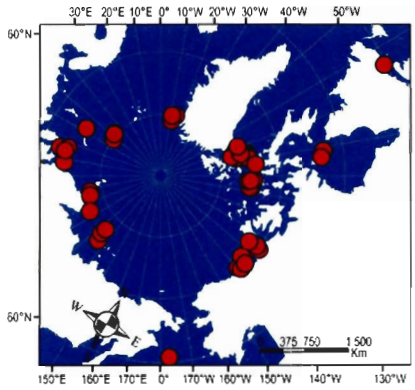

Carotte 009

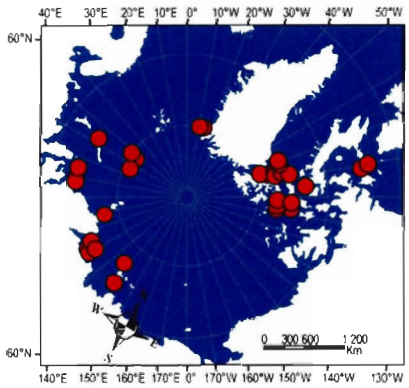

Carotte 004

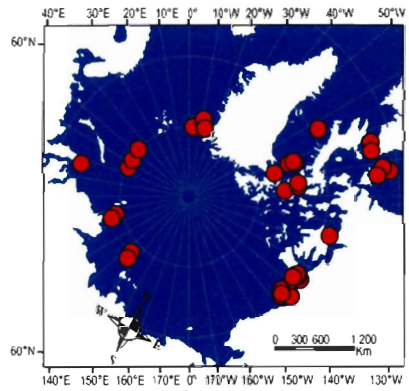

Carotte 006

APPENDICE 14

DISTANCE DES ANALOGUES POUR LES CAROTTES 009 PC, 004 PC ET 006 PC

Distance des analogues

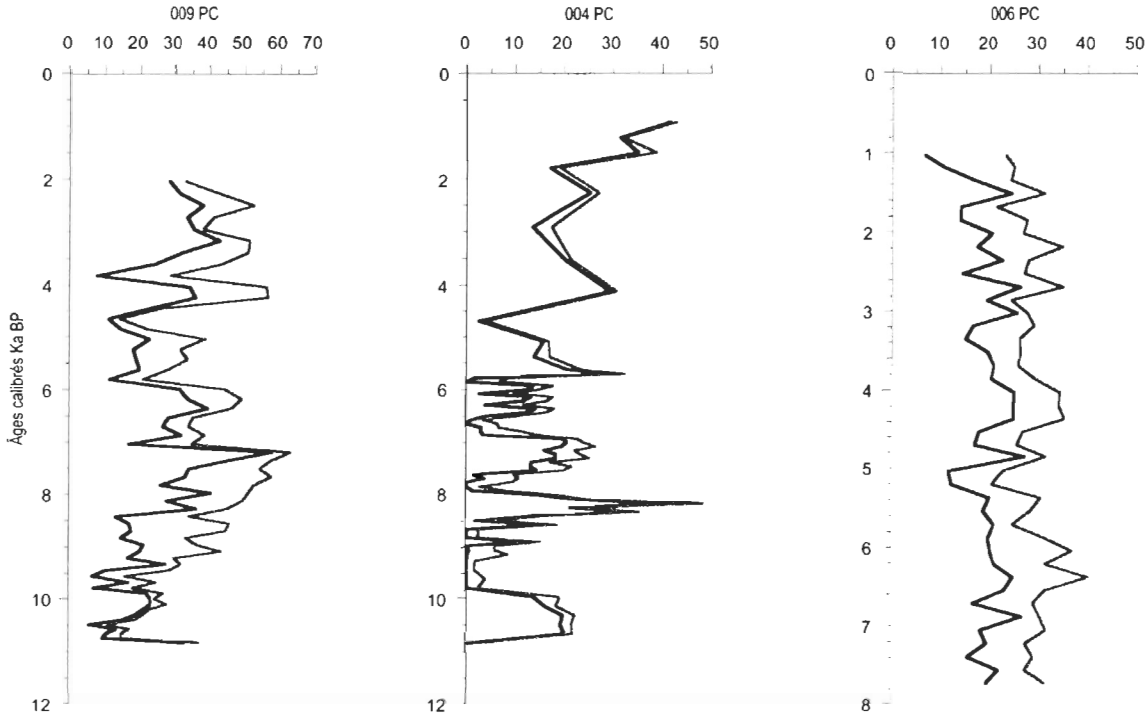

La ligne noire représente la distance du premier analogue tandis que la ligne grise représente la distance du cinquième analogue.

APPENDICE 15

RECONSTITUTIONS 009 BC, 004 BC ET 006 BC

Reconstitutions des carottes à boîtes

Carotte	Profondeur (cm)	T°C (Août)	T°C (Août min)	T°C (Août max)	Salinité (Août)	Salinité (Août min)	Salinité (Août max)	Durée couvert de glace (mois/année)	Durée couvert de glace (min, mois/année)	Durée couvert de glace (max, mois/année)
009	0	2.20	1.73	5.28	31.43	-3.55	33.16	8.07	7.06	8.28
009	5	1.29	-0.12	2.66	28.36	-2.78	28.24	9.78	7.72	11.52
009	10	2.08	-0.12	3.33	31.51	-3.45	31.39	8.50	7.72	11.52
009	15	1.97	0.66	2.61	31.96	-1.95	32.62	7.85	7.72	8.28
009	20	2.34	-0.66	6.34	23.82	-7.00	23.16	9.39	8.30	11.36
009	25	2.34	-0.66	6.34	28.83	-7.00	28.17	9.29	8.12	11.36
009	30	2.12	-0.66	5.16	19.50	-5.82	18.84	9.92	8.56	11.36
009	35	1.50	-0.66	3.55	23.35	-4.21	22.69	9.84	8.30	11.36
004	0	2.25	1.1	4.75	22.52	16.60	30.61	9.58	8.32	10.48
004	5	1.99	0.12	4.75	24.84	16.60	30.61	9.81	8.32	11.28
004	10	3.03	1.1	4.75	21.49	16.60	24.41	9.92	9.48	10.48
004	15	2.50	1.1	4.75	21.17	16.60	24.41	9.97	9.48	10.48
004	20	3.03	1.1	4.75	21.50	16.60	24.41	9.92	9.48	10.48
004	25	3.04	1.1	4.75	21.48	16.60	24.41	9.92	9.48	10.48
004	30	3.85	1.67	5.85	21.59	10.60	30.61	9.34	8.32	10.30
004	35	4.18	1.1	5.85	20.69	10.60	25.64	9.61	8.80	10.48
006	0	5.11	0.21	6.79	27.53	14.93	33.71	7.14	0.00	10.24
006	5	1.10	-0.49	2.75	32.04	30.74	33.19	9.63	7.64	11.92
006	10	0.19	-0.77	1.96	31.60	30.53	33.18	10.37	8.30	11.50
006	15	-0.34	-0.77	0.21	31.54	30.53	33.18	11.21	10.24	11.92
006	20	0.20	-1.88	2.83	33.14	30.53	33.19	10.24	7.64	11.50
006	25	-0.36	-0.77	0.21	31.38	29.36	33.18	10.89	10.24	11.50
006	30	0.16	-0.77	1.96	31.61	30.53	33.19	10.41	8.30	11.50
006	35	0.23	-0.77	2.83	32.13	30.53	33.18	10.36	7.64	11.50

APPENDICE 16

RECONSTITUTIONS 009 PC

Reconstitutions 009 PC

Modèle d'âge	Profondeur non corrigée (cm)	T°C (Août)	T°C (Août min)	T°C (Août max)	Salinité (Août)	Salinité (Août min)	Salinité (Août max)	Durée couvert de glace (mois/année)	Durée couvert de glace (min, mois/année)	Durée couvert de glace (max, mois/année)
2034.70	0.00	1.51	-0.66	3.55	23.40	7.08	31.14	9.86	8.30	11.36
2268.20	10.00	2.54	-0.66	6.34	24.00	7.08	31.14	9.35	8.30	11.36
2499.10	20.00	2.15	0.25	3.60	18.68	7.08	28.06	9.72	8.56	10.74
2727.10	30.00	2.84	-0.49	6.34	31.01	27.31	32.74	8.82	7.64	11.92
2952.30	40.00	2.27	0.25	3.55	25.36	7.08	32.44	8.53	7.64	10.52
3174.90	50.00	1.46	-0.66	3.60	22.46	9.83	32.05	9.78	8.28	11.36
3394.50	60.00	2.77	-0.49	6.34	29.31	20.84	33.71	9.33	8.12	11.92
3611.50	70.00	3.90	2.29	6.34	25.73	14.93	32.24	8.56	7.72	9.62
3825.50	80.00	1.85	-0.49	3.39	32.65	30.74	33.84	9.01	7.72	11.92
4036.80	90.00	3.36	0.85	6.34	29.46	20.84	33.71	8.46	8.12	8.86
4245.40	100.00	2.65	0.85	3.39	32.78	32.30	33.71	8.04	7.64	8.60
4451.00	110.00	4.22	2.66	6.00	23.85	19.23	28.33	9.24	8.60	9.96
4654.10	120.00	3.33	2.68	5.16	28.27	11.07	32.74	7.95	7.64	8.68
4854.10	130.00	3.48	2.68	5.16	28.08	11.07	32.74	8.08	7.64	8.68
5051.50	140.00	4.49	3.79	6.34	22.16	16.60	27.95	8.97	8.56	9.62
5246.10	150.00	4.27	2.26	6.33	26.41	11.07	32.66	8.13	7.20	8.86
5437.80	160.00	4.83	3.79	6.46	20.64	16.60	31.86	8.96	6.58	9.96
5626.90	170.00	4.16	2.66	6.00	24.22	19.23	28.33	9.24	8.60	9.96
5812.90	180.00	3.28	1.26	4.85	23.67	16.60	33.84	9.22	8.12	9.94
5996.40	190.00	4.65	3.03	6.33	28.42	20.97	32.66	8.42	7.36	9.82
6177.00	200.00	4.78	3.79	6.46	21.66	16.60	31.86	8.73	6.58	9.96
6354.80	210.00	4.09	1.26	6.33	26.12	16.60	33.84	8.97	6.58	9.94
6529.90	220.00	3.22	1.26	4.85	24.89	16.60	33.84	9.11	8.12	9.94
6702.10	230.00	3.51	1.26	4.85	24.42	16.60	33.84	9.07	8.12	9.94
6871.60	240.00	3.45	1.26	4.85	23.51	16.60	33.84	9.43	8.86	9.94
7038.20	250.00	3.29	2.19	5.53	32.13	30.39	32.74	7.88	7.36	8.16
7202.10	260.00	3.21	2.19	5.28	31.03	28.33	32.66	8.18	7.20	9.82
7363.20	270.00	3.12	0.58	4.90	29.58	16.60	33.45	8.13	6.58	9.62
7521.40	280.00	2.63	-0.49	6.34	29.08	20.84	33.45	9.38	8.12	11.92
7677.10	290.00	2.71	-0.49	6.34	28.44	20.84	33.45	9.53	8.56	11.92
7829.60	300.00	1.69	-0.49	6.34	30.94	27.31	33.45	9.54	8.28	11.92
7979.60	310.00	1.64	-0.66	6.34	30.30	27.31	33.45	9.69	8.30	11.92
8126.70	320.00	2.36	-0.49	6.34	30.55	27.31	33.45	9.26	7.72	11.92
8271.00	330.00	2.49	0.58	3.99	29.92	20.84	33.45	8.33	7.72	8.86
8412.60	340.00	1.10	-0.49	6.34	31.30	27.31	33.45	10.00	8.28	11.92
8551.30	350.00	1.45	-0.49	6.34	31.06	27.31	33.45	9.69	8.28	11.92
8687.40	360.00	1.69	-0.49	6.34	31.04	27.31	33.45	9.52	7.72	11.92
8820.40	370.00	2.56	-0.49	6.34	30.60	27.31	33.45	9.34	8.12	11.92
8950.80	380.00	1.80	-0.49	6.34	31.67	27.31	33.45	9.48	8.12	11.92
9078.50	390.00	2.81	-0.49	6.34	28.59	19.43	33.19	9.61	8.30	11.92
9203.20	400.00	1.03	-0.49	3.39	32.43	30.74	33.45	9.44	8.12	11.92
9325.40	410.00	1.01	-0.49	2.83	32.25	30.74	33.45	9.32	7.64	11.92
9444.40	420.00	0.95	-0.49	3.39	32.56	30.74	33.45	9.30	8.12	11.92
9560.90	430.00	0.19	-1.88	2.83	32.39	30.53	33.45	9.96	7.64	11.50
9674.60	440.00	1.17	0.21	2.38	32.04	30.53	33.45	9.26	8.30	11.18
9785.40	450.00	0.09	-1.88	3.50	31.94	30.32	33.40	9.93	8.10	11.38
9893.60	460.00	1.54	0.02	2.48	28.88	18.27	31.89	9.67	8.34	11.18
9998.70	470.00	2.54	1.48	3.50	29.33	18.27	32.95	8.42	7.64	9.72
10101.00	480.00	1.54	0.02	2.48	28.76	18.27	31.89	9.66	8.34	11.18
10201.00	490.00	1.20	-1.88	3.50	32.37	31.78	33.19	8.99	8.10	11.38
10298.00	500.00	1.40	0.02	2.48	30.71	29.91	31.35	9.96	8.34	11.72
10392.00	510.00	1.55	0.02	2.48	31.06	30.37	31.73	9.43	8.30	11.18
10483.00	520.00	1.75	0.02	2.48	31.08	17.69	31.62	9.26	8.30	11.18
10572.00	530.00	1.23	-0.63	4.87	31.29	30.48	31.92	9.10	6.58	11.50
10657.00	540.00	1.00	-1.88	2.48	31.22	30.53	31.89	9.93	8.34	11.38
10740.00	550.00	1.18	-1.88	3.50	32.37	15.19	33.00	9.01	8.10	11.38
10821.00	560.00	3.51	1.25	6.61	22.37	7.12	23.04	8.76	7.78	10.20

APPENDICE 17

RECONSTITUTIONS 004 PC

Reconstitutions 004 PC

Modèle d'âge	Profondeur non corrigée (cm)	T°C (Août)	T°C (Août min)	T°C (Août max)	Salinité (Août)	Salinité (Août min)	Salinité (Août max)	Durée couvert de glace (mois/année)	Durée couvert de glace (min. mois/année)	Durée couvert de glace (max. mois/année)
914.02	0.00	3.75	1.10	5.85	20.33	10.60	24.41	9.77	8.80	10.48
1200.00	10.00	2.73	1.25	4.75	27.00	19.77	31.86	9.12	7.78	10.20
1486.00	20.00	4.16	1.25	5.85	21.67	10.60	31.86	9.08	7.78	9.82
1772.00	30.00	1.81	0.11	4.75	25.69	16.60	29.78	10.46	9.48	11.78
2252.70	40.00	3.04	1.10	4.75	21.50	16.60	24.41	9.92	9.48	10.48
2898.10	50.00	2.69	0.26	5.67	29.49	20.82	32.23	8.61	6.58	10.48
3538.20	60.00	2.88	1.25	4.75	24.18	16.60	31.86	9.36	7.78	10.20
4118.60	70.00	3.99	2.30	5.85	18.82	10.60	23.79	9.60	8.80	10.30
4699.00	80.00	2.11	0.11	4.75	23.81	16.60	29.78	10.20	9.48	11.78
5095.00	90.00	2.02	0.11	4.75	24.61	16.60	29.78	10.29	9.48	11.78
5380.40	100.00	2.81	1.10	4.75	22.52	16.60	29.78	9.90	9.48	10.48
5630.80	110.00	1.80	0.11	4.75	26.23	16.60	31.71	10.48	9.48	11.78
5706.40	120.00	4.22	1.25	5.85	22.10	10.60	31.86	9.08	7.78	9.82
5781.90	130.00	0.45	0.11	2.30	29.28	16.60	31.71	11.23	9.56	11.78
5854.60	140.00	-1.27	-1.88	3.50	31.62	31.44	33.40	10.93	8.10	11.38
5926.10	150.00	0.81	0.11	2.30	27.80	16.60	31.71	10.90	9.56	11.78
5997.50	160.00	1.43	0.02	2.48	31.06	30.48	31.89	9.50	8.30	11.18
6068.70	170.00	0.55	0.11	2.30	28.96	16.60	31.71	11.16	9.56	11.78
6139.90	180.00	0.85	0.11	2.30	27.79	16.60	31.71	10.88	9.56	11.78
6211.30	190.00	1.51	0.02	2.48	31.07	30.48	31.89	9.44	8.30	11.18
6282.90	200.00	0.21	-0.91	1.76	30.41	29.56	31.71	11.32	10.20	11.78
6354.70	210.00	1.48	0.02	2.48	31.06	30.48	31.89	9.46	8.30	11.18
6426.80	220.00	1.49	0.02	2.48	31.06	30.48	31.89	9.46	8.30	11.18
6499.00	230.00	0.66	0.11	2.30	28.60	16.60	31.71	11.06	9.56	11.78
6571.80	240.00	1.53	0.02	2.48	31.00	30.48	31.89	9.66	8.30	11.18
6644.60	250.00	-1.42	-1.88	3.50	31.58	31.44	33.40	11.04	8.10	11.38
6717.80	260.00	0.97	0.11	2.30	28.43	16.60	31.86	10.42	7.78	11.78
6791.40	270.00	0.50	0.11	2.30	29.18	16.60	31.71	11.18	9.56	11.78
6865.10	280.00	-0.11	-1.88	3.50	31.81	30.32	33.19	10.34	8.10	11.38
6939.40	290.00	1.44	0.02	2.48	31.06	30.48	31.89	9.49	8.30	11.18
7013.80	300.00	1.46	0.02	2.48	31.06	30.48	31.89	9.47	8.30	11.18
7088.60	310.00	1.08	-1.88	3.50	32.34	31.44	33.40	9.09	8.10	11.38
7163.90	320.00	1.08	-1.88	3.50	32.33	31.44	33.40	9.10	8.10	11.38
7239.10	330.00	0.85	0.11	2.30	27.74	16.60	31.71	10.87	9.56	11.78
7315.10	340.00	0.47	0.11	1.76	30.37	29.56	31.71	11.20	10.20	11.78
7391.10	350.00	1.48	-0.91	4.87	31.03	29.00	32.23	8.92	6.58	11.22
7467.60	360.00	1.04	-0.91	4.87	30.76	29.00	32.23	9.36	6.58	11.50
7544.40	370.00	1.38	-0.91	4.87	31.02	29.00	32.23	9.00	6.58	11.22
7621.40	380.00	0.65	-0.91	4.87	30.75	29.00	32.23	9.71	6.58	11.22
7699.00	390.00	0.38	0.11	1.76	30.41	29.56	31.71	11.30	10.20	11.78
7776.70	400.00	-0.86	-1.88	2.25	30.36	30.32	32.23	11.16	7.78	11.50
7854.90	410.00	-0.30	-1.88	3.50	31.90	31.44	33.40	10.26	8.10	11.38
7933.40	420.00	0.49	0.11	2.30	29.12	16.60	31.71	11.24	9.56	11.78
8012.00	430.00	0.80	0.11	2.02	30.51	29.56	31.87	10.54	7.78	11.78
8091.30	440.00	2.82	1.10	4.75	22.64	16.60	29.78	9.90	9.48	10.48
8170.60	450.00	3.69	-0.66	6.61	14.48	8.98	28.74	9.51	8.68	11.36
8250.50	460.00	2.99	1.10	4.75	21.50	16.60	24.41	9.93	9.48	10.48
8330.70	470.00	3.02	1.10	4.75	21.50	16.60	24.41	9.92	9.48	10.48
8411.00	480.00	1.38	0.02	2.48	31.05	30.48	31.89	9.54	8.30	11.18
8491.60	490.00	1.65	0.02	2.48	31.05	30.48	31.89	9.40	8.30	11.18
8572.30	500.00	1.08	0.11	2.30	28.09	16.60	31.86	10.20	7.78	11.78
8653.00	510.00	0.42	-1.88	3.50	32.11	31.44	33.40	9.78	8.10	11.38
8733.70	520.00	-0.07	-1.88	3.50	31.97	31.44	33.40	10.10	8.10	11.38
8814.40	530.00	0.76	-1.88	3.50	32.21	31.44	33.40	9.54	8.10	11.38
8895.10	540.00	1.68	-0.66	5.85	25.12	9.74	31.71	10.40	8.28	11.78
8975.80	550.00	-1.57	-1.88	3.50	31.53	31.44	33.40	11.16	8.10	11.38
9056.60	560.00	1.90	0.02	2.48	30.99	28.36	31.89	9.19	8.34	11.72
9137.40	570.00	-0.48	-0.91	4.87	30.42	29.00	32.23	10.81	6.58	11.50
9261.10	580.00	1.45	-1.88	3.50	32.41	31.44	33.40	9.10	8.10	11.38
9435.60	590.00	1.26	0.02	2.48	30.90	30.48	31.89	10.27	8.30	11.18
9610.00	600.00	2.01	0.02	2.48	31.04	28.36	31.89	9.01	8.34	11.72
9784.40	610.00	0.39	-1.88	3.50	32.10	31.44	33.40	9.79	8.10	11.38
9958.90	620.00	1.39	0.02	2.48	30.72	28.36	31.89	9.98	8.34	11.72
10133.00	630.00	1.18	-1.88	3.50	32.37	31.44	33.40	9.01	8.10	11.38
10308.00	640.00	1.19	-1.88	3.50	32.37	31.44	33.40	9.01	8.10	11.38
10482.00	650.00	1.19	-1.88	3.50	32.37	31.44	33.40	9.00	8.10	11.38
10657.00	660.00	1.20	-1.88	3.50	32.37	31.44	33.40	8.99	8.10	11.38
10831.00	670.00	1.07	-1.88	3.50	32.30	31.44	33.40	9.34	8.10	11.38

APPENDICE 18

RECONSTITUTIONS 006 PC

Reconstitutions 006 PC

Modèle d'âge	Profondeur non corrigée (cm)	T°C (Août)	T°C (Août min)	T°C (Août max)	Salinité (Août)	Salinité (Août min)	Salinité (Août max)	Durée couvert de glace (mois/année)	Durée couvert de glace (min, mois/année)	Durée couvert de glace (max, mois/année)
1023.60	0.00	0.23	-1.88	2.83	32.01	29.74	33.19	10.18	7.64	11.50
1174.90	10.00	1.35	-0.63	5.47	28.43	14.93	33.19	9.91	7.64	11.50
1343.00	20.00	3.23	1.73	5.47	26.54	14.93	32.40	8.31	7.06	9.62
1511.10	30.00	0.65	-0.77	2.26	31.82	30.53	33.19	9.74	7.72	11.50
1679.20	40.00	0.04	-0.77	2.26	31.73	30.53	33.19	10.56	7.72	11.50
1847.30	50.00	1.85	-0.66	6.34	29.24	24.61	33.19	9.54	8.30	11.36
2015.40	60.00	2.06	0.25	3.55	25.87	7.08	32.12	8.53	7.72	10.52
2183.50	70.00	2.54	-0.49	6.34	31.76	27.31	33.71	9.06	8.12	11.92
2351.60	80.00	4.42	1.96	6.34	24.35	19.43	31.14	8.71	8.30	9.02
2519.70	90.00	4.96	3.79	5.88	21.37	14.93	26.36	9.01	8.86	9.62
2687.80	100.00	2.24	-0.49	6.34	31.48	27.31	33.71	9.37	8.12	11.92
2855.90	110.00	5.00	2.26	6.33	25.58	19.80	32.12	8.26	7.20	8.86
3024.00	120.00	4.99	2.26	6.33	28.74	20.97	32.12	7.72	7.20	8.86
3192.10	130.00	4.61	1.96	6.34	23.83	19.43	31.14	8.74	8.30	9.02
3360.20	140.00	5.28	3.79	6.74	23.24	19.43	28.68	8.85	8.56	9.02
3528.30	150.00	3.63	0.77	5.88	21.02	7.08	31.14	8.93	8.30	10.32
3696.40	160.00	5.05	3.79	5.88	20.81	14.93	26.36	9.05	8.86	9.62
3864.50	170.00	5.98	4.43	8.42	21.67	14.93	26.53	7.99	2.50	9.96
4032.60	180.00	3.55	-0.12	6.34	23.84	7.08	31.14	9.09	8.30	11.52
4200.70	190.00	2.60	-0.12	6.34	30.62	27.31	33.71	8.92	8.12	11.52
4368.80	200.00	3.15	1.67	5.88	28.58	21.90	32.12	8.90	7.72	10.88
4536.90	210.00	2.43	0.25	5.47	21.00	7.08	31.14	9.35	8.30	10.52
4705.00	220.00	1.72	0.25	3.55	24.27	7.08	31.14	9.09	8.30	10.52
4856.30	230.00	3.99	1.96	5.88	21.29	7.08	31.14	9.26	8.30	10.88
5041.20	240.00	5.01	3.79	5.88	21.50	14.93	26.36	9.01	8.86	9.62
5209.30	250.00	6.04	5.80	6.74	23.77	21.41	28.68	8.81	8.56	8.90
5377.40	260.00	2.52	-0.12	6.34	23.90	7.08	31.14	9.35	8.30	11.52
5545.50	270.00	5.69	3.99	6.74	24.91	20.84	28.68	8.77	8.56	8.90
5713.60	280.00	5.00	3.79	5.88	20.80	14.93	26.36	9.04	8.86	9.62
5881.70	290.00	3.79	0.77	5.88	20.37	7.08	31.14	9.14	8.30	10.32
6049.80	300.00	3.86	0.85	6.34	27.29	19.43	33.71	8.61	8.12	9.02
6217.90	310.00	2.59	-0.12	6.34	24.36	7.08	31.14	9.36	8.30	11.52
6386.00	320.00	1.58	-0.49	3.80	32.58	30.74	33.71	9.41	8.12	11.92
6554.10	330.00	4.16	0.85	6.34	25.13	19.43	33.71	8.80	8.56	9.02
6722.20	340.00	3.01	0.21	6.34	31.12	27.31	33.71	8.72	8.12	10.24
6890.30	350.00	2.58	-0.77	5.88	26.78	14.93	33.19	9.55	7.72	11.46
7058.40	360.00	3.10	0.21	6.34	26.85	14.93	33.19	9.33	8.30	10.40
7226.50	370.00	5.05	3.79	6.34	22.97	19.43	27.31	8.84	8.56	9.02
7394.60	380.00	3.15	-0.66	6.34	26.27	7.08	32.74	8.82	8.12	11.36
7562.70	390.00	4.97	3.79	5.88	20.90	14.93	26.36	9.03	8.86	9.62
7730.80	400.00	2.84	-0.12	6.34	30.48	27.31	33.71	8.91	8.12	11.52